JOURNAL OF GEOPHYSICAL RESEARCH

The continuation of

TERRESTRIAL MAGNETISM AND ATMOSPHERIC ELECTRICITY
(1896-1948)

An International Quarterly

VOLUME 60 December, 1955 NUMBER 4

CONTENTS

(Contents concluded on outside back cover)

Part one of two parts, December, 1955

Published at

THE WILLIAM BYRD PRESS, INC.

P. O. BOX 2-W, SHERWOOD AVE. AND DURHAM ST.

RICHMOND 5, VIRGINIA

Address all correspondence to

JOURNAL OF GEOPHYSICAL RESEARCH

5241 BROAD BRANCH ROAD, NORTHWEST

WASHINGTON 15, D.C., U.S.A.

SIX DOLLARS A YEAR

SINGLE NUMBERS, TWO DOLLARS

JOURNAL OF GEOPHYSICAL RESEARCH

The continuation of

Terrestrial Magnetism and Atmospheric Electricity
(1896-1948)

An International Quarterly

Founded 1896 by L. A. BAUER *Continued 1928-1948 by* J. A. FLEMING

Fields of Interest

Terrestrial Magnetism
Atmospheric Electricity
The Ionosphere
Solar and Terrestrial Relationships
Aurora, Night Sky, and Zodiacal Light
The Ozone Layer
Meteorology of Highest Atmospheric Levels
The Constitution and Physical States of the Upper Atmosphere
Special Investigations of the Earth's Crust and Interior, including experimental seismic waves, physics of the deep ocean and ocean bottom, physics in geology
And similar topics

This Journal serves the interests of investigators concerned with terrestrial magnetism and electricity, the upper atmosphere, the earth's crust and interior by presenting papers of new analysis and interpretation or new experimental or observational approach, and contributions to international collaboration. It is not in a position to print, primarily for archive purposes, extensive tables of data from observatories or surveys, the significance of which has not been analyzed.

Forward *manuscripts* to one of the Associate Editors, or to the editorial office of the Journal at 5241 Broad Branch Road, Northwest, Washington 15, D. C., U. S. A. It is preferred that manuscripts be submitted in English, but communications in French, German, Italian, or Spanish are also acceptable. A brief abstract, preferably in English, must accompany each manuscript. A *publication charge* of $8 per page will be billed by the Editor to the institution which sponsors the work of any author; private individuals are not assessed page charges. Manuscripts from outside the United States are invited, and should not be withheld or delayed because of currency restrictions or other special difficulties relating to page charges. Costs of publication are roughly twice the total income from page charges and subscriptions, and are met by subsidies from the Carnegie Institution of Washington and international and private sources.

Back issues and *reprints* are handled by the Editorial Office, 5241 Broad Branch Road, N.W. Washington 15, D.C., U.S.A.

Subscriptions are handled by the Editorial Office, 5241 Broad Branch Road, N.W., Washington 15, D.C., U.S.A.

Second-class mail privileges authorized at Richmond, Virginia

Journal of

GEOPHYSICAL RESEARCH

The continuation of

Terrestrial Magnetism and Atmospheric Electricity

VOLUME 60 DECEMBER, 1955 No. 4

GEOMAGNETIC SECULAR VARIATION AT THE CORE-MANTLE BOUNDARY

BY KEITH LEON MCDONALD*

Department of Physics, University of Utah, Salt Lake City, Utah

(Received June 15, 1955)

ABSTRACT

From maps of the geomagnetic secular variation, the time derivative of the radial component of the magnetic intensity is extrapolated to the core-mantle boundary. This problem is divided into two parts, the first of which is a purely geometrical extrapolation on the basis of potential theory for an insulating mantle. The effects of a finite conductivity of the mantle are to be considered in a later paper. Assuming the mantle an insulator, a quantitative description is given of the topography of the magnetic field variation at that boundary. Although the projection is carried out here in terms of circular hills and dales, it is found that the magnetic topography at the core is far better described in terms of an extensive system of long ridges radiating out from a set of focal points. Frequently, a near-illusion of the existence of hills or valleys is brought about by neighboring ridges. A typical ridge has a half-width of from 150 to 600 km at the core's surface, and extends over several thousand kilometers, being paralleled on each side by ridges of opposite sign. The maximum heights of the ridges frequently occur at large distances from the focal points. The integrated effects at the core are such that, for an insulating mantle, radial field intensities of 2 to 5

*Supported by the U. S. Office of Naval Research.

gauss are common, whereas intensities ranging from 5 to 15 gauss occur in the more active regions. A lower limit of the total root-mean-square value of the time derivative of the vertical component at the core is estimated to be 0.18 ($\pm$0.05) gauss per year.

I. *Introduction*

The geomagnetic secular variation may be attributed to the distortion of the main magnetic field within the earth's core by convective motions (Elsasser, 1950). The hydromagnetic effects at the core boundary may be correlated with the observed field at the earth's surface by extrapolating this field to the surface of the core. The purpose of the work reported here is to determine the extrapolated field from maps of the secular variation. Earlier investigations may be found in the works of McNish (1940), Vestine (1947), Bullard (1948), and Lowes and Runcorn (1951).

In the first part of this work, we employ a simplified earth model; it is presumed that the magnetic characteristics of the earth's mantle are those of free space. This assumption seems well justified only for the magnetic permeability μ; a preliminary dimensional analysis indicates that the electrical conductivity σ offers certain limitations which cannot be overlooked. For this reason, we shall qualify the suitability of our model before proceeding to our method of approximation.

Chapman and Whitehead (cf. ref. 5) inferred that the magnetic permeability of the earth was about unity to depths of a few hundred kilometers, disregarding the negligible percentage of magnetic surface rocks. At even lesser depths, however, the Curie point will be reached, judging from the work of Adams and Green (1931) on the shift of Curie point with increasing pressure. We are thus quite safe in presuming a constant permeability throughout the mantle. On the other hand, the studies of Chapman and Price (1930) and Lahiri and Price (1939) suggest a very rapid rise in the earth's conductivity at about the 700-km depth. From consequences of electromagnetic induction in relation to measured aperiodic storm-time variations and periodic diurnal variations, Lahiri and Price inferred a rise in σ from a value of order 10^{-13} emu to at least 10^{-11} emu, and possibly much higher. Below the 700-km depth, the radial distribution of σ is unknown, but may be expected to increase monotonically with depth. In spite of the large periods involved in the secular field, a uniform conductivity as small as 10^{-11} emu is not negligible.

As is characteristic of conductive media, the magnitude and phase velocity of each of the harmonic field components diminish monotonically with increasing σ. It follows that the field extrapolated to the core surface, assuming $\sigma \equiv 0$, represents a *lower limit* to the actual field prevailing there.

Assuming now that $\sigma = 0$ in the mantle, we may express the *instantaneous* time variation of the geomagnetic potential by the series

$$\dot{v}(r, \theta, \varphi, t)_{t=0} = a \sum_{n=0}^{\infty} \left(\frac{a}{r}\right)^{n+1} \sum_{m=0}^{n} P_n^m(\cos\theta)[a_{nm} \cos m\varphi + b_{nm} \sin m\varphi] \quad \ldots (1)$$

P_n^m (cos θ) is taken here as the usual associated Legendre functions of the first kind (cf. ref. 12). The absence of external sources seems well justified by Vestine's

latest spherical harmonic analysis (1947), which does not reveal the existence of any permanent external field. The above expansion is therefore valid for all r greater than the radius of the core, R_c (= 3,473 km). A knowledge of $\dot{v}(R_e, \theta, \varphi, 0)$, at the earth's surface, is sufficient to uniquely determine the three components of $\dot{\mathbf{H}}$ at all points of space for which $r \geq R_e$. Likewise, since all sources are assumed to be contained within the core, a knowledge of $\dot{H}_r(R_e, \theta, \varphi, 0) = -(\partial \dot{v}/\partial r)$ uniquely determines the two remaining components $\dot{H}_\theta$ and $\dot{H}_\varphi$, as well as the potential $\dot{v}$. For this reason, we shall require only the observed values of $\dot{H}_r$. Of the four available maps of $\dot{H}_r$ (Vestine, 1947), the 1922.5 epoch was chosen to be analyzed because of its relative simplicity and intermediary position in the sequence.

From Eq. (1), with $a = R_e$, it would appear that we could calculate the secular variation at the core from the spherical harmonic coefficients at the earth's surface. The success of such a method of analytical continuation, however, depends mainly on the rapidity of convergence of the series. The factor $(R_e/r)^{n+1}$ becomes increasingly important at depths approaching the core-mantle boundary, especially for larger values of n. Thus, for $r = R_e/2$, $n = 10$, we see that the 10th surface harmonic is multiplied by the factor 2,048, whereas at the earth's surface this factor becomes unity. Since the series of surface harmonics converges rather slowly, especially in a representation of the secular variation as compared with the main field, one may expect the contributions from the 10th solid harmonics, together with their errors, to be as large as 100, or more, times those of the second or third harmonics. The variation of the field at the core is too violent to be represented by an expansion, evaluated at the earth's surface, of degree only *six*.

To circumvent these difficulties, an alternate method is here employed. Essentially the procedure is one of trial and error. Assumed functions, judiciously placed at the core, are extrapolated to the earth's surface. The extrapolated field is then subtracted from the observed field. This furnishes us a new field which we designate as the *difference field*. By repeated approximations, using successive difference fields, one obtains a reasonable estimate of the field at the core. Details of the method are discussed in Chapter II, where a first and second approximation are carried out. The results of the analysis are discussed in Chapter III.

II. *Approximation to the Vertical Intensity*

We first want to find out how a "hill" of magnetic intensity at the core's boundary appears at the surface of the earth. For purposes of orientation, several arbitrary functions $\dot{H}_r(R_c, \theta)$, of axial symmetry, were placed at the core surface and expanded in terms of zonal harmonics. These same functions were then extrapolated to the earth's surface by means of the rapidly converging series

$$\dot{H}_r(r, \theta) = \dot{H}_{r0} \frac{R_c}{r} \sum_n A_n \left(\frac{R_c}{r}\right)^{n+1} P_n(\cos \theta), \qquad r = R_e \ldots\ldots\ldots (2)$$

where $\dot{H}_{r0}$ is a scale factor, made equal to $\dot{H}_r(R_c, 0)$. The results of some of these computations are shown in Figure 1, wherein several distributions of $\dot{H}_r$ at the core and their corresponding distributions at the earth's surface are plotted as functions of the great-circle arc (degrees) from their common axis of symmetry. For simplicity, the ratio R_e/R_c was set equal to two and the peak values $\dot{H}_r(R_e, 0)$

were chosen as 100 γ per year ($1\ \gamma \equiv 10^{-5}$ gauss). We may note two facts of significance. Firstly, the magnitude and shape of a function at the earth's surface depend primarily on the magnitude and spread of its source function; the shape of the latter function is immaterial so long as the bulk of the function is contained within a given half-angle. Thus, in Figure 1, it is evident that we could choose a step function with half-angle roughly intermediate to those represented by Curves 1 and 3, such that its extrapolated values would differ from Curve 2′ by an amount less than approximately one gamma per year. Curve 4′ has a large spread because of the large spread of its source function. Secondly, the spread of all functions at the earth's surface is considerable, regardless of the shape of the core functions. We may, therefore, anticipate a strong interaction between neighboring functions.

Because of its simplicity, a universal source function which depends only on one parameter, α, was finally adopted:

$$\left.\begin{aligned} \dot{H}_r(R_c\ ,\ \theta) &= \dot{H}_{r0}\left\{\frac{\cos\theta - \cos\alpha}{1 - \cos\alpha}\right\}, \qquad \theta \leq \alpha \\ \dot{H}_r(R_c\ ,\ \theta) &\equiv 0, \qquad \alpha \leq \theta \leq \pi \end{aligned}\right\} \qquad (3)$$

The expansions of (3) in the form (2) were obtained for values of α equal to 1°, 5°, 10°, $\cdots$, 40°, and for the ratio R_c/R_e equal to 35/64. The functions (3), for several values of α, together with their extrapolated values, are plotted in Figure 2. Curves 1′, 2′, $\cdots$, 7′ correspond to values of α equal to 10°, 15°, $\cdots$, 40°, respectively. The curve below the 10° curve is for $\alpha = 5°$ and the dashed curve for $\alpha = 1°$, the corresponding peak values at the core being 0.472 and 11.7 gauss per year, respectively. It should be observed that with decreasing values of α, the curves rapidly approach a limit which corresponds effectively to a δ-function at the core.

After a careful initial analysis of Vestine's map, the source functions were distributed over the core surface, with estimated half-angles and heights. To improve the estimate of the heights, the great-circle arc between centers of every pair of functions was measured, using a specially constructed flexible ruler in conjunction with a globe. With the help of Figure 2, the sum of the contributions from each of the functions at the position of any given function was compared with the value read off the observational map. The mean difference was then subtracted from the height of the given function so as not to exaggerate the correction. After several repetitions of this readjustment procedure, the over-all extrapolated field was made to agree, at the positions of the source functions, with the observed field within two or three gammas per year, except for a few points where the discrepancy was somewhat larger.

To determine the accuracy of this first approximation, the total extrapolated field was computed and compared with observation. The results are represented here in terms of the difference map (observed field minus computed field), Figure 3. In computing the extrapolated field, use was again made of the flexible rule and globe. Great-circle distances were measured from the center of each function to each of the grid points on that portion of the globe (graduated in 5° intervals of latitude and longitude) shown in Figure 3. The contribution from each function at

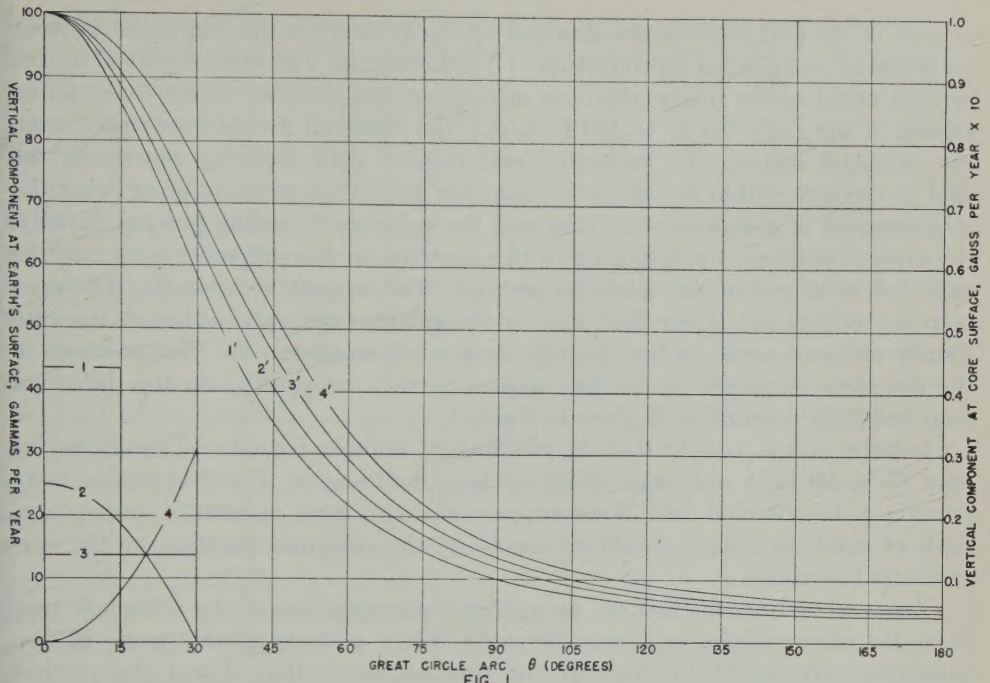

FIG. 1

each of the grid points was then scaled off from large-scale graphs of the functions, of the type shown in Figure 2, one graph for each function. Observational values

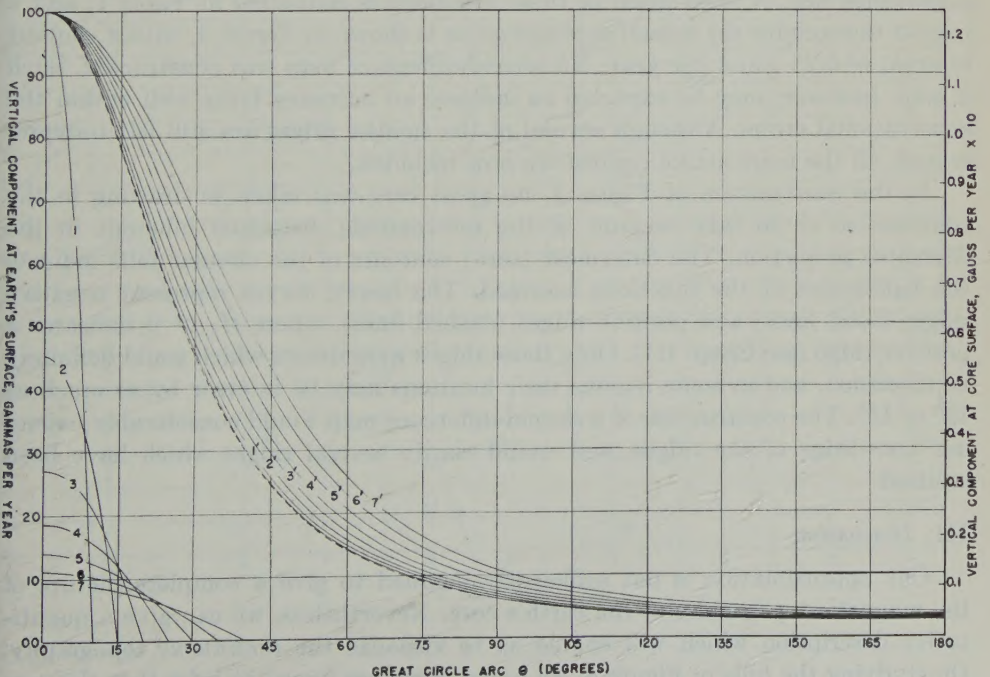

FIG. 2

at each of the grid points were obtained by linear interpolation along the contour gradients of an enlarged reproduction of Vestine's map. The error involved in this process would not be greater than one or two gammas per year. Of the overlapping regions of the globe (80 E. to 120 E. long.), the observed values were scaled from the left-hand region. The computed extrapolated field correctly represents the field at the core within five or six gammas per year, the sources of error being the measurement of great-circle distance and the subsequent scaling process. Finally, the error introduced by sketching in the contours in the difference map may be expected to be one or two gammas per year. The over-all error in the difference map is therefore not larger than nine or ten gammas per year, although the continuity obtained seems in fact to indicate a much smaller error. The positions of the functions employed in the first approximation are marked on the difference map and their description is given in Table 1.

Initially, it was thought that the secular field could be reproduced by employing only 15 or 20 hills and dales of rather large half-angles. The first attempts to reproduce the observed field, however, proved that a large number of source functions of small half-angle would be required—the potential function at the core oscillates too wildly.

For a second approximation, an enlarged superposition of the difference map upon the observational map was prepared. From a study of this map, 26 new functions were added to those of the first approximation. Using the method previously described, the heights of all functions were made compatible with observation, within two or three gammas per year, except in the more active regions, where the discrepancy was purposely left somewhat larger, always on the *conservative* side. A description of these functions is contained in Table 1, and a map of the core for the second approximation is shown in Figure 4, with a contour interval of 0.25 gauss per year. No second-difference map was constructed. Such a map, however, may be expected to indicate an accuracy lying well within the observational errors. Although several of the smaller ridges are still left unrepresented, all the more active regions are now included.

In the construction of Figure 4, no great care was taken in drawing in the contours so as to take account of the unavoidable distortion inherent in the Mercator projection. The outermost (zero) contours of the circular hills indicate the half-angles of the functions assumed. The heavy curves represent negative ridges (solid lines) and positive ridges (dashed lines), where $\dot{H}_r > 0$ indicates a positive ridge (see Chap. III). Only those ridges were drawn which could definitely be discerned, and in some regions their locations may be in error by as much as 10° or 15°. The construction of a second-difference map would considerably extend our knowledge of the ridges, and would clarify several ridges which have been omitted.

III. *Discussion*

Our approximation is not sufficiently detailed to give a complete picture of the magnetic topography of the earth's core. Nevertheless, we can give a quantitative description which will enable us to visualize the *continuous* topography. On studying the hills in Figure 4, we found ourselves forced to infer that the core

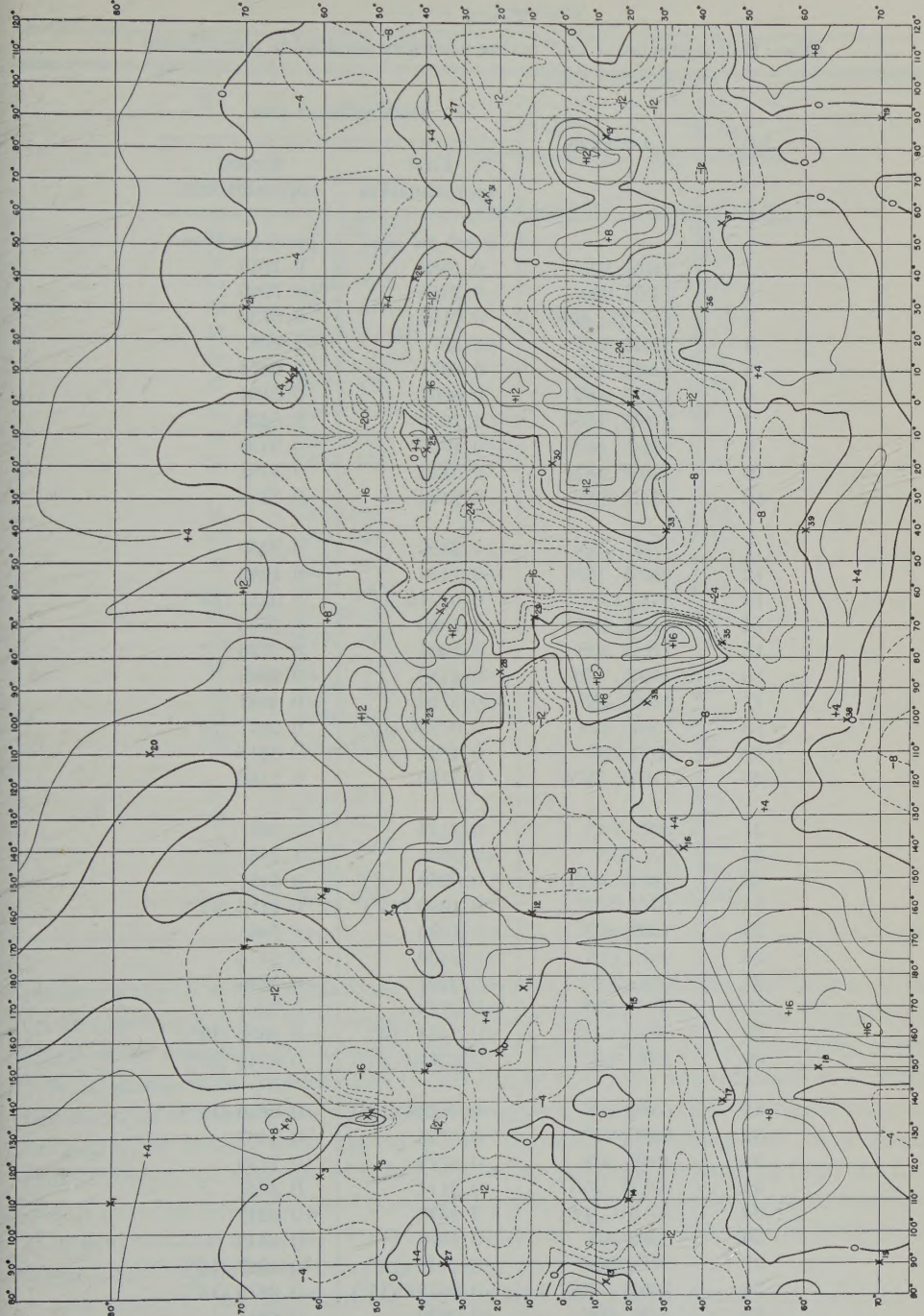

FIG. 3

TABLE 1

(*Note*: Half-angles are $\alpha = 5°$ unless otherwise specified in parentheses)

No.	Location	Peak value at core	
		First approximation	Second approximation
		gauss per year	*gauss per year*
1	110E, 80N	0.1888	0.1038
2	133E, 65N	−0.2359	−0.7786
3	117.5E, 60N	0.6182	0.8730
4	136E, 52N	−1.557	−2.265
5	120E, 50N	0.6371	0.9674
6	150E, 40N	0.6607	0.5191
7	170W, 70N	0.2973	0.6229
8	155W, 60N	−0.4719	−0.9438
9	160W, 48N	0.3822	0.5191
10	155E, 20N	−0.2124	−0.2218
11	176E, 13N	0.2359	0.2359
12	160W, 10N	−0.1416	−0.1982
13	84E, 13S	0.07716 (15°)	0.0811 (15°)
14	110E, 20S	0.1699	0.1793
15	170E, 20S	0.1604	0.1793
16	140W, 35S	−0.1180	−0.0802
17	140E, 45S	−0.4719	−0.4247
18	150E, 62S	0.07886 (15°)	0.2837 (10°)
19	90E, 70S	0.1321	0.2218
20	110W, 78N	0.1180	0.1180
21	30E, 70N	0.2124	1.033
22	8E, 65N	−0.3634	−1.746
23	100W, 40N	0.3256	0.5427
24	66W, 36N	0.1089 (15°)	0.1112 (15°)
25	15W, 40N	−0.1085	−1.586
26	39E, 43N	−0.2359	−0.5474
27	90E, 35N	−0.2407	−0.3398
28	85W, 20N	−0.3728	−0.7267
29	68W, 10N	−0.2484 (10°)	−0.2630 (10°)
30	19W, 5N	0.02789 (30°)	0.0245 (30°)
31	65E, 24N	−0.06298 (15°)	−0.0539 (15°)
32	95W, 25S	0.1793	0.2407
33	40W, 30S	0.4719	0.1793
34	0E-W, 20S	0.3114	0.2737
35	76.5W, 44S	−0.1982	−0.4247
36	30E, 40S	−0.1699	−0.2548
37	57E, 44S	−0.1146 (15°)	−0.1027 (15°)
38	100W, 66S	−0.08737 (15°)	−0.0879 (15°)
39	40W, 60S	−0.2973	−0.5615
40	135E, 38N	.....	0.1888

TABLE 1—*Concluded*

No.	Location	Peak value at core	
		First approximation	Second approximation
		gauss per year	*gauss per year*
41	152.3E, 55N	.....	0.5663
42	171E, 64N	.....	0.1652
43	110E, 20N	.....	0.0330
44	120E, 57S	.....	−0.3303
45	180E-W, 60S	.....	−0.3917
46	140W, 0N-S	.....	0.0849
47	95W, 40S	.....	0.3586
48	120W, 50S	.....	−0.0897
49	72W, 33S	.....	−1.038
50	60W, 43S	.....	1.099
51	28E, 10S	.....	0.4766
52	48E, 13S	.....	−0.3114
53	62W, 20S	.....	0.4011
54	93W, 10N	.....	0.4341
55	104W, 5S	.....	−0.1935
56	92W, 52N	.....	−0.2218
57	0E-W, 53N	.....	2.123
58	3.5E, 38N	.....	1.562
59	30W, 30N	.....	0.6795
60	12E, 47N	.....	−2.123
61	16E, 31N	.....	−1.298
62	23E, 40N	.....	1.675
63	55W, 70N	.....	0.0472
64	16W, 53N	.....	0.0944
65	26E, 50N	.....	−0.2359

surface is traversed by numerous *ridges* as shown. The large hills and dales occurring on the earth's surface map sometimes appear as foci for the ridges. Sometimes a single ridge branches out into two ridges. A typical ridge has a half-width of from 3 to 10 great-circle degrees (150 to 600 km at the core) and extends over several thousand kilometers, being paralleled by ridges of opposite sign. A ridge of moderate or negligible height may extend a few thousand kilometers and then become quite intense. An example of this is shown by the ridges extending from the function X_{31} in the Arabian Sea. Likewise, the ridge near X_{20} passes close to the North Pole and returns to partly enclose the function X_4 near Manchuria. Only in the latter neighborhood does this ridge become very large.

At present, the structure of certain foci must still remain speculative. As viewed from the earth's surface, these regions appear as vast expanses where the variation of the field at the core seems to have a maximum or minimum value. Our representations show this to be usually a near-illusion; these regions are relatively quite gentle. The case of the source function X_4 is an exception. A

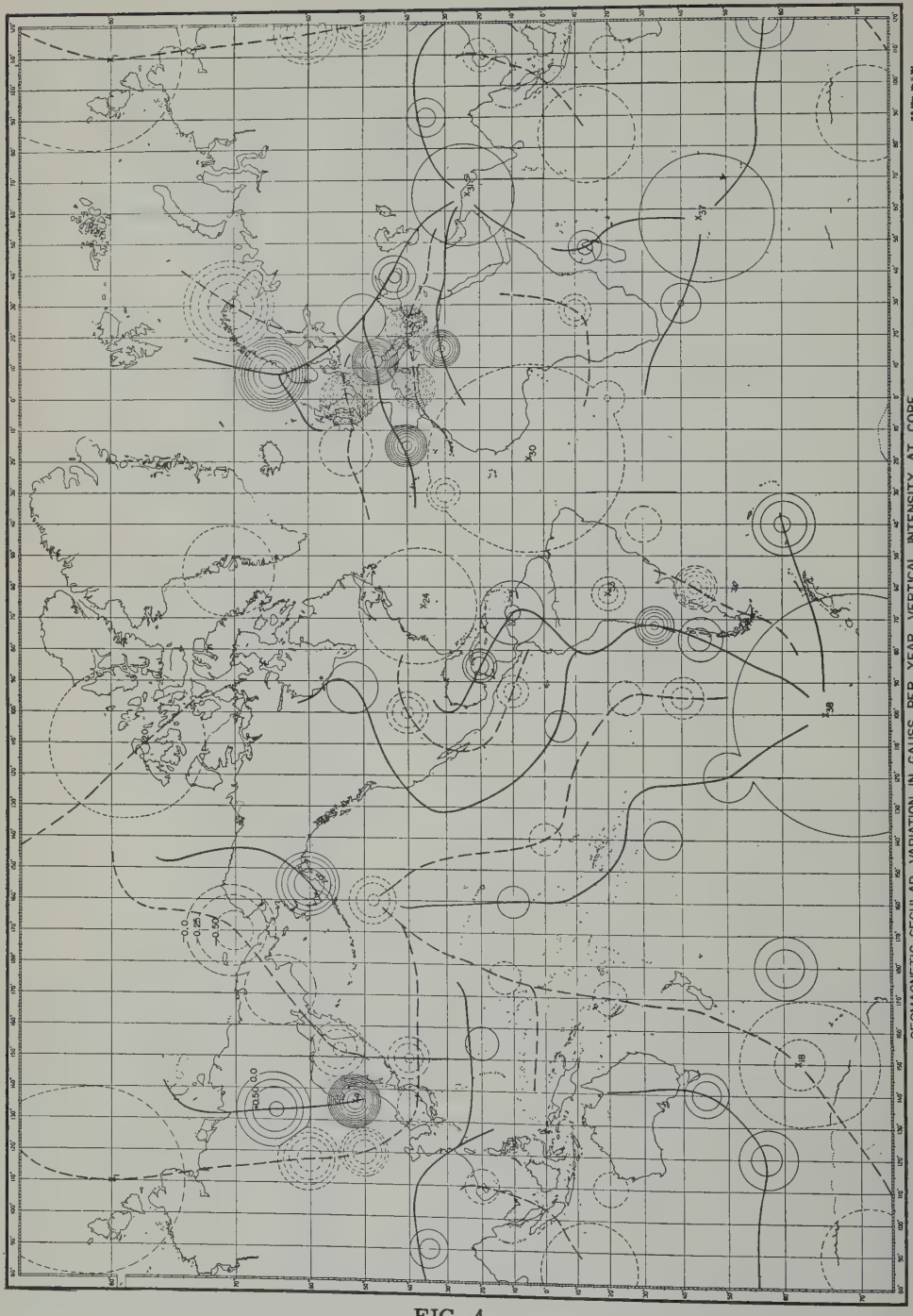
GEOMAGNETIC SECULAR VARIATION IN GAUSS PER YEAR, VERTICAL INTENSITY AT CORE

FIG. 4

typical example is the negative function X_{38} in the Antarctic, which has a half-angle, α, of 15°. This implies a rather broad region of only moderate activity, since the source functions of larger half-angles manifest themselves more readily at the earth's surface. The extent to which the two positive ridges shown in Figure 4 penetrate this region is unknown. Because of the close proximity of the positive and negative ridges in this region, however, it would not be surprising to find positive values of $\dot{H}_r$ near the center of X_{38} ; that is, these broad centers could contain considerably more activity than that indicated here. Likewise, the broadest hill at the earth's surface, centered at X_{30} , is a region of relatively gentle activity. The illusion of a large source function at the core is caused partly by the neighboring ridges. Unfortunately, this region is still somewhat obscure. Several of the neighboring ridges could not be continued— a second-difference map may be expected to clarify this region. Questions concerning the cross-sectional shapes of the hills and ridges would require approximations correct to within a few tenths gamma per year. This remark follows from our discussion of Figure 1 in Chapter II.

From Figure 4 or Table 1, we find several regions of the core where the variation of the radial component is greater than 0.5 gauss per year. The region of greatest activity occurs between Manchuria and Siberia, the negative hill X_4 showing a peak value of $\dot{H}_r = -2.26$ gauss per year. The ridges in Europe are of nearly comparable size.

From the sequence of experimental maps of $\dot{Z} = -\dot{H}_r$ (cf. ref. 11), we may estimate the value of H_r . The earliest map of the sequence, the 1912.5 epoch, shows that the general region about the hill X_4 is quite similar to that shown for the 1922.5 epoch. (Although the peak of X_4 is only slightly larger numerically than 20 γ/yr, the contour gradient in the general neighborhood indicates that the region is no less violent.) In 1932.5, however, the hill has *moved* southward and is considerably attenuated. If it is assumed that the field at X_4 maintains a constant rate of change for a period of 10 years, we conclude that the variation of the field during this period is -22.6 gauss. At some time during this period, the radial field must therefore be at least half this value, or -11 gauss.

A vertical component of this magnitude appears to be large compared to the remaining regions. For example, the hill X_{18} has a peak value of 0.28 gauss per year. During the period 1912.5 to 1942.5, this variation may be assumed constant, although there arise some modifications in the neighboring contours. Accordingly, we obtain a total variation of 11.2 gauss.

A further study of the sequence of observational maps shows that the more violent regions at the core possess a relatively short lifetime, roughly, from 5 to 20 years, whereas the broad regions of relative inactivity may persist for as long as 70 or 80 years. In Vestine's map, the field in the regions of X_{29} , X_{37} , and X_{38} changes by roughly 0.05 to 0.2 gauss per year. The radial field intensity may, nevertheless, reach a peak value of 4 or 5 gauss in these vast regions because of the long lifetime.

The surface average of $[\dot{H}_r(R_c\,,\,\theta)]^2$, computed from Eq. (3), is $\dot{H}_{r0}^2\,(1 - \cos\alpha)/6$. The total rms value of the vertical component at the core is therefore

$$h = \left[\frac{1}{4\pi R_c^2}\int \dot{H}_r^2\,\mathrm{d}S\right]^{1/2} = [\sum \dot{H}_{r0}^2(1 - \cos\alpha)/6]^{1/2} \quad \ldots\ldots\ldots (4)$$

Using the values of $\dot{H}_{r0}$ and α given in Table 1, we find that $h = 0.158$ gauss per year. It is interesting to compare this value with the surface average of $\dot{H}_r$ ($= \sum A_0 \dot{H}_{r0} = 5.4 \times 10^{-5}$ gauss per year.). The divergenceless nature of **H** would rigorously require the vanishing of the latter number.

From the evaluation of our first and second approximations, we may anticipate the deductions from a more elaborate portraiture of the core surface. First, we would require a second-difference map which would depict the discrepancies of our second approximation. Employing a total of approximately 120 source functions, we may then expect to reproduce the surface field within three or four gammas per year. Our present approximation roughly includes all the more active regions at the core, but several smaller ridges are only scarcely represented. Accordingly, we estimate a further rise in the rms value of the field to a value close to 0.18 gauss per year. Further refinements can hardly be expected to alter this value appreciably.

The rms value of the vertical component of the main dipole field, for 1945, is approximately 0.35 gauss (computed from Vestine's data, cf. ref. 10). We therefore infer that, taken over about 16 years, the rms secular variation of the field at the core approximately equals the permanent dipole field there.

In conclusion, we may expect radial field intensities of from 2 to 5 gauss at the more gentle regions of the core. Intensities ranging from 5 to 10 gauss occur in the moderately active regions, and intensities greater than 10 gauss occur only in a few violent regions of small extent. These violent fields will persist for only one or two years and their occurrence will be sparse in both time and location. The rms value at the core may be estimated, from all considerations, to be 0.18 ± 0.05 gauss per year. The small precision results partly from the large observational errors.

Our estimates assume a vanishing electrical conductivity in the mantle. The distribution of conductivity and its influence on our present results will be discussed in a subsequent paper.

References

[1] Elsasser, W. M. (1950); Rev. Mod. Phys., **22**, 1.
[2] McNish, A. G. (1940); Trans. Amer. Geophys. Union, 21st annual meeting, Pt. 2, 287.
[3] Bullard, E. C. (1948); Mon. Not. R. Astr. Soc., Geophys. Sup., **5**, 248.
[4] Lowes, F. J., and S. K. Runcorn (1951); Phil. Trans. R. Soc., A, **243**, 525.
[5] Chapman, S., and J. Bartels (1940); Geomagnetism, Oxford, Clarendon Press, Vols. 1 and 2.
[6] Adams, L. H., and J. W. Green (1931); Phil. Mag., **12**, 361.
[7] Chapman, S., and A. T. Price (1930); Phil. Trans. R. Soc., A, **229**, 427.
[8] Lahiri, B. N., and A. T. Price (1939); Phil. Trans. R. Soc., A, **237**, 509.
[9] Vestine, E. H., L. Laporte, and C. Cooper (1946); Trans. Amer. Geophys. Union, **27**, 814.
[10] Vestine, E. H., L. Laporte, I. Lange, and W. E. Scott (1947); Carnegie Inst. Wash., Pub. No. 580.
[11] Vestine, E. H., L. Laporte, I. Lange, C. Cooper, and W. C. Hendrix (1947); Carnegie Inst. Wash., Pub. 578.
[12] Jahnke, E., and F. Emde (1945); Tables of functions, Dover Publications, Inc., New York.
[13] Lowan, A. N. (1945); Tables of associated Legendre functions, Columbia University Press, New York.
[14] Tallqvist, H. (1938); Helsinki, Acta Societatis Scientiarum Fennicae, Nova Series A, **2**, No. 11.

THE DIURNAL VARIATION OF IRREGULAR GEOMAGNETIC FLUCTUATIONS

By Seth B. Nicholson

Mount Wilson and Palomar Observatories,
Carnegie Institution of Washington,
California Institute of Technology
Pasadena, California

AND

Oliver R. Wulf

United States Weather Bureau,
California Institute of Technology,
Pasadena, California

(Received April 21, 1955)

ABSTRACT

The authors have studied the diurnal variation of irregular geomagnetic fluctuations in moderately low latitudes using the eight daily K numbers (three-hour-range indices) for the seven years 1940-1946 and for the six observatories Alibag, Watheroo, Honolulu, Tucson, San Juan, and San Fernando. These observatories were chosen because they are fairly uniformly distributed in longitude, being at 73°, 116°, 202°, 249°, 294°, and 354° east, respectively.

A local time variation, to be expected from the work of earlier investigators, is apparent also in these data. The present data indicate a minimum near sunrise and a maximum in the late evening. This diurnal variation appears to have a small seasonal change.

When the local time variation is deducted from the original data for each observatory, the remainders suggest a universal time variation which exhibits a pronounced seasonal change.

A hypothesis is developed to explain the nocturnal prevalence of the irregular fluctuations in terms of atmospheric turbulence in the ionosphere. The turbulent motions are regarded as hindered during the day by electromagnetic damping. It is suggested that features of the large-scale circulation of the atmosphere may contribute to the universal time component.

The irregular fluctuations of the earth's magnetic field are known to exhibit a diurnal variation [see 1 of "References" at end of paper] that proceeds on local time. In middle latitudes, such geomagnetic disturbance is usually more prevalent during the hours of darkness, being, in the average, at a maximum in the late evening. This is a rather surprising phenomenon, for which, so far as we are aware,

no explanation has yet been offered. An understanding of it should help toward an understanding of magnetic disturbance in general.

One measure of the irregular geomagnetic fluctuations is contained in the three-hour-range index K, which is given for each of the eight three-hour intervals of the Greenwich day by a number of observatories distributed over the earth. In the present work, we have studied the diurnal variation of the irregular fluctuations in moderately low latitudes by means of the eight daily K numbers, for the seven years 1940-1946 and for the six observatories Alibag, Watheroo, Honolulu, Tucson, San Juan, and San Fernando. These observatories were chosen because they are fairly uniformly distributed in longitude, being at 73°, 116°, 202°, 249°, 294°, and 354° east, respectively. Their latitudes are 19°N, 30°S, 21°N, 32°N, 18°N, and 37°N, respectively. The data were taken from the compilation of Johnston, Scott, and Balsam [2].

When these data for each three-hour interval of Greenwich time are arranged on the local time of each observatory as nearly as such data permit, a local time diurnal variation is apparent. The results so arranged for each observatory and averaged for all the days of the seven years are shown in the six graphs in Figure 1, where the value for the Greenwich interval 0-3 hours has been placed under the

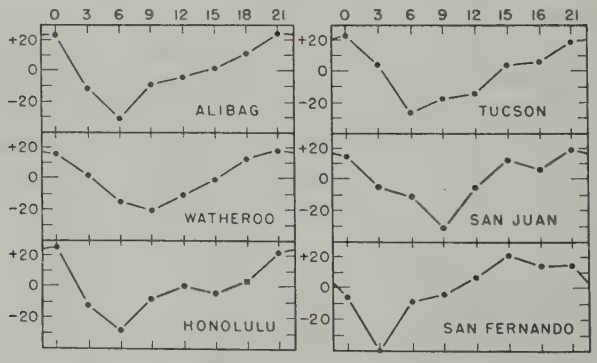

FIG. 1—Mean departures of geomagnetic disturbance, K, for each three-hour interval, 1940–1946, arranged on local time for each of six observatories

local time 6 hours for Alibag, 9 hours for Watheroo, 15 hours for Honolulu, 18 hours for Tucson, 21 hours for San Juan, and 0 hours for San Fernando, and so on for the other seven three-hour Greenwich time intervals. Actually, the centers of these intervals correspond to times a few minutes later than these even hours for the first five observatories, and a little more than an hour later for San Fernando.*

*In the arrangement of the K numbers on the local times of these six observatories, a word is necessary concerning the positions of these observatories relative to the three-hour Greenwich time interval in which they lie. The first five observatories lie near the middle of their respective intervals, averaging a little to the east of the center. San Fernando, however, lies near the beginning of its interval, considerably to the east of the relative positions of the other observatories in their respective intervals. To average the K numbers, as is done below in deriving the local time variation, represents therefore an approximation, but it was not felt that an arbitrary interpolation to correct for this was warranted in this study. Thus, San Fernando lies actually almost an hour to the east, in its respective three-hour time interval, of the average of the positions of the other five

The local time diurnal variation, as obtained by averaging the results shown in Figure 1 for these six observatories, is given in Figure 2. This indicates a minimum in the general vicinity of 6 hours and a maximum in the late evening.

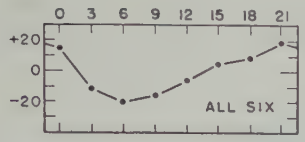

FIG. 2—Local time component of the diurnal variation of K, 1940–1946, derived from the six observatories

The six graphs of Figure 1 show considerable differences from their average in Figure 2. It is of interest, therefore, to study the remainders obtained by deducting the local time variation (shown in Fig. 2) from the results for each observatory. But, anticipating a little, it is also of interest to inquire if the local time daily variation shows an appreciable seasonal change.

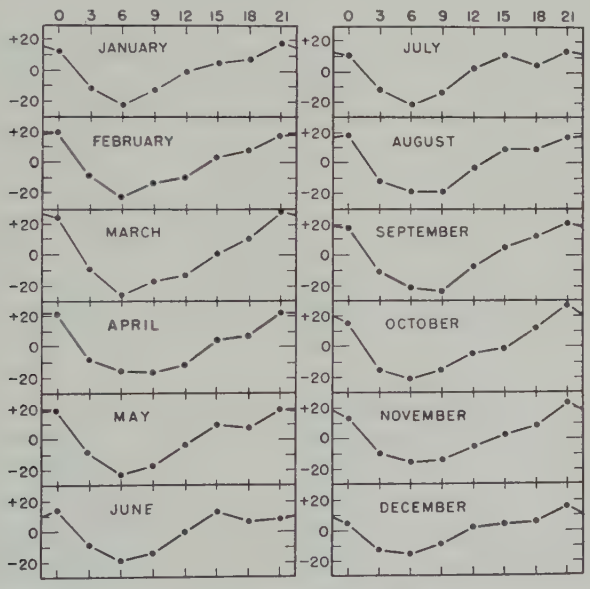

FIG. 3—Local time component of the diurnal variation of K, 1940–1946, for each month of the year from the six observatories

One answer to this is contained in Figure 3, which shows the 12 individual monthly graphs, corresponding to the one of Figure 2 where all months are averaged together. Each graph in Figure 3 is the local time variation obtained by averaging the data for all six observatories for the particular month for all seven years.

It is clear that there is no major seasonal change in the local time diurnal

---

stations in theirs. As an average of all six observatories, the centers of the three-hour Greenwich time intervals lie about 18 minutes later than the even hours of local time under which they have been tabulated, and under which their averages are plotted in the Figures.

variation, but there are nevertheless some seasonal differences, such as the subsidiary maximum in summer in the 15-18 hour interval [3].

After subtracting the local time diurnal variations shown in Figure 3 separately for each month, the six remainders (one for each observatory) were then arranged on Greenwich time and averaged for each month. The results are shown in the 12 graphs of Figure 4.

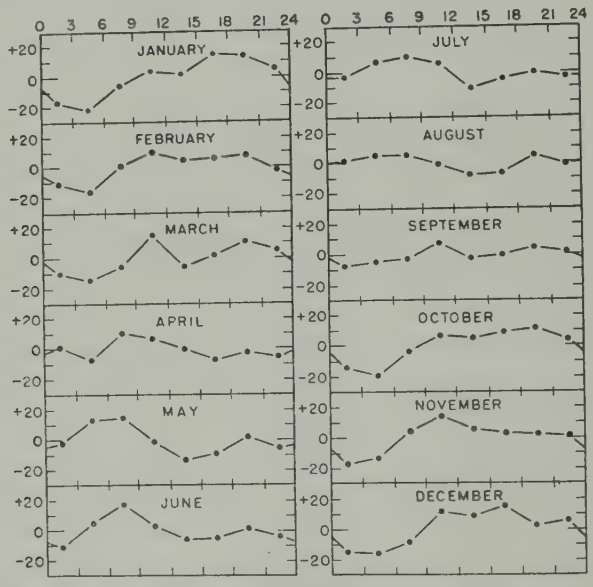

FIG. 4—Universal time component of the diurnal variation of K, 1940–1946, after subtracting the local time component for each month

These results suggest that there is also a component of the diurnal variation that proceeds on universal time and that this component exhibits a pronounced seasonal change. The months near the December solstice agree with one another reasonably well, but show a behavior noticeably different from that of the months near the June solstice, which in their turn agree reasonably well with one another. The months near the equinoxes appear rather as transition months, especially September and April. However, the behaviors near the two solstices are not mirror images of one another, and the seasonal change is not closely symmetrical with respect to the solstices.

DISCUSSION

Though an explanation of these diurnal variations of the irregular geomagnetic fluctuations seems at present difficult, we should like, nevertheless, to call attention to certain points of correspondence with other geophysical features, and to make one or two suggestions.

The nocturnal prevalence of such geomagnetic disturbance is probably the principal feature to be explained. The phenomenon of spread F, or F scatter, which arises from irregularly distributed ionization in the F layer of the ionosphere

also shows a pronounced nocturnal prevalence [4, 5, 6]. One might then ask whether irregular F layer ionization may in some way be related to the irregular geomagnetic fluctuations. An indication that it is related appears to us to be contained in the finding of Little and Maxwell [7] that the rate of scintillation of radio stars is approximately proportional to the K index of geomagnetic disturbance. It seems to be generally agreed that the scintillation of radio stars is produced mainly by the movement across the line of sight of irregular ionization in the F layer [7, 8]. Hence, spread F in motion appears to be correlated with irregular geomagnetic fluctuations.

If we assume that the horizontal motion of an irregularly distributed F layer does produce irregular geomagnetic fluctuation (in some manner by dynamo action), the question remains as to why the irregularities in the ion density in the F layer are essentially a night-time phenomenon.

The behavior in the F layer, when spread F, or F scatter, is present, is suggestive of turbulence there [6]. But vertical turbulence might be thought more likely to occur in the daytime than at night, if its source were thermal convection. Such turbulence in a relatively thin horizontal layer might be cellular in structure [9]. However, vertical turbulence could also be produced by vertical wind shear. Increase of wind velocity with height has been observed in the ionosphere [10]. In this case, there seems to be no evident reason for expecting the turbulence to be more prevalent during the day than during the night. Probably both sources contribute. And since the rate of recombination of ions and electrons depends on gas density, it would seem that vertical turbulence might lead to the observed irregularities of ion density. The following hypothesis may possibly explain the nocturnal prevalence of spread F and of irregular geomagnetic fluctuations.

During the day, the sun ionizes deeply in the ionosphere in the E and D layers and produces molecular dissociation, especially of oxygen. Heat is deposited in these regions both as actual heat and, in some measure, as heat latent in the ionization and in molecular dissociation. This lower ionization and dissociation undergoes recombination rapidly as the sun goes down because of the relatively high gas density, setting free this latent heat. The general heating in the lower ionosphere during the day would aid vertical turbulence were it not for electromagnetic damping [11] which tends to prevent the motions of turbulence across the earth's magnetic field. This electromagnetic damping may arise chiefly from the deep ionization in the E and D layers, where the direct current conductivity is relatively large. With the recombination of this ionization as the sun goes down, the braking force is in large measure removed, permitting turbulence to increase as darkness approaches, the effect of which is felt in the F layer. This appears to reach a maximum near midnight. The decrease following the maximum may be due partly to a spending of the potential energy causing the turbulence, and partly to the electromagnetic damping that sets in when solar radiation begins again to produce photoionization in the lower ionosphere.

In the irregular geomagnetic fluctuations and in the rate of radio star scintillation, a second factor is involved, namely, the motion of the irregularly distributed F layer (wind in the ionosphere). Thus, the correspondence between spread F and the irregular geomagnetic fluctuations need not be one to one, but, in general,

with some spread F and some wind in this region of the ionosphere, irregular geomagnetic fluctuations (and radio star scintillation) would be expected.

The universal time component of the diurnal variation implies that the irregular fluctuations are greater (or lesser) all around the earth, at the same universal solar time, that is, when the sun is in the vicinity of some particular longitude. Near the June solstice, there is indication of a semi-diurnal wave on universal time, with minima near the 0-3 hour and 12-15 hour Greenwich intervals. The 12-15 hour minimum comes a little before the time when the sun is near the meridian of the north geomagnetic pole. Near the December solstice, any tendency toward a semi-diurnal wave is much less pronounced, and the minimum comes just before the time when the sun is near the meridian of the south geomagnetic pole. However, even if the position of the sun relative to the geomagnetic axis may result in maxima and minima in the diurnal variation of geomagnetic activity, as discussed by Bartels [12], the lack of symmetry of these curves about the solstices suggests that irregularities of the earth's magnetic field and atmospheric factors may also be involved.

Near the June solstice, the maxima are in the 6-9 hour and 18-21 hour Greenwich intervals. At this season, the sun is north of the equator and at these two times of the Greenwich day the sun is approximately over the larger and the smaller of the two main land masses of the northern hemisphere, respectively. Near the December solstice, with the sun over the southern hemisphere where there is much less land-water differentiation, any tendency toward a semi-diurnal wave is much less pronounced. At this season, the minimum roughly replaces in position the major maximum near the June solstice. It is suggested that the irregular distribution of land and water over the earth's surface affects the large-scale atmospheric circulation even in the ionosphere, and introduces geographical peculiarities in the universal time component of geomagnetic disturbance. Such peculiarities, an example of which might be the monsoons, would be expected to change with the seasons.

References

[1] S. Chapman, The earth's magnetism, Methuen and Co., Ltd., London (1951); see p. 97.
[2] H. F. Johnson, W. E. Scott, and E. Balsam, Bull. No. 12, Assoc. of Terr. Mag. Electr., Internat. Union Geod. Geophys., Washington, D. C. (1948).
[3] A similar subsidiary maximum was found by J. M. Stagg, Geophys. Mem., **4**, No. 32, Meteorological Office, London, 1926, in data taken from the Kew magnetograms. For a discussion of these results, see Geomagnetism, by S. Chapman and J. Bartels, Clarendon Press, Oxford, 1940, p. 386.
[4] M. Ryle and A. Hewish, Mon. Not. R. Astr. Soc., **110**, 381–394 (1950).
[5] G. Reber, J. Geophys. Res., **59**, 257–265 (1954).
[6] H. W. Wells, J. Geophys. Res., **59**, 273–277 (1954).
[7] C. G. Little and A. Maxwell, J. Atmos. Terr. Phys., **2**, 356–360 (1952).
[8] A. Maxwell and C. G. Little, Nature, **169**, 746–747 (1952).
[9] In this connection, see K. Chandra, Proc. R. Soc., A, **164**, 231–242 (1938); O. G. Sutton, Proc. R. Soc., A, **204**, 297–309 (1950).
[10] J. S. Greenhow, Phil. Mag., **45**, 471–490 (1954).
[11] In this connection, see Y. Nakagawa, Nature, **175**, 417–419 (1955).
[12] J. Bartels, Met. Zs., **42**, 147–152 (1925); S. Chapman and J. Bartels, Geomagnetism, Clarendon Press, Oxford, 1940, p. 391.

SOME RESULTS OF A SWEEP-FREQUENCY PROPAGATION EXPERIMENT OVER AN 1150-KM EAST-WEST PATH

BY BERNARD WIEDER

National Bureau of Standards, Boulder, Colorado

(Received September 19, 1955)

ABSTRACT

Data from an oblique-incidence time-delay measurement experiment over an 1150-km east-west path between Sterling, Virginia, and St. Louis, Missouri, are used to examine the accuracy of the transmission-curve method of determining oblique-incidence ionosphere characteristics from vertical-incidence soundings. The experiment employed a pulsed sweep-frequency ionosphere recorder at each of the endpoints and another at the midpoint of the great-circle path. A small but consistent difference between the maximum usable frequencies (MUF) observed at the endpoint stations and the MUF determined from the vertical-incidence soundings was found. Seasonal trends of this difference are presented. The results of the analysis indicate that the average error of the transmission-curve-derived MUF varies between zero and 5 per cent too low, depending on time of day and season. Random variations result in a spread of about 10 per cent between the upper and lower decile errors.

INTRODUCTION

High-frequency radio communication over long distances involves the refraction of radio waves that are incident obliquely upon the ionized layers of the upper atmosphere. Several experiments have been conducted to determine the effect of the ionosphere on long-distance radio-wave paths, but most of the information available about radio-wave propagation through the ionosphere has been obtained from vertical-incidence radio soundings. It has been left to theory to deduce and describe the oblique-incidence phenomena from the vertical-incidence observations.

In the latter part of 1951, the National Bureau of Standards initiated an extensive sweep-frequency time-delay measurement experiment that was designed to examine the validity of the theories used in the determination of oblique-incidence characteristics from the vertical-incidence data [see 1 of "References" at end of paper]. From August 1951 to December 1952, measurements were made over a path between Sterling, Virginia, and St. Louis, Missouri, a distance of approximately 1150 km; since that time, the experiment has been operating over a path of twice this distance between Sterling, Virginia, and Boulder, Colorado.

Experiments similar to the one to be described in this paper have been conducted by other investigators [2]. The results of these experiments indicated

excellent agreement of median values predicted from vertical-incidence data with the oblique-incidence observations. The paths involved, however, were comparatively short, so that the effects of ionospheric curvature on the wave path were small and difficult to evaluate. In addition, the quantitative accuracy of the comparison of the oblique-incidence characteristics with the vertical-incidence data in these experiments is limited because the ionospheric conditions near the midpoint of the path were estimated from vertical-incidence soundings of the ionosphere at considerable distances from the midpoint. In some cases, the time involved in making a single series of observations was so long that changes in ionospheric conditions during each series were appreciable.

One purpose of the present experiment, of major interest, is to check the accuracy of the transmission-curve method [3] of obtaining oblique-incidence maximum usable frequencies (MUF) from the vertical-incidence soundings. The results of the comparison of the MUF predicted from vertical-incidence data with the MUF determined from the oblique-path data are presented in this paper.

THEORY

Figure 1 illustrates the well-known fact that one-hop propagation between two points on the earth's surface at frequencies higher than the vertical-incidence

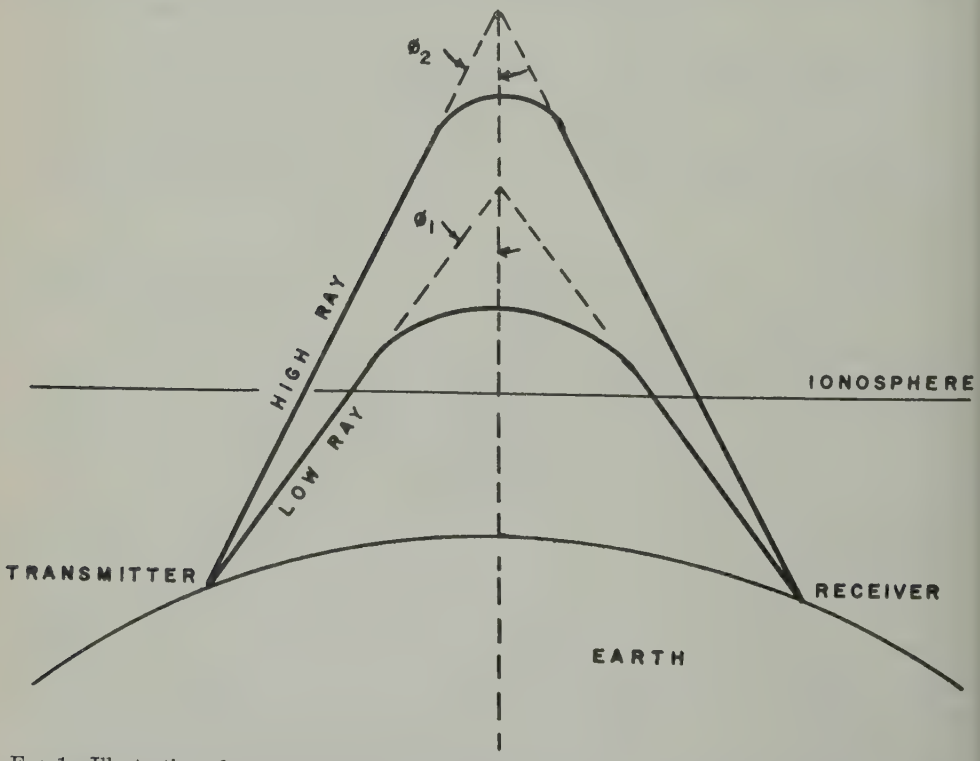

Fig. 1—Illustration of one-hop propagation between two points on the earth's surface; ionosphere is idealized as plane and its height is greatly exaggerated; ϕ_1 and ϕ_2 are half-vertex angles of equivalent triangular paths for low and high rays, respectively

itical frequency may take place by two different paths—a high path and a low th. At frequencies below the critical frequency, transmissions occur only by y of a single path. This effect is independent of the earth's magnetic field. The agneto-ionic components each shows these characteristics. Other rays will come wn short of or beyond the receiving site, or will not be returned to earth at all. the MUF, the high and the low rays merge, while above the MUF neither ray received.

For reflection by a plane stratified ionospheric layer in the absence of a magnetic ld, the relationship between the frequency (f') of a wave with angle of incidence

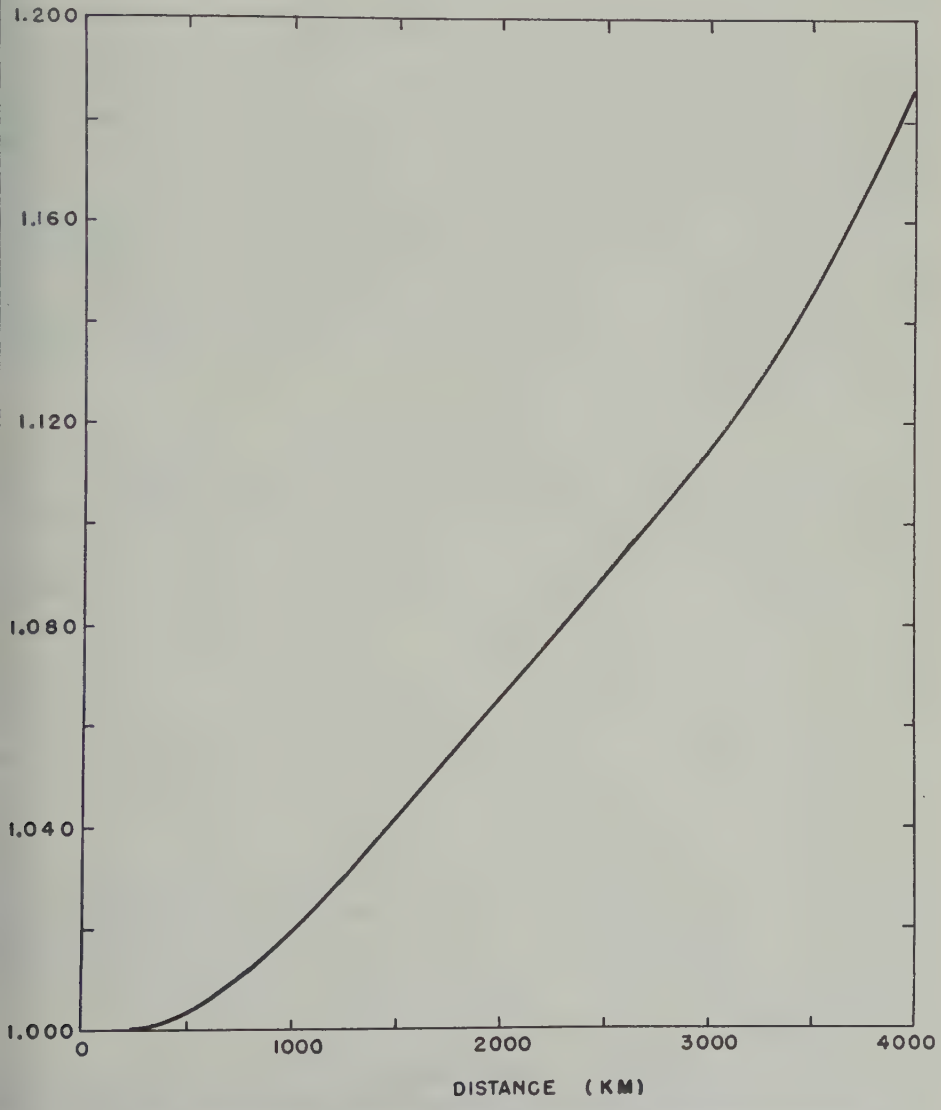

FIG. 2—Correction factor k as derived by N. Smith for virtual heights greater than 200 km

ϕ and the frequency (f) of a wave incident vertically which is reflected at the sam height in the layer is given by the well-known "secant law" approximation

$$f' = f \sec \phi \quad (1$$

This equation holds regardless of the vertical distribution of ionization. Fo propagation of radio waves through a *spherically* stratified ionosphere, on th other hand, the ionization distribution enters into the equation in a complicate way, and the "secant law" must be modified somewhat to correct for the effec of curvature. Following N. Smith [3], we may write a modified secant law a follows:

$$f' = kf \sec \phi \quad (2$$

where k is a quasi-empirical factor which is a constant for a given distance an represents the average correction to the plane-ionosphere transmission equatio when ionospheric curvature and ionization distributions are considered. Figu 2 gives k as a function of distance as derived by Smith and which is incorporate in the transmission curves used in this experiment for finding the MUF fro vertical-incidence ionograms. The theory is based on a ray or geometric-opti treatment of radio-wave propagation. Smith concluded that in the case of prop gation of the ordinary wave over an east-west path in the United States the effe of the earth's magnetic field on the relationship of f' to f could be neglecte Horizontal uniformity is assumed.

EXPERIMENTAL

At each of the endpoints of the path, modified pulsed sweep-frequency ion spheric recorders [4] were operated synchronously, so that each received th

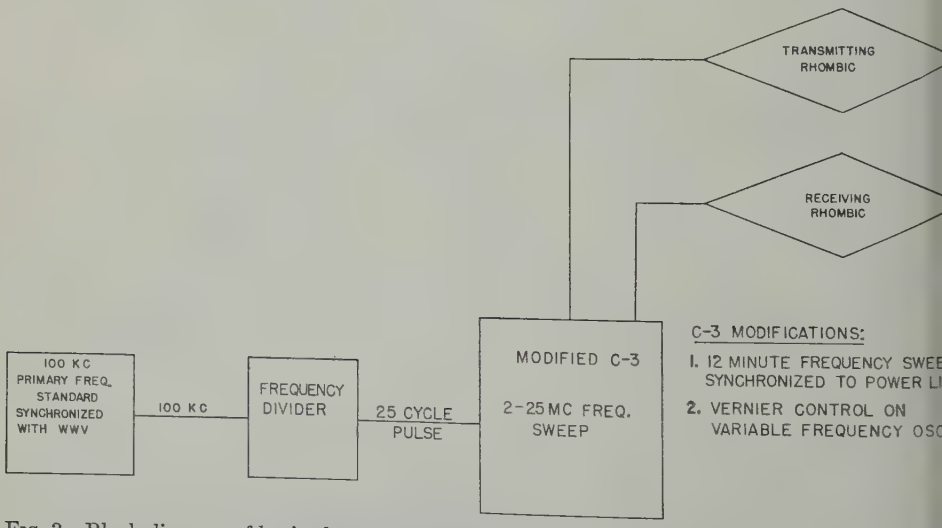

FIG. 3—Block diagram of basic elements of endpoint equipment; 100-kc primary standard at ea endpoint provided excellent synchronization stability

ulses transmitted by the other. Synchronization stability was maintained by a 00-kc primary frequency standard at each endpoint that was periodically nchronized with WWV. Horizontal rhombic antennas were used for both trans- itting and receiving to obtain suitable directivity and gain. The equipment perated through a frequency range of 3 to 25 Mc, linearly in 12 minutes, and was un continuously for a 24-hour period once each week. The pulse repetition rate as 25 cycles. A block diagram of the endpoint equipment is shown in Figure 3.

At the midpoint of the great-circle path near Batavia, Ohio, a standard iono- pheric recorder made approximately simultaneous vertical-incidence records. he equipment at the midpoint was operated in the usual manner for a vertical- ncidence ionosphere station; a frequency range of 1 to 25 Mc was swept in 15 econds. In the early months of the experiment, midpoint records were made nce every 12 minutes; later, in order to improve the temporal correspondence etween the observed MUF and the vertical-incidence records, the rate was hanged to once every 6 minutes, and then finally to once every 3 minutes.

Figure 4 shows typical oblique records made at Sterling, and below each of hem the associated vertical-incidence records made at the midpoint of the path. ecords similar to the Sterling records were, of course, made at St. Louis. The ecords shown are for a winter morning and a summer afternoon. The vertical cale on all the records shows time delay after the local transmitter pulse, each nterval corresponding to 200 km of free-space path distance. On the vertical- ncidence records, each interval therefore corresponds to 100 km of virtual height. n the oblique-incidence records, the sum of the relative delay times observed at ach endpoint station is equal to the round-trip delay time of the pulse. The orizontal scales show frequency in megacycles.

The endpoint records have a linear frequency scale and the midpoint records a garithmic frequency scale. The vertical-incidence trace at the low-frequency nd of the endpoint records is the result of pulses transmitted vertically at Sterling nd received by the Sterling equipment. The oblique-incidence trace is caused by ulses received at Sterling that were transmitted by the St. Louis equipment.

Figures 5 and 6 are examples of one of the operations that can be performed ith the data. In each Figure, the solid curve of (*A*) is traced from the oblique- ncidence record, and the solid curve in (*B*) is traced from the corresponding idpoint vertical-incidence record. The time marked on (*A*) is the time the carrier equency reached 23 Mc, and the time marked on (*B*) is within a minute or two the time when the oblique-incidence trace on (*A*) went through the *F*2 MUF ssociated with (*B*). Superimposed on each vertical-incidence trace are the trans- ission curves for the path, parametric in the oblique-incidence frequency. The elay time, in units of equivalent path length, for the one-way oblique path is own to the left of Figures (*A*) and is the average of the relative delay times on he two endpoint records.

At each point where the transmission curve intersects the vertical-incidence ace, there should be a corresponding point on the oblique-incidence records. A mple trigonometric equation relates the virtual height at vertical incidence with he equivalent triangular path length. The dotted curves in Figures (*A*) show the oints that correspond to the intersections of the transmission curves with the

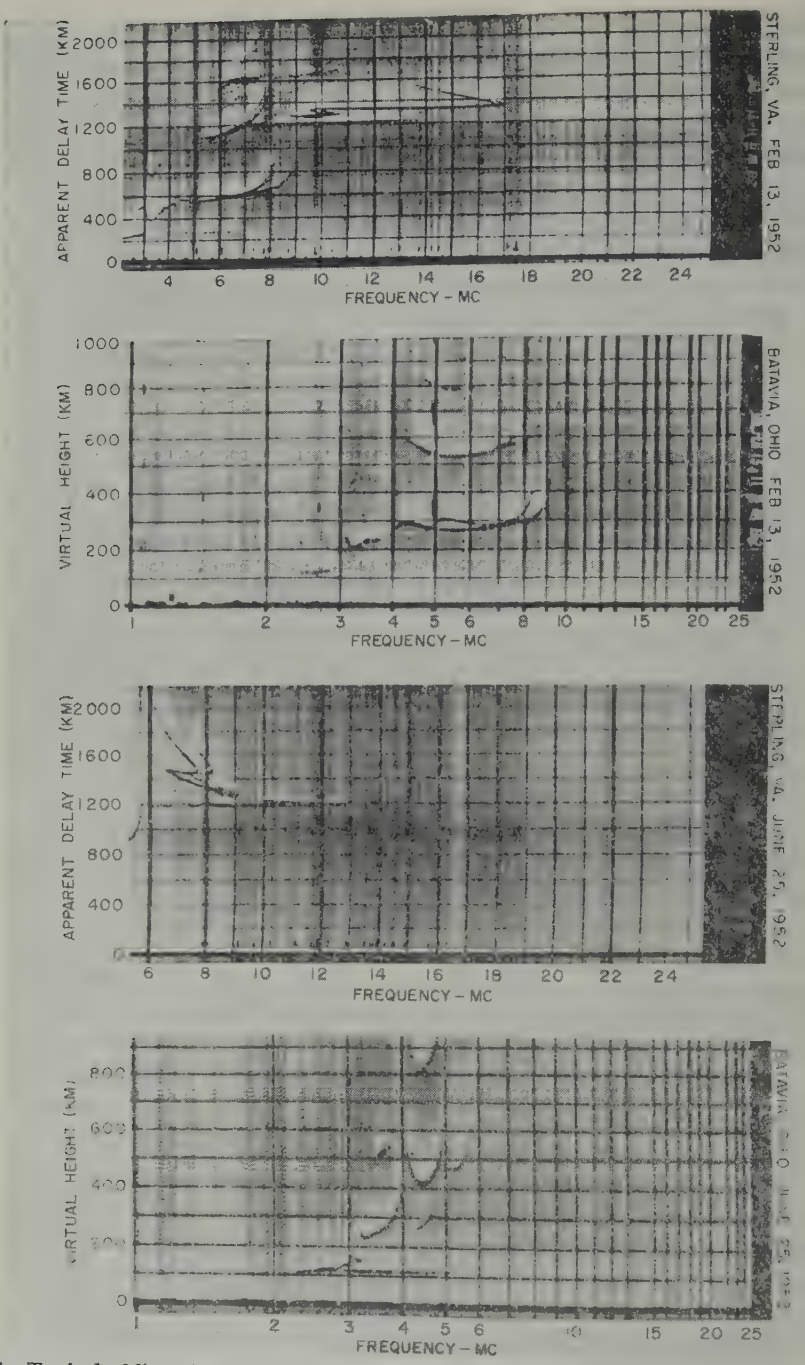

FIG. 4—Typical oblique-incidence records made at Sterling, Virginia, and associated vertic incidence midpoint records made at Batavia, Ohio; a winter morning and a summer afterno record are shown

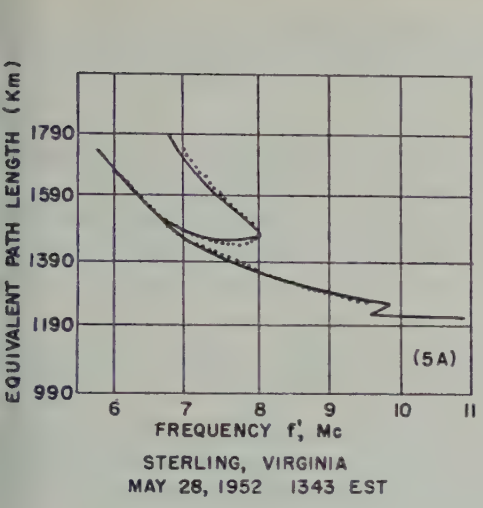

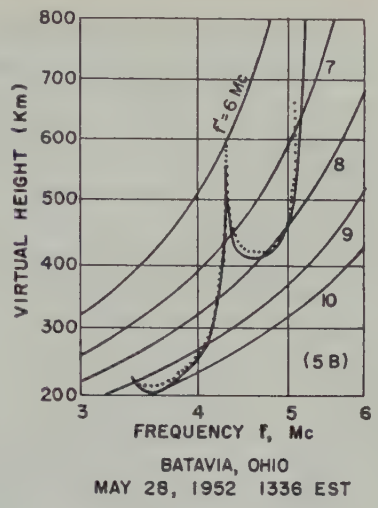

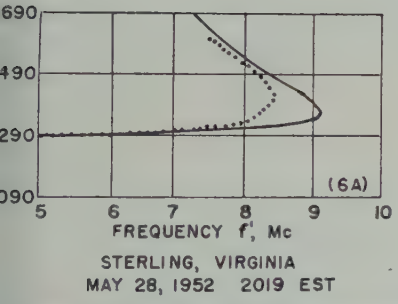

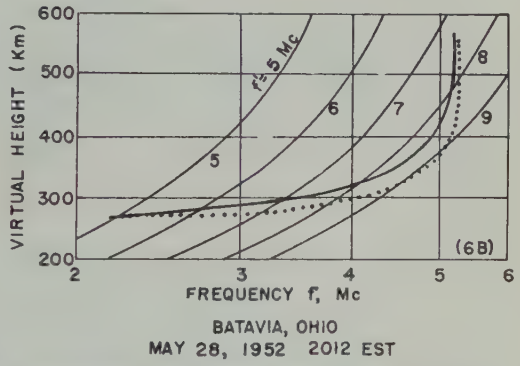

s. 5 and 6—Solid lines in illustrations are traced from the records; dotted lines are derived ves; dotted curve of (*A*) is derived from traced (solid) curve of (*B*); and, conversely, dotted curve of (*B*) is derived from solid curve of (*A*)

tical-incidence traces in Figures (*B*). The inverse procedure can also be per-med and results in the dotted curves of Figures (*B*).

Figure 5 is an example in which the *F*2 MUF derived from the vertical-incidence ord agrees with the *F*2 MUF observed over the oblique path. There is also stantial agreement between the derived and observed delay times at all fre-ncies. Figure 6 is an example in which the derived and the observed curves er considerably.

ANALYSIS

The *F*2 layer rather than the *F*1 or *E* layers was chosen for the analysis of the uracy of the transmission curve for the following reasons:

1) The *F*2 MUF is the controlling MUF for long distances during most of the year.

2) The $F2$ layer is a comparatively thick layer. Hence, the low ray and the high ray are well separated in delay time at frequencies just below the MUF, making for more precise scaling of the MUF from the endpoint records.
3) The $F2$ layer exists throughout the day and night, and its trace is nearly always scalable on both the endpoint and the midpoint records.
4) The diurnal and seasonal variations of the ionization in the underlying E and $F1$ regions of the ionosphere provide an opportunity to examine the effect of multilayer ionization distributions on the accuracy of the transmission curve.

The ordinary magneto-ionic component was used in the analysis. The Appleton-Hartree [5] equation shows that, for radio paths transverse to the earth's magnetic field, the refractive index for the ordinary component is identical with the refractive index in the absence of the magnetic field. The effect of the earth's magnetic field was considered negligible for the quasi-transverse east-west path under consideration.

TESTS FOR NON-RECIPROCITY EFFECTS

Two tests for non-reciprocity effects were made. The simplest test was to compare the MUF recorded at Sterling with that recorded simultaneously at St. Louis. Combined results for a day in January and a day in May are shown in Figure 7. The MUF on each of the endpoint records could be scaled to within

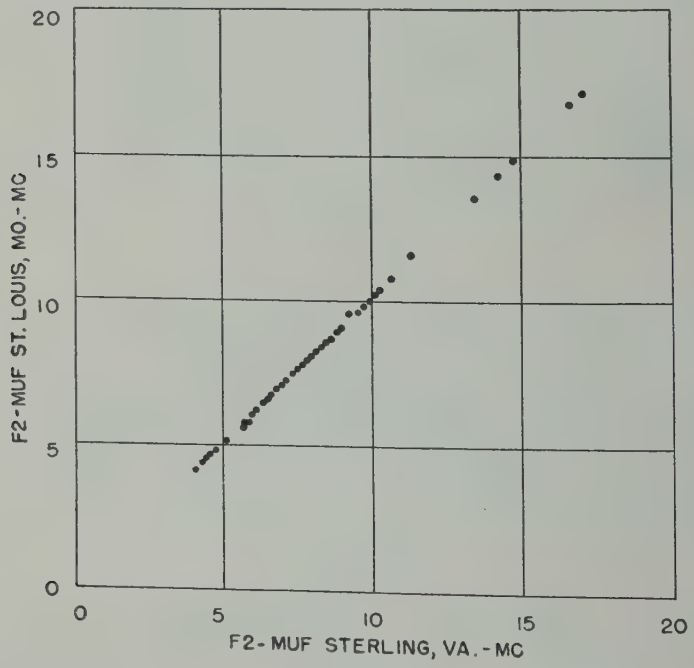

FIG. 7—Comparison of $F2$ MUF (ordinary wave) observed at Sterling and St. Louis on January 16–17 and May 7–8, 1952

out ± 0.1 Mc. This scaling error takes account of slight errors in the calibration the frequency scale on the records, as well as the error in scaling. Since the quency scale was linear, an error of ± 0.1 Mc is equivalent to a per cent error tween ± 0.5 and ± 1 per cent for the daytime data and between ±1 and ±2 r cent for the night-time data. Within the limits of the scaling error, the difference tween the two MUF was very nearly zero in all cases, and there was no net ference to indicate a systematic dependence of the MUF on the direction of opagation. Another check on propagation reciprocity was made by plotting the ference of the relative delay times of the simultaneous oblique transmissions a function of frequency for several pairs of endpoint records in different seasons d at different hours of the day. Figure 8 is an example of this test. At the top of e illustration are reproductions of the paired endpoint records. At the bottom,

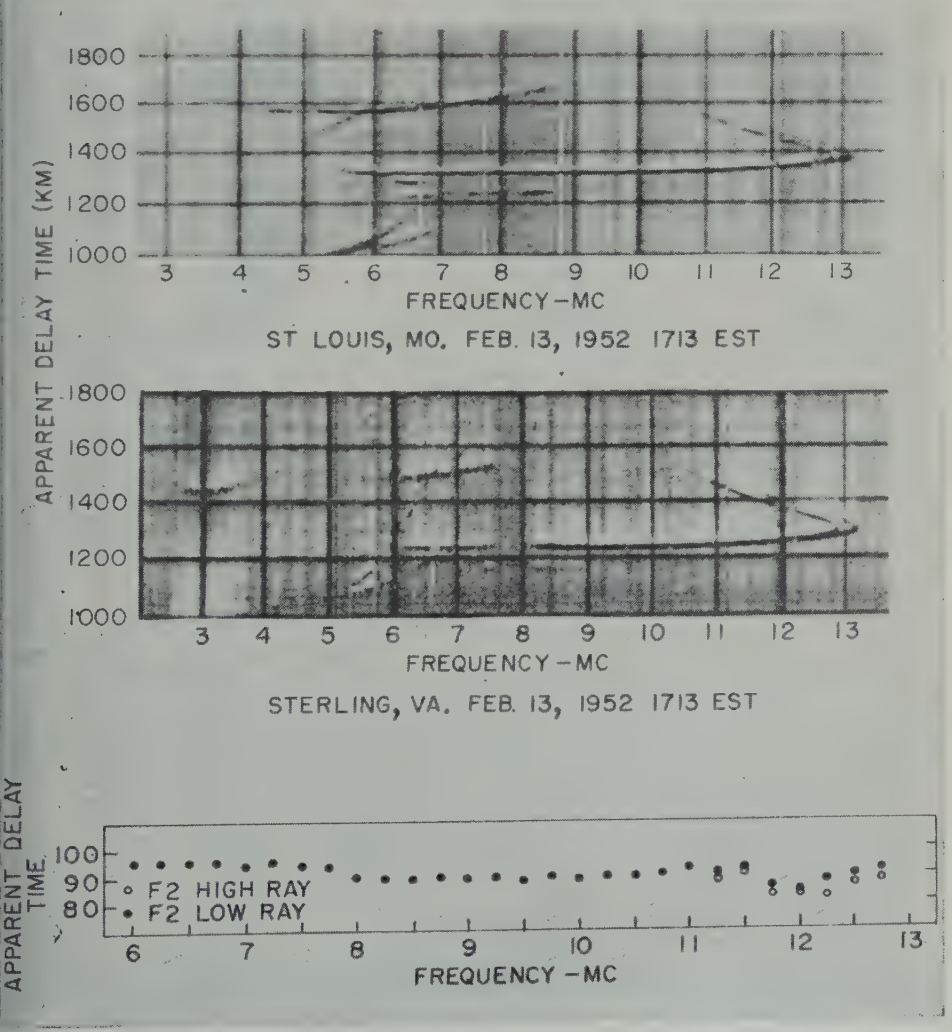

g. 8—Comparison of *F*2 ordinary-wave apparent delay times in units of equivalent path length

the relative delay-time differences, in units of equivalent path length, for bot the low and the high rays, are plotted as a function of frequency. Although th endpoint equipments were pulsed at the same rate, they normally operated wit a small phase difference. The ordinate of the graph is a measure of this phas difference, plus any actual difference in the propagation times. A change in th apparent phase difference with frequency, not attributable to scaling error or difference in the pulse repetition rates, would indicate the existence of a frequenc dependent non-reciprocity effect. No such dependence was found.

MUF COMPARISON

With the reciprocal behavior of the data established for the endpoint station the $F2$ ordinary wave MUF from the records of one of the two endpoint station (usually the Sterling station) was compared with the MUF derived by applyin the transmission curve to the corresponding vertical-incidence record obtaine at the midpoint station. The scaling error for the derived MUF, including smal frequency and virtual-height calibration errors and errors in the transmissio curve overlay, is estimated to be about $\pm$ 1.5 per cent. The error of the per cen difference between the observed oblique incidence MUF and the derived MU is therefore between about $\pm$ 1.6 and $\pm$ 1.8 per cent of the MUF for the daytim data, or between about $\pm$ 1.8 and $\pm$ 2.5 per cent for the night-time data. Figur 9 shows the point to point comparison of the $F2$ ordinary-wave MUF for a day i

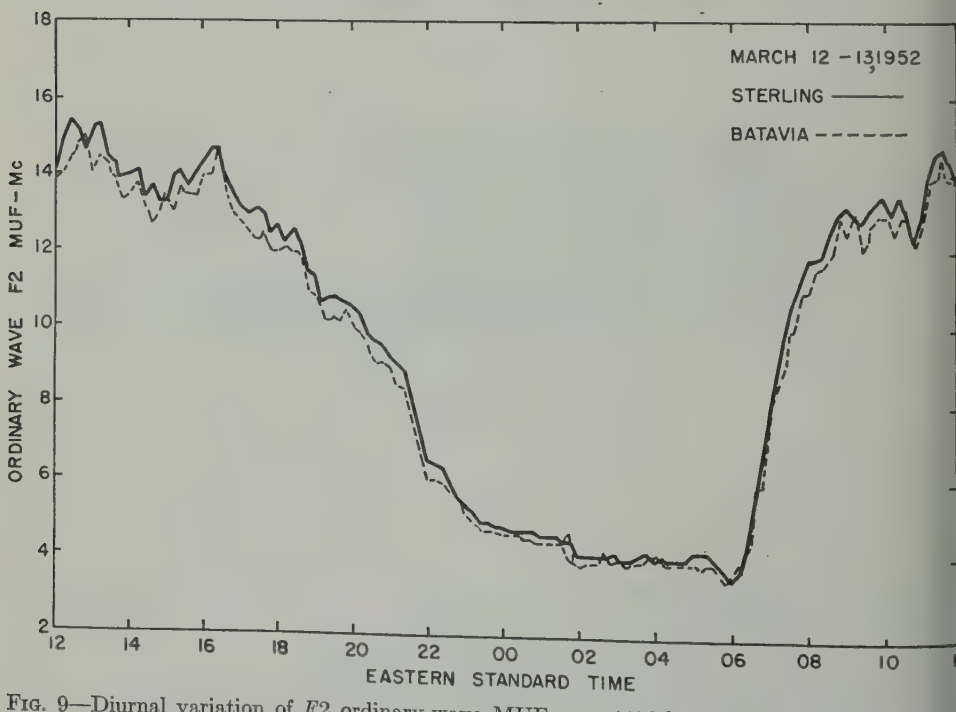

Fig. 9—Diurnal variation of $F2$ ordinary-wave MUF over 1150-km east-west path; solid lin shows MUF scaled from endpoint records; dashed line shows MUF derived from vertical-incidenc records at midpoint of great-circle path

March 1952 plotted against time of day. The solid line shows the MUF scaled at the endpoint station, and the dashed line shows the MUF scaled from the midpoint records by use of the transmission-curve overlay. These curves are typical of what is found throughout the experiment. The two curves follow each other in detail very well. There is, however, a small but consistent difference between the observed MUF and the MUF derived from the vertical-incidence records, the observed MUF being the larger of the two.

The distributions of the per cent differences between the observed MUF and the derived MUF for three different months of 1952 are shown in Figure 10. For this

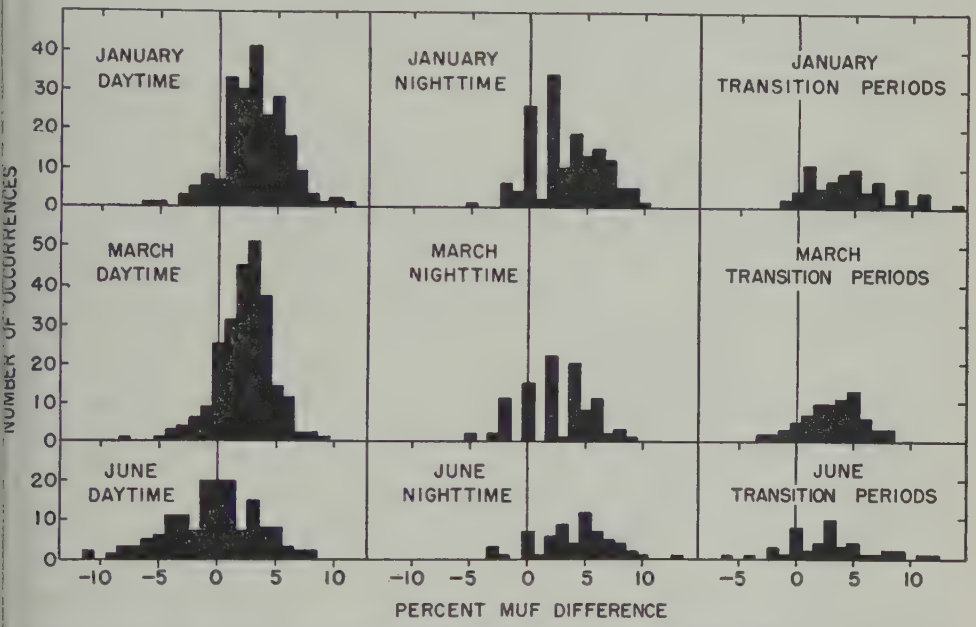

FIG. 10—Distribution of per cent difference between observed ordinary wave *F*2 MUF for St. Louis-Sterling path and MUF scaled from midpoint records, 1952

analysis, the day was divided into four periods—a daytime period when the MUF was highest; a night-time period when the MUF was lowest; and two transition periods, one starting just after sunrise, and the other starting just after sunset, when the MUF was varying rapidly. Data that were doubtful because of noise or interference, or because of excessively spread echoes, were not included in the analysis. Since the large part of these obscuring effects occurred at night or during the transition periods, the data used for these periods are not so numerous as those for daytime. These distributions include four or five days in each month and the distributions are for a winter, an equinoctial, and a summer month. Data for the two transition periods are grouped together.

The daytime data show a tendency for the mean value of the per cent difference to become smaller from winter to summer, and for the dispersion of the data to increase. The mean values of the night-time data, on the other hand, appear to have a trend in the opposite direction, although the dispersion of the data increases

toward summer. The trend of the mean and dispersion for the transition periods is intermediate between those for day and night.

Figure 11 brings out the trends more clearly. The means, the upper and lower decile values, and the 95 per cent confidence limits for the means of the parent populations (from Student's "t" distribution) are plotted for each month from

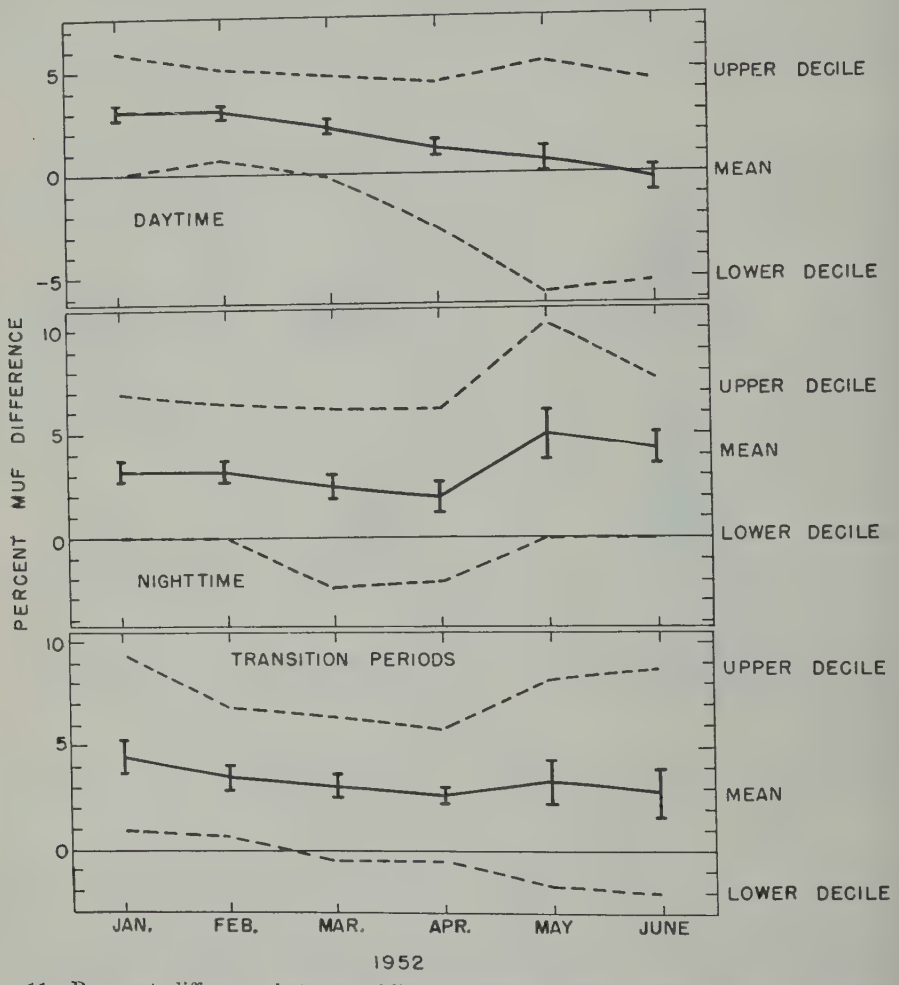

Fig. 11—Per cent difference between oblique-incidence ordinary-wave $F2$ MUF recorded at Sterling, Virginia, and MUF determined from vertical-incidence records taken at Batavia, Ohio, 1952; vertical bars through mean values show 95 per cent confidence limits

January to June, 1952. Taking account of the confidence limits for the mean, the following seasonal trends appear to be significant. The mean per cent MUF difference for daytime changes from about 3 per cent in winter to about zero per cent in summer. At night, the mean follows the trend of the daytime mean through April, but then jumps suddenly to about 5 per cent in May and June. The dispersion tends to increase toward summer in all periods.

DISCUSSION

The problem presented by the above data is to account for the apparently significant systematic difference between the observed and derived MUF and the rather large dispersion of the difference about its mean.

A factor which may contribute to both the mean and the dispersion of the differences is the effect of the earth's magnetic field on the refractive index of the ionosphere and on the ray paths, both for the oblique transmissions and the vertical-incidence soundings. In the presence of the earth's field, the direction of energy flow, except in certain restricted cases, does not coincide with the direction of phase propagation [6]. The wave is reflected from the level where the group direction is horizontal, rather than where the phase direction is horizontal. Furthermore, the energy is deviated laterally out of the plane of the great-circle path. The geographical point over which the group path is horizontal, is, in general, an appreciable distance from the midpoint of the great-circle path.

For the quasi-transverse E-W path under consideration, calculations, using Booker's development of the magnetic-ionic theory [7], show that the effect of the earth's field on the ordinary component of the obliquely propagated wave is small with respect to both the effect of the field on the refractive index of the ionosphere and the lateral deviation of the radio energy out of the great-circle path. (The angle between the great-circle arc joining the endpoint stations and the magnetic meridian at the midpoint is 85° 42′.) At vertical incidence, however, the propagation conditions are quasi-longitudinal. While the solution of the magneto-ionic equation indicates that the electron density at which the refractive index for the ordinary wave becomes zero is independent of the earth's field, there is a considerable deviation of the ordinary wave toward the north magnetic pole. The distance the ray is deviated depends upon the strength of the earth's field and upon the ionization distribution. Hence, the information given by the ordinary-wave trace on the vertical-incidence ionogram describes the conditions of the ionosphere at a distance that may be appreciably to the north of the station [8]. These factors, coupled with somewhat uncorrelated minute-to-minute variations of the ionization densities in the separate regions traversed by the obliquely and vertically incident waves (for example, see the variability of the diurnal curves shown in Figure 9), probably account for much of the dispersion shown in Figures 10 and 11.

Several possible explanations of the systematic difference may be mentioned, none of which have been examined carefully enough at the time of this writing for quantitative evaluation.

The first is an error in the "k" factor, which is introduced to correct the sec ϕ relationship for the effect of ionosphere curvature. This correction depends upon the horizontal distance traversed by the wave in the region where the refractive index is appreciably less than unity, which in turn depends upon the height and thickness of the region. In summer daytime, the effective thickness of the region is greater than in winter or at night. A higher value of k should then be required for summer daytime. The derived MUF using a constant k should then be less with respect to the observed MUF in summer daytime than in winter daytime, contrary to the experimentally determined difference. In this connection, it is curious that the sudden increase in the night-time MUF difference between April and May occurs

at the same time as a sudden increase in the occurrence of sporadic E [9]. But it seems unlikely that the sporadic-E reflections represent enough ionization to cause the observed increase in MUF difference. A tentative conclusion, then, is that some other effect is more important than the "k" error.

Another condition of the ionosphere which could cause a systematic difference between the observed and derived MUF is the systematic north-south gradient of the maximum electron density, with density decreasing toward the north, which occurred across the transmission path and caused the northward deviated vertical-incidence ordinary wave to encounter systematically lower densities than the obliquely incident wave. Since the gradient was steeper in winter daytime than in summer daytime, such an effect would account for the decrease of the MUF difference from winter to summer. However, the gradient was also small at night in summer. The high MUF difference for summer night-time is therefore not accounted for on this basis.

A third condition which could cause a systematic MUF difference is a systematic "tilt" of the ionosphere, especially in the presence of a gradient of maximum electron density transverse to the axis of the tilt. Such a condition would cause the oblique wave to pass through a greater or less dense portion of the layer than the vertical-incidence wave (depending upon the sign of the gradient), since the tilt would cause a greater deviation of the oblique wave.

CONCLUSIONS

The results of this experiment over an E-W path of 1150 km indicate that, to within an average error of about 3 per cent, the method used in determining the oblique-incidence $F2$ MUF from vertical-incidence data is satisfactory, at least for east-west paths up to about 1200 km in length. The derived MUF, however, underestimates the true value of the MUF by about 3 per cent on the average during most of the year. It would appear that the simplest way of improving the transmission-curve technique would be to make the factor k multiplying the right side of equation (2) depend on time of day and on season. Such dependence might, of course, be different for different geographical locations and for different stages of the sunspot cycle. The values of k could take account not only of the effect of ionospheric curvature but of ray deviations and other magneto-ionic effects, and possibly of sporadic-E effects if need be. Empirical values could be used for time of day, season, direction of propagation, distance, and geomagnetic location. One purpose of possible future experiments would be to obtain enough information for an analytical determination of k for any set of conditions.

ACKNOWLEDGMENT

The author is indebted to Messrs. T. N. Gautier, R. Silberstein, and V. L. Agy for helpful discussions and advice, and to J. W. Wright, A. R. Mitz, and J. H. Puerner for assistance with data scaling.

References

[1] (*a*) P. G. Sulzer and E. E. Ferguson, Sweep-frequency oblique-incidence ionospheric measurements over an 1,150 km path, Proc. Inst. Radio Eng., 40, 1124 (1952).

(*b*) P. G. Sulzer, Sweep-frequency pulse-transmission measurements over a 2400-km path, J. Geophys. Res., **60**, 411 (1955).

[2] (*a*) W. J. G. Beynon, Measurements with oblique incidence in the ionosphere, Wireless Eng., **25**, 322 (1948). [This paper gives references to earlier investigations.]

(*b*) J. W. Cox and K. Davies, Oblique incidence pulse transmission over a 2360 km path via the ionosphere, Wireless Eng., **32**, 35 (1955).

(*c*) Report on sweep frequency pulse tests at oblique incidence, Japan, VIIth Plenary Assembly, C.C.I.R., London, 1953.

[3] N. Smith, The relation of radio sky-wave transmission to ionospheric measurements, Proc. Inst. Radio Eng., **27**, 332 (1939).

[4] J. H. Carroll, Automatic ionosphere recorder, Electronics, **25**, No. 5, 128 (1952).

[5] E. V. Appleton, Wireless studies of the ionosphere, J. Inst. Elec. Eng., London, **71**, 642 (1932).

[6] H. G. Booker, An outline of magneto-ionic theory, Part 1, Studies on propagation in the ionosphere, Cornell University, School of Electrical Engineering, Tech. Rep. No. 1 (March, 1950).

[7] H. G. Booker, Application of the magneto-ionic theory to radio waves incident obliquely upon a horizontally-stratified ionosphere, J. Geophys. Res., **54**, 243 (1949).

[8] J. C. W. Scott, The Poynting vector in the ionosphere, Proc. Inst. Radio Eng., **38**, 1057 (1950).

[9] E. K. Smith, The effect of sporadic *E* on television reception, Trans. Inst. Radio Eng. Prof. Group, **AP-2**, 54 (March, 1952).

SWEEP-FREQUENCY PULSE-TRANSMISSION MEASUREMENTS OVER A 2400-KM PATH

By Peter G. Sulzer

National Bureau of Standards, Washington 25, D. C.

(Received July 1, 1955)

ABSTRACT

The paper shows some sweep-frequency pulse-transmission records obtained over a 2400-km path during the winter of 1953-1954. Although a detailed analysis of the records has not been completed, some preliminary results are given. Among the most significant of these is observed oblique-incidence propagation on numerous occasions at frequencies considerably above the maximum usable frequency as computed from vertical-incidence ionospheric observations at the midpoint of the path.

Since September 1953, the National Bureau of Standards has been conducting a radio propagation experiment between Sterling, Virginia, and Boulder, Colorado, a distance of approximately 2400 km. This experiment is the continuation of an earlier experiment over a 1150-km path, reported elsewhere in this issue [see 1 and 2 of "References" at end of paper]. Pulse transmitters and receivers at both sites are simultaneously swept through the frequency range from 2 to 25 megacycles, and photographic records of relative delay time *vs* frequency are obtained at both ends of the path. At approximately the same time, although not strictly simultaneously, conventional vertical-incidence sweep-frequency ionosphere records are produced at the midpoint of the path, which is located near Carthage, Illinois.

The principal purpose of the experiment is to check the transmission-curve method of obtaining maximum usable frequencies from vertical-incidence ionospheric data. Extensive experience has indicated that in many cases it is possible to maintain communication over long paths at frequencies considerably higher than the maximum usuable frequency calculated by the transmission curve method from vertical-incidence records made near the midpoint of the path. The cause of this anomalous propagation has not been understood. In the earlier experiment, conducted over a 1150-km path, no unusual propagation phenomena were noticed. Satisfactory agreement was obtained with the maximum usable frequency computed from vertical-incidence data. However, in the present experiment, large numbers of records have been obtained which exhibit propagation above the computed maximum usable frequency and supply some indication of its nature. The abundance of excellent records obtained has permitted the study of various other phenomena as well. It is the purpose of this paper to display some typical records obtained during the winter of 1953-1954. Detailed analysis of all the records is being carried out by a National Bureau of Standards group at Boulder, Colorado.

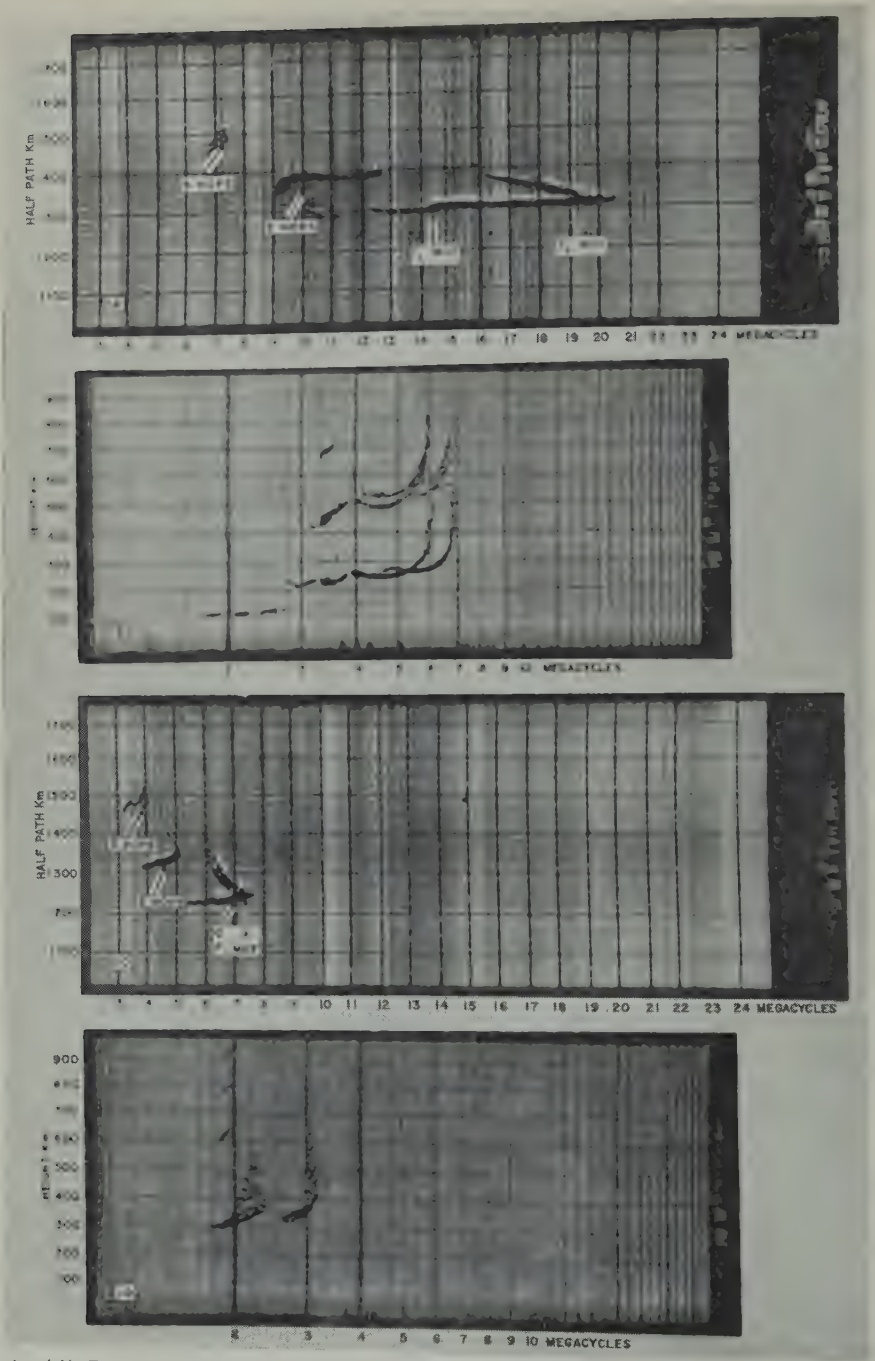

Fig. 1—(*A*) Boulder, Colorado, winter 2:00 PM oblique-incidence record; (*B*) corresponding midpoint record; (*C*) Boulder winter 1:12 AM oblique-incidence record; (*D*) corresponding midpoint record

The records are produced with modified type C-3 ionosphere recorders, which for this experiment employ moderately large horizontal rhombic antennas for transmitting and receiving. Frequency tracking is obtained by using synchronous motors to drive the frequency-change mechanisms. A relatively constant time-reference over a 24-hour period is produced by the use of highly stable oscillators to control the transmitter pulse rates and recording oscilloscopes. The frequency range is covered in one sweep, requiring approximately 12 minutes.

Figure 1(*A*) is a Boulder (oblique-incidence) record obtained at 2:00 PM CST, February 10, 1954. In this and in most of the following Figures, the pulse traces have been darkened to bring them out more vividly. Figure 1(*A*) is a typical midday record obtained during an undisturbed period. *F*1-layer and *F*2-layer MUF are noted, as are the presence of two-hop and three-hop transmission. The MUF marked on the record is not the highest frequency at which transmission is recorded. It is rather the estimated "classical" MUF or frequency at which the junction of the high-angle and low-angle rays of the ordinary wave is estimated

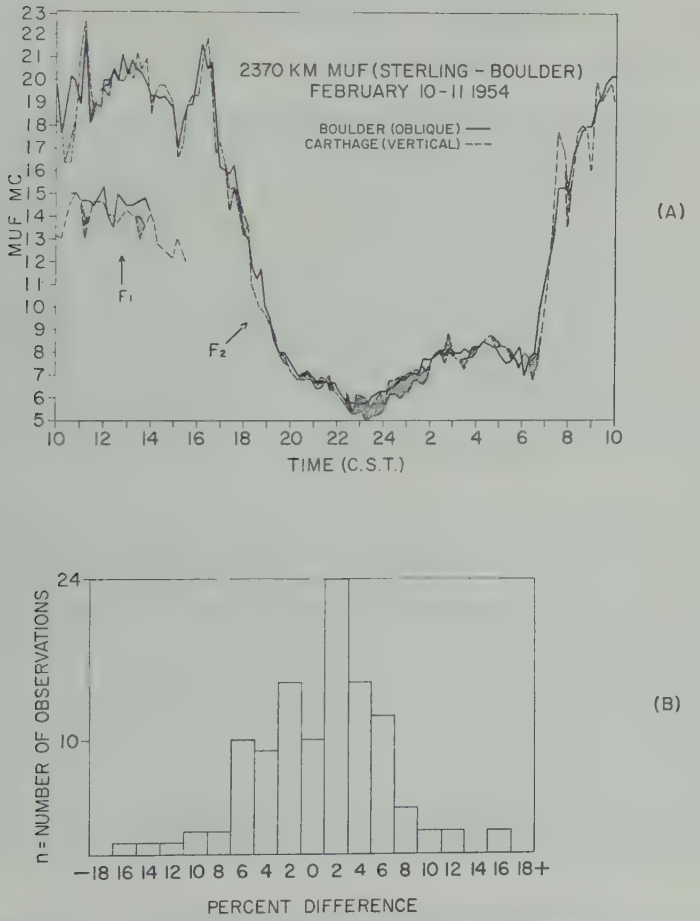

Fig. 2—(*A*) Diurnal comparison plot of Boulder-Sterling maximum usable frequencies; (*B*) histogram for the data on Figure 2*A*

to occur. In this record, a form of scatter transmission extends the $F2$ trace to a practical maximum usable frequency approximately one megacycle above the "classifical" MUF. This phenomenon is discussed further below.

Figure 1(*B*) is the midpoint record made at a time corresponding to the $F2$-layer maximum usable frequency of Figure 1(*A*). Figure 1(*C*) is a Boulder record obtained

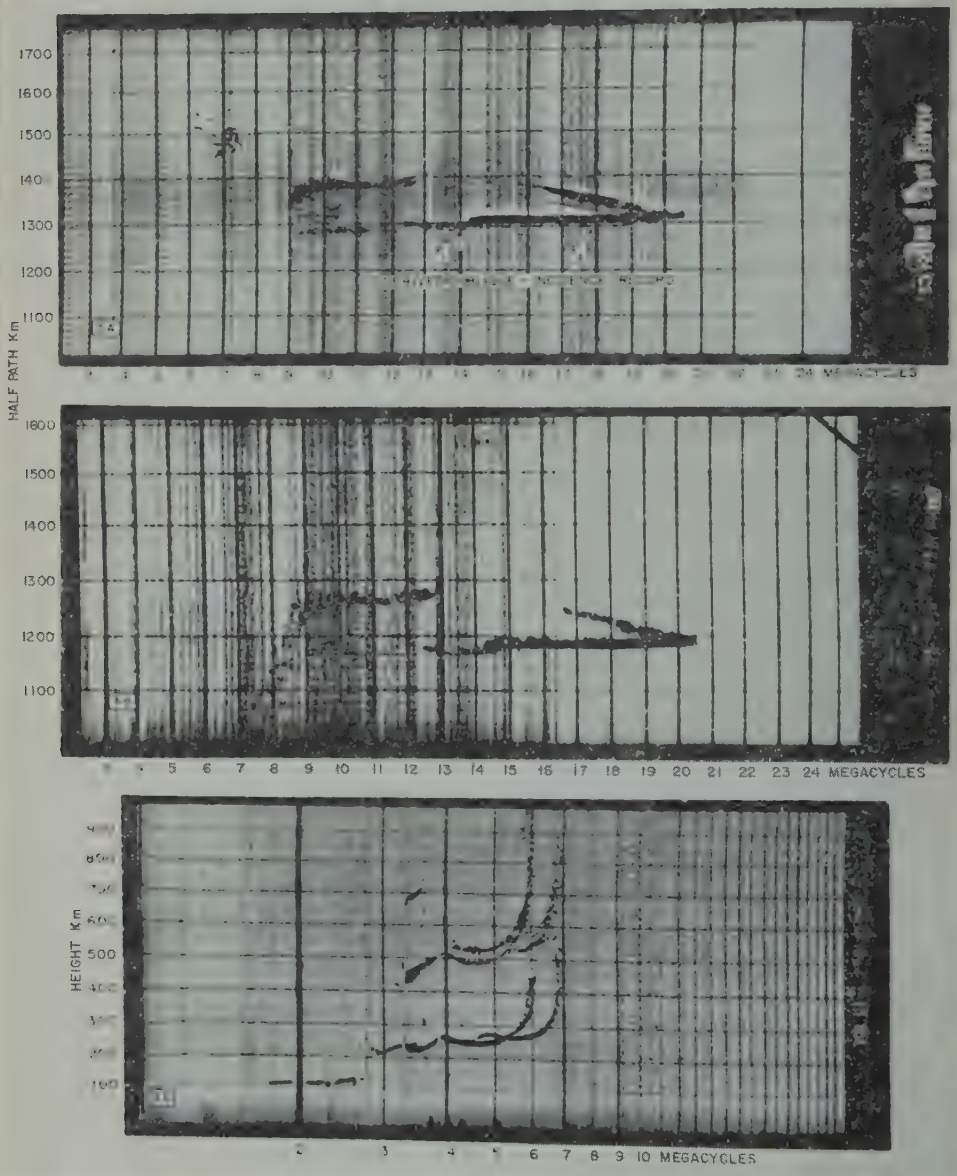

FIG. 3—(*A*) Boulder oblique-incidence record showing theoretical curve derived from midpoint data; (*B*) corresponding oblique-incidence record obtained at Sterling, Virginia; (*C*) midpoint record corresponding to Figures 3.1 and 3*B*

at 1:12 AM of the following day. Here the ordinary and extraordinary components of the high ray are resolved. Figure 1(*D*) is the corresponding midpoint record, which incidentally indicates the presence of spread echoes.

Figure 2(*A*) is a 24-hour plot of estimated "classical" maximum usable frequencies (solid line), scaled directly from the (Boulder) endpoint records, and of the usual theoretical maximum usable frequencies (dashed line), scaled from the midpoint vertical-incidence records by means of a transmission curve. The Figure contains the results of approximately 120 observations made at 12-minute intervals during February 10-11, 1954, which was an undisturbed period. The shaded areas indicate the presence of spread echoes on the midpoint records. It will be noted that there is normally an excellent agreement between the observed and derived maximum usable frequencies, although occasional large differences are obtained. These differences can be explained partly in terms of timing errors, where, because of rapid rates of change, the records may not portray corresponding conditions at the endpoint and midpoint stations. It should also be mentioned that the records are often difficult to interpret, or a particular value may be obscured by noise or interference.

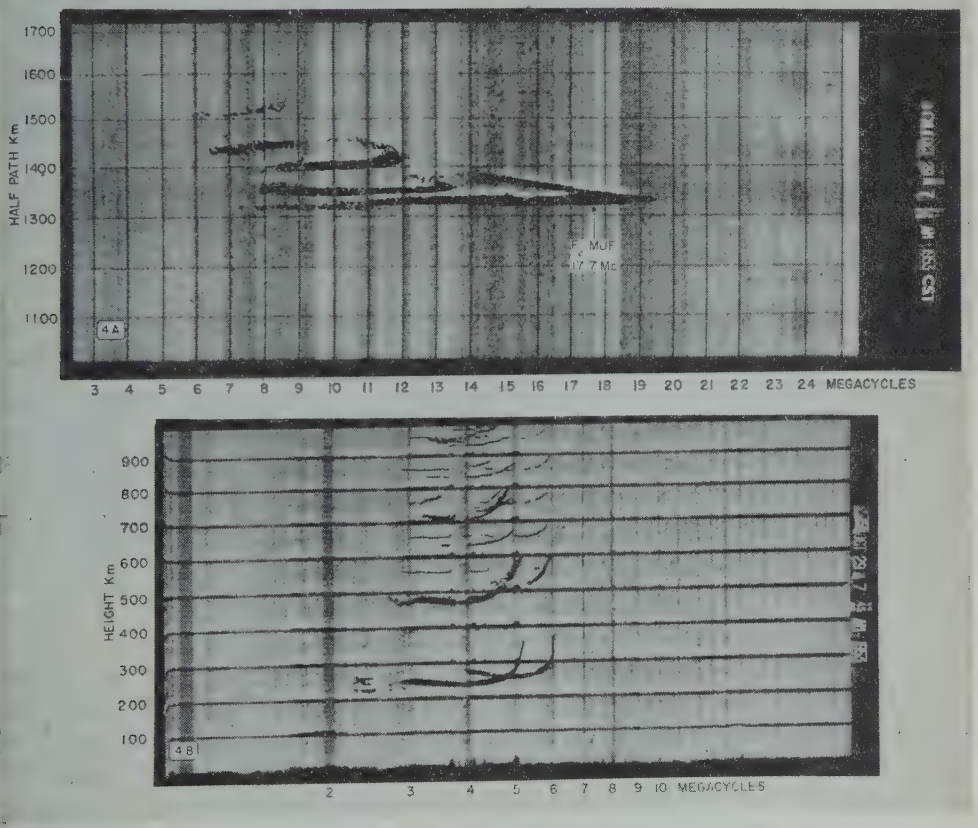

Fig. 4—(*A*) Boulder oblique-incidence record showing extension of normal curve; (*B*) corresponding midpoint record

Figure 2(*B*) is a histogram for the same 24-hour period, showing the distribution of percent differences between the oblique-incidence and vertical-incidence values of MUF plotted in 2(*A*). The difference is positive if the oblique-incidence MUF exceeded the MUF derived from the corresponding vertical-incidence record. The mean difference is + 0.5 percent, while the standard deviation is 5.25 percent, indicating a small systematic difference but a rather large spread in individual differences.

Figures 3(*A*) and 3(*B*) contain, respectively, the Boulder and Sterling records for February 10, 1954. The corresponding midpoint record is shown in Figure 3(*C*). A comparison of these two endpoint records indicates that their shapes are essen-

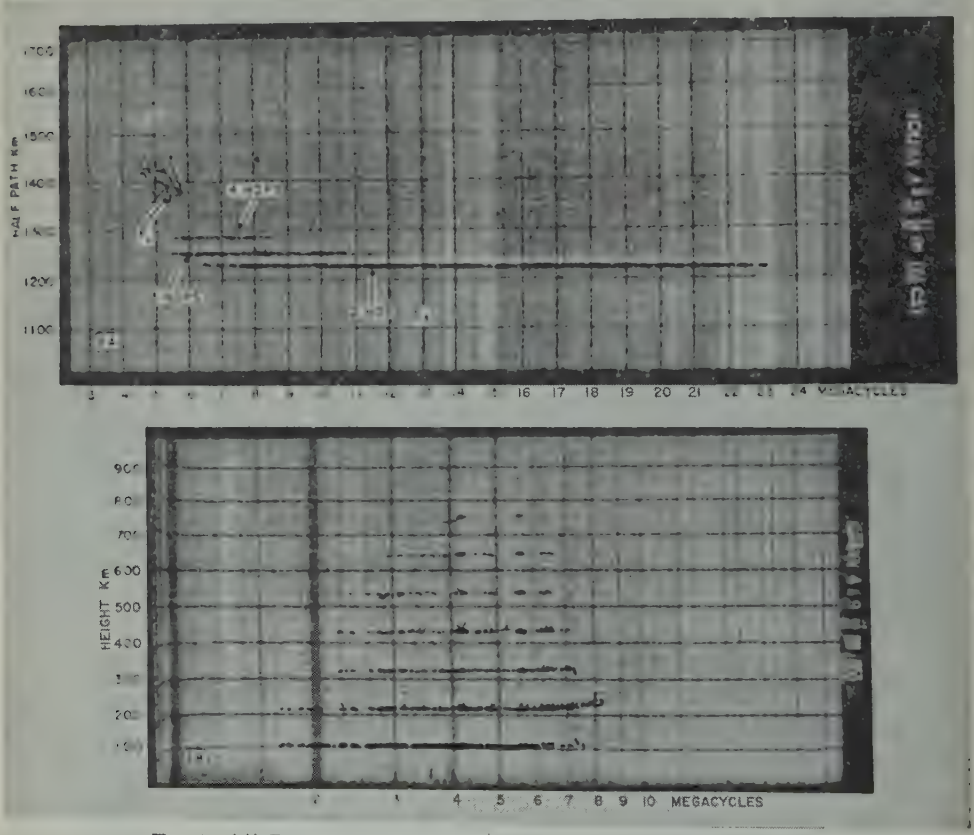

FIG 5—(*A*) Boulder record showing sporadic-*E* layer transmission; (*B*) corresponding midpoint record

tially identical. Small differences in the appearance of these and other simultaneous records can be explained in terms of differences in receiver gain and overload characteristics, and differences in transmitter power and antenna characteristics.

If reciprocity is assumed, a delay time reference can be established by averaging the delays (recorded as half-path lengths) indicated by the two records. Considering a frequency of 18.5 Mc, the apparent half-path length of the lower ray

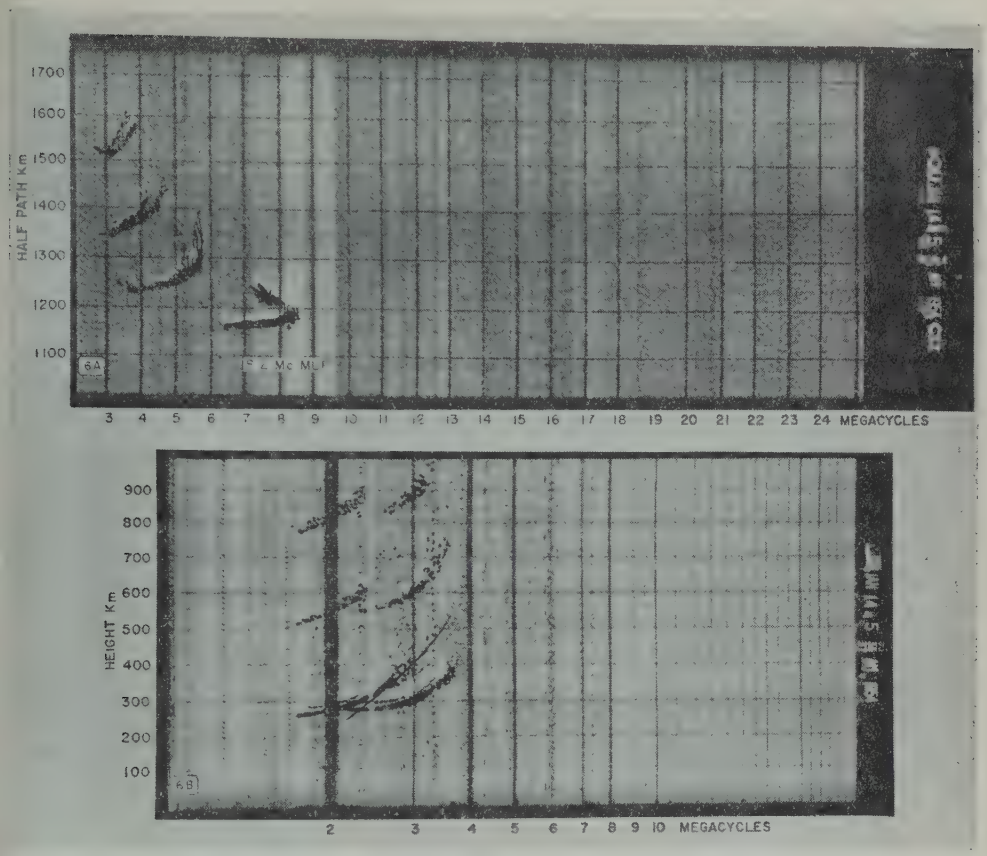

FIG. 6—(*A*) Early morning Boulder record showing four modes of *F*-layer transmission; (*B*) corresponding midpoint record

recorded at the Boulder station is 1300 km, and 1180 km at the Sterling station. This difference indicates merely that the transmitters at the two ends of the path were not pulsing at the same instant. The average of these two values, 1240 km, is then taken to be the half-path length of the lower *F*2 ray at this frequency, thus establishing a time reference for use with either record.

Application of the transmission curve to the midpoint records gives information on reflecting height *vs* frequency. The half-path length corresponding to a given reflecting height can be obtained from simple geometric considerations, permitting the synthesis of an oblique-incidence record from a midpoint record. The curve so produced is drawn in Figure 3(*A*) as a dashed line. Its shape is similar to that of the recorded trace (except for the extended nose on the latter), although small timing and frequency errors are evident.

A better example of a nose extension, sometimes referred to as a "tail," is shown in Figure 4(*A*), with the corresponding midpoint record in Figure 4(*B*). The maximum usable frequency derived from the midpoint record is marked on Figure 4(*A*). The interpretation of this phenomenon is difficult, although it has been suggested by D. K. Bailey [3] that forward *E*-region scattering, which could

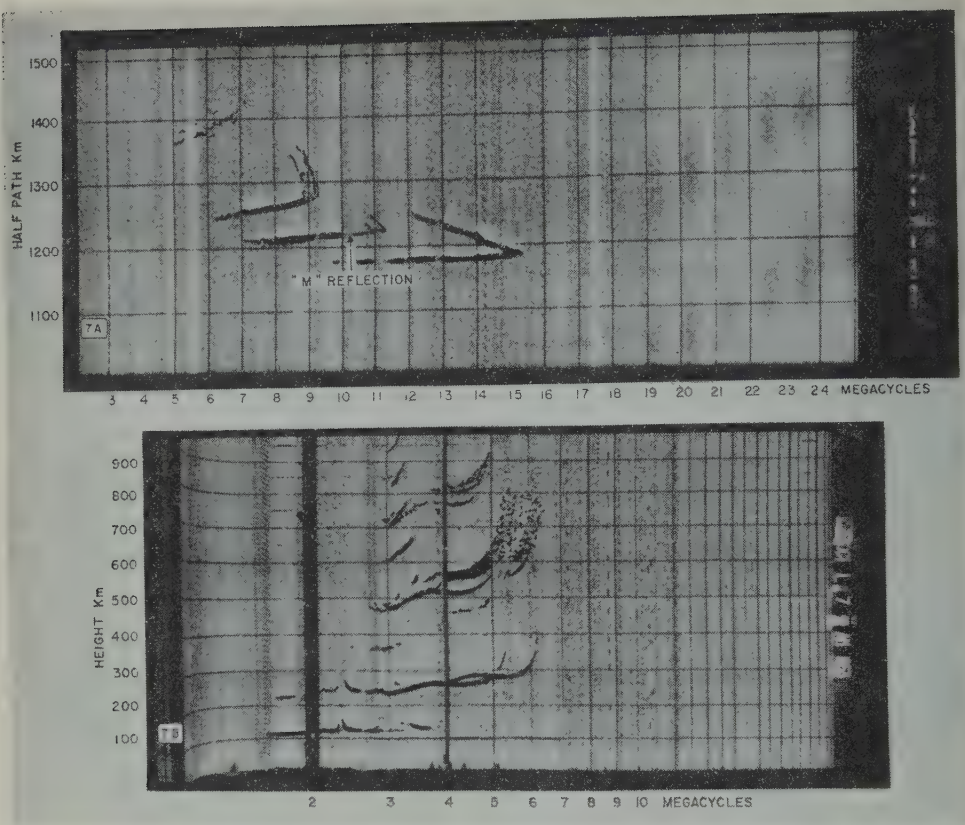

FIG. 7—(*A*) Early morning Boulder record with a strong "*M*" reflection; (*B*) corresponding midpoint record

produce a distribution of sources with a wide range of apparent take-off angles, might be responsible. The presence of *E*-layer reflections will be noted on Figure 4(*B*). A consequence of this mode of transmission, whatever may be the source, is, as far as this record is concerned, transmission two megacycles above the normal predictable maximum usable frequency. Such transmission is probably of great practical importance. Examination of the pulses comprising such an extended nose indicates that they are incoherent in nature, apparently consisting of a scattered return over a moderate range of time delays. Their appearance is quite different from that of the separate, distinct low-ray and high-ray pulses normally observed below the maximum usable frequency. It is significant that prominent extensions of the nose were not observed over the shorter 1150-km path, nor are they observed on the two-hop *F*2 traces over the present path.

Figure 5(*A*) and its corresponding vertical-incidence record, Figure 5(*B*), show winter-time evening sporadic-*E* layer transmission between Sterling and Boulder. The 4-hop, 3-hop, and 2-hop modes are observed, respectively, from left to right. Single-hop *E*-layer transmission has rarely been observed over this distance because of the limitation imposed by earth curvature. A trace of *F*-layer

transmission appears at the left end of the record. It is interesting to note that, although F-layer reflections were only partially blanketed by E at oblique incidence, they were completely blanketed at vertical incidence.

Figure 6(A) shows four modes of early morning F-layer transmission. A spread echo is observed on the ordinary component of Figure 6(B), the vertical-incidence

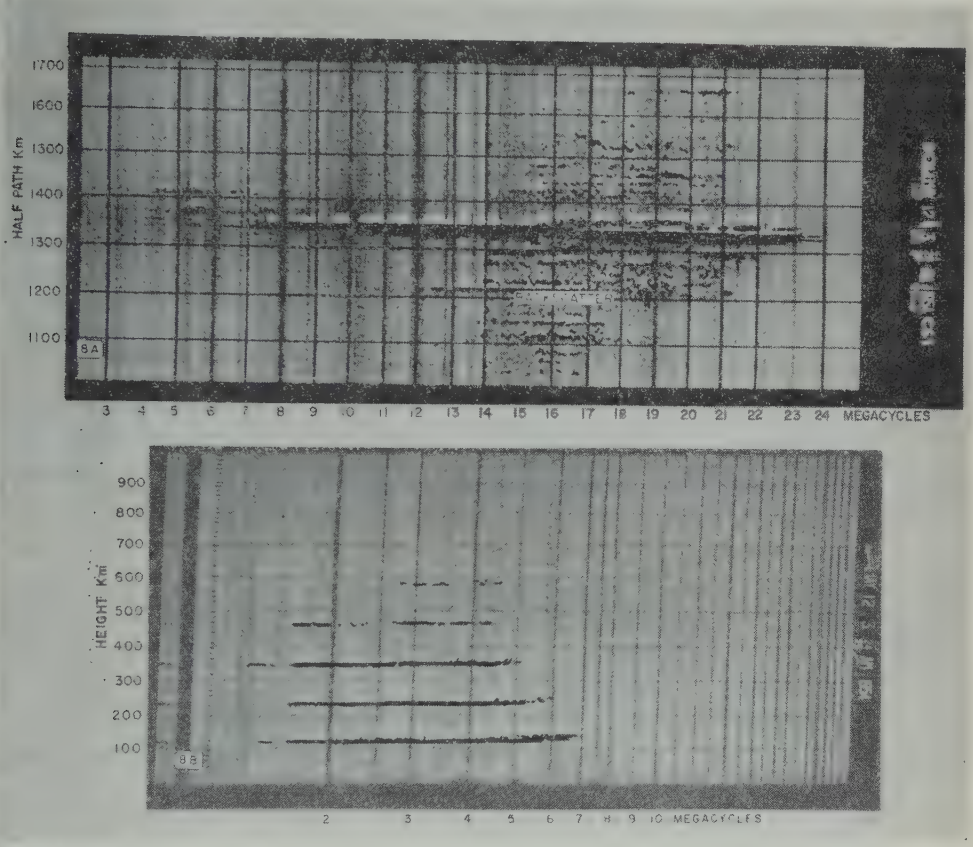

FIG. 8—(A) Boulder record showing sporadic-E layer transmission and backscatter from the Boulder transmitter; (B) corresponding midpoint record

record. A slight spread will be noted here at oblique incidence, although its magnitude does not compare with that at vertical incidence. A transmission curve corresponding to the observed maximum usable frequency is drawn in Figure 6(B). This transmission curve passes through the ordinary-ray spread, rather than through its upper or lower boundary.

In the oblique-incidence record of Figure 6(A), the absence of any appreciable nose extension of the type discussed earlier seems to be more characteristic of records which have maximum usable frequencies at the lower end of the frequency sweep than of records showing high MUF. Another feature of Figure 6(A) is that as frequency is increased 4-hop transmission is observed first, then 3-hop, then 2-hop, and lastly 1-hop. The higher mode orders have lower minimum observable

frequencies, principally because of the increase in elevation angle of the antenna-system major lobe at the low frequencies.

Figure 7(*A*) is a morning record showing 1-hop, 2-hop, and 3-hop *F*-layer propagation. It is shown here because of the presence of a strong *M*(2*F*-*E*) reflection, indicating reflection from the top of the *E*-layer. However, direct *E*-layer transmission is absent, although the presence of a strong *E* reflection is observed on the midpoint record, Figure 7(*B*). Since *E*-layer transmission would normally occur *via* two or more hops over this long a path, it can be concluded that an *E*-layer had not developed at a point one-quarter the distance from Boulder to Sterling.

Figure 8(*A*) is an oblique-incidence record obtained at Boulder from the Boulder transmitter during a period of widespread sporadic-*E* transmission. It will be noted that, in addition to 2-hop, 3-hop, and 4-hop transmission from Sterling, there is also a large amount of backscatter. The striated appearance of the backscatter echoes is believed to be due to a 10-kc modulation of the receiver gain. Figure 8(*B*) is the corresponding midpoint record. Studies of backscatter recorded on narrow-band receivers, using the oblique-incidence transmitter of the experiment, are being conducted in Boulder, and some of the early work has been reported elsewhere [4, 5].

The experiment obviously required careful team-work in its execution. Credit for expert operation of the equipment is due to H. E. Petrie, Lowell H. Tveten, J. W. Caldwell, J. H. Puerner, A. R. Mitz, and David Sands. Thanks for assistance in scaling the records are due particularly to D. R. Paquette.

References

[1] P. G. Sulzer and E. E. Ferguson, Sweep-frequency oblique-incidence ionosphere measurements over a 1150-km path, Proc. Inst. Radio Eng., **40**, 1124 (1952).

[2] B. Wieder, Some results of a sweep frequency propagation experiment over an 1150-km east-west path, J. Geophys. Res., **60**, 395–409 (1955).

[3] Presented at the Commission III sessions at the XIth General Assembly of the International Scientific Radio Union, The Hague, August-September 1954.

[4] R. Silberstein, A note on sweep-frequency backscatter observations, J. Geophys. Res., **59**, 138 (1954).

[5] R. Silberstein, Sweep-frequency backscatter—some observations and deductions, Trans. Inst. Radio Eng., AP-2, No. 2, 56 (1954).

ON THE COOLING OF THE UPPER ATMOSPHERE AFTER SUNSET

By Arnold N. Lowan

Yeshiva University, New York 33, N. Y., and
Naval Research Laboratory, Washington 25, D. C.

(Received June 23, 1955)

ABSTRACT

The cooling of the "upper atmosphere" (region between the altitude $h_0 = 100$ km and the altitude $h_1 = 380$ km) after sunset was investigated under the assumptions that (*a*) the temperature at the altitude h_0 is constant and equals 240°K, (*b*) the temperature gradient at the altitude h_1 is equal to zero, and (*c*) the process of heat transfer takes place solely by conduction. Assumed initial temperature is that given by the Rocket Panel, ranging from 240°K at altitude h_0 to 1250°K at altitude h_1 . For the sake of simplicity, thermal conductivity K and specific heat c were assumed constant and dependence of density ρ on temperature was ignored, the differential equation of heat conduction being solved numerically on the assumption that the density ρ and, therefore, the thermal diffusivity $\alpha = K/c\rho$ varies with altitude but is independent of time, the variation of ρ with altitude being that given by the Rocket Panel. The computations revealed that after 2-1/2 hours the temperature has not changed at altitudes below 160 km, and that the maximum drop at altitude h_1 is 440°K. From the computed temperatures at time $t = 2^h$ (2 hours), the densities were computed from formula (2) below. Computations revealed that a certain settling of the atmosphere takes place, the densities at time $t = 2^h$ being larger than at time $t = 0$ in some region, and correspondingly lower at altitudes above the upper limit of this region. Analysis of the ion density led to the conclusion that there is an appreciable increase of the ion density in the F-layer in spite of the recombination of ions which takes place after sunset.

SECTION I

The cooling of the upper atmosphere is of importance because it affects the ion density in the F-layer. The subsequent investigation will show that the anticipated decrease in ion density after sunset due to the process of recombination of ions is in part offset at certain altitudes by the settling of the atmosphere, that is, the increase in atmospheric density at certain altitudes and the decrease at higher altitudes, the last-mentioned effect being due to the cooling of the upper atmosphere. The region of interest is approximately the region between 100 and 380 km. In the subsequent discussion, the last-mentioned altitudes will be denoted by h_0 and h_1, respectively.

The problem of cooling of the upper atmosphere may be formulated as follows. If the temperature is known at time $t = 0$ (the instant of sunset) in the region between h_0 and h_1 , what will the temperature be at any later time? The initial temperature is that given by the "Rocket Panel"* and is shown in the second column of Table 1 of temperatures, densities, and pressures on page 426 of this article. The problem will be solved under the following assumptions:

(*a*) The temperature gradient at the altitude h_1 is $= 0$ at all times (in the interval between sunset and sunrise)
(*b*) The temperature at the altitude h_0 is $= 240°\text{K} =$ constant
(*c*) The process of heat transfer takes place by conduction only

The limits of the region of the atmosphere under investigation were chosen merely as a matter of convenience. As far as the upper limit (380 km) is concerned, there is evidence that the temperature is essentially constant and equals 1250°K in the region between 360 and 500 km. This justifies the assumption under (*a*) that the temperature gradient vanishes at the altitude h_1 . As to the assumption under (*b*), its validity was first conjectured and then proved *a posteriori*, at least for values of t up to 2-1/2 hours.

Since the initial temperature increases monotonically with altitude, and since at any subsequent time the temperature continues to increase monotonically with altitude (as will be seen below), it is reasonable to assume that the major contribution to the heat transfer is due to conduction. For the sake of simplicity, it was assumed that heat transfer takes place solely by conduction. Accordingly, it is governed by the differential equation

$$\frac{\partial T}{\partial t} = \alpha \frac{\partial^2 T}{\partial x^2}\,; \qquad \alpha = \frac{K}{c\rho} \qquad (1)$$

where $K =$ thermal conductivity and where, for the sake of convenience, x denotes the difference $h_1 - h$, where h is a variable altitude.

The thermal conductivity K is proportional with the square root of the absolute temperature. However, the variation of α with temperature due to the factor K is negligible compared to its variation with altitude due to the variation of ρ with altitude. For this reason and for the sake of expediency, it was assumed that K has the constant value 5.68×10^{-5} in cgs units; the value of the specific heat used in the computation is 0.2404 cal/gm. As to the density ρ, it varies both with altitude and temperature in accordance with the formula†

$$\rho = \frac{\rho_0 T_0}{T} \exp\left[-10^5 \frac{M}{R} \int_0^h \frac{g\,dh}{T}\right] \qquad (2)$$

where 10^5 is the conversion factor between kilometers and centimeters and $\rho_0 =$ density at the temperature $T_0 = 273°\text{K}$, $M = 28.966 =$ mean molecular mass of

*"Pressures, densities, and temperatures in the upper atmosphere," Phys. Rev., 85, 1027-1032 (1952).

†See, for instance, "High altitude rocket research," p. 111, by H. E. Newell, Jr., Academic Press, Inc., New York (1953).

ir, $R = 8.314 \times 10^7$ ergs/°K mole = gas constant, and $g = g(h)$ is the acceleration f gravity at the altitude h. Clearly

$$g = g(h) = g_0\left(\frac{a}{a+h}\right)^2 \quad \ldots\ldots(3)$$

where $g_0 = g(0) = 980$ cm/sec^2 and $a = 6370$ km = radius of the earth. Using he numerical values of M and R just given, (2) becomes

$$\rho = \frac{\rho_0 T_0}{T} \exp\left[-0.03484 \int_0^h \frac{g\,dh}{T}\right] \quad \ldots\ldots(4)$$

t should be emphasized that in (2) and in (4) the upper limit of integration h is xpressed in kilometers. It may be readily shown that if ρ_H and T_H denote the lensity and the temperature at the altitude H then the density at the altitude $> H$ is given by

$$\rho = \frac{\rho_H T_H}{T} \exp\left[-0.03484 \int_H^h \frac{g\,dh}{T}\right] \quad \ldots\ldots(5)$$

The desired solution of the differential equation (1) must satisfy the initial condition

$$T = f(x) \quad \text{for} \quad t = 0 \quad \ldots\ldots(6)$$

where $f(x)$ is given (in tabular form) by the Rocket Panel, and the boundary conditions

$$\frac{\partial T}{\partial x} = 0 \quad \text{for} \quad x = 0 \qquad (h = h_1) \quad \ldots\ldots(7)$$

$$T = 240°\text{K} \quad \text{for} \quad x = 280 \text{ km} \qquad (h = h_0) \quad \ldots\ldots(8)$$

In accordance with the customary procedure, the differential equation (1) and the boundary conditions (7) and (8) were replaced by

$$\frac{T_{m,n+1} - T_{m,n}}{\Delta t} = \alpha_{m,n} \cdot \frac{T_{m-1,n} - 2T_{m,n} + T_{m+1,n}}{(\Delta x)^2} \quad \ldots\ldots(9)$$

$$T_{0,n} = T_{1,n} \quad \ldots\ldots(10)$$

$$T_{M,n} = 240°K \quad \ldots\ldots(11)$$

where $T_{m,n}$ denotes the value of $T(x, t)$ for $x = m\Delta x$ and $t = n\Delta t$, $m\Delta x = 280$ km, $\alpha_{m,n} = K/c\rho_{m,n}$, and

$$\rho_{m,n} = \frac{\rho_0 T_0}{T_{m,n}} \exp\left[-0.03484 \int_0^{h_m} \frac{g\,dh}{T}\right] \quad \ldots\ldots(12)$$

In (12), h_m denotes $h_1 - m\Delta x$, and the variable T in the integrand is the temperature at the time $t = n\Delta t$ considered as a function of altitude. From (9) we get

$$T_{m,n+1} = (1 - 2\lambda_{m,n})T_{m,n} + \lambda_{m,n}(T_{m-1,n} + T_{m+1,n}) \quad \ldots\ldots(13)$$

where

$$\lambda_{m,n} = \alpha_{m,n} \frac{\Delta t}{(\Delta x)^2} = \frac{K}{c\rho_{m,n}} \cdot \frac{\Delta t}{(\Delta x)^2} \quad \ldots\ldots(14)$$

From (14) and (12) it is seen that the $\lambda_{m,n}$'s depend not only on the altitude but also on temperature, and therefore on time. Nevertheless, to a first approximation, the variation of the $\lambda_{m,n}$'s with time may be ignored. If this is done, equations (13) and (14) assume the form

$$T_{m,n+1} = (1 - 2\lambda_m)T_{m,n} + \lambda_m(T_{m-1,n} + T_{m+1,n}) \quad \ldots\ldots\ldots\ldots (15)$$

$$\lambda_m = \frac{K}{c\rho_m} \cdot \frac{\Delta t}{(\Delta x)^2}$$

where ρ_m denotes the density at the altitude $h_m = h_1 - m\Delta x$ at time $t = 0$. A rough estimate of the possible errors in the computed temperatures due to the replacement of $\lambda_{m,n}$ defined in (14) by λ_m defined in (16) will be given in Section II.

Starting with the known values of the temperature at time $t = 0$, the iterated use of (15) in conjunction with (16), (10), and (11) yields in succession the values of the temperature at time $t = \Delta t$, $t = 2\Delta t$, $t = 3\Delta t$, $\cdots$ etc., and for $x = \Delta x$, $x = 2\Delta x$, $x = 3\Delta x$, $\cdots$ etc.

The computations were first carried out "by hand," that is, with the aid of a desk calculator,* and subsequently on the "Mark 22." The latter computations were carried out with $\Delta t = 10^3$ (10 seconds) and $\Delta x = 20$ km for t ranging from 0 to 2-1/2 hours. The over-all consistency of the computed values was tested by means of the formula

$$\int_0^t K\left(\frac{\partial T}{\partial x}\right)_{h=h_0} \mathrm{d}t = \int_{h_0}^{h_1} c\rho[T(h) - T_0(h)]\,\mathrm{d}h \quad \ldots\ldots\ldots\ldots (17)$$

where $T(h)$ denotes the temperature at altitude h at time t and $T_0(h)$ denotes the temperature at the altitude h at time $t = 0$. Since the temperature gradient vanishes at the altitude h_1 , it is clear that the first member of (17), where the integrand is a function of time, represents the amount of heat transferred by a column of air of unit cross-section extending from $h = h_0$ to $h = h_1$ across the lower base of the column. The second member of (17) evidently represents the decrease in the heat content of the column of air in question between the time t and the time $t = 0$.

The thermal history of the upper atmosphere for the first 2-1/2 hours after sunset is portrayed on the accompanying graphs. An examination of these graphs reveals the fact that during the first 2-1/2 hours after sunset, the temperature has not changed at altitudes below 160 km and that the maximum drop in temperature is about 440°K at the altitude h_1 . The computations have thus corroborated the conjecture that the temperature remains constant at the altitude h_0 , at least for several hours after sunset.

CALCULATION OF ATMOSPHERE DENSITY

Since the temperature does not change during the first 2-1/2 hours after sunset, at altitudes below 160 km, it follows from (4) that the atmospheric density remains equally unchanged below 160 km during the same interval of time. It follows further that the density at altitudes above 160 km may be computed with the aid of the formula (5), where we may choose for ρ_H and T_H the density and the tem-

*Details of these computations are discussed in Section II.

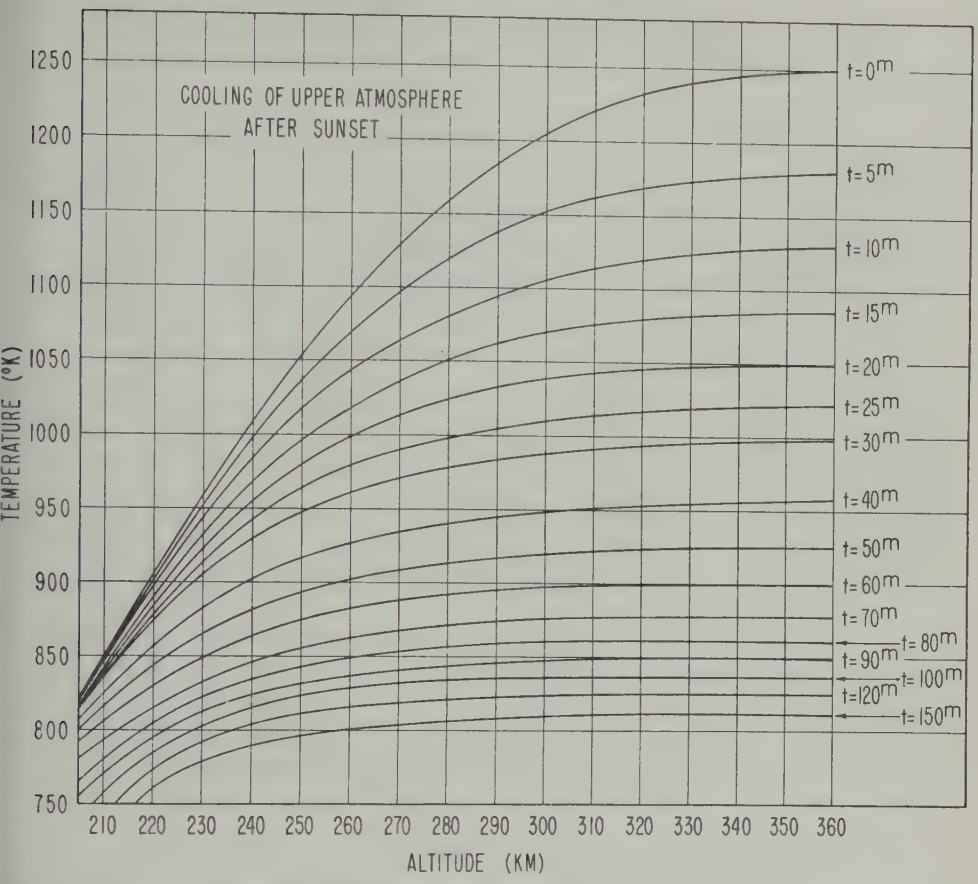

FIG. 1—Cooling of upper atmosphere after sunset

perature at the altitude h_0 given by the Rocket Panel. The computation of the densities was carried out for $t = 2^h$ (two hours). The temperatures, densities, and pressures [the latter calculated with the aid of the relation $p = (R/M)\rho T$] at times $t = 0$ and $t = 2^h$ are given in the accompanying Table 1.

As already stated, the values for $t = 0$ are those given by the Rocket Panel.

Examination of the values of ρ at times $t = 0$ and $t = 2^h$ reveals the fact that the densities at time $t = 2^h$ are larger than those at time $t = 0$ in an altitude region extending from some altitude h_2 between 160 and 180 km to some altitude h_3 between 220 and 240 km. Moreover, this increase in density at time $t = 2^h$ is compensated by a decrease at altitudes $h > h_3$. This is the phenomenon of the settling of the atmosphere referred to at the beginning of this article.

CALCULATION OF ION DENSITIES

We shall investigate the effect on the ion density of the F-layer arising both from the settling of the atmosphere as well as the process of recombination of ons, since both effects take place after sunset.

Let p and $p + dp$ denote the pressures at the altitudes h_1 and $h_1 + dh_1$ at time

TABLE 1—*Temperature, density, and pressure*

h	T		ρ		p	
	$t = 0$	$t = 2^h$	$t = 0$	$t = 2^h$	$t = 0$	$t = 2^h$
100	240	240	8.56 (−10)	8.56	5.90 (−1)	5.90 (−1)
120	330	330	5.80 (−11)	5.80	5.49 (−2)	5.49
140	447	447	7.62 (−12)	7.62	9.77 (−3)	9.77
160	560	560	1.64 (−12)	1.64	2.63 (−3)	2.63
180	677	665	4.71 (−13)	4.75	9.15 (−4)	9.23
200	792	730	1.67 (−13)	1.72	3.80 (−4)	3.60
220	907	774	6.83 (−14)	6.91	1.78 (−4)	1.54
240	1010	804	3.15 (−14)	2.97	9.13 (−5)	6.86
260	1095	816	1.59 (−14)	1.34	5.00 (−5)	3.14
280	1160	821	8.62 (−15)	6.20	2.87 (−5)	1.46
300	1205	824	4.89 (−15)	2.89	1.69 (−5)	6.84 (−6)
320	1230	825	2.88 (−15)	1.36	1.02 (−5)	3.22 (−6)
340	1245	825	1.73 (−15)	6.45 (−16)	6.18 (−6)	1.53 (−6)
360	1250	825	1.05 (−15)	3.07 (−16)	3.77 (−6)	8.76 (−7)

$t = 0$. (In the present discussion, h_1 is a variable altitude and not the altitude of 380 km previously denoted by h_1 .) Let similarly p and $p + \mathrm{d}p$ be the pressure at the lower altitudes h_2 and $h_2 + \mathrm{d}h_2$ at time $t = 2^h$. Let further ρ_1 denote the density at the altitude h_1 at time $t = 0$ and ρ_2 the density at the altitude h_2 at time $t = 2^h$. Then, since $\mathrm{d}p = -\rho_1 g_1 \, \mathrm{d}h_1$, where g_1 is the value of g (the acceleration of gravity) at the altitude h_1 , and similarly $\mathrm{d}p = -\rho_2 g_2 \, \mathrm{d}h_2$, it follows that

$$\rho_1 g_1 \, \mathrm{d}h_1 = \rho_2 g_2 \, \mathrm{d}h_2$$

If now n_1 and n_2 denote the ion densities at time $t = 0$ and $t = 2^h$ at the altitudes h_1 and h_2 above considered, it is reasonable to assume

$$n_1 g_1 \, \mathrm{d}h_1 = n_2 g_2 \, \mathrm{d}h_2$$

whence

$$n_2 = \frac{g_1}{g_2} \frac{\mathrm{d}h_1}{\mathrm{d}h_2} n_1 \qquad (18)$$

It should be emphasized that in the last equation $\mathrm{d}h_1$ and $\mathrm{d}h_2$ are the altitude increments corresponding to the same pressure increment $\mathrm{d}p$ and that, moreover, h_1 and h_2 are such that the pressure at the altitude h_1 at $t = 0$ is identical with the pressure at the altitude h_2 at time $t = 2^h$.

Consider now the effect of recombination of ions. From the well-known equation

$$\mathrm{d}N = -\beta N^2 \, \mathrm{d}t$$

it follows that

$$N_f = \frac{N_i}{1 + \beta N_i t} \cong N_i(1 - \beta N_i t) \qquad (19)$$

where N_i and N_f denote the initial and final ion densities, respectively. If in the

last equation we replace N_i by the expression of n_2 from (18) and write N for N_f, we obtain

$$N \cong \frac{g_1}{g_2}\frac{dh_1}{dh_2} n_1\left(1 - \beta \frac{g_1}{g_2}\frac{dh_1}{dh_2} n_1 t\right) \quad \ldots\ldots\ldots\ldots\ldots\ldots\ldots\ldots (20)$$

The values of n_1 as a function of altitude up to 300 km is known from the work of Seddon, Pickar, and Jackson;* beyond 300 km, the ion-density curve is obtained by extrapolation of the Seddon-Pickar-Jackson curve, on the basis of a static ion atmosphere with a mean molecular weight of 8 (corresponding to ions of atomic oxygen and free electrons). The value of β may be taken as 10^{-10}. The value of N

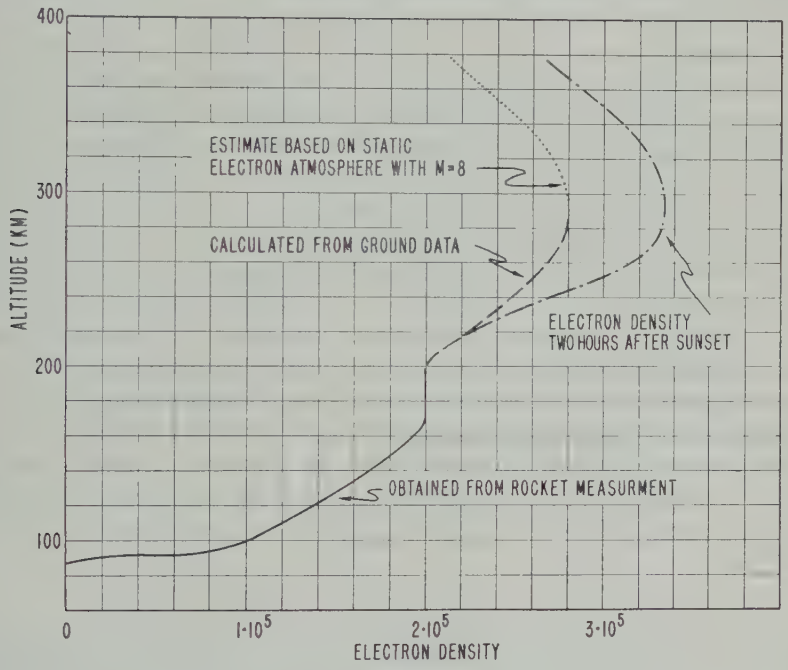

FIG. 2—Electron density before and two hours after sunset

as a function of altitude for $t = 2^h$ is shown in the accompanying graph, together with the original Seddon-Pickar-Jackson curve. It will be seen that the ion density increases considerably in the F-layer, in spite of the recombination of ions which takes place after sunset.

It should be pointed out that in the above treatment we have neglected the downward diffusion of ions and electrons. When such diffusion is taken into account, it is likely that there will be little or no increase in ion density in the F-layer, in most latitudes, with the possible exception of the equator, where the magnetic field tends to offset diffusion.

In the above treatment of the cooling of the upper atmosphere, we ignored the heat set free in the process of recombination of ions. On the other hand, we

*"Continuous electron density measurements up to 200 km," by J. C. Seddon, A. D. Pickar, and J. E. Jackson, J. Geophys. Res., 59, 513-524 (1954).

have neglected radiation. The error entailed by ignoring the heat set free in the process of recombination of ions may partly offset the errors due to ignoring radiation.

SECTION II—ANALYSIS OF COMPUTING SCHEME

The choice of the intervals Δt and Δx is governed by two important considerations: (*a*) The intervals must be such that the difference equation (9) will be a sufficiently good substitute for the differential equation (1); (*b*) the intervals must be such that, when formula (15) is iterated as often as is required in order to cover the full time interval desired, the aggregate of the computational errors, which are inevitably introduced at every step of the computations, remains tolerably small.

With regard to (*a*), it may be loosely stated that if the intervals Δt and Δx are chosen so that $\delta^2 T$ and $(1/12)\delta^4 T$ are negligibly small compared to $\delta_t T$ and $\delta_x^2 T$ (where $\delta_t^2 T$ denotes the second central difference of the computed values with respect to t, for fixed x and where $\delta_x^2 T$ and $\delta_x^4 T$ have similar meaning), then the values generated by iterated use of (15) and (16) are "very close" to the values which would be obtained from the differential equation (1). Unfortunately, it is not possible in the present case to estimate *a priori* for what values of Δt and Δx these conditions are satisfied. Neither is it possible to estimate the differences between the values generated by means of (15) and (16) and the true values corresponding to the solution of the differential equation (1) when $\delta_t^2 T$ and $(1/12)$ $\delta_x^4 T$ are not negligibly small compared to $\delta_t T$ and $\delta_x^2 T$, respectively. In view of the uncertainty which attaches to the optimum choice of the intervals Δt and Δx, the importance of the over-all test embodied by formula (17) is self-evident.

With regard to (*b*) above, it is a well-known fact that if Δt and Δr are chosen so that

$$\lambda = \alpha \frac{\Delta t}{(\Delta x)^2} < \frac{1}{2} \qquad (21)$$

the solution of the difference equation (15) is stable, that is, the values generated by iterated use of (15) in conjunction with (16) remain bounded. It is important to realize, however, that condition (21) is sufficient but not necessary.

As previously stated, the computations on Mark 22 were carried out with $\Delta t = 10^s$ and $\Delta x = 20$ km. With this choice of intervals, all the λ_m's are smaller than 0.5 with the exception of λ_1, which is slightly larger than 0.5.

With few exceptions, the choice of Δx in the hand computations was the same as in the Mark 22 computations, namely, $\Delta x = 20$ km. The choice of Δt in the interval between $t = 0$ and $t = 30^m$ may be indicated by the symbol $0^m(10^s)$ $3^m(1^m)$ $5^m(5^m)$ 30^m, each quantity in a parenthesis denoting the value of Δt in the range between the two values of t preceding and following the parenthesis. Since the values of several λ_m's were larger than 0.5 in the computations with $\Delta t = 5^m$, the temperatures were recomputed by the process of "upward integration," starting with $h = h_0 = 100$ km and making use of the boundary condition (8), thus generating in succession the values of the temperature for $h = 120$ km, 140 km, $\cdots$ etc.

The values of the temperature for $t = 40^m$, 50^m, and 60^m were obtained by the

rocess of upward integration, with $\Delta t = 10^m$ and $\Delta x = 20$ km, up to the altitude = 240 km. Since the values of λ beyond $h = 240$ km were appreciably larger than 5, it was deemed advisable to adopt an alternative procedure. The values of ie temperature for $h = 260$ km, $h = 280$ km, etc., were plotted as functions of me up to $t = 30^m$ and the resulting curves were extrapolated up to what appeared o be a safe distance beyond $t = 30^m$, the values of the temperatures for $t = 40^m$ eing read on the extrapolated curves. The correctness of the temperatures btained by this procedure was tested by means of formula (17).

When values obtained by the extrapolation procedure above described were und to "pass the test" of formula (17) satisfactorily, the curves T *vs* t for various titudes were further extrapolated a certain safe distance and the new temperatures ius obtained were again subjected to the test of formula (17). In this manner, was possible to obtain the thermal history of the upper atmosphere for a period f 2-1/2 hours. The values of the temperature computed "by hand" were found to gree with those obtained on Mark 22 to within not more than 3.5 per cent, except r the values for $t = 2.5^h$, where the maximum discrepancy was 6.5 per cent.

It may be shown that the values of the temperatures above 240 km, computed n the basis of the simplified scheme consisting of equations (15) and (16), tend to e somewhat lower than those which would be obtained on the basis of (13) and 14). The truth of this statement follows from the following considerations:

From the computations carried out on the basis of (15) and (16), it is apparent iat (*a*) the coefficient of λ in the expression of $T_{m,n+1}$ in (15) is negative, and (*b*) ie densities at altitudes above 240 km at time $t = 2^h$ are smaller than at time = 0. It is reasonable to assume that (*c*) the coefficient of λ in the expression of $_{m,n+1}$ in (13) is also negative, and (*d*) the densities at altitudes above 240 km ecrease monotonically with time. From (*c*) and (*d*) it follows that since the values f λ at time $t = 0$ are smaller than their values at a later time, the temperatures alculated on the basis of these λ's (at time $t = 0$) are larger than their true values. o illustrate this effect, suffice it to state that the temperature at the altitude = 300 km at time $t = 10^m$, when computed on the basis of the value of λ at = 5^m, is 1.75°K lower than the temperature computed on the basis of the value f λ at time $t = 0$. Assuming that the difference in temperatures computed by the vo schemes under discussion is approximately constant at each step of the mputations, this would give rise to a discrepancy of about 42°K in two hours. ince the computed drop in temperature at $h = 300$ km in two hours is 408°K, e conclude that this figure may be in error by about 10 per cent, the true drop temperature being perhaps closer to 408 − 42 = 366°K. It seems reasonable o conjecture that all the values of the temperature drops computed on the basis (15) and (16) are higher by about 10 per cent than the corresponding values mputed on the basis of (13) and (14).

ACKNOWLEDGMENTS

The writer wishes to express his appreciation to Dr. H. E. Newell, Jr., and to r. R. J. Havens for suggesting the above problem and for very stimulating scussions in the course of the investigation. He is also indebted to Mr. Campbell . Chrisman, of the Applications Research Division, for carrying out the compu-tions on the Mark 22.

HEIGHTS OF IRREGULARITIES GIVING RISE TO THE FADING OF 150-KC WAVES*

By R. B. Banerji

Ionosphere Research Laboratory, The Pennsylvania State University, University Park, Pennsylvania

(Received April 11, 1955)

ABSTRACT

Evidences are quoted which show that the fading of 150-kc waves is due to random absorption rather than random scattering from the ionosphere. On the basis of this, a statistical theory has been worked out for the relationship between phase and amplitude of a wave which has encountered random absorption on its downward passage. The predicted behaviour shows excellent agreement with experiment and yields a method for the estimation of the collisional frequency at the region where the absorption is taking place. Experimental results pertaining to 150-kc waves at State College are described and discussed.

The method has possibilities for supplementing wind-measurement results to provide information regarding the heights of winds.

Introduction

The random fading of pulsed radio waves is known to be due to the motion irregularities in the ionosphere [see 1 of "References" at end of paper] and has rved as a basis for the measurement of ionospheric winds [2, 3, 4, 5]. However, ie heights of the irregularities giving rise to the fading, and hence that of the ind system, cannot be obtained by this method. In fact, the irregularities can be tuated at any point, at or below the level of reflection for the wave.

Existing evidences [6, 7] on the fading of 150-kc waves seem to indicate that ie irregularities giving rise to the fading are situated below the reflection level. he irregularities, hence, serve as random absorbers to the waves. This, together ith the random variations of the phase retardation, gives rise to an amplitude id phase modulated wave. Jones, Millman, and Nertney [6] have shown that ie relationship between the phase and amplitude fluctuations can give us indi- tions of the collisional frequency at the height of the irregularities and hence the height itself. The present work deals with certain improvements of this ethod and the results.

A direct comparison of the phase and amplitude of the downcoming wave ould not be sufficient to determine the height unless the comparison were carried

*The research reported in this paper has been sponsored by the Geophysics Research Directo- e of the Air Force Cambridge Research Center, Air Research and Development Command, der Contracts AF19(122)-44 and AF19(604)-1304.

out at the height of the irregularities. If the measurement were to be carried out at the ground, however, one has to keep in mind the fact that the variation of amplitude at the ground is different from the variation of amplitude at the irregularities. We have, hence, to use, instead of the actual value of the amplitude, some statistical property of the amplitude which is independent of the height. Such a property is to be found in the autocorrelogram of the amplitude. Hence, if instead of comparing the amplitude and phase we compare their autocorrelograms, we could expect a smaller amount of scatter and hence more precise determination than obtained by previous investigators.

Theory indicates that the parameter obtained by the above comparison ($\delta\chi/\delta\mu$, where χ is the attenuation coefficient and μ the refractive index) is a function of N, the electron density, and ν, the collisional frequency. In regions of high electron density, the quantity is nearly independent of N, and hence is equal in magnitude to the parameter discussed by the previous workers $[\chi/(1 - \mu)]$. However, at the low electron densities in which we are interested, the variation with N is quite pronounced, and we have had to take account of this by considering a model for the lower ionosphere. This removes a source of anomaly present in the previous determination.

2. *Theoretical Considerations*

We assume a plane wave, coming down through a horizontally stratified ionosphere, to be incident upon a layer where the electron density is variable laterally and in time, so that μ, the refractive index at a point, and χ, the attenuation coefficient there, both undergo a random variation. Let the resulting standard deviation of μ be σ_μ and let $\rho_\mu(\tau)$ be the correlation between its values at a point at two instants separated by a lag τ. The change in χ will also be random with related statistical properties. We may assume that within the thickness b of the screen, variations in these quantities may be neglected by choosing a mean value of the refractive index and attenuation coefficient over the thickness. Let these have instantaneous values $\mu + \mu'$ and $\chi + \chi'$, respectively. Here μ and χ designate the average values of the quantities; μ' and χ' the local deviations therefrom. Let z be the distance measured downwards, so that the downcoming wave at the upper boundary of the layer may be represented by

$$E_0 = A \exp\left[-jK_0 \int_{z_0}^{z_1} (\mu - j\chi)\, dz\right]$$

where z_0 is an initial point and z_1 the upper boundary of the irregular layer.

This wave, on emerging from the screen, will have the form

$$E' = A \exp\left[-jK_0 \int_{z_0}^{z_1} (\mu - j\chi)\, dz - jK_0 b\{\mu + \mu' - j(\chi + \chi')\}\right]$$

while, in the absence of irregularities, it would have the form

$$E_0 = A \exp\left[-jK_0 \int_{z_0}^{z_1+b} (\mu - j\chi)\, dz\right]$$

Hence we can represent E' as a random function of time represented by the orm

$$E' = E_0 e^{-jK_0 b(\mu' - j\chi')} \quad \ldots\ldots(1)$$

Let, at the instant t and $t + \tau$, the deviations of the refractive index be μ' and $''$, and those of the attenuation coefficient χ' and χ'', respectively. Then at these wo instants the amplitude of the wave will have the values

$$R' = |E_0| e^{-K_0 b\chi'}$$

$$R'' = |E_0| e^{-K_0 b\chi''}$$

espectively. For small variations of μ and χ, we can write

$$\chi' = \frac{\delta\chi}{\delta\mu}\mu' = \alpha\mu' \quad \ldots\ldots(2)$$

here

$$\frac{\delta\chi}{\delta\mu} = \frac{\partial\chi}{\partial N}\bigg|_{\nu=\text{const}} \Big/ \frac{\partial\mu}{\partial N}\bigg|_{\nu=\text{const}}$$

we suppose the variations to be entirely due to changes in the electron density and not to any change in ν, the collisional frequency.

The autocorrelogram $\rho_R(\tau)$ of the amplitude R is defined as

$$\rho_R(\tau) = \frac{\overline{R'R''} - \overline{R}^2}{\overline{R^2} - \overline{R}^2}$$

here the bars stand for averages, either over all possibilities or over a long duration f time. This can be found theoretically by carrying out the averaging process over l possibilities. The first term in the numerator is found by multiplying the product $'R''$ by the joint probability distribution of the two random quantities μ' and $''$ (assumed normal)

$$(\mu', \mu'') = \frac{1}{2\pi\sigma_\mu^2\sqrt{1 - \rho_\mu(\tau)^2}} \exp\left[-\frac{1}{2\sigma_\mu^2\{1 - \rho_\mu(\tau)^2\}}\{\mu'^2 - 2\rho_\mu(\tau)\mu'\mu'' + \mu''^2\}\right]$$

nd integrating over the range of possibilities. We thus obtain

$$\overline{R'R''} = \int_{-\infty}^{\infty}\int_{\infty}^{\infty} R'R''P(\mu', \mu'')\,d\mu'\,d\mu'' = |E_0|^2 \exp\left[K_0^2 b^2\sigma_\mu^2\alpha^2\{1 + \rho_\mu(\tau)\}\right]$$

The first term in the denominator is obtained by putting $\rho_\mu(\tau) = 1$ for $\tau = 0$.

$$\overline{R^2} = |E_0|^2 \exp\left[2K_0 b^2\sigma_\mu^2\alpha^2\right]$$

can be found by a similar integration after multiplying R' (or R'') by the distri- ution of μ' (or μ'') and integrating over the range of possibilities. This yields

$$\overline{R}^2 = |E_0|^2 \exp\left[K_0^2 b^2\sigma_\mu^2\alpha^2\right]$$

hence we obtain

$$\rho_R(\tau) = \frac{\exp\left[K_0^2 b^2\sigma_\mu^2\alpha^2\rho_\mu(\tau)\right] - 1}{\exp\left[K_0^2 b^2\sigma_\mu^2\alpha^2\right] - 1} \quad \ldots\ldots(3)$$

The autocorrelogram is dependent only on the power spectrum of the wave and hence is the same at all points below the level of irregularities.

Now, it has been pointed out by Hewish [8] that in a purely phase-modulated screen the form of the phase variation at the ground is very similar to the phase variation at the screen. This analysis has been extended by Jones, Millman, and Nertney to the case of a wave which is both amplitude and phase modulated with a similar result. We are, therefore, safe in concluding that the autocorrelogram of phase is the same at the ground and at the screen.

Now, in Equation (1), if ϕ' and ϕ'' are the phases at two instants t and $t + \tau$, then

$$\phi' = K_0 b \mu'$$

$$\phi'' = K_0 b \mu''$$

so that

$$\rho_\phi(\tau) = \frac{\overline{\phi'\phi''} - \bar{\phi}^2}{\overline{\phi^2} - \bar{\phi}^2} = \frac{\overline{\mu'\mu''} - \bar{\mu}^2}{\overline{\mu^2} - \bar{\mu}^2} = \rho_\mu(\tau)$$

and we can write equation (3) as

$$\rho_R(\tau) = \frac{\exp\left[K_0^2 b^2 \sigma_\mu^2 \alpha^2 \rho_\phi(\tau)\right] - 1}{\exp\left[K_0^2 b^2 \sigma_\mu^2 \alpha^2\right] - 1}$$

Under conditions when the exponential term is large enough, we can write

$$ln\rho_R(\tau) + K_0^2 b^2 \sigma_\mu^2 \alpha^2 = K_0^2 b^2 \sigma_\mu^2 \rho_\phi(\tau)$$

Also since

$$\phi' = K_0 b \mu'$$

$$\sigma_\phi^2 = K_0^2 b^2 \sigma_\mu^2$$

which indicates that if we plot $ln\rho_R(\tau)$ against $\rho_\phi(\tau)$, for different values of τ, we would get a straight line of slope $\sigma_\phi^2 \alpha^2$. Hence, from experimentally determined values of $\rho_R(\tau)$, $\rho_\phi(\tau)$, and σ_ϕ^2, we can obtain α or $\delta\chi/\delta\mu$. $\delta\chi/\delta\mu$ is a function of N and ν. Its value can be obtained from magneto-ionic theory and plotted as contours of constant $\delta\chi/\delta\mu$ on the (N, ν) plane. On the other hand, from theoretical models of the electron-density distribution in the ionosphere, we can plot the value of N for different values of ν (corresponding to the different heights) at different hours of the day, on the (N, ν) plane, there being one curve for each hour of the day.

The determination of $\delta\chi/\delta\mu$ at a certain hour gives us a relationship that must exist between N and ν at the diffracting layer as determined by the contour for this value of $\delta\chi/\delta\mu$. The intersection of this curve with the (N, ν) curve for the hour determines the value of ν uniquely at the diffracting screen. Since the value of N as a function of height can be computed theoretically, this value fixes the height of the screen uniquely.

3. *Experimental Observations and Results*

The method of analysis presented above was applied to winter-time data obtained at the Ionosphere Research Laboratory of the Pennsylvania State

niversity [9, 10] on the fading of 150-kc pulsed waves reflected from the lower E gions. The formula for $\rho(\tau)$ was slightly modified to take account of the finite ngth of the fading data. Instead of using the formula

$$\rho(\tau) = \frac{\frac{1}{n-\tau}\sum_{t=1}^{n-\tau} R(t)R(t+\tau) - \left[\frac{1}{n}\sum_{t=1}^{n} R(t)\right]^2}{\frac{1}{n}\sum_{t=1}^{n}[R(t)]^2 - \left[\frac{1}{n}\sum_{t=1}^{n} R(t)\right]^2}$$

hich assumes a very long time-series, we computed

$$\tau) = \frac{\frac{1}{n-\tau}\sum_{t=1}^{n-\tau} R(t)R(t+\tau) - \left[\frac{1}{n-\tau}\sum_{t=1}^{n-\tau} R(t)\right]\left[\frac{1}{n-\tau}\sum_{t=\tau}^{n} R(t)\right]}{\sqrt{\left[\frac{1}{n-\tau}\sum_{t=1}^{n-\tau}\{R(t)\}^2 - \left\{\frac{1}{n-\tau}\sum_{t=1}^{n-\tau} R(t)\right\}^2\right]\left[\frac{1}{n-\tau}\sum_{t=\tau}^{n}\{R(t)\}^2 - \left\{\frac{1}{n-\tau}\sum_{t=\tau}^{n} R(t)\right\}^2\right]}}$$

hich is the conventional statistical definition of correlation between two time-ries obtained by lagging a series on itself.

The plot of $ln\rho_R(\tau)$ against $\rho_\phi(\tau)$ obtained on two typical occasions is shown in igure 1. It will be noticed that the fit is very close to linear up to values of ρ_ϕ of

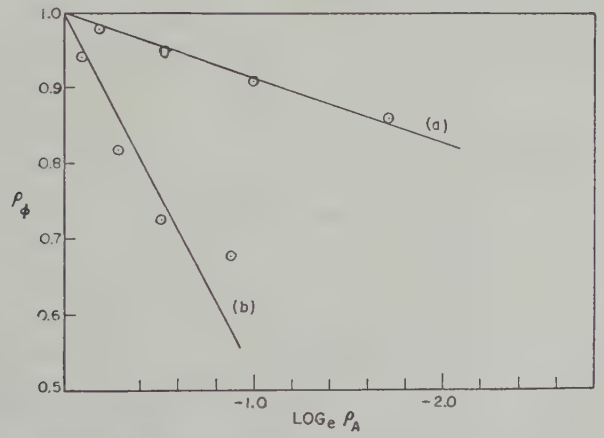

G. 1—Comparison plots obtained on (*a*) January 28, 1952, at 2100 hours LMT, and (*b*) February 23, 1952, at 2100 hours LMT

8. The time in which this value is reached depends on the rapidity of phase fading. n the average, this corresponds to a time range of about two minutes. It will be called that the variation of phase is much slower than the variation of amplitude.

For our electron-distribution model, we used the one obtained for the D-region Mitra on theoretical and experimental considerations [11] for the daytime ectron distribution. The night-time models were obtained by using a model for nset condition suggested by him as a starting point and computing the night-ne distributions from it on the basis of the recombination-coefficient gradient tained by him [12].

The model for the collisional frequency as a function of height was as obtained

by Nicolet [13] from theoretical considerations. The model is shown in Figure 2. This, combined with the electron-distribution model, enables us to draw the (N, ν) curves for the different hours in winter-time in State College.

The contours for $\delta\chi/\delta\mu$ were computed from the tables of complex refractive

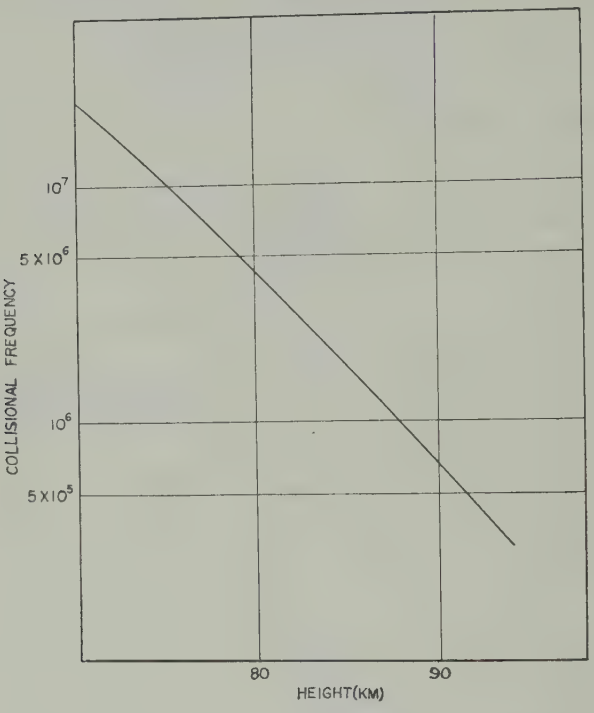

Fig. 2—Collisional frequency as a function of height

index for 150-kc waves obtained by Kelso [14]. These are shown as solid lines superposed on the electron-density contours in Figure 3.

The values obtained for the heights of the irregularities at different hours of the day are shown in Figure 4.

4. *Conclusions*

The results above clearly establish the diurnal trend of height variations observed by Jones, Millman, and Nertney. The uncertainties in the actual height, however, are much reduced because of the larger available precision.

Our method enables us also to determine the mean electron density of the diffracting screen. This did not show any consistent diurnal variation, but, except for one or two values at noon-time, remained confined near the value of 150 electrons per cm^3. This is what could be expected from the general trend of the diurnal variation, since the level of occurrence of a certain fixed electron density would show the same kind of diurnal variation that the height of irregularities exhibit. There does not seem to be any known reason, however, why this electron

nsity and this alone should be such as to affect the waves most profoundly and nce to give rise to a diffraction effect in the presence of irregularities.

Atmospheric turbulence is known to exist [16, 18] in the whole height range th which we have been dealing so far, and it is conceivable that the heights nich we have determined are really average heights of a very wide region, the whole which contributes to the fading.

The upper boundary of the region that can affect the 150-kc wave is located at e reflection height. If the lower boundary of the region were at a fixed height he lower boundary of the region of turbulence), the effective height measured r us ought to have a variation less pronounced than the height variation of the flecting region. Comparison with the variation of reflection height as obtained by nes [15] at State College from phase data shows, however, that the amount of ariation is almost the same in the two cases. This seems to indicate that the

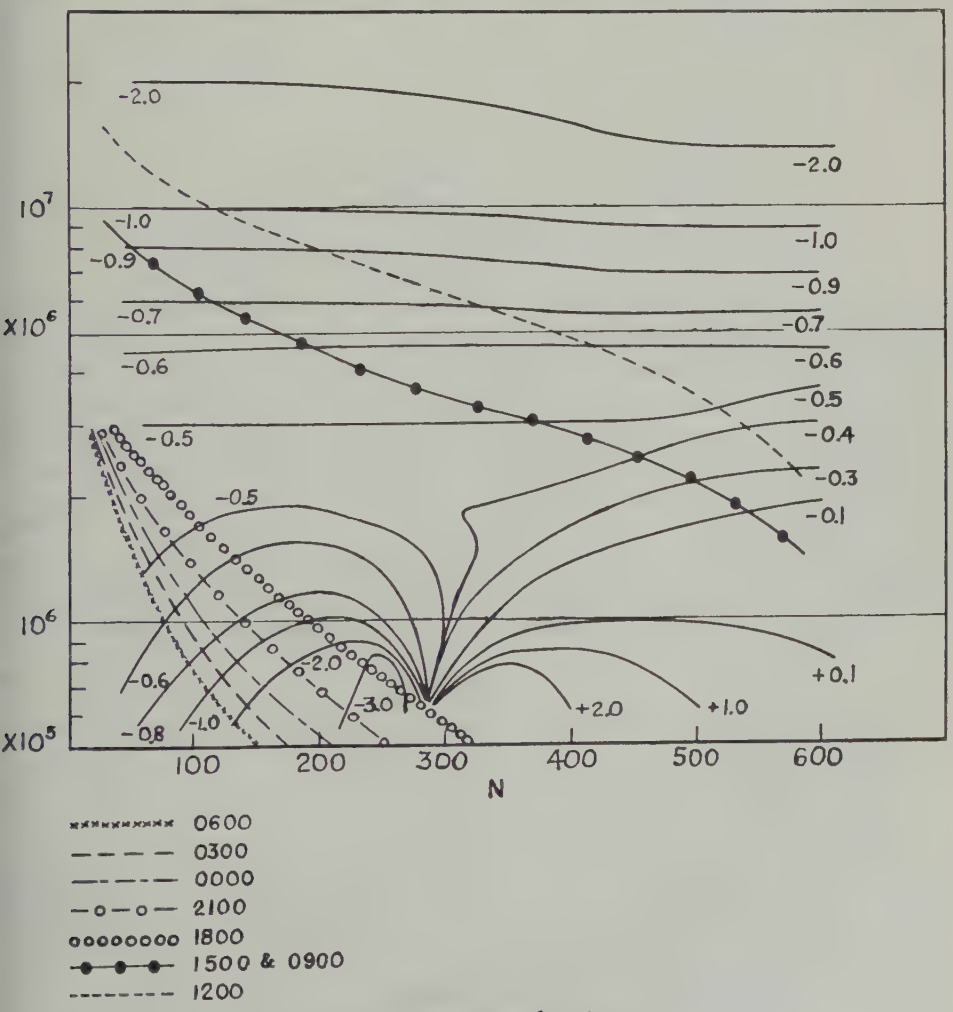

Fig. 3—The fundamental contours

region of irregularity does not have a lower boundary but moves with the whole ionized region. This seems very reasonable on physical grounds, since the whole ionized region below the reflection level can give rise to irregularities in propagation, if subjected to turbulence. However, from the results it is clear that the region of ionization never moves out of a region of turbulence. In the light of the available *D*-region models, which are supposed to extend down to heights of 60 km, we can say that the region of tubulence extends down to this height. This might be ex-

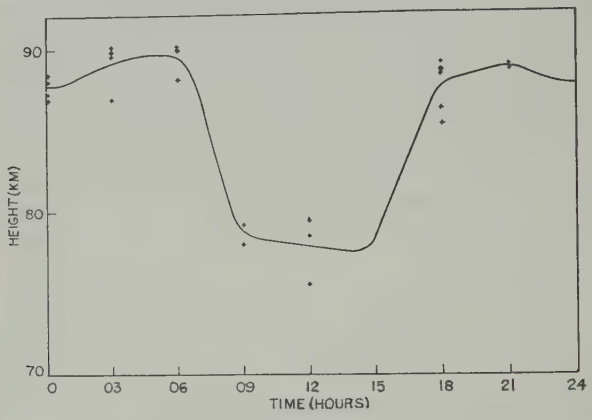

Fig. 4—The diurnal variation of the height of irregularities

pected from the fact that at these heights the temperature increases with height and no convective equilibrium can be maintained.

Since collisional frequency and electron-density distributions, other than those with which we have worked, have been proposed, it was considered of interest to see how far the models affect our results. The models obtained by Parkinson [17] were used as a check on this. The results differed from those obtained above by about one kilometer. This is not considered significant in view of the larger experimental scatter of the results.

This work was carried out under the sponsorship of the Geophysics Research Directorate, of the Air Force Cambridge Research Center. I am thankful to Dr. R. E. Jones for his very helpful cooperation during the progress of the work.

References

[1] H. G. Booker, J. A. Ratcliffe, and D. H. Shinn, Phil. Trans. R. Soc., A, **262**, 579 (1950).
[2] S. N. Mitra, Proc. Inst. Elec. Eng., Pt. 3, **96**, 441 (1949).
[3] G. J. Phillips, J. Atmos. Terr. Phys., **2**, 140 (1952).
[4] C. D. Salzberg and R. Greenstone, J. Geophys. Res., **56**, 521 (1951).
[5] J. H. Chapman, Can. J. Phys., **31**, 120 (1953).
[6] R. E. Jones, G. H. Millman, and R. J. Nertney, J. Atmos. Terr. Phys., **3**, 79 (1953).
[7] R. E. Jones and R. W. Parkinson, The amplitude and phase variation of 150 kc signals reflected from the *E* layer, presented at the meeting of the U.S.A. National Committee of the International Scientific Radio Union (URSI), Washington, D. C., May 3–5, 1955.
[8] A. Hewish, Proc. R. Soc., A, **209**, 81 (1951).
[9] G. H. Millman, Ann. Géophys., **8**, 365 (1952).
[10] R. E. Jones, Rev. Sci. Inst., **24**, 433 (1953).

[11] A. P. Mitra, private communication, in modification of his results published in J. Atmos. Terr. Phys., **5**, 28 (1954).
[12] A. P. Mitra, The Pennsylvania State University, Ionosphere Res. Lab., Sci. Rep. No. 68 (1954).
[13] M. Nicolet, J. Atmos. Terr. Phys., **3**, 200 (1953).
[14] J. M. Kelso, The Pennsylvania State University, Ionosphere Res. Lab., Tech. Rep. No. 24 (1951).
[15] R. E. Jones, J. Atmos. Terr. Phys., **6**, 1 (1955).
[16] P. M. Millman, Proceedings of the Conference on Motions in the Upper Atmosphere, University of New Mexico, Albuquerque (1951).
[17] R. W. Parkinson, The Pennsylvania State University, Ionosphere Res. Lab., Sci. Rep. No. 73 (1955).
[18] W. Liller and F. L. Whipple, High altitude winds by meteor train photography, p. 112, Rocket Exploration of the Upper Atmosphere, Pergamon Press, Ltd., London (1954).

THE INTERACTION BETWEEN ELASTIC WAVE MOTIONS AND A MAGNETIC FIELD IN ELECTRICAL CONDUCTORS*

By L. Knopoff

Institute of Geophysics, University of California, Los Angeles, California

(Received May 16, 1955)

ABSTRACT

The propagation of elastic waves in an electrically conducting solid permeated by a uniform, static magnetic field is discussed. In the case of plane wave motions, two systems of waves arise: simple uncoupled systems and a trimodal coupled system of waves. In the uncoupled case, in which polarizations are unaltered, two dispersive, complex phase velocities exist. For a weak impressed magnetic field, one of these velocities is close to the elastic wave velocity of the polarized wave in the absence of the field. The other wave, called an eddy current wave, although strongly attenuated, cannot be neglected in the solution of boundary value problems.

When the theory of magnetoelastic interactions is applied to seismic motions in the conducting core of the earth, it is found that compressional waves are virtually unattenuated in the core for the pertinent values of frequency, conductivity, and magnetic intensity. It is concluded that magnetoelastic interactions are not a significant mechanism in the earth's core.

. *Introduction*

Alfvén (1950) has studied the interaction of hydrodynamic and magnetic henomena in electrically conducting fluids. It is of interest to investigate the orresponding cases of the coupling of elastic and electrodynamic forces in elec-rically conducting materials.

Examples of cases of the interaction of elastic wave motions with magnetic elds are found in the laboratory and in nature. The parallel in nature to the aboratory case of propagation of sound waves in metallic conductors in the resence of strong magnetic fields is to be found in the propagation of seismic aves through the earth's conducting core. The earth's core is a fluid permeated y a magnetic field whose intensity is somewhat greater than that which is found n the earth's surface. The excitation of magnetohydrodynamic waves in the uid core by seismic waves passing through the core has been considered by ikitake (1952). However, it is of interest to determine the influence of the agnetoelastic interactions upon the seismic core waves themselves.

The equations of motion of hydrodynamic, elastic, and acoustic systems differ

*Publication No. 57, Institute of Geophysics, University of California.

only in the descriptions of the respective mechanical restoring forces. Before investigating the special problems of magnetoelasticity, we shall, in this paper, write the linearized equations of motion of a massive conductor in the presence of a uniform magnetic field in which arbitrary mechanical restoring forces are assumed.

II. *Linearized Magnetomechanical Equations*

Consider a massive, homogeneous, isotropic, conducting region permeated by a magnetic induction $\mathbf{B}_0$ in the absence of motions. Let $\mathbf{F}$ be the sum of the inertial and the mechanical restoring forces per unit volume, and let $\mathbf{f}$ be the magnetic interaction forces per unit volume. Then,

$$\mathbf{F} + \mathbf{f} = 0 \qquad (1)$$

If the restoring forces are elastic, then

$$\frac{\mathbf{F}}{\rho} = \alpha^2 \nabla\nabla\cdot\mathbf{U} - \beta^2 \nabla \times \nabla \mathbf{U} - \frac{\partial^2 \mathbf{U}}{\partial t^2} \qquad (2)$$

where α and β are the velocities of longitudinal (P $-$) and transverse (S $-$) waves, ρ is the density of matter, and $\mathbf{U}$ is the displacement of a particle. The first two terms in the right-hand side of equation (2) are the stress gradients due to the dilatation and the torsion of matter, respectively, while the third is the inertial term. If the restoring forces are those of an incompressible, non-viscous fluid,

$$-\mathbf{F} = \nabla p + \rho \frac{\mathrm{d}\mathbf{v}}{\mathrm{d}t} \qquad (3)$$

where p is the pressure and $\mathbf{v}$ is the velocity of a particle. If the restoring forces are those of a compressible fluid,

$$\frac{1}{\rho}\frac{\mathrm{d}\mathbf{F}}{\mathrm{d}t} = -\frac{\mathrm{d}^2\mathbf{v}}{\mathrm{d}t^2} + c^2 \nabla\nabla\cdot\mathbf{v} \qquad (4)$$

where c is the velocity of sound.

The magnetic forces are obtained from the interaction of the motion with the induction $\mathbf{B}$. As the conductors move, or are moved, through the field, currents are induced in them and these currents in turn interact with the field in such a way as to retard the motion. The electromagnetic forces are

$$\mathbf{f} = \mathbf{j} \times \mathbf{B} + \rho_e \mathbf{E} \qquad (5)$$

where $\mathbf{j}$ is the current density, ρ_e is the electric charge density, and $\mathbf{E}$ is the induced electric field. The current is obtained from the electric field by the expression

$$\mathbf{j} = \sigma(\mathbf{E} + \mathbf{v} \times \mathbf{B}) + \rho_e \mathbf{v} \qquad (6)$$

where σ is the electrical conductivity and $\mathbf{v}$ is the particle velocity. In the case in which the restoring forces are elastic, $\mathbf{v} = \partial\mathbf{U}/\partial t$. In the derivation, the two time-dependent Maxwell equations will be required:

$$\nabla \times \mathbf{H} = \mathbf{j} + \dot{\mathbf{D}} \qquad (7)$$

$$\nabla \times \mathbf{E} = -\dot{\mathbf{B}} \qquad (8)$$

The Maxwell equation defining the electric charge density

$$\nabla \cdot \mathbf{D} = \rho_e \quad \ldots\ldots (9)$$

will also be used.

Let us assume the medium to be a conductor with dielectric constant ϵ and constant magnetic permeability μ. Then among equations (1), (5), (6), (7), and (9), we can eliminate the quantities $\mathbf{f}$, $\mathbf{j}$, and ρ_e

$$\mathbf{F} + \sigma\mathbf{E} \times \mathbf{B} + \sigma(\mathbf{v} \times \mathbf{B}) \times \mathbf{B} + \epsilon(\mathbf{v} \times \mathbf{B})\nabla \cdot \mathbf{E} + \epsilon\mathbf{E}\nabla \cdot \mathbf{E} = 0 \quad \ldots\ldots (10)$$

$$\frac{1}{\mu}\nabla \times \mathbf{B} = \sigma\mathbf{E} + \sigma\mathbf{v} \times \mathbf{B} + \epsilon\dot{\mathbf{E}} + \epsilon\mathbf{v}\nabla \cdot \mathbf{E} \quad \ldots\ldots (11)$$

Equations (8), (10), and (11) are linearized by assuming a uniform, static magnetic induction $\mathbf{B}_0$ exists throughout the region if motions are absent. We let

$$\left.\begin{aligned} \mathbf{B} &= \mathbf{B}_0 + \mathbf{b} \\ \mathbf{E} &= \mathbf{e} \end{aligned}\right\} \quad \ldots\ldots (12)$$

The lower case symbols represent first-order quantities, while the capital letter $\mathbf{B}_0$ is a zeroth-order quantity. Upon substitution of equations (12) into equations (8), (10), and (11), we shall neglect second-order terms of the type *be*, *vb*, and *ve*. Performing the indicated substitution and dropping the subscript from $\mathbf{B}_0$, there are obtained the three equations

$$\mathbf{F} + \sigma\mathbf{e} \times \mathbf{B} + \sigma(\mathbf{v} \times \mathbf{B}) \times \mathbf{B} = 0 \quad \ldots\ldots (13)$$

$$\frac{1}{\mu}\nabla \times \mathbf{b} = \sigma\mathbf{e} + \sigma\mathbf{v} \times \mathbf{B} + \epsilon\dot{\mathbf{e}} \quad \ldots\ldots (14)$$

$$\nabla \times \mathbf{e} = -\dot{\mathbf{b}} \quad \ldots\ldots (15)$$

The induced magnetic field, $\mathbf{b}$, is easily eliminated between equations (14) and (15):

$$-\frac{1}{\mu}\nabla \times \nabla \times \mathbf{e} = \sigma\dot{\mathbf{e}} + \sigma\mathbf{v} \times \mathbf{B} + \epsilon\ddot{\mathbf{e}} \quad \ldots\ldots (16)$$

The vector $\mathbf{e}$ may be eliminated between equations (13) and (16), obtaining an equation in $\mathbf{F}$, $\mathbf{B}$, and $\mathbf{v}$ only—that is to say, an equation in the mechanical terms and the external field. This is accomplished by writing equation (16) as

$$\nabla^2\mathbf{e} - \nabla\nabla \cdot \mathbf{e} = \sigma\mu\dot{\mathbf{e}} + \sigma\mu\dot{\mathbf{v}} \times \mathbf{B} + \epsilon\mu\ddot{\mathbf{e}} \quad \ldots\ldots (17)$$

Taking the divergence of equation (14)

$$\left(\sigma + \epsilon\frac{\partial}{\partial t}\right)\nabla \cdot \mathbf{e} = -\sigma\nabla \cdot (\mathbf{v} \times \mathbf{B}) \quad \ldots\ldots (18)$$

and substituting this quantity into expression (17), we obtain

$$\left(\sigma + \epsilon\frac{\partial}{\partial t}\right)\nabla^2\mathbf{e} + \sigma\nabla\nabla \cdot \mathbf{v} \times \mathbf{B} = \left(\sigma + \epsilon\frac{\partial}{\partial t}\right)(\mu\sigma\dot{\mathbf{e}} + \sigma\mu\dot{\mathbf{v}} \times \mathbf{B} + \epsilon\mu\ddot{\mathbf{e}}) \quad \ldots\ldots (19)$$

If the vector product of equation (19) is taken with **B** on the right, and it is noted that if **B** is a constant, the identity

$$(\nabla^2\mathbf{e}) \times \mathbf{B} \equiv \nabla^2(\mathbf{e} \times \mathbf{B}) \quad \ldots\ldots(20)$$

holds, then

$$\left(\sigma + \epsilon\frac{\partial}{\partial t}\right)\nabla^2(\mathbf{e} \times \mathbf{B}) + \sigma(\nabla\nabla\cdot\mathbf{v} \times \mathbf{B}) \times \mathbf{B}$$

$$= \left(\sigma + \epsilon\frac{\partial}{\partial t}\right)\{\sigma\mu\dot{\mathbf{e}} \times \mathbf{B} + \sigma\mu(\dot{\mathbf{v}} \times \mathbf{B}) \times \mathbf{B} + \epsilon\mu\ddot{\mathbf{e}} \times \mathbf{B}\} \quad \ldots\ldots(21)$$

Now from equation (13),

$$-\mathbf{e} \times \mathbf{B} = \mathbf{F}/\sigma + (\mathbf{v} \times \mathbf{B}) \times \mathbf{B} \quad \ldots\ldots(22)$$

Substituting equation (22) into equation (21), we obtain the desired equation in the mechanical terms:

$$\left(-\nabla^2 - \frac{\epsilon}{\sigma}\frac{\partial}{\partial t}\nabla^2 + \sigma\mu\frac{\partial}{\partial t} + 2\epsilon\mu\frac{\partial^2}{\partial t^2} + \frac{\epsilon^2\mu}{\sigma}\frac{\partial^3}{\partial t^3}\right)\mathbf{F}$$

$$= \left(\sigma\nabla^2 + \epsilon\frac{\partial}{\partial t}\nabla^2 - \sigma\epsilon\mu\frac{\partial^2}{\partial t^2} - \epsilon^2\mu\frac{\partial^3}{\partial t^3}\right)(\mathbf{v} \times \mathbf{B}) \times \mathbf{B}$$

$$- \sigma(\nabla\nabla\cdot\mathbf{v} \times \mathbf{B}) \times \mathbf{B} \quad \ldots\ldots(23)$$

Equation (23) is the linearized vector equation of motion of the complex electromagnetic-mechanically coupled system. It contains the terms due to waves traveling with the velocity of light in the conducting medium, terms due to waves traveling with velocities determined by the mechanical restoring forces, and terms due to the interactions of these two wave types with the magnetic field. In order to simplify the computations, assume that the mechanical waves propagate much more slowly than the velocity of electromagnetic radiation. If the magnetic fields are established instantaneously, equation (23) becomes

$$\left(\nabla^2 - \sigma\mu\frac{\partial}{\partial t}\right)\mathbf{F} = \sigma\{\nabla \times \nabla \times (\mathbf{v} \times \mathbf{B})\} \times \mathbf{B} \quad \ldots\ldots(24)$$

Equation (24) is obtained by neglecting the displacement currents; that is, by allowing ϵ to vanish.

III. *Plane Magnetoelastic Motions in Infinite Media*

Consider the system of equations (24) for the case of the mechanical system specified by equation (2), and specialize to the case of plane waves in infinite media. Let the waves be propagated in the z-direction of a Cartesian system and let the induction **B** be located in the $y - z$ plane. This specification of coordinates may be made without loss of generality.

$$\mathbf{U} = U_x(z, t)\mathbf{x}_1 + U_y(z, t)\mathbf{y}_1 + U_z(z, t)\mathbf{z}_1 \quad \ldots\ldots(25)$$

$$B_x = 0 \quad \ldots\ldots(26)$$

The three equations (24) become

$$\left(\frac{\partial^2}{\partial z^2} - \sigma\mu\frac{\partial}{\partial t}\right)\left(\beta^2\frac{\partial^2}{\partial z^2} - \frac{\partial^2}{\partial t^2}\right)U_x = \frac{\sigma}{\rho}\frac{\partial^3}{\partial z^2\,\partial t}U_xB_z^2 \quad \ldots\ldots(27)$$

$$\left(\frac{\partial^2}{\partial z^2} - \sigma\mu\frac{\partial}{\partial t}\right)\left(\beta^2\frac{\partial^2}{\partial z^2} - \frac{\partial^2}{\partial t^2}\right)U_y = \frac{\sigma}{\rho}\frac{\partial^3}{\partial z^2\,\partial t}(U_yB_z^2 - U_zB_yB_z) \quad \ldots\ldots(28)$$

$$\left(\frac{\partial^2}{\partial z^2} - \sigma\mu\frac{\partial}{\partial t}\right)\left(\alpha^2\frac{\partial^2}{\partial z^2} - \frac{\partial^2}{\partial t^2}\right)U_z = \frac{\sigma}{\rho}\frac{\partial^3}{\partial z^2\,\partial t}(U_zB_y^2 - U_yB_yB_z) \quad \ldots\ldots(29)$$

Equations (28) and (29) are a coupled system in U_z and U_y, indicating that an interaction exists between the longitudinal (or compressional) wave and the transverse (or shear) wave polarized in the plane of the field, and that these two types of motions no longer represent independent modes of propagation as they do in the absence of the field. However, equation (27) is independent of the components of displacement U_y and U_z; it represents a shear wave polarized normal to the plane of the magnetic field and interacting only with the component of the field parallel to the direction of propagation.

If the magnetic field is parallel to one of the coordinate axes, then at least one of the polarizations of the elastic wave motion is unaffected by the magnetic field. If the magnetic field is parallel to the direction of propagation ($B_y = 0$), compression waves do not interact with the field; if the magnetic field is transverse to the direction of propagation ($B_z = 0$), shear waves do not interact with the field.

IV. *Uncoupled Plane Waves*

The simplest cases of plane wave motions interacting with the magnetic field are the uncoupled waves. Uncoupled waves are plane polarized waves whose polarizations are unaltered by propagation through the magnetic field. From equations (27) to (29), it is seen that uncoupled waves can arise in two ways, as follows: (1) From the propagation of shear waves polarized transverse to the magnetic field; and (2) from the propagation of compression waves through a transverse magnetic field. In each case, the differential equation which holds is

$$\left(\frac{\partial^2}{\partial z^2} - \sigma\mu\frac{\partial}{\partial t}\right)\left(\xi^2\frac{\partial^2}{\partial z^2} - \frac{\partial^2}{\partial t^2}\right)U(z, t) = \frac{B^2\sigma}{\rho}\frac{\partial^3 U(z, t)}{\partial z^2\,\partial t} \quad \ldots\ldots(30)$$

where $U(z, t)$ is the particle displacement, B is the magnitude of the induction, and ξ is the velocity of shear waves, β, in the absence of the field for case 1, and is the velocity of compression waves α in the absence of the field for case 2.

For harmonic motions, the complex wave number k associated with the frequency of the vibratory motion ω is

$$(k^2 - i\omega\sigma\mu)(\omega^2 - \xi^2k^2) = -i\omega B^2\sigma\frac{k^2}{\rho} \quad \ldots\ldots(31)$$

The magnetohydrodynamic case of Alfvén occurs in case 1 if the shear velocity vanishes and the conductivity σ is assumed infinite. Then,

$$k^2 = \frac{\mu\rho\omega^2}{B^2} \quad \ldots\ldots(32)$$

and the phase velocity of magnetohydrodynamic waves is

$$V_h = \frac{B}{\sqrt{\mu\rho}} \quad \ldots\ldots\ldots\ldots\ldots\ldots\ldots\ldots\ldots\ldots (33)$$

It is desirable to write the biquadratic expression (31) in more convenient units. Let the phase velocity of the motion be

$$V = \omega/k \quad \ldots\ldots\ldots\ldots\ldots\ldots\ldots\ldots\ldots\ldots (34)$$

and introduce a quantity V_e, having the dimensions of a velocity (and equal to the product of the sonic frequency ω and the skin depth of electromagnetic waves at this frequency).

$$V_e \equiv \left(\frac{\omega}{\mu\sigma}\right)^{1/2} \quad \ldots\ldots\ldots\ldots\ldots\ldots\ldots\ldots\ldots\ldots (35)$$

This notation, using the four velocities V, V_e, V_h, and ξ, effectively isolates the magnetic, conductive, and elastic properties of the medium. Equation (28) may be rewritten as

$$(V^2 - \xi^2)(V^2 + iV_e^2) = V^2 V_h^2 \quad \ldots\ldots\ldots\ldots\ldots\ldots\ldots\ldots (36)$$

whose solution is

$$2V^2 = V_h^2 + \xi^2 - iV_e^2 \pm \{(V_h^2 + \xi^2 - iV_e^2)^2 + 4iV_e^2\xi^2\}^{1/2} \quad \ldots\ldots (37)$$

The two modes reduce, in the field-free case ($V_h = 0$), to the ordinary elastic wave and to the eddy current attenuation of the electromagnetic waves induced in the conductor.

The relatively complex equation (37) can be approximated by considering typical numbers occurring in nature. For magnetic inductions up to 10,000 gauss, a reasonable approximation seems to be $V_h^2 \ll \alpha^2$ in solids and liquids and $V_h^2 \ll \beta^2$ in solids. However, in ionized gases in strong magnetic fields, it is possible to have an Alfvén velocity comparable to or larger than the velocity of sound. For the cases of the propagation of vibratory motions through liquids and solids, and in weak fields in ionized gases, the two roots of equation (37) are

$$V_1 \approx \xi\{1 + \tfrac{1}{2}V_h^2(\xi^2 + iV_e^2)^{-1}\} \quad \ldots\ldots\ldots\ldots\ldots\ldots\ldots\ldots (38)$$

and

$$V_2 \approx i^{3/2}V_e\{1 - \tfrac{1}{2}V_h^2(\xi^2 + iV_e^2)^{-1}\} \quad \ldots\ldots\ldots\ldots\ldots\ldots\ldots\ldots (39)$$

One mode is seen to be a perturbation of the elastic wave motion, while the other mode is a perturbation of the eddy currents.

The particle motions have phase velocities which are perturbed only in the second order. The particle motions have attenuations given by

$$\frac{\omega}{2\beta}\frac{V_h^2 V_e^2}{\beta^4 + V_e^4} = \frac{\omega^2 B^2}{2\xi\rho\mu^2\sigma}\left(\xi^4 + \frac{\omega^2}{\sigma^2\mu^2}\right)^{-1} \text{ nepers} \quad \ldots\ldots\ldots\ldots\ldots\ldots (40)$$

In the case of infinite conductivity, $V_e = 0$, and

$$V = (\xi^2 + V_h^2)^{1/2} \quad \text{.....(41)}$$

is the phase velocity for the only mode. The phase velocity is not the magnetohydrodynamic velocity if elastic restoring forces are present. Indeed, the phase velocity may differ greatly from the magnetohydrodynamic velocity and may be only slightly shifted from the elastic velocity.

V. *Coupled Shear-Compression Waves*

If the induction is not aligned along one of the coordinate axes in the $y - z$ plane, but is inclined at an angle θ to the direction of propagation, the coupled system represented by equations (28) and (29) holds. These equations are solved, as in the preceding section, by assuming harmonic motions of frequency ω and determining the phase velocities of the system. If the component U_y vibrates with amplitude C and the component U_z vibrates with amplitude D, the equations reduce to the pair

$$(V^2 - \beta^2)(V^2 + iV_e^2)C = V^2V_h^2(C\cos^2\theta - D\sin\theta\cos\theta) \quad \text{.....(42)}$$

$$(V^2 - \alpha^2)(V^2 + iV_e^2)D = V^2V_h^2(D\sin^2\theta - C\sin\theta\cos\theta) \quad \text{.....(43)}$$

The relative amplitudes of the two components are

$$\frac{C}{D} = -\cot\theta\,\frac{V^2 - \alpha^2}{V^2 - \beta^2} \quad \text{.....(44)}$$

while the equation for the phase velocity is

$$(V^2 - \alpha^2)(V^2 - \beta^2)(V^2 + iV_e^2) = V^2V_h^2(V^2 - \beta^2\sin^2\theta - \alpha^2\cos^2\theta) \quad \text{....(45)}$$

Under the usual assumption $V_h^2 \ll \beta^2 \leq \alpha^2/2$, the three roots to equation (43) are

$$\left.\begin{aligned} V_1 &\approx \alpha\left(1 + \frac{1}{2}\frac{V_h^2\sin^2\theta}{\alpha^2 + iV_e^2}\right) \\ V_2 &\approx \beta\left(1 + \frac{1}{2}\frac{V_h^2\cos^2\theta}{\beta^2 + iV_e^2}\right) \\ V_3 &\approx i^{3/2}V_e\left(1 - \frac{1}{2}V_h^2\frac{iV_e^2 + \beta^2\sin^2\theta + \alpha^2\cos^2\theta}{(iV_e^2 + \beta^2)(iV_e^2 + \alpha^2)}\right) \end{aligned}\right\} \quad \text{.....(46)}$$

The first two sonic roots are similar to the corresponding uncoupled values given by equation (38), where the magnetic induction to be used is the appropriate component in each case. In both the coupled and uncoupled waves, the root corresponding to the eddy current solution is damped out in distances of the order of the skin depth corresponding to the frequency of the vibratory motion. This distance is, in general, small compared with the extent of the field. For instance, at a frequency of 1 Mc, the skin depth in aluminum is 0.02 cm. In the earth, where the frequencies of motion are lower, of the order of 1/6 cps, for a conductivity equal to that of iron at standard conditions, the skin depth is of the order of 100 cm, a distance quite small compared with the distances over which seismic waves are propagated.

In the case of the coupled waves, the general motions in plane waves, when B is small, are

$$U_x = (\alpha^2 + iV_e^2)(\alpha^2 - \beta^2)Ee^{i\omega(z/V_1 - t)} - \beta^2 V_h^2 F \sin\theta \cos\theta e^{i\omega(z/V_2 - t)} - (iV_e^2 + \beta^2)G \sin\theta e^{i\omega(z/V_3 - t)} \quad (47)$$

$$U_y = -\alpha^2 V_h^2 E \sin\theta \cos\theta e^{i\omega(z/V_1 - t)} + (\beta^2 + iV_e^2)(\beta^2 - \alpha^2)Fe^{i\omega(z/V_2 - t)} + (iV_e^2 + \alpha^2)G \cos\theta e^{i\omega(z/V_3 - t)} \quad (48)$$

where E, F, and G are three arbitrary constants to be determined from the boundary conditions. Thus, the motion, which in the field-free case would be purely transverse and propagating with the velocity β, is now a mixed wave of two velocities, one close to the velocity of the compressional wave, the other to that of the shear wave. The third wave is rapidly damped. In a similar way, the longitudinal term is composed of two waves propagating with velocities close to α and β, respectively. If, initially, a pure plane polarized wave, of either longitudinal type or shear type (polarized in the plane of the magnetic field), is produced at some coordinate z, then as this wave propagates, the component of motion, absent at z, is induced. The remaining component of the displacement will be generated and the relative amplitudes of each of the two components will change with distance.

VI. *Boundary Value Problems in Magnetoelasticity*

In this section, there is investigated the propagation of elastic waves through magnetic, conducting media of infinite extent, in which the regions of magnetization are limited. The discontinuities between the magnetized and unmagnetized regions will all be assumed to be perpendicular to the direction of propagation. Only those problems will be considered in which the electric fields are parallel to the magnetic discontinuities; that is, where the vector $\mathbf{v} \times \mathbf{B}$ is perpendicular to the direction of propagation. This can occur in two ways, as follows: Either (1) the magnetic field is parallel to the direction of propagation, or (2) the particle displacement lies in the plane of the magnetic field and the direction of propagation.

Three sets of boundary conditions must be satisfied at the discontinuities in the magnetic fields: (1) the displacement vector $\mathbf{U}$ must be continuous across the boundaries, (2) the total compressional stress T_{zz} and the total shear stresses T_{zz} and T_{zy} must each be continuous across the boundaries, and (3) the tangential component of the total electric field, $\mathbf{e} + \mathbf{v} \times \mathbf{B}$, must be continuous across the boundaries. The physical properties of α, β, σ, and ρ will be assumed continuous in all cases considered here, but this is a mathematical restriction which does not invalidate the above conditions for the more general cases.

The tangential component of the electric field is obtained by taking the vector product of all terms in equation (13) with the uniform induction $\mathbf{B}$. Then,

$$\mathbf{F} \times \mathbf{B} - \sigma\mathbf{e}B^2 - \sigma B^2 \mathbf{v} \times \mathbf{B} = 0 \quad (49)$$

since the scalar product $\mathbf{e} \cdot \mathbf{B}$ vanishes. The condition for the continuity of the tangential component of the total electric field is thus equivalent to the condition for the continuity of the vector $\mathbf{F} \times \mathbf{B}/(\sigma B^2)$.

The total stress T, is defined as the tensor sum of the mechanical stresses and the electromagnetic stresses (Appendix I),

$$T_{ij} = \rho(\alpha^2 - 2\beta^2)e_{kk}\delta_{ij} + 2\rho\beta^2 e_{ij} + \frac{1}{\mu}(B_i b_j + B_j b_i - B_k b_k \delta_{ij}) \ldots\ldots (50)$$

where e is the strain tensor,

$$e_{ij} = \frac{1}{2}\left(\frac{\partial u_i}{\partial x_j} + \frac{\partial u_j}{\partial x_i}\right)$$

and δ_{ij} is the Kronecker delta. If equations (15) and (49) are substituted into equation (50), the total stress rate may be written as

$$\dot{T}_{ij} = \rho(\alpha^2 - 2\beta^2)\dot{e}_{kk}\delta_{ij} + 2\rho\beta^2\dot{e}_{ij} + \frac{1}{\mu}(B_i \mathbf{a}_j + B_j \mathbf{a}_i - B_k \mathbf{a}_k \delta_{ij}) \ldots\ldots (51)$$

where

$$\mathbf{a} = \nabla \times \{[(\mathbf{F}/\sigma B^2) - \mathbf{v}] \times \mathbf{B}\}.$$

When the magnetic field is parallel to the direction of propagation, only shear waves interact with the field. In this case, the three boundary conditions to be satisfied are the continuity of the quantities

$$U_x, \quad \left(\beta^2 \frac{\partial^2 U_x}{\partial z^2} - \frac{\partial^2 U_x}{\partial t^2}\right)B^2\rho, \quad \text{and} \quad \rho \frac{\partial}{\partial z}\left(\beta^2 \frac{\partial U_x}{\partial t} - \frac{\beta^2}{\sigma\mu}\frac{\partial^2 U_x}{\partial z^2} + \frac{1}{\sigma\mu}\frac{\partial^2 U_x}{\partial t^2} - V_h^2 \frac{\partial U_x}{\partial t}\right)$$

across all the plane boundaries.

When the shear motions U_x are absent, the boundary conditions to be satisfied are continuity of the five quantities

$$U_y, \quad U_z, \quad \frac{\partial}{\partial z}\left\{\rho\alpha^2 \frac{\partial U_z}{\partial t} - \frac{B_y}{\mu}(c_y B_z - c_z B_y)\right\}, \quad \frac{\partial}{\partial z}\left\{\rho\beta^2 \frac{\partial U_y}{\partial t} - \frac{B_z}{\mu}(c_z B_y - c_y B_z)\right\}$$

and

$$\left(\rho\beta^2 \frac{\partial^2 U_y}{\partial z^2} - \rho \frac{\partial^2 U_y}{\partial t^2}\right)B_z - \left(\rho\alpha^2 \frac{\partial^2 U_z}{\partial z^2} - \rho \frac{\partial^2 U_z}{\partial t^2}\right)B_y$$

across all the plane boundaries, where

$$c_y = \frac{\rho\beta^2}{\sigma B^2}\frac{\partial^2 U_y}{\partial z^2} - \frac{\rho}{\sigma B^2}\frac{\partial^2 U_y}{\partial t^2} - \frac{\partial U_y}{\partial t}$$

and

$$c_z = \frac{\rho\alpha^2}{\sigma B^2}\frac{\partial^2 U_z}{\partial z^2} - \frac{\rho}{\sigma B^2}\frac{\partial^2 U_z}{\partial t^2} - \frac{\partial U_z}{\partial t}$$

A. *Uncoupled Waves in a Semi-infinite Magnetic Field*

Consider an elastic conductor of infinite extent in which a uniform magnetic field exists in a semi-infinite portion bounded by the plane surface, $z = 0$. The two regions may be considered to be continuous in all properties except in the magnetic permeability in order to permit the existence of significant discon-

tinuities in the static magnetic field. Let the magnetic induction be aligned in the z-direction. Let plane shear waves of polarization U_x be transmitted from the field-free region in the positive z-direction toward the magnetic discontinuity. The propagation of such a shear wave in the magnetic region is a case of an uncoupled wave considered earlier (case 1, part IV).

Two waves traveling with velocities V_1 and V_2 [given by equation (37)] will be transmitted across the discontinuity. In the field-free region, a reflected shear wave must be anticipated.

Subject to the three boundary conditions above, the solutions for the transverse vibrations in the two regions are

$$U_x = \{a_2(1 + g_1) - a_1(1 + g_2)\}Ae^{i\omega(z/\beta - t)} + \{a_1(g_2 - 1) - a_2(g_1 - 1)\}e^{-i\omega(z/\beta + t)} \qquad z < 0 \ldots\ldots (52)$$

$$U_x = 2a_2Ae^{i\omega(z/V_1 - t)} - 2a_1Ae^{i\omega(z/V_2 - t)} \qquad z > 0 \ldots\ldots (53)$$

where

$$g_i = \frac{\beta}{V_i}\left(1 + \frac{iV_e^2a_i\beta}{V_i(\beta^2 - V_h^2)}\right), \qquad a_i = \frac{\beta^2}{V_i^2} - 1$$

The reflected shear and the transmitted eddy current waves become vanishingly small as the magnetic field decreases. To the order of approximation used in the evaluation of the two roots given in equations (38) and (39), the transmission coefficient at large distances from the boundary, where the eddy current wave has been strongly attenuated, is

$$1 + \frac{1}{2}\frac{V_h^2}{\beta^2 + iV_e^2}\left\{\frac{1}{2} + \frac{iV_e^2}{\beta^2} + \frac{2iV_e^2 + \beta^2 - i^{3/2}V_e\beta}{\beta^2 + iV_e^2}\right\} \ldots\ldots (54)$$

It should be noted that the electromagnetic conditions, appearing in both the electric field and stress boundary conditions, are essential, despite the fact that the eddy current wave is rapidly damped: if the eddy current wave is ignored and the ordinary continuity conditions of elastic theory applied, the transmission coefficient is

$$1 + \frac{V_h^2}{4(\beta^2 + iV_e^2)} \ldots\ldots (55)$$

in disagreement with the result obtained above.

B. *Uncoupled Waves in a Magnetic Field in a Slab of Infinite Extent*

Consider an elastic conductor of infinite extent in which a magnetic field, B_z, is confined to a region bounded by the planes $z = 0$ and $z = d$. Let plane shear waves of polarization U_x be propagated from the field-free region toward the magnetic discontinuity in the positive z-direction. This problem is the extension of the preceding one, in which the magnetic induction is limited in both the positive and negative z-directions.

The interaction with the magnetic field yields six waves whose amplitude coefficients are to be determined. Besides the reflected shear and the transmitted

shear waves, within the magnetic region four waves exist; these are waves propagating in both the positive and negative directions with both velocities of propagation V_1 and V_2. Simplification of the computation results if it is assumed that the electromagnetic terms within the magnetic region start from the appropriate boundary but do not reach the opposite boundary with any significant amplitude. This approximation is satisfactory when the slab thickness is large compared with the skin depth.

The three boundary conditions of the preceding problem must be satisfied at each boundary. The transmission coefficient, comparing the emerging shear wave with the incident shear, is found to be

$$\frac{4a_2g_1(a_1 - a_2)e^{-i\omega d/\beta}}{\{a_2(g_1 - 1) + a_1(g_2 + 1)\}^2 e^{i\omega d/V_1} - \{a_2(g_1 + 1) - a_1(g_2 + 1)\}^2 e^{-i\omega d/V_1}} \quad \ldots\ldots(56)$$

This expression will be of importance in the theory of the propagation of seismic waves through the earth's core.

C. *Coupled Waves in a Semi-infinite Magnetic Field*

Consider a semi-infinite elastic conductor permeated by a uniform steady magnetic field. The magnetic induction is inclined at an angle to the normal to the plane boundary to the magnetic region. Let the excitation of this medium be produced by the oscillations of a conducting unmagnetized piston of infinite extent placed along the plane boundary and vibrating harmonically and normal to the interface. Let A be the amplitude of vibration of the piston.

Within the semi-infinite medium, the motions are given by equations (47) and (48). As seen above, the three boundary conditions which determine the three coefficients E, F, and G are

(1) $\qquad U_z = A, \qquad z = 0$

(2) $\qquad U_y = 0, \qquad z = 0$

(3) $\qquad \rho B_z\left(\frac{\partial^2 U_y}{\partial z^2}\beta^2 - \frac{\partial^2 U_y}{\partial t^2}\right) - \rho B_y\left(\alpha^2\frac{\partial^2 U_z}{\partial z^2} - \frac{\partial^2 U_z}{\partial t^2}\right) = 0, \qquad z = 0$

On the basis of the weak field approximation for which equation (46) was derived, the approximate solutions for U_z and U_y are

$$U_z = A\left(1 + \frac{iV_e^2V_h^2\sin^2\theta}{(\alpha^2 + iV_e^2)^2}\right)e^{i\omega(z/V_1 - t)} - A\frac{iV_e^2V_h^2\sin^2\theta}{(\alpha^2 + iV_e^2)^2}e^{i\omega(z/V_3 - t)} \quad \ldots\ldots(57)$$

$$U_y = \frac{AV_h^2\sin\theta\cos\theta}{(\alpha^2 + iV_e^2)^2(\beta^2 - \alpha^2)}\left\{\alpha^2(\alpha^2 + iV_e^2)e^{i\omega(z/V_1 - t)}\right.$$
$$\left. - \beta^2(\beta^2 + iV_e^2)e^{i\omega(z/V_2 - t)} + (\beta^2 - \alpha^2)\frac{iV_e^2(\alpha^2 + iV_e^2)}{\beta^2 + iV_e^2}e^{i\omega(z/V_3 - t)}\right\} \ldots\ldots(58)$$

At large distances, the "eddy current" wave, of velocity V_3, disappears and the motion consists of the following three waves: (1) A longitudinal wave propagated with constant amplitude at a velocity of almost the value α; (2) a weak transverse wave, which, though vanishing on the boundary, is a curious mixture

of two waves with velocities almost α and β. The two components of the transverse motion are of comparable amplitude, differing by less than a factor of 4. The amplitude of the term whose velocity is almost α is always the larger.

VII. *Good Conductors and Strong Fields*

In this section, we consider two limiting cases. In the first of these, the conductivities are assumed to be infinite so that a condition, assumed by Alfvén, is approached; however, the medium is an elastic solid rather than a fluid. In the second example, the case of extremely strong fields in elastic media of any assigned conductivity is considered.

A. Good conductors—In the case of the perfectly conducting medium, the eddy current waves vanish. As already noted in Section IV, only one type of uncoupled wave exists, for which the velocity is

$$V = (V_h^2 + \beta^2)^{1/2} \quad \ldots\ldots(59)$$

The phase velocity is not the Alfvén velocity, V_h, in an elastic medium.

The high conductivity condition for the coupled waves, when applied to equation (45), yields, for the weak field approximation, the two phase velocities

$$\left.\begin{aligned} V_1^2 &= \alpha^2 + V_h^2 \sin^2\theta \\ V_2^2 &= \beta^2 + V_h^2 \cos^2\theta \end{aligned}\right\} \quad \ldots\ldots(60)$$

These velocities are similar to the uncoupled values in which the magnetohydrodynamic velocity is determined from the proper component of the induction. The major difference between the coupled and the uncoupled systems is that in the coupled case the longitudinal and transverse terms each contain both the velocities V_1 and V_2.

B. Strong fields—The strong field case arises as a limiting case of the equations of motion in which the magnetohydrodynamic term is allowed to become large. The cases of interest are the coupled motions.

The solution in the uncoupled case is a phase velocity V, given by

$$V^2 = V_h^2 + \beta^2 - iV_e^2 \quad \ldots\ldots(61)$$

In the coupled case, the two phase velocities for large V_h are

$$V_1^2 = V_h^2 + \alpha^2 \sin^2\theta + \beta^2 \cos^2\theta - iV_e^2 \quad \ldots\ldots(62)$$

$$V_2^2 = \beta^2 \sin^2\theta + \alpha^2 \cos^2\theta \quad \ldots\ldots(63)$$

The third root is of order $1/V_h^2$. The ratios of the amplitudes for these two cases are, from equation (44),

$$\left(\frac{C}{D}\right)_1 = -\cot\theta\left[1 + \frac{\beta^2 - \alpha^2}{V_h^2}\right] \quad \ldots\ldots(64)$$

and

$$\left(\frac{C}{D}\right)_2 = \tan\theta\left[1 + \frac{\alpha^2 - \beta^2}{V_h^2}\left(1 + \frac{iV_e^2}{\beta^2 \sin^2\theta + \alpha^2 \cos^2\theta}\right)\right] \quad \ldots\ldots(65)$$

Thus, the first mode propagates with almost the magnetohydrodynamic velocity t an angle almost perpendicular to the magnetic field. The second mode propagates t velocity which is between the shear and compression wave velocities and is arallel to the magnetic field vector.

Thus, if in the problem of the skew field excited by the normally vibrating iston considered in Section VI the fields are considered to be very strong, the notions are not principally longitudinal and transverse; the influence of the trong field is to twist about the two independent modes of vibration, so that a ast magnetohydrodynamic wave propagates polarized perpendicular to the eld and an elastic wave, with a rather unusual velocity value, propagates polarized arallel to the magnetic field. The two angles by which the polarizations of the ew independent modes differ from parallelism and perpendicularity to the field re

$$\frac{\alpha^2 - \beta^2}{2V_h^2} \sin 2\theta \qquad (66)$$

or large conductivities.

III. *Propagation in the Earth's Core*

The propagation of uncoupled waves through a magnetic slab, a problem onsidered in Section VI, may be construed as a rough model for the propagation f seismic waves through the earth's conducting, magnetic core. Compression aves propagated through the less conducting mantle interact with the magnetic, onducting core and emerge into the mantle. The transmission coefficient given equation (56), in which the shear wave velocity β is replaced by the compression ave velocity α, will provide a rough evaluation of the interactions of the core aves with the magnetic field in the core.

The transmission coefficient,

$$= \frac{4a_2g_1(a_1 - a_2)e^{-i\omega d/\alpha}}{\{(g_1 - 1)a_2 + (g_2 + 1)a_1\}^2 e^{i\omega d/V_1} - \{(g_1 + 1)a_2 - (g_2 + 1)a_1\}^2 e^{-i\omega d/V_1}} \qquad (67)$$

of sufficient complexity that certain approximations will have to be made. It is interest to investigate this expression for certain numerical properties of the rth's core. The following lumped constants will be assumed for the core: velocity seismic waves $\alpha = 10^6$cm/sec, density $\rho = 10$ gm/cm^3, magnetic permeability $= 1$ cgs unit. It is reasonable to assume that the magnetic induction within e earth's core is less than 10^3 gauss [Elsasser (1950), Bullard and Gellman (1954)]. or the above values, the magnetohydrodynamic velocity is less than 300 cm/sec, d the ratio V_h/α is less than 3×10^{-4}. As a consequence, the small field approximations of Section IV are suitable. The resulting transmission coefficient is

$$T = \left\{1 + \frac{V_h^2(\alpha^2 + iV_e^2 - i^{3/2}V_e\alpha)}{(\alpha^2 + iV_e^2)^2}\right\} \exp\left[i\frac{\omega d}{\alpha} V_h^2 \frac{(\alpha^2 - iV_e^2)}{\alpha^4 + V_e^4}\right] \qquad (68)$$

he expansion is valid for all values of the parameter V_e/α. It is only for larger

values of the magnetic field that reverberation of the V_1 waves within the slab becomes important. The absolute value of the transmission coefficient is

$$| T | = \left(1 + \frac{V_h^2}{\alpha^2} \frac{\sqrt{2} + x - 2x^3 - x^5 + \sqrt{2}x^4}{\sqrt{2}(1 + x^4)^2}\right) \exp\left[-\frac{\omega d V_h^2 V_e^2}{2\alpha(\alpha^4 + V_e^4)}\right] \quad (69)$$

where $x = V_e/\alpha$.

Equation (69) shows that the transmission coefficient depends upon two effects: the attenuation of magnetoelastic waves in a slab of thickness d [compare with equation (40)] and reflections at the slab boundaries.

$$| T | = T_a T_r \quad (70)$$

The contribution to the transmission coefficient from the reflections at the boundaries is

$$T_r = 1 + \frac{V_h^2}{\alpha^2} \frac{\sqrt{2} + x - 2x^3 + \sqrt{2}x^4 - x^5}{\sqrt{2}(1 + x^4)^2} \quad (71)$$

Since the coefficient of V_h^2/α^2 in this expression is always less than 1.2, the effect of reflections is less than 10^{-7}.

The contribution to the transmission coefficient from attenuation within the core is

$$T_a = \exp\left[-\frac{\omega d}{2\alpha} \frac{V_h^2 V_e^2}{\alpha^4 + V_e^4}\right] \quad (72)$$

If the propagation of seismic waves through the earth's core were appreciably influenced by the presence of the magnetic field, two effects would be observed. First, the propagation of compression waves through a filter such as that described by equation (72) would be selective in frequency over the frequency band of interest; over the frequency band, the high frequency components would be strongly attenuated. Second, the passage of a broad spectrum of energy through a filter such as given by equation (72) would yield terms in the output having frequency components predominating in the region of the cut-off frequency of the spectrum (Goldman, 1948). The cut-off frequency ω_0 of this spectrum is

$$\omega_0 = \frac{\alpha^4 \mu \sigma}{\left(\frac{dB^2}{2\alpha\rho}\right) - \frac{1}{\sigma}} \quad (73)$$

The solution to equation (73) is presented in Figure 1 for a suitable set of values for α, ρ, and μ.

Seismic core waves predominate in the frequency band $\omega = 0.6$ to 10 radians/sec (Denson, 1952). Thus, the observed frequencies create an inconsistency in the weak field ($B < 10^3$ gauss)-high conductivity ($\sigma > 10^{-8}$cgs emu) hypothesis.

If it be assumed that the characteristic core frequencies as observed are due to some cause other than the propagation of a broad band of frequencies through the filter of equation (72), then an attenuation of these frequencies must occur for the interaction to be a significant mechanism in the propagation of seismic waves in the core. At a frequency of $\omega \sim 1$ rad/sec, $V_e < 10^4$ cm/sec, since it seems assured that $\sigma > 10^{-8}$ cgs emu. Thus, at this frequency, $V_e \ll \alpha$ and

$$T_a = \exp\left[-\frac{\omega^2 Bd}{2\alpha^5 \rho\sigma\mu^2}\right] \quad \ldots\ldots\ldots\ldots\ldots\ldots\ldots\ldots\ldots\ldots (74)$$

For the values of the induction up to 10^3 gauss and conductivities above 10^{-8} cgs emu, this part of the transmission coefficient is $1 > | T_a | > e^{-3.5\times10^{-9}}$. The two contributing factors are each negligible at these frequencies and for the

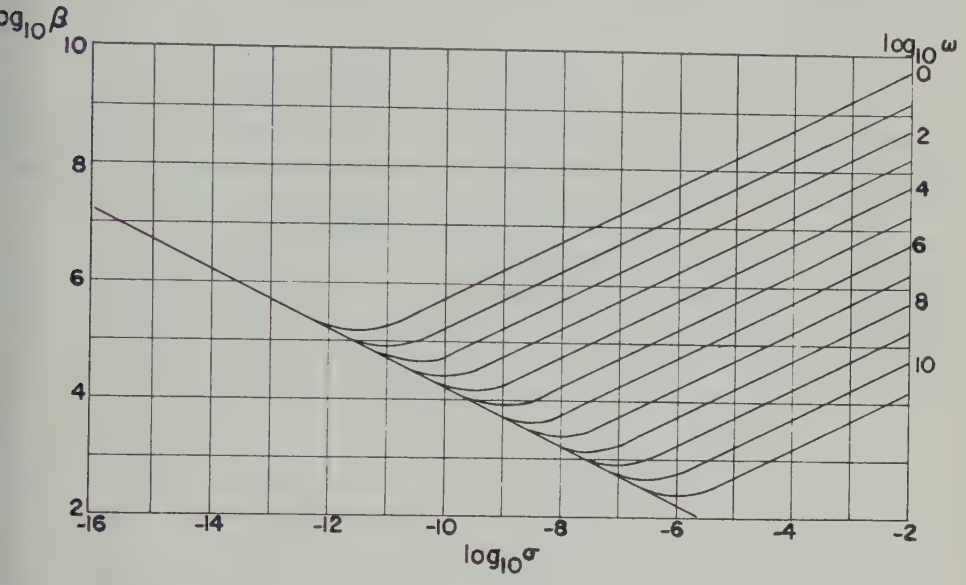

FIG. 1—Numerical solution to the cut-off equation (71) for $\alpha = 10$ km/sec, $\mu = 1$ cgs emu, $= 10$ gm/cm^3, $d = 7{,}000$ km; the induction B, conductivity σ, and angular frequency ω_0 are in cgs emu

allowable range of conductivities and fields. The attenuation of seismic waves by the magnetic field is not significant and the interaction with the magnetic field is not an important mechanism in the propagation of seismic waves through the earth's core.

References

Alfvén, H. (1950); Cosmical electrodynamics, Oxford, Clarendon Press, 76–91.
Bullard, E. C., and H. Gellman (1954); Phil. Trans. R. Soc. London, A, **247**, 213–278.
Denson, M. E., Jr. (1952); Bull. Seis. Soc. Amer., **42**, 119–134.
Elsasser, W. M. (1950); Revs. Mod. Phys., **22**, 1–35.
Goldman, S. (1948); Frequency analysis, modulation and noise, McGraw-Hill Book Co., Inc., New York, 72–81.
Rikitake, T. (1952); Bull. Earthquake Res. Inst., Tokyo Univ., **30**, 191–221.

APPENDIX I—*The Total Stress Tensor*

We define the total stress T as the tensor sum of the elastic stress τ and the electromagnetic stress S. The elastic stress tensor for an isotropic medium is the familiar expression

$$\tau_{ij} = \rho(\alpha^2 - 2\beta^2)e_{kk}\delta_{ij} + 2\rho\beta^2 e_{ij}$$

where e is the strain tensor

$$e_{ij} = \frac{1}{2}\left(\frac{\partial u_i}{\partial x_j} + \frac{\partial u_j}{\partial x_i}\right)$$

and δ_{ij} is the Kronecker delta. The elastic constants have been written in terms of the density and the velocities.

The electromagnetic stress tensor is the expression

$$S_{ij} = \epsilon\left(E_iE_j - \frac{1}{2}E_kE_k\delta_{ij}\right) + \frac{1}{\mu}\left(B_iB_j - \frac{1}{2}B_kB_k\delta_{ij}\right)$$

where $\mathbf{B}$ is the sum of the impressed and the induced fields. Substituting the linearizing conditions of equation (12) and neglecting second-order quantities,

$$S_{ij} = \frac{1}{\mu}(B_ib_j + B_jb_i - B_kb_k\delta_{ij})$$

where $\mathbf{B}$ is now merely the impressed field, the subscript upon $\mathbf{B}_0$ having been dropped.

POLARIZATION OF ELECTROMAGNETIC WAVES FOR VERTICAL PROPAGATION IN THE IONOSPHERE

By R. Roy and J. K. D. Verma

Institute of Nuclear Physics, Calcutta, India

(Paper transmitted by Prof. M. N. Saha; received July 25, 1955)

ABSTRACT

A theoretical study of the variation of the state of polarization of a vertically incident electromagnetic wave while in propagation in the ionosphere has been made on the basis of an approximate solution of the wave equations obtained by Saha, Banerjee, and Guha. It has been shown that the major axes of the polarization ellipses of both the ordinary and the extraordinary waves would lie in the N-E quadrant in the northern hemisphere and in the N-W quadrant in the southern hemisphere. A new method has been outlined for the determination of the electron density and the collision frequency in the ionized layers from the value of the tilt-angle and the ratio of axes of the elliptic patterns.

An analysis of the characteristics of the experimentally observed polarization patterns indicates that in E layer the value of ν is 1.7×10^6 per second. They further show that the polarization of the downcoming waves corresponds to their respective reflection levels, rather than a limiting region below the E layer.

§1. *Introduction*

The polarization of radio waves in the ionosphere has been the subject of intensive study since the formulation of the Appleton-Hartree equations. The relation between the complex polarization and the polarization characteristics at the wave-front had been studied by Taylor (1934), Bailey (1934), Martyn (1935), Ghosh (1938), and recently by Scott (1953). These investigations are based on the ray-theory of propagation. The object of this paper is to study—on the basis of the wave-theory—the changes in the orientation and ellipticity of the polarization ellipse of any of the split waves with the electron density, the collision frequency, and the magnetic field vector in the ionosphere. It will be shown that it is possible to deduce the electron density and collision frequency in the ionized layers from the tilt-angle and the ratio of axes of the experimentally recorded elliptical patterns of the downcoming o- and x-waves.

The coupled wave-equations for the case of vertical propagation in the ionosphere were given by Försterling (1942), Rydbeck (1944), and Saha, Banerjee, and Guha (1947, 1951). The pair of equations obtained by these workers are

identical, as pointed out by Kelso (1953). We write out these equations in the form given by Saha, Banerjee, and Guha

$$\left.\begin{aligned} \dot{V} + (q_o^2 - \dot{\phi}^2)V &= 2\dot{\phi}\dot{W} + \ddot{\phi}W \\ \dot{W} + (q_e^2 - \dot{\phi}^2)W &= -2\dot{\phi}\dot{V} - \ddot{\phi}V \end{aligned}\right\} \quad \ldots\ldots\ldots\ldots\ldots\ldots (1.1)$$

where q_o and q_e are the ordinary and extraordinary refractive indices,

$$\dot{V} = \frac{dV}{du} = \frac{c}{p}\cdot\frac{dV}{dz}, \qquad \text{etc.}$$

the positive direction of z-axis is the direction of propagation and the y-axis is perpendicular to the magnetic meridian, and

$$V = (E_x + i\rho_1 E_y)/\sqrt{1 + \rho_1^2}$$

$$W = (E_x + i\rho_2 E_y)/\sqrt{1 + \rho_2^2}$$

$$\dot{\phi} = \frac{d\rho}{du}\Big/(1 + \rho^2)$$

$$\rho_1 = \tan\phi = G - \sqrt{1 + G^2}$$

$$\rho_2 = -\cot\phi = G + \sqrt{1 + G^2}$$

For describing the ionospheric parameters, Saha, *et al.*, also adopted the following notations:

$$p_0^2 = \frac{4\pi Ne^2}{m}, \qquad r = p_0^2/p^2, \qquad \omega = -\frac{|e|H}{mcp}$$

$$\omega_z = -|\omega|\cos\Theta, \qquad \omega_x = -|\omega|\sin\Theta$$

$$\nu_c = p\omega_x^2/2\omega_z = -|p_h|\sin^2\Theta/2\cos\Theta$$

$$\beta = 1 - i\delta, \qquad \delta = \nu/p, \qquad \delta_c = \nu_c/p$$

$$q_o^2 = 1 - \frac{r}{\beta + \rho_1\omega_z}, \qquad q_e^2 = 1 - \frac{r}{\beta + \rho_2\omega_z}$$

$$\xi = \delta/\delta_c = \nu/\nu_c, \qquad \eta = (1 - r)/\delta_c, \qquad \tan\nu = \frac{\delta}{1 - r} = \frac{\xi}{\eta}$$

$$G = \omega_x^2/2\omega_z(r - \beta) = -i/(\xi + i\eta),$$

and Θ represents the angle between the positive z-direction and the positive direction of the magnetic lines of force, and it varies from zero over the south pole to $\pi/2$ on the geomagnetic equator, and from $\pi/2$ to π in the nothern hemisphere, attaining the value π over the north pole. The value of ν_c (and hence ξ) is positive in the northern hemisphere and negative in the southern hemisphere, and it varies from zero at the geomagnetic poles to infinity at the geomagnetic equator.

§2. *The coupling term and the ξ-η plane*

The expression for the coupling term $\dot{\phi}$ may be written in terms of ξ and η as

$$\dot{\phi} = \frac{1}{2} \cdot \frac{(\dot{\eta} - i\dot{\xi})}{(1 - \xi^2 + \eta^2) - 2i\xi\eta} \quad \ldots\ldots\ldots\ldots\ldots\ldots (2.1)$$

For a model ionosphere obeying the Chapman distribution,

$$N = N_{\max} \exp \tfrac{1}{2}(1 + x - e^x)$$

where $x = (z_0 - z)/l$, l being the scale height, and also an exponential distribution of the collision frequency given by

$$\nu = \nu_0 e^x$$

ν_0 being the value of electron collisions at the height of maximum ionization, it can be shown that

$$\dot{\xi} = -\frac{c}{pl}\xi \quad \text{and} \quad \dot{\eta} = \frac{c}{2pl}(1 - e^x)\left(\frac{1}{\delta_c} - \eta\right)$$

The magnitude of the coupling factor is then given by

$$|\dot{\phi}| = \frac{\lambda}{4\pi l}\left\{\frac{k^2(1/\delta_c - \eta)^2 + \xi^2}{(1 + \eta^2 - \xi^2)^2 + 4\xi^2\eta^2}\right\}^{1/2} \quad \ldots\ldots\ldots\ldots\ldots\ldots (2.2)$$

where

$$k = \tfrac{1}{2}(1 - e^x)$$

The right-hand side of equation (2.2) shows that as long as ξ is constant the maximum value of $|\dot{\phi}|$ is attained at an electron-density level where $\eta = 0$. Thus,

$$|\dot{\phi}|_{\eta=0} = \frac{\lambda}{4\pi l}\left\{\frac{k^2/\delta_c^2 + \xi^2}{(1 - \xi^2)^2}\right\}^{1/2} \quad \ldots\ldots\ldots\ldots\ldots\ldots (2.3)$$

It may be seen that, even when ξ is assumed to vary within a layer, $|\dot{\phi}|$ becomes maximum at a level very near to one where $\eta = 0$. Equation (2.3) shows that $|\dot{\phi}|_{\eta=0}$ becomes extremely large as ξ tends to one, but is zero when ν_c is zero or infinity (at the poles or the equator). To illustrate the variation of the coupling factor with propagation angle Θ, in both E and F layers, the following parameters may be assumed:

E layer (100 km)—$f = 3$ Mc/sec, $l = 10$ km, $N_{\max} = 1.5 \times 10^5$, $\nu = 10^6$/sec

F layer (300 km)—$f = 8$ Mc/sec, $l = 70$ km, $N_{\max} = 1.5 \times 10^6$, $\nu = 10^3$/sec

and the earth being considered as a uniformly magnetized sphere of moment 8.19×10^{25} cgs units.

A study of the curves (Figs. 1 and 2) showing the variations of $|\dot{\phi}|_{\eta=0}$ with Θ for E and F layers reveals that at stations of low and intermediate geomagnetic latitudes, the value of the coupling term in E layer is higher than that in the F layer. Hence, for a comparative study of the values of $|\dot{\phi}|$, $|\ddot{\phi}|$, $|q_o^2|$, $|q_e^2|$, it is sufficient to consider the case of propagation at a place of low magnetic dip like Calcutta (dip = 31° 45′) in E layer on the basis of a Chapman distribution of electron density and an exponential distribution of collision frequency. The values

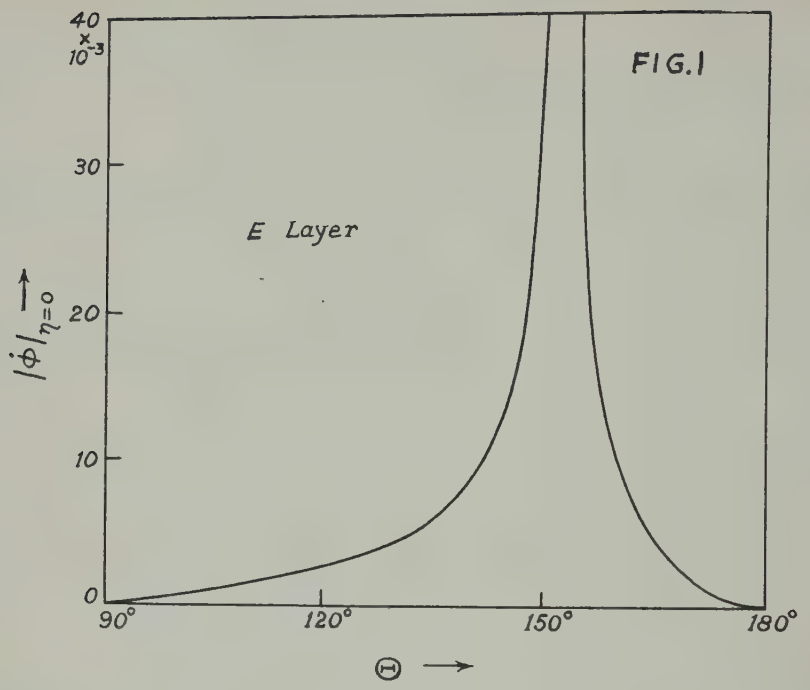

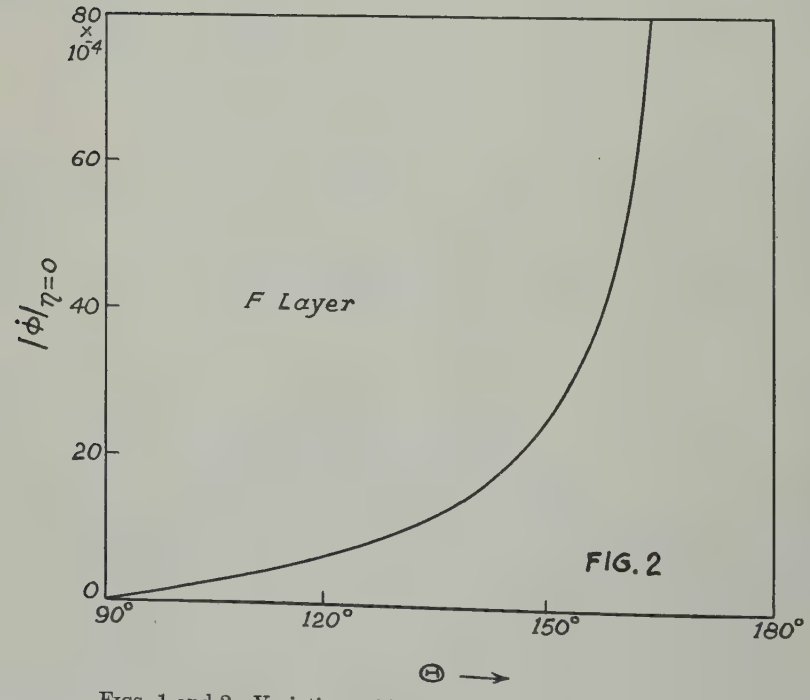

FIGS. 1 and 2—Variations of $|\dot{\phi}|$ with Θ for E and F layers

$|\ddot{\phi}|$, $|q_o^2|$, and $|q_e^2|$, when expressed in terms of ξ and η, are given by the following expressions:

$$\left.\begin{aligned} |\ddot{\phi}| &= \sqrt{A^2 + B^2} \\ |q_o^2| &= \sqrt{\frac{K_o^2 + L_o^2}{M_o^2 + N_o^2}} \\ |q_e^2| &= \sqrt{\frac{K_e^2 + L_e^2}{M_e^2 + N_e^2}} \end{aligned}\right\} \quad \ldots\ldots\ldots\ldots\ldots\ldots\ldots\ldots (2.4)$$

where

$$A = \frac{1}{2}\frac{\{(1-\xi^2+\eta^2)^2 - 4\xi^2\eta^2\}C + 4\xi\eta(1-\xi^2+\eta^2)D}{\{(1-\xi^2+\eta^2)^2 + 4\xi^2\eta^2\}^2}$$

$$B = \frac{1}{2}\frac{\{(1-\xi^2+\eta^2)^2 - 4\xi^2\eta^2\}D - 4\xi\eta(1-\xi^2+\eta^2)C}{\{(1-\xi^2+\eta^2)^2 + 4\xi^2\eta^2\}^2}$$

$$C = (1-\xi^2+\eta^2)\ddot{\eta} - 2\xi\eta\ddot{\xi} - 2\dot{\eta}(\eta\dot{\eta} - \xi\dot{\xi}) + 2\dot{\xi}(\xi\dot{\eta} + \xi\eta)$$

$$D = (1-\xi^2+\eta^2)\ddot{\xi} + 2\xi\eta\ddot{\eta} - 2\dot{\xi}(\eta\dot{\eta} - \xi\dot{\xi}) - 2\dot{\eta}(\xi\dot{\eta} + \xi\eta)$$

$$\ddot{\xi} = \frac{c^2}{p^2 l^2}\cdot\xi, \qquad \ddot{\eta} = \frac{c^2}{2p^2 l^2}\left[e^x - \frac{(1-e^x)^2}{2}\right]\left(\frac{1}{\delta_e} - \eta\right)$$

$$K_o = \eta^2 - \xi^2 - \frac{2\omega_z^2}{\omega_x^2}(1-E)$$

$$M_o = \frac{\eta p}{\nu_c} - \xi^2 - \frac{2\omega_z^2}{\omega_x^2}(1-E)$$

$$L_o = 2\xi\eta + \frac{2\omega_z^2}{\omega_x^2}F$$

$$N_o = \xi\eta + \frac{\xi p}{\nu_c} + \frac{2\omega_z^2}{\omega_x^2}\cdot F$$

$$K_e = \eta^2 - \xi^2 - \frac{2\omega_z^2}{\omega_x^2}(1+E)$$

$$M_e = \frac{\eta p}{\nu_c} - \xi^2 - \frac{2\omega_z^2}{\omega_x^2}(1+E)$$

$$L_e = 2\xi\eta - \frac{2\omega_z^2}{\omega_x^2}F$$

$$N_e = \xi\eta + \frac{\xi p}{\nu_c} - \frac{2\omega_z^2}{\omega_x^2}\cdot F$$

$$E = \frac{1}{\sqrt{2}}[\{(\xi^2+\eta^2)^2 - 2\xi^2 + 2\eta^2 + 1\}^{1/2} + (1-\xi^2+\eta^2)]^{1/2}$$

$$F = \frac{1}{\sqrt{2}}[\{(\xi^2+\eta^2)^2 - 2\xi^2 + 2\eta^2 + 1\}^{1/2} - (1-\xi^2+\eta^2)]^{1/2}$$

With the help of equations (2.2) and (2.4), curves (Figs. 3 and 4) depicting the variations of $|\dot{\phi}|$, $|\ddot{\phi}|$, $|q_o^2|$, and $|q_e^2|$, with the reduced height x in the E layer, have been drawn with $f = 3$ Mc/sec, $\nu_c = 4.112 \times 10^6$/sec, $\nu_0/\nu_c = 0.1$, $N_{max} = 1.5 \times 10^5$, and $l = 10$ km.

It will be apparent from a scrutiny of these curves that the maximum values of $|\dot{\phi}|$ and $|\ddot{\phi}|$ in the layer are negligibly small in comparison to the minimum values of $|q_o^2|$ or $|q_e^2|$.* Thus, for all stations of low and intermediate geomagnetic latitudes and also the poles (where $|\dot{\phi}| = 0$), the terms involving $\dot{\phi}$ and $\ddot{\phi}$ in equation (1.1) can be neglected in comparison to q_o^2 and q_e^2. Hence, the fundamental equations of propagation of the waves take the simplified form

$$\left.\begin{aligned} \frac{d^2V}{du^2} + q_o^2 V &= 0 \\ \frac{d^2W}{du^2} + q_e^2 W &= 0 \end{aligned}\right\} \quad \ldots\ldots\ldots\ldots\ldots\ldots\ldots\ldots (2.5)$$

These equations show that the incident wave is split into two waves V (the o-wave) and W (the x-wave), and they propagate independently of each other in the ionosphere with the refractive indices q_o and q_e, respectively.

The general solution of the equation pair (2.5) can be written in the form

$$\left.\begin{aligned} V &= (E_x + i\rho_1 E_y)/\sqrt{1 + \rho_1^2} = e^{ipt} \cdot f_V(z) \\ W &= (E_x + i\rho_2 E_y)/\sqrt{1 + \rho_2^2} = e^{ipt} \cdot f_W(z) \end{aligned}\right\} \quad \ldots\ldots\ldots\ldots (2.6)$$

Since ρ_1 and ρ_2 are functions of z, the equation pair (2.6) gives

$$\left.\begin{aligned} E_x + i\rho_1 E_y &= e^{ipt} \cdot F_V(z) \\ E_x + i\rho_2 E_y &= e^{ipt} \cdot F_W(z) \end{aligned}\right\} \quad \ldots\ldots\ldots\ldots\ldots\ldots (2.7)$$

But $\rho_1 \cdot \rho_2$ being equal to -1, the following expressions for ρ_1 and ρ_2 can be written:

$$\left.\begin{aligned} i\rho_1 &= Re^{i\alpha} = iG\{1 - \sqrt{1 + 1/G^2}\} \\ i\rho_2 &= R^{-1}e^{-i\alpha} = iG\{1 + \sqrt{1 + 1/G^2}\} \end{aligned}\right\} \quad \ldots\ldots\ldots\ldots (2.8)$$

From (2.8), after some simplification, the following relations giving R and α may be obtained:

$$\left(\frac{\xi}{\zeta^2}\right)^2 \cdot \left(\frac{2R}{1 + R^2}\right)^2 + \left(\frac{\eta}{\zeta^2}\right)^2 \cdot \left(\frac{2R}{1 - R^2}\right)^2 = 1 \quad \ldots\ldots\ldots\ldots (2.9)$$

$$\frac{(\xi/\zeta^2)^2}{\cos^2\alpha} - \frac{(\eta/\zeta^2)^2}{\sin^2\alpha} = 1 \quad \ldots\ldots\ldots\ldots\ldots\ldots (2.10)$$

where $\zeta^2 = \xi^2 + \eta^2$

*It is worth while to point out that at stations like Calcutta, $|\dot{\phi}|_{max}$ becomes of the same order as that of $|q_o^2|_{min}$ or $|q_e^2|_{min}$ when the wave-length of the incident wave exceeds 300 metres; hence, the terms involving the coupling factor cannot be neglected for frequencies less than 1 Mc/sec.

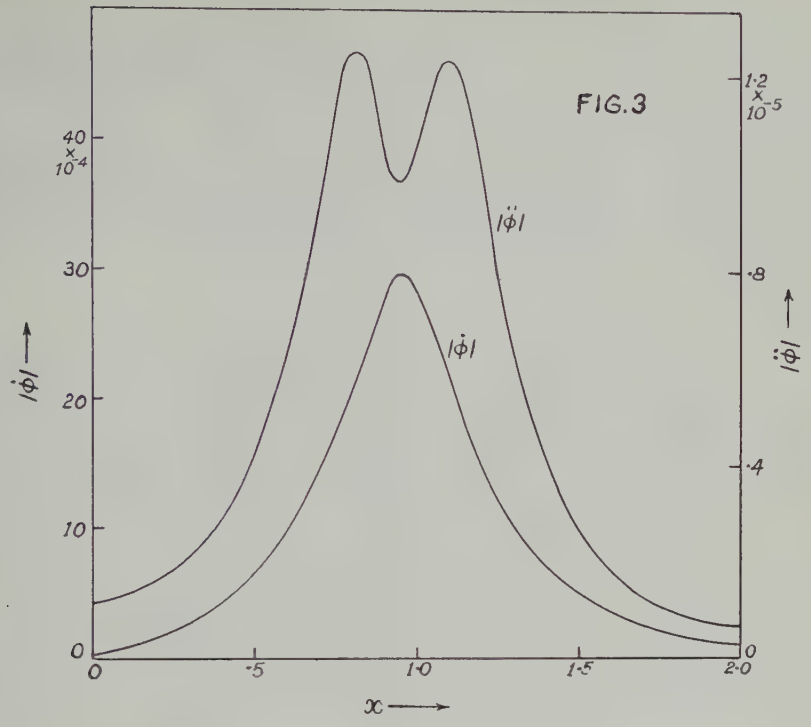

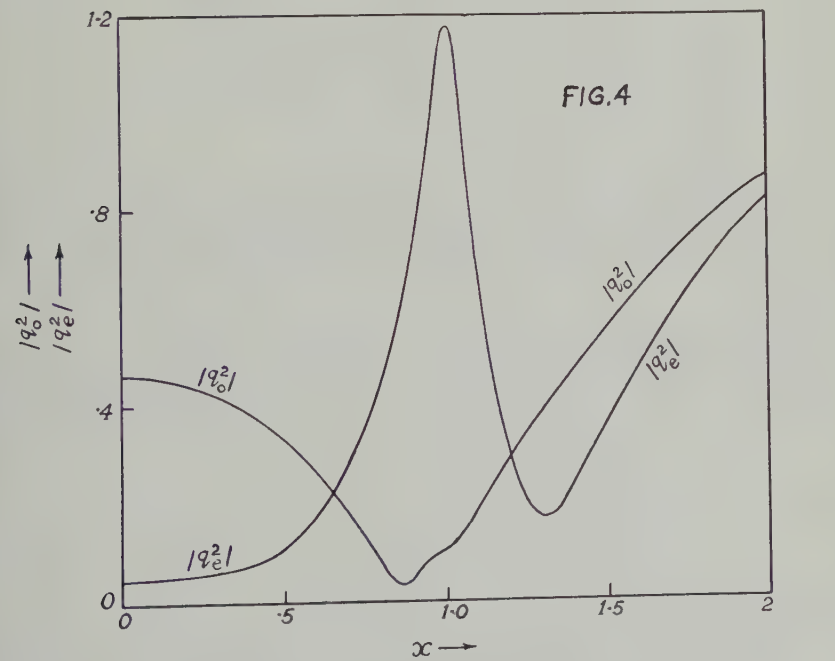

FIGS. 3 and 4—Variations of $|\dot{\phi}|$, $|\ddot{\phi}|$, $|q_o^2|$, and $|q_e^2|$ with reduced height x in the E layer

It may be noted that equations (2.9) and (2.10) remain unchanged if $1/R$ is substituted for R, and $-\alpha$ for α, respectively. Thus, corresponding to any value of ξ and η, in the ξ-η plane, the values of R and α cannot be determined uniquely. The ambiguity arises due to the fact that $(1 + 1/G^2)^{1/2} = \{(1 - \xi^2 + \eta^2) - 2i\xi\eta\}^{1/2}$ in (2.8) is a double-valued function, and it can be removed only after detailed discussions (Appendix) on the possible values of R and α in the ξ-η plane. For the northern hemisphere where $\xi > 0$, the unambiguous ranges of R and α for different values of ξ and η have been shown in Figure 5.

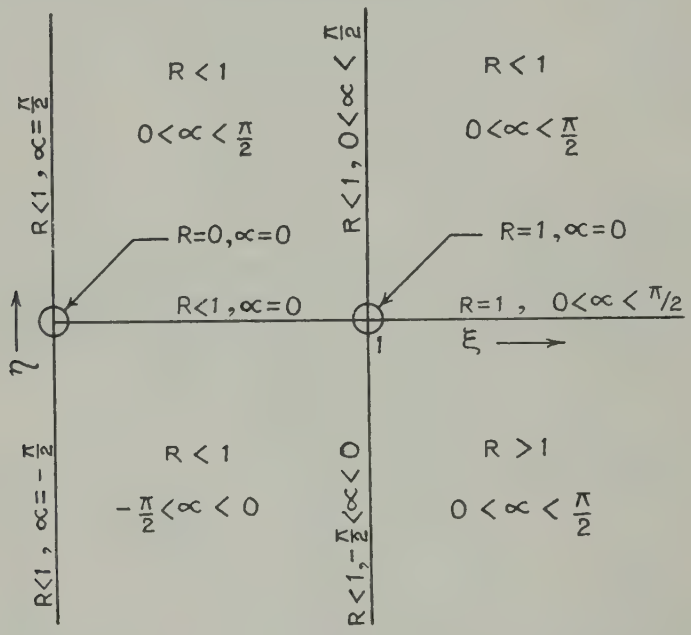

FIG. 5—Range of R and α in the ξ-η plane in northern hemisphere

§3. *Polarization*

Substituting the values of $i\rho_1$ and $i\rho_2$ from (2.8) in (2.7), the following expressions for the components of the electric vector of the o-wave can be written

$$\left.\begin{aligned} E_x^V &= \frac{C_V}{\sin\alpha}\cdot\sin(pt + \theta_V + \pi - \alpha) \\ E_y^V &= \frac{C_V}{R\sin\alpha}\cdot\sin(pt + \theta_V) \end{aligned}\right\} \qquad \text{.....(3.1)}$$

where

$$C_V = \sqrt{A_V^2 + B_V^2}\,, \qquad \theta_V = \tan^{-1}(B_V/A_V)$$

$$A_V = Re\{F_V(z)\}, \qquad B_V = Im\{F_V(z)\}$$

he phase difference between the component electric vectors E_x^V and E_y^V is thus $r - \alpha$). Similarly, for the x-wave, we have

$$\left.\begin{aligned} E_x^W &= \frac{C_W}{\sin\alpha}\sin(pt + \theta_W + \alpha) \\ E_y^W &= \frac{RC_W}{\sin\alpha}\sin(pt + \theta_W + \pi) \end{aligned}\right\} \quad \ldots\ldots(3.2)$$

here

$$C_W = \sqrt{A_W^2 + B_W^2}\,, \qquad \theta_W = \tan^{-1}(B_W/A_W)$$
$$A_W = Re\{F_W(z)\}, \qquad B_W = Im\{F_W(z)\}$$

nd the phase difference between E_x^W and E_y^W is $(\alpha - \pi)$. The equation pairs (3.1) nd (3.2) yield the following equations for the ellipses described by the component lectric vectors of the o- and x-waves:

$$\left.\begin{aligned} E_x^{V^2} + 2R\cos\alpha E_x^V E_y^V + R^2 E_y^{V^2} &= C_V^2 \\ E_x^{W^2} + 2R^{-1}\cos\alpha E_x^W E_y^W + R^{-2} E_y^{W^2} &= C_W^2 \end{aligned}\right\} \quad \ldots\ldots(3.3)$$

he axes of these polarization ellipses are inclined to the x-axis, that is, the NS-axis hrough an angle ψ (measured in the anticlockwise direction) given by

$$\left.\begin{aligned} \tan 2\psi^V &= \frac{2R\cos\alpha}{1 - R^2} \\ \tan 2\psi^W &= -\frac{2R\cos\alpha}{1 - R^2} \end{aligned}\right\} \quad \ldots\ldots(3.4)$$

quation (3.4) gives a pair of values for ψ^V (and ψ^W), which are evidently the tilt-ngles of the major and minor axes with the x-axis. But it can be shown from these quations that the expression for the tilt-angle made by the major axis of the liptic pattern with the x-axis, is for the o-wave,

$$\tan\psi_{\text{major}}^V = -\frac{1 - R^2 + \sqrt{(1 - R^2)^2 + 4R^2\cos^2\alpha}}{2R\cos\alpha} \quad \ldots\ldots(3.5)$$

nd that for the x-wave

$$\tan\psi_{\text{major}}^W = \frac{1 - R^2 - \sqrt{(1 - R^2)^2 + 4R^2\cos^2\alpha}}{2R\cos\alpha} \quad \ldots\ldots(3.6)$$

nd hence

$$\tan\psi_{\text{major}}^V \cdot \tan\psi_{\text{major}}^W = 1 \quad \ldots\ldots(3.7)$$

hich gives

$$\psi_{\text{major}}^V + \psi_{\text{major}}^W = (2n + 1)\frac{\pi}{2} \quad \ldots\ldots(3.8)$$

For the northern hemisphere, it has already been shown (Fig. 5) that α always lies between zero and $\pm \pi/2$. Immediately the range of values for ψ^{W}_{major} or ψ^{V}_{major} becomes uniquely determined,* namely,

$$\pi/2 < \psi^{V,W}_{\text{major}} < \pi \quad \ldots\ldots\ldots\ldots\ldots\ldots\ldots\ldots (3.9)$$

So the major axes of both o- and x-ellipses lie in the same N-E quadrant. Combining the relation (3.9) with the equation (3.8), it follows that

$$\psi^{V}_{\text{major}} + \psi^{W}_{\text{major}} = 3\pi/2 \quad \ldots\ldots\ldots\ldots\ldots\ldots\ldots\ldots (3.10)$$

which shows that the major axes of the polarization ellipses of the two split waves are never perpendicular to each other (Aden, DeBettencourt, and Waterman, 1950) unless $\psi^{V}_{\text{major}} = \pi/2$ or π.

It may be pointed out that the ellipses having the tilt-angles ψ and $(\psi + \pi)$ are one and the same; so the values of ψ which lie in the range $0 \leq \psi \leq \pi$ need only be considered.

The direction of rotation in the polarization pattern is determined uniquely by the value of the phase difference (Appleton and Ratcliffe, 1928). As long as the phase difference ϵ lies between 0 and π, the direction of rotation is anticlockwise; and when the phase difference lies between 0 and $-\pi$, the rotation is clockwise. It has been shown earlier that for the o-wave, $\epsilon = (\pi - \alpha)$, and for the x-wave, $\epsilon = (\alpha - \pi)$. Hence, the sense of rotation for the o- and x-waves corresponding

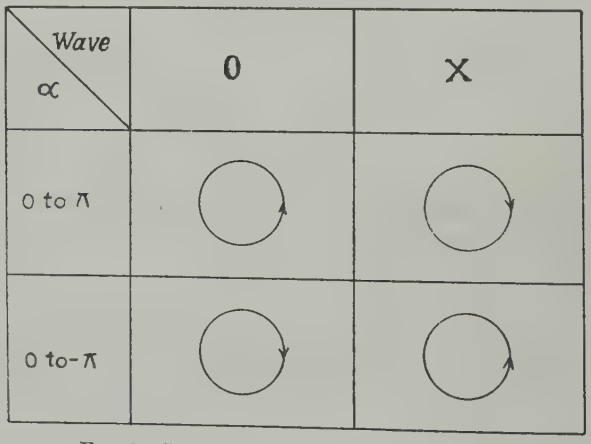

FIG. 6—Sense of rotation of o- and x-waves

to different values of α can be determined as illustrated in the diagram (Fig. 6). Whenever $\alpha = 0$ or π, the polarization of either wave is linear. The ratio of minor to major axes of the polarization ellipse, designated by $\tan \theta$, is given by the expression

*As long as $\xi < 1$, we have $R \leq 1$ and α lies between 0 and $\pm\pi/2$; under these conditions, equations (3.5) and (3.6) indicate that ψ^{V}_{major} lies in the range $\pi/2 \leq \psi^{V}_{\text{major}} \leq 3\pi/4$, and ψ^{W}_{major} in the range $3\pi/4 \leq \psi^{W}_{\text{major}} \leq \pi$.

$$\left.\begin{aligned}\tan\theta &= \left\{\frac{1+R^2-\sqrt{(1+R^2)^2-4R^2\sin^2\alpha}}{1+R^2+\sqrt{(1+R^2)^2-4R^2\sin^2\alpha}}\right\}^{1/2} \\ &= \frac{1+R^2-\sqrt{(1+R^2)^2-4R^2\sin^2\alpha}}{2R\sin\alpha}\end{aligned}\right\} \quad \ldots\ldots\ldots(3.11)$$

Thus, the magnitude of the ratio of axes of both the waves at any particular oint of propagation is the same. The values of θ may be associated with the sense rotation in the following way: If $+\theta^V$ is a measure of the ratio of axes of the llipse which has an anticlockwise sense of rotation, then $-\theta^W$ may be taken to present the ratio of axes of the x-ellipse having a clockwise sense of rotation. he values of θ^V and θ^W must always satisfy the relation

$$\theta^V = -\theta^W$$

A change in the sign of θ will mean that the wave suffers a change of sense of tation, namely, anticlockwise to clockwise, or *vice versa*.

. *Polarization characteristics at Calcutta*

To determine the values of ψ^V and θ^V at any place, it is necessary to find the lues of R and α for different values of r. From equations (2.8), the following pressions can be readily derived:

$$R = \left|\left\{\frac{\xi\tan\alpha-\eta}{\xi\tan\alpha+\eta}\right\}^{1/2}\right| \quad \ldots\ldots\ldots\ldots\ldots\ldots(4.1)$$

$$\cos 2\alpha = \frac{1}{\xi^2} - \sqrt{1+\frac{2}{\xi^2}\cos 2\gamma+\frac{1}{\xi^4}} \quad \ldots\ldots\ldots\ldots\ldots(4.2)$$

Thus, corresponding to some graded values of λ and ν, the values of R and α n be determined, provided the ranges possible for them in the ξ-η plane as shown Figure 5 are kept in view. Immediately the respective values of ψ^V_{major} and θ^V can evaluated with the help of equations (3.5) and (3.11).

Curves (Figs. 7 and 8) depicting the variations of ψ^V_{major} and θ^V for increasing lues of r (and hence N) have been drawn for $\lambda = 100$ metres and 200 metres, and $= 0$, $1/2\ \nu_c$, and $2\nu_c$ (that is, $\xi = 0$, 0.5, and 2). For $\nu < \nu_c$, $\Theta = \pi/4$, Martyn d plotted a set of curves. The difference between the curves of Martyn and those the authors is that the two sets differ in respect to the sign of θ^V. But in either case, e representative curves indicate that for $\nu < \nu_c$, the o-wave is elliptically polarized th its rotation in the anticlockwise direction; as the wave enters the ionosphere, ecomes linearly polarized at $r = 1$, and the character of the polarization becomes ckwise if the wave penetrates into regions of higher electron density. But when $> \nu_c$, the direction of rotation remains anticlockwise for all values of N.

It will be apparent from the values of ψ^V_{major} in the curves (Figs. 7 and 8) that ajor lies in the same range $\pi/2 < \psi^V_{\text{major}} < \pi$ (that is, the major axis of the o-wave s in the same N-E quadrant), irrespective of the wave frequency, electron density, d the collision frequency. Further, the effect of the collision on the downcoming

*The case when $\xi = 1$, that is, $\nu = \nu_c$, is not taken into account, since $|\phi|_{\eta=0}$ becomes infinity l it cannot therefore, be neglected in comparison to q_o^2 or q_e^2.

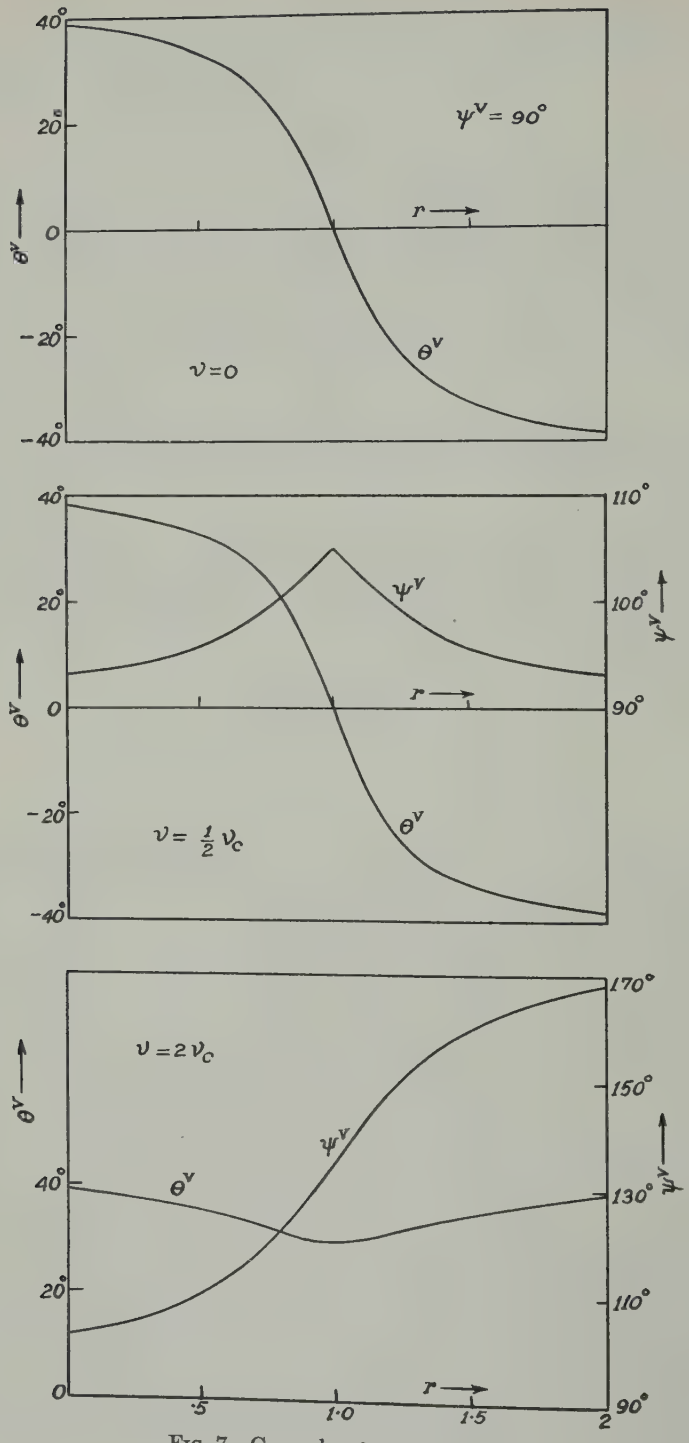

FIG. 7—Case when $\lambda = 100$ metres

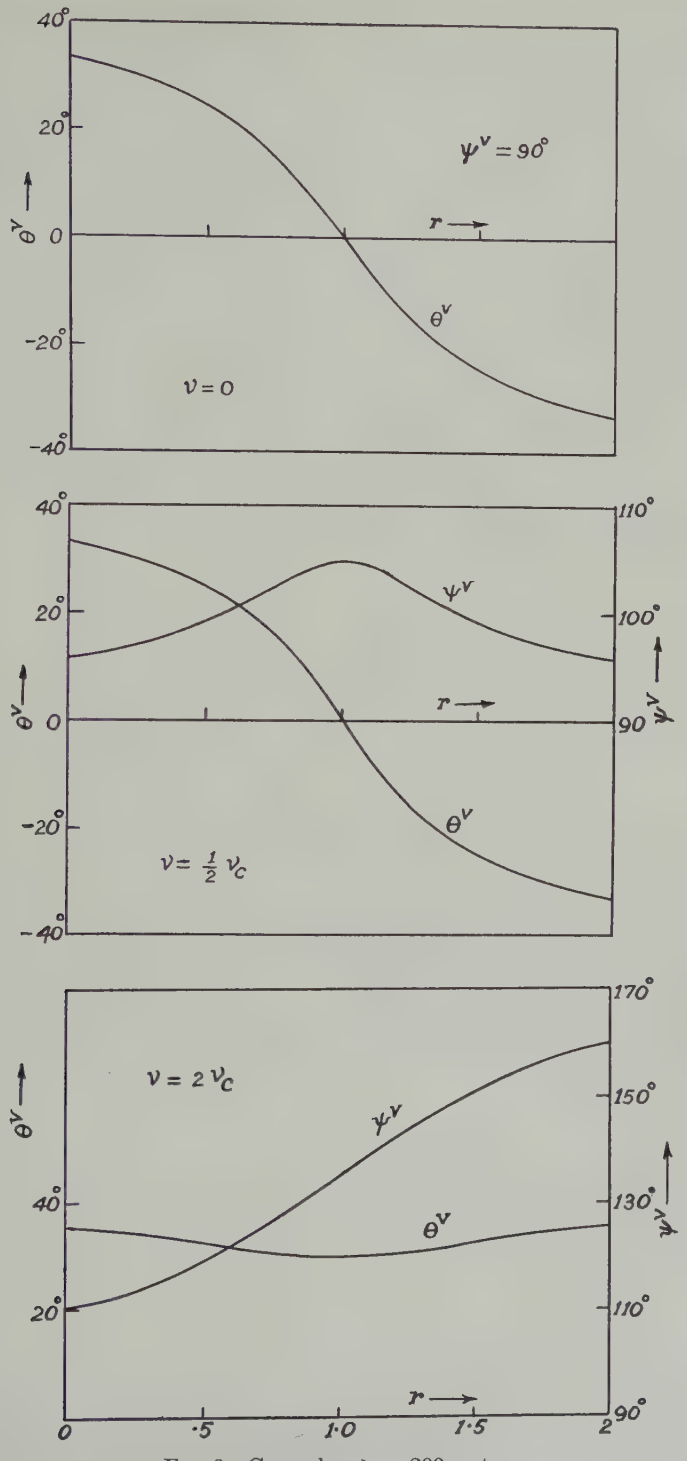

FIG. 8—Case when $\lambda = 200$ metres

wave is to increase the ratio of axes of the polarization ellipse, whereas an increase in wave-length decreases the ratio; the tilt-angle ψ^{V}_{major} increases for increase in collision and wave-length.

In the southern hemisphere, ν_c is negative; the negative values of η, therefore, correspond to values of r less than one. Following the same arguments as in the

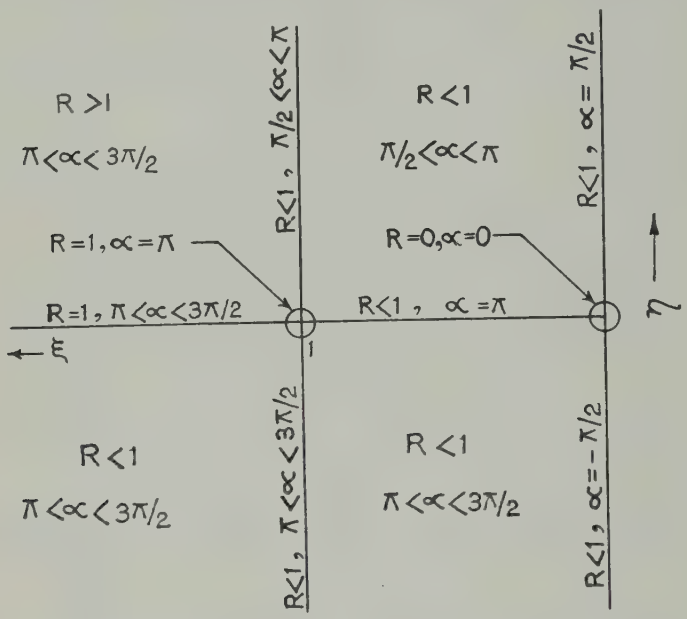

FIG. 9—Range of R and α in the ξ-η plane in southern hemisphere

case of the northern hemisphere, the possible ranges of values of R and α in the ξ-η plane can be determined (Fig. 9). These ranges of R and α may be utilized along with equations (3.5) and (3.11) for finding out the polarization characteristics θ^{V} and ψ^{V}_{major} for southern latitudes. The sense of rotation of the downcoming waves will be clockwise and anticlockwise for the o- and x-waves, respectively. The major axes of both the polarization ellipses will lie in the same N-W quadrant, the sum of their tilt-angles ($\psi^{V}_{\text{major}} + \psi^{W}_{\text{major}}$) being equal to $\pi/2$.

§5. *Limiting polarization and collision frequency*

The limiting polarization of the downcoming waves is believed to be determined at the lower part of the ionosphere where the electron density is small. Booker (1936) showed that this critical level lies at a region where the following relation for the split waves holds:

$$| q_o - q_e | \simeq | \dot{q}_o | \quad \text{or} \quad | \dot{q}_e |$$

Budden (1952) from considerations of approximate solutions of the coupled wave equations showed that for frequencies greater than 1 Mc/sec, incident on a Chapman region, the value of the coupling coefficient determining the limiting polarization is given by

$$|\dot{\phi}|^2 \simeq \tfrac{1}{4}\,|\,q_o - q_e\,|^2$$

and for frequencies less than 500 kc/sec,

$$|\dot{\phi}|^2 \simeq \tfrac{1}{2}\,|\,\dot{q}_o - \dot{q}_e\,|$$

But for stations of low magnetic dip where the coupling between the two waves is negligible, the polarization characteristics of the downcoming wave no longer depend on the coupling factor ϕ. The limiting polarization of the waves would still correspond to some region of the ionized layer from which they have been reflected or through which they have propagated. The analysis of the polarization characteristics as developed in the earlier sections is perfectly general and it holds for any point in the ionosphere; hence, it is possible to identify the region in the ionosphere to which the polarization characteristics of the downcoming waves correspond—from the data of the experimentally recorded polarization patterns.

Rewriting the expressions for the ratio of axes as

$$x = \tan\theta = \left\{\frac{1 + R^2 - \sqrt{1 + 2R^2\cos 2\alpha + R^4}}{1 + R^2 + \sqrt{1 + 2R^2\cos 2\alpha + R^4}}\right\}^{1/2} \qquad (5.1)$$

and substituting

$$y = \frac{2R\cos\alpha}{1 - R^2} \qquad (5.2)$$

(which shows $y = \tan 2\psi^V$ for o-wave and $y = -\tan 2\psi^W$ for x-wave), the following relations for R and α can be deduced:

$$R = \left\{\frac{\sqrt{1 + y^2}(1 + x^2) - (1 - x^2)}{\sqrt{1 + y^2}(1 + x^2) + (1 - x^2)}\right\}^{1/2} \qquad (5.3)$$

$$\cos\alpha = \frac{y(1 - x^2)}{[(1 + y^2)(1 + x^2)^2 - (1 - x^2)^2]^{1/2}} \qquad (5.4)$$

No ambiguity arises about the value of α, since it may be recalled that as long as the wave does not penetrate the layer α lies between 0 and $\pi/2$. From the values of R and α, the values of γ and ζ^2 are obtained from equations (4.1) and (2.10), which may be rewritten as

$$\tan\gamma = \frac{\xi}{\eta} = \frac{1 + R^2}{1 - R^2}\cot\alpha \qquad (5.5)$$

$$\zeta^2 = -\frac{2(\cos 2\alpha + \cos 2\gamma)}{\sin^2 2\alpha} \qquad (5.6)$$

Hence, the values of r and ν can be determined from

$$\left.\begin{aligned}\eta &= (1 - r)p/\nu_e = \zeta\cos\gamma\\ \xi &= \nu/\nu_e = \eta\tan\gamma\end{aligned}\right\} \qquad (5.7)$$

It should be pointed out that, if the limiting polarization is determined at a level where the electron density is small, the analysis of the polarization character-

istics of the downcoming waves should yield a value of η which corresponds to a small value of r.

§6. *Experimental studies*

For the experimental study of the polarization patterns of the downcoming waves, a radio polarimeter adopting the method of echo-selection—evolved by Eckersley and Farmer (1945)—has been in use. The polarimeter utilizes a crossed pair of tuned loop antennae, oriented in the NS and EW directions, two wide-band receivers (band-width 50 kc/sec), and an indicator oscilloscope. Each of the receiving systems is adjusted for identical phase and amplification. The echoes are selected by means of a delayed gate generator, which provides a positive square wave pulse of duration 8 μsecs to itensify the CRO beam. This delay of the intensifying gate from the transmitter pulse can be adjusted over an interval 0.4 to 4 milliseconds. The transmitter radiates by means of a vertical delta antenna, terminated at the top—R/F pulses of duration 25 μsecs—and the echoes are displayed on a raster time-base (Banerjee and Roy, 1950) of 12 lines. Each line

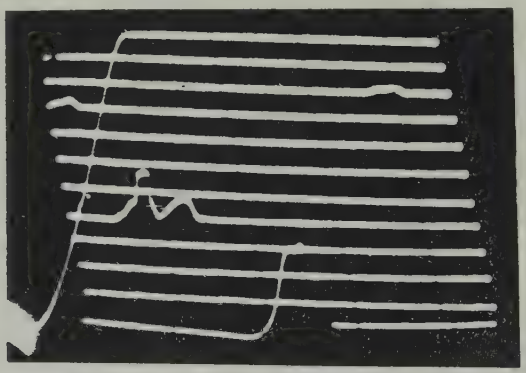

PLATE I—Illustrating selection of x-echo when its separation from the o-echo was only 5 km

corresponds to 50 km of equivalent height and is executed from right to left. With the help of this sounding equipment (Banerjee and Roy, 1952), it is possible to separate the magneto-ionic components completely from each other and also from the echoes arising out of back-scattering from electron clouds (Roy and Verma, 1953). Any of these echoes may be selected by the delayed gate generator for the display of their polarization patterns on the CRO of the polarimeter. Plate I illustrates how the x-echo had been selected when its separation from the o-echo was only 5 km. It may be pointed out that with the conventional equipments the selection of echoes with such a small separation between them is not possible. The high resolution afforded by the equipment facilitated the delineation of the true polarization patterns of the individual echoes.

Experimental observations, during both day and night for a period of 15 months—January 1954 to March 1955—showed that all the reflected waves from both E and F layers are, in general, elliptically polarized. The major axes of these elliptic patterns mostly lie in N-E quadrant, but on occasions they have also been

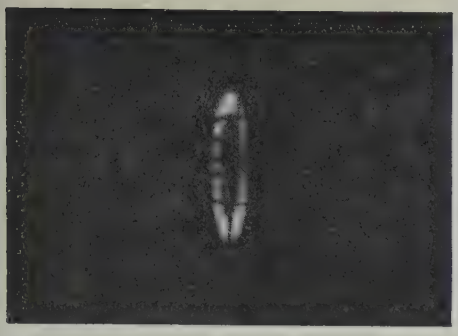

PLATE II—The *o*-ellipse

PLATE III—The *x*-ellipse

observed to be oriented in N-W quadrant. The *o*-ellipse (Plate II) due to *F*-layer reflection has been found most frequently to have a tilt-angle ψ^V_{major} lying between 90° and 92° (Fig. 10), whereas the pattern of the *x*-echo (Plate III) from the same layer has ψ^W_{major} lying generally in the neighborhood of 176° (Fig. 11). The *o*-ellipses due to *E*-layer reflections frequently show a tilt-angle lying between 100° and 104° (Fig. 12), but the *x*-ellipses show a wider scatter in the value of their tilt-angles (Fig. 13) than those for the *F*-layer. It may be noted, however, that the most frequent values of ψ^V_{major} and ψ^W_{major} in the patterns are in the ranges

$$\pi/2 \leq \psi^V_{\text{major}} \leq 3\pi/4 \quad \text{and} \quad 3\pi/4 \leq \psi^W_{\text{major}} \leq \pi$$

and their sum $(\psi^V_{\text{major}} + \psi^W_{\text{major}})$ is approximately equal to $3\pi/2$, as deduced earlier.

The patterns of the *o*- and *x*-waves were most frequently found to have a ratio of axes lying between 0.22 to 0.30 and 0.42 to 0.5 for *F*-layer reflections (Figs. 14 and 15) and between 0 to 0.1 and 0.38 to 0.46 for *E*-layer reflections (Figs. 16 and 17). The ratio of axes for *x*-ellipse was always observed to be greater than that for the *o*-ellipse for reflections from any of the layers.

§7. *The collision frequency and the electron concentration*

The formulae for the determination of the collision frequency and the electron concentration from the data of the polarization patterns of the echoes were developed in §5. The application of these formulae (5.1 to 5.6) can now be illustrated with the following data, which may be considered to be typical in view of the histograms given in Figures 10 to 17.

Patterns for F-layer reflections observed at 4.22 *Mc/sec*

$$o\text{-ellipse}, \; x = 0.26, \qquad \psi^V_{\text{major}} = 92° \tag{a}$$

$$x\text{-ellipse}, \; x = 0.46, \qquad \psi^W_{\text{major}} = 176° \tag{b}$$

Patterns for E-layer reflections observed at 3.1 *Mc/sec*

$$o\text{-ellipse}, \; x = 0.02, \qquad \psi^V_{\text{major}} = 102° \tag{c}$$

$$x\text{-ellipse}, \; x = 0.42, \qquad \psi^W_{\text{major}} = 162° \tag{d}$$

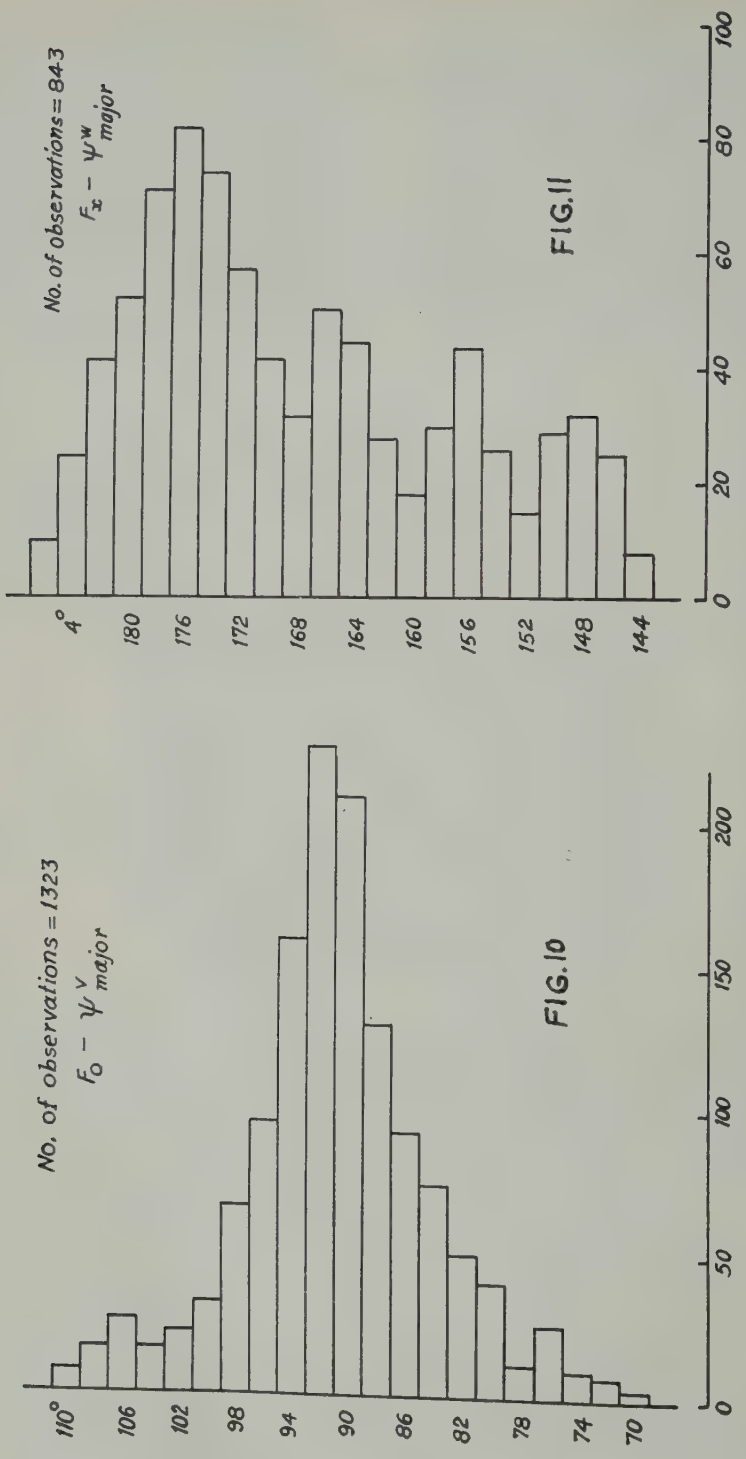

FIGS. 10 and 11—Tilt-angles of o- and x-ellipses, respectively, for F-layer reflections

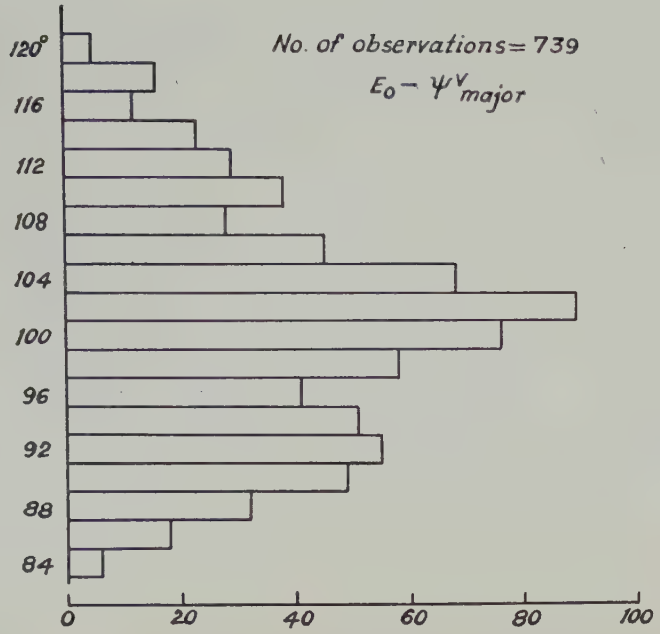

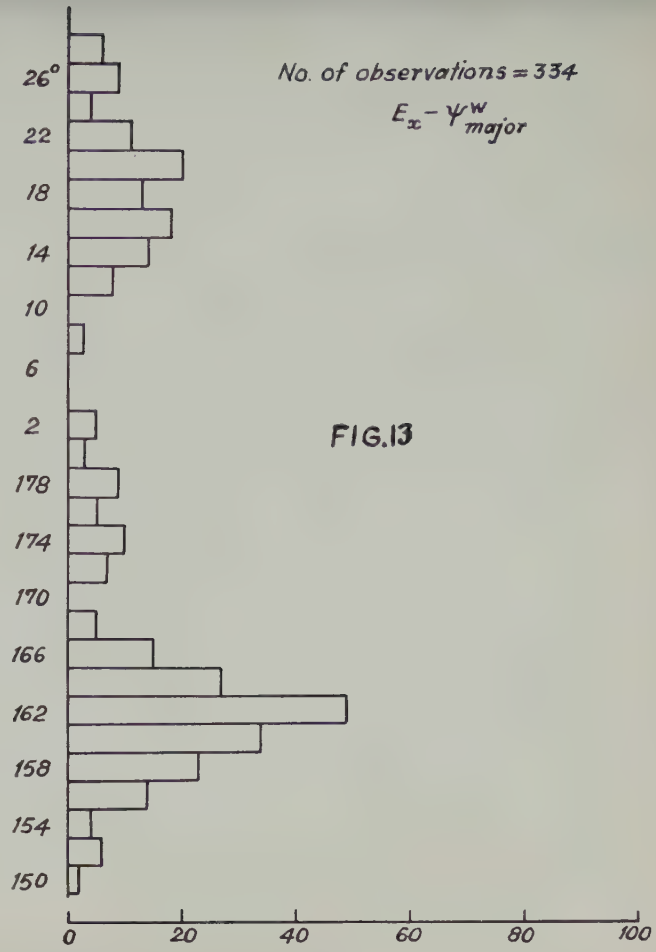

FIGS. 12 and 13—Tilt-angles of *o*- and *x*-ellipses, respectively, for *E*-layer reflections

FIG. 14

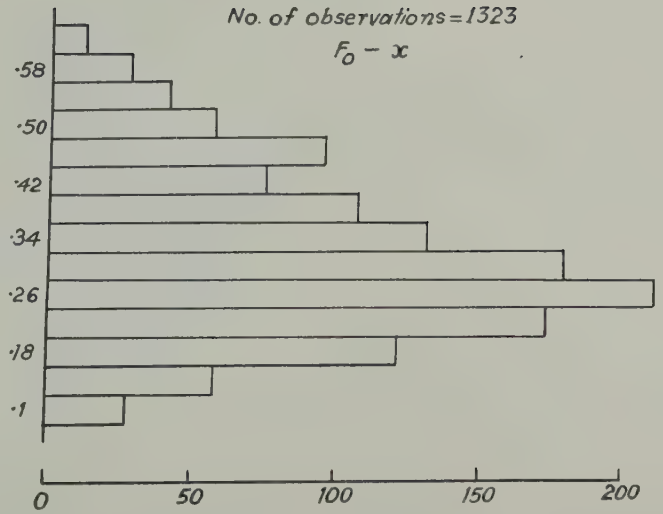

FIG. 15

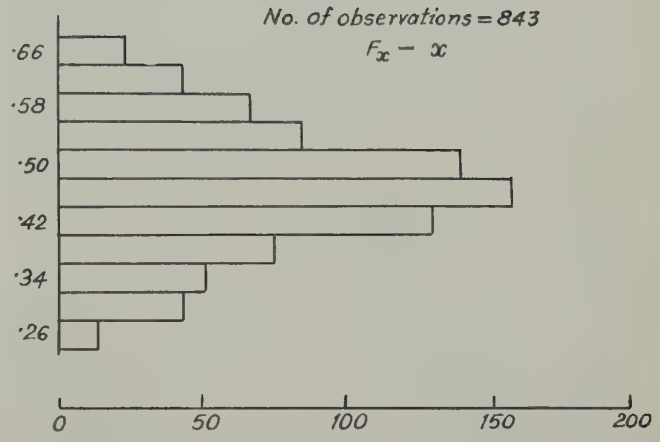

FIGS. 14 and 15—Ratios of axes of o- and x-waves for F-layer reflections

FIG. 16

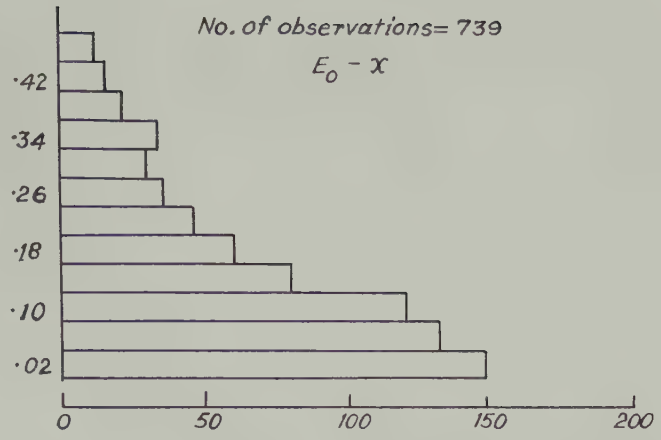

FIG. 17

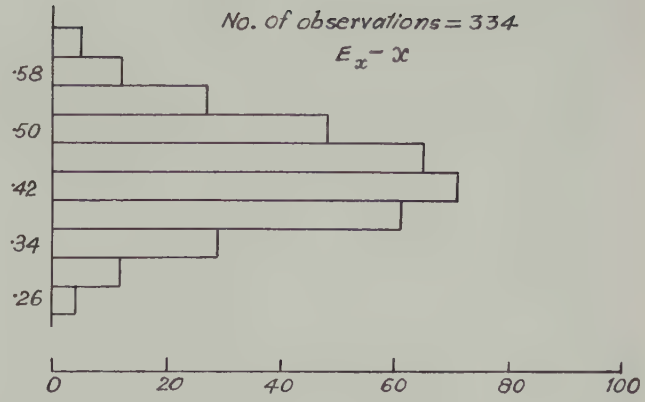

FIGS. 16 and 17—Ratios of axes of *o*- and *x*-waves for *E*-layer reflections

Taking $\nu_c = 3.753 \times 10^6$/sec at F layer (300 km), we get for the case (a), $R = 0.2622$, $\alpha = 82° 53'$. Then, $\tan\gamma = 0.1434$, $\xi^2 = 0.3207$. Hence, $\xi = 0.08037$, $\eta = 0.5606$. But, $\eta = (1 - r)p/\nu_c$ and $\xi = \nu/\nu_c$. Thus, we obtain

$$r = 0.92, \nu = 3.016 \times 10^5/\text{sec}.$$

Similarly, for the case (b), $r = 0.84$, $\nu = 8.054 \times 10^5$/sec. Repeating the same process for patterns of the o- and x-waves from E layer and taking ν_c at E layer (100 km) to be 4.112×10^6, we get for the case (c)

$$r = 0.9966, \qquad \nu = 1.706 \times 10^6/\text{sec}$$

and for the case (d),

$$r = 0.83, \qquad \nu = 3.448 \times 10^6/\text{sec}$$

It may be noted that the value of the collision frequency estimated for the E layer agrees well with the results of other workers, specially of Shaw (1951), who from his experiments on the cross-modulation of the waves in E region found the value of ν to lie between 1.48×10^6/sec to 2.96×10^6/sec. The magnitude of the collision frequency in F layer evaluated above seems to be abnormally high. It is worth while to point out that there is a limitation in this method of determining the collision frequency from the polarization characteristics of the echoes. A record of the elliptical pattern of the o-wave from F layer at 4.22 Mc/sec, having $\psi^V_{\text{major}} = 91°$ and $x = 0.28$, gives a value of $\nu = 1.56 \times 10^5$/sec, but for those patterns whose ψ^V_{major} lies between 90° and 91°, it is not practicable to measure the tilt accurately and hence the value of ν cannot be correctly estimated. Polarization patterns of the o-wave from F layer having a $\psi^V_{\text{major}} = 90°$ have frequently been recorded both during the day and night; they represent the cases when the collision frequency in F layer was below 10^5/sec, but cannot be analysed for the above-mentioned limitation inherent in the method.

In §5, it was pointed out that if the idea of a limiting region below the E layer, determining the final polarization characteristics of the downcoming waves, is true, then the value of the electron concentration evaluated from the above analysis of the polarization data should be small. The electron density in the limiting region being low, the value of r should be extremely small compared to its value corresponding to the critical electron densities of the waves. But contrary to the expected low value, the value of r corresponding to the o-ellipse is nearly unity and that for the x-ellipse is slightly smaller than unity. The ray-theory gives the reflection levels of the o- and x-waves as $r = 1$ and $r = 1 - p_h/p$ ($= 0.79$ in the F region when $f = 4.22$ Mc/sec). The exact reflection levels of the waves in an ionized region where collision cannot be neglected have not yet been determined and they may be different from the values given for the collision-free case. Nevertheless, the high values of r, evaluated from the data of the polarization patterns, definitely go against the concept of a limiting region below the E layer.

Further, if the emergent polarizations of the waves were solely determined by a low-lying region of small electron density, it is expected that the o- and x-waves should have identical ratio of axes. The experimental observations showed that the x-ellipse had, in general, a greater ratio of axes than the o-ellipse. At the reflection

level, the ratio of axes of the elliptical pattern of the x-wave is bigger than that of the o-wave, since the x-wave is reflected from a comparatively lower electron-density level. Thus, it appears that the polarization characteristics of the down-coming waves correspond more to their reflection levels than any limiting region below the E layer.

§8. *Acknowledgment*

The authors are deeply indebted to Prof. M. N. Saha, D.Sc., F.R.S., for his keen interest and constant guidance. They are also grateful to Dr. A. K. Saha, D.Sc., and Dr. S. S. Baral, D.Sc., for their valuable suggestions.

References

Appleton, E. V., and J. A. Ratcliffe (1928); Proc. R. Soc., A, **117**, 576.
Aden, A. L., J. T. deBettencourt, and A. T. Waterman, Jr. (1950); J. Geophys. Res., **55**, 53.
Bailey, V. A. (1934); Phil. Mag., **18**, 516.
Banerjee, B. M., and R. Roy (1950); Indian J. Phys., **24**, 411.
Banerjee, B. M., and R. Roy (1952); Indian J. Phys., **26**, 473.
Booker, H. G. (1936); Proc. R. Soc., A, **155**, 235.
Budden, K. G. (1952); Proc. R. Soc., A, **215**, 215.
Eckersley, T. L., and F. T. Farmer (1945); Proc. R. Soc., A, **184**, 196.
Försterling, K. (1942); Hochfrequenztechnik u. Elektroakustik, **59**, 10.
Ghosh, S. P. (1938); Indian J. Phys., **12**, 341.
Kelso, J. M. (1953); J. Geophys. Res., **58**, 431.
Martyn, D. F. (1935); Phil. Mag., **19**, 376.
Roy, R., and J. K. D. Verma (1953); J. Geophys. Res., **58**, 473.
Rydbeck, O. E. H. (1944); Chalmer Tekn. Högsk. Handl., No. 34.
Saha, M. N., B. K. Banerjee, and U. C. Guha (1947); Indian J. Phys., **21**, 181.
Saha, M. N., B. K. Banerjee, and U. C. Guha (1951); Proc. Nat. Inst. Sci. India, **17**, 205.
Scott, J. C. W. (1953); J. Geophys. Res., **58**, 437.
Shaw, I. J. (1951); Proc. Phys. Soc., B, **64**, 1.
Taylor, M. (1934); Proc. Phys. Soc., B, **46**, 408.

Appendix

To obtain the unambiguous values of R and α in the ξ-η plane, it is necessary to discuss in detail the course of the double-valued function $(1 + 1/G^2)^{1/2}$ in the complex plane. In terms of ξ and η, the expression $(1 + 1/G^2)$ may be written as

$$1 + 1/G^2 = (1 - \xi^2 + \eta^2) - 2i\xi\eta$$

Confining the discussion to the case of propagation in the northern hemisphere, where $\xi > 0$, $Im\{1 + 1/G^2\} = -2\xi\eta$ is negative for $\eta > 0$. Hence, $(1 + 1/G^2)$ may lie in the third or fourth quadrant. So for $\eta > 0$, $(1 + 1/G^2)^{1/2}$ may lie in the second or fourth quadrant. Under these conditions, it may be shown that (*i*) when $(1 + 1/G^2)^{1/2}$ lies in the second quadrant, R is greater than one, and α lies in the range $3\pi/2 < \alpha < 2\pi$; (*ii*) when $(1 + 1/G^2)^{1/2}$ lies in the fourth quadrant, R is less than one, and α lies in the range $0 < \alpha < \pi/2$. But for $\xi = 0$, $\eta > 0$, it will be shown from the expression

$$i\rho_1 = Re^{i\alpha} = iG\{1 - \sqrt{1 + 1/G^2}\}$$

that $R = (\sqrt{1+\eta^2} - 1)/|\eta|$, a quantity which is less than one, and $\alpha = \pi/2$. Thus, it follows from considerations of continuity that the root of $(1 + 1/G^2)^{1/2}$, which lies in the fourth quadrant, is associated with $i\rho_1$. Then, the following conclusions regarding the value of this root of $(1 + 1/G^2)^{1/2}$ for different values of ξ and r may be arrived at:

Case I. $\xi \leq 1$

(*a*) $r < 1$, that is, $\eta > 0$.

According to the above arguments, $(1 + 1/G^2)^{1/2}$ lies in the fourth quadrant.

(*b*) $r = 1$, that is, $\eta = 0$.

$Im\{1 + 1/G^2\} = 0$, and $Re\{1 + 1/G^2\}$ lies on the real axis as long as $\xi < 1$ and vanishes when $\xi = 1$. Thus, $(1 + 1/G^2)^{1/2}$ lies on the positive real axis, the negative value being inadmissible, since earlier, for $r < 1$, $(1 + 1/G^2)^{1/2}$ was in the fourth quadrant.

(*c*) $r > 1$, that is, $\eta < 0$.

$Re\{1 + 1/G^2\}$ and $Im\{1 + 1/G^2\}$ are both positive. Hence, for $\xi \leq 1$, $(1 + 1/G^2)^{1/2}$ is represented by a point in the first quadrant.

Case II. $\xi > 1$

(*a*) $r < 1$.

$(1 + 1/G^2)^{1/2}$ lies in the fourth quadrant.

(*b*) $r = 1$.

$Im\{1 + 1/G^2\} = 0$, and $Re\{1 + 1/G^2\} = 1 - \xi^2$, which is a negative quantity. Hence, $(1 + 1/G^2)^{1/2}$ is now represented by a point on the negative imaginary axis.

(*c*) $r > 1$.

The imaginary part of $(1 + 1/G^2)$ is positive, which means $(1 + 1/G^2)$ lies in the first or second quadrant. Hence, $(1 + 1/G^2)^{1/2}$ lies in the third quadrant. It is clear from these arguments, that $Re\{1 + 1/G^2\}^{1/2}$ is always positive, except when $r > 1$, $\xi > 1$. In the latter case, $Re\{1 + 1/G^2\}^{1/2}$ is negative.

Now, from the equations (2.8), it can be easily shown that

$$R^2 = \frac{|\rho_1|}{|\rho_2|} = \left\{\frac{1 - 2A' \cos\beta' + A'^2}{1 + 2A' \cos\beta' + A'^2}\right\}^{1/2}$$

where

$$A' \cos\beta' = Re\{1 + 1/G^2\}^{1/2}$$

Hence, the following conclusions regarding the value of R^2 are immediately arrived at: for

$$\xi < 1, r \lesseqgtr 1 \cdots R^2 < 1$$

$$\xi = 1, r \lesseqgtr 1 \cdots R^2 < 1$$

$$\xi > 1, r < 1 \cdots R^2 < 1$$

$$\xi > 1, r > 1 \cdots R^2 > 1$$

At $r = 1$, equation (2.8) gives

$$Re^{i\alpha} = \frac{1}{\xi}\{1 - \sqrt{1 - \xi^2}\} \quad \ldots\ldots\ldots\ldots\ldots\ldots\ldots\ldots (A)$$

Hence, for $\xi = 1$, $r = 1$, we have $R = 1$, $\alpha = 0$; and for $\xi > 1$, $r = 1$, we have $R = 1$, $\alpha = \cos^{-1}(1/\xi)$. At $\xi = 0$, similarly from (2.8),

$$Re^{i\alpha} = -\frac{i}{\eta}\{1 - \sqrt{1 + \eta^2}\}$$

which gives

$$R = \frac{\sqrt{1 + \eta^2} - 1}{|\eta|} < 1$$

and $\alpha = \pi/2$ when $r < 1$ and $\alpha = -\pi/2$ when $r > 1$. To find the values of R and α at the point $\xi = 0$, $\eta = 0$, the expression (A) may be considered at values of ξ slightly greater than zero. Considering the limit of the expression as $\xi \to 0$, it follows that

$$R = 0, \qquad \alpha = 0$$

Equations (2.8) also yield the following expressions:

$$\sin\alpha = \frac{2\eta}{\zeta^2} \cdot \frac{R}{1 - R^2}$$

$$\cos\alpha = \frac{2\xi}{\zeta^2} \cdot \frac{R}{1 + R^2}$$

The expression for $\cos\alpha$ indicates that it is always positive, since ξ is positive in the northern hemisphere. Remembering the possible values of R in the ξ-η plane, the following conclusions can be drawn up: for

$$\xi < 1, r < 1, \cdots \sin\alpha > 0$$

$$\xi < 1, r > 1, \cdots \sin\alpha < 0$$

$$\xi < 1, r = 1, \cdots \quad \alpha = 0$$

$$\xi = 1, r < 1, \cdots \sin\alpha > 0$$

$$\xi = 1, r > 1, \cdots \sin\alpha < 0$$

$$\xi = 1, r = 1, \cdots \quad \alpha = 0$$

$$\xi > 1, r < 1, \cdots \sin \alpha > 0$$

$$\xi > 1, r > 1, \cdots \sin \alpha > 0$$

$$\xi > 1, r = 1, \cdots \quad \alpha = \cos^{-1}(1/\xi) > 0$$

the positive value of α being chosen in the last case from the consideration of continuity, since for $\xi > 1$, but $r \lesseqgtr 1$, α lies in the range $0 < \alpha < \pi/2$. Thus, the ambiguities regarding the values of R and α are removed. In the northern hemisphere, α always lies between 0 and $\pm \pi/2$. All these conclusions about the values of R and α in the ξ-η plane have been outlined in Figure 5.

JOURNAL OF GEOPHYSICAL RESEARCH VOLUME 60, No. 4 DECEMBER, 1955

THERMAL AND GRAVITATIONAL EXCITATION OF ATMOSPHERIC OSCILLATIONS

BY HARI K. SEN AND MARVIN L. WHITE

National Bureau of Standards, Boulder, Colorado

(Received August 12, 1955)

ABSTRACT

Previous work on the excitation of large-scale oscillations in an atmosphere on a rotating globe is extended to include a unified treatment for both gravitational and thermal forcing functions and is applied to the solar and lunar semi-diurnal pressure variation, that is, S_2 and L_2 , respectively. It is assumed that the heating is applied only at the base of the atmosphere and that the temperature gradient is constant in this region as in the actual troposphere. The solution of the problem consists of the usual Bessel's functions characteristic of a purely gravitational forcing function found by Pekeris [see 1 of "References" at end of paper], plus a particular integral found by the method of variation of parameters. The total resonant amplification is obtained for the various atmospheric models used by Jacchia and Kopal [2]. The hitherto neglected phase of the dynamical tidal oscillation is included in a treatment where complex variables are systematically employed to represent the magnitude and phase of observables. It is found that current atmospheric models favor the conclusion that thermal effects are far more important than the gravitational in producing the S_2 variation ($\simeq 15$) as compared with Chapman's [3] 1924 conclusion that they are of nearly equal importance. However, if one assumes, as did Chapman, that eddy motion at the ground is the only heating source, then our conclusion is at odds with observed values of eddy conductivity found by Eiffel Tower measurements. A possible resolution of this paradox is the consideration of other heating sources. Balloon observations by Riehl and the analysis of Haurwitz [4] are cited in support of this possibility.

1. *Introduction*

The historical introduction to lunar and solar air tides has been given in detail by Wilkes [see 5 of "References" at end of paper] and by Chapman [6], covering, among others, the early contributions by Laplace, Lamb, Lord Kelvin, Hough, and Chapman to the subject. The resonance theory of atmospheric oscillations on a rotating globe was developed by Taylor [7] and Pekeris [1] for free and gravitationally excited oscillations, respectively. These works were extended by Weekes and Wilkes [8], who reduced the radially dependent differential equation

of motion to wave equation form. In 1951, Wilkes [9], in a highly formalized treatment, extended the Pekeris gravitational analysis to purely thermal oscillations for an atmosphere with an isothermal base.

A purpose of the present paper [10] is to extend the resonant theory of atmospheric oscillations on a rotating globe to include a unified treatment for both gravitational and thermal forcing functions. The results for the semi-diurnal pressure variations may be expressed as

$$\frac{S_2 \text{ (observed)}}{S_2 \text{ (equilibrium tidal)}} = \mathbf{M}\left(1 + \frac{R\tau'(0)}{\gamma\beta\Omega(0)}\right)$$

where $\mathbf{M}$ is a factor depending on the atmospheric temperature profile, γ is the ratio of specific heats, $\Omega(0)$ is the ground value of the solar tidal potential, and R is the gas constant per unit mass. If we suppose, as was originally done by Chapman, that the thermal excitation is a variation of air temperature τ conducted upward from the ground and expressible in terms of the height z and time t, we have his $\tau'(z, t) = \tau'(0)\, e^{-\beta z + i\sigma t}$, where β is a complex constant and $\tau'(z)$ is the actual temperature variation corrected for adiabatic heating and cooling. The second term in parentheses is the ratio of thermal to tidal part of S_2 or S_2(thermal)/S_2(tidal). This equation obtained by Chapman [3] in 1924 for a plane parallel atmosphere with a linear temperature profile is shown here to be more generally valid. However, the fact that $\mathbf{M}$ (= dynamical tidal/equilibrium tidal) depends on the atmospheric profile was not fully appreciated until 1937 [Pekeris, 1]. Jacchia and Kopal [2], using the purely gravitational analysis of Wilkes and Weekes [8], have by numerical integration recently determined the magnitude (but not the phase) of $\mathbf{M}$ for a number of current atmospheric models. $\mathbf{M}$ is ordinarily complex and is treated as such by present authors. Chapman used a real $\mathbf{M}$, which is valid for the simple models treated by him.

The value of the ratio on the left of the above equation is known from observation ($\simeq$ 100), as is also $\tau'(0)$. We infer from the work by Jacchia and Kopal [2] that $M \ll 100$ (for current atmospheric models) and therefore S_2 (thermal)/S_2 (tidal) $\simeq$ 15; however, this implies a β-value much larger than accords with Eiffel Tower observations of eddy conductivity of the atmosphere. In Chapman's [3] discussion of the data, Eiffel Tower measurements were used, giving a ratio S_2 (thermal)/S_2 (tidal) $\simeq$ 1. Present authors prefer to resolve the paradox by supposing other heating sources. Balloon observations by Riehl and the analysis of Haurwitz [4] are cited in support of this possibility.

2. *General Solution*

Unless otherwise specified, the notation used will be that of Wilkes [9], reproduced below for the reader's convenience:

a = radius of the earth

ω = angular velocity of the earth

g = acceleration of gravity

C_v , C_p = specific heats of the gas composing the atmosphere at constant volume and pressure

$\gamma = C_p/C_v$

R = gas constant for unit mass of gas

θ, ϕ, z = co-latitude, east longitude, height (above earth's surface) of a point in the atmosphere

u, v, w = southward, eastward, upward components of air velocity at (θ, ϕ, z)

$\chi(u, v, w)$ = divergence of velocity $= \chi(z)\, \psi(\theta, \phi)$

$$= \frac{1}{a \sin \theta} \frac{\partial}{\partial \theta} (u \sin \theta) + \frac{1}{a \sin \theta} \frac{\partial v}{\partial \phi} + \frac{\partial w}{\partial z}$$

p_0 , ρ_0 , T_0 = static pressure, density, absolute temperature (functions of z only)

p, ρ, T = departures, supposed small, from static values of pressure, density, temperature during oscillations (functions of θ, ϕ, z)

$\bar{p}, \bar{\rho}, \overline{T}$ = total pressure, density, temperature; that is, $p_0 + p$, $\rho_0 + \rho$, $T_0 + T$

$H = RT_0/g$ = scale height of atmosphere (function of z only)

$\Omega(z, \theta, \phi) = \Omega(z)\, \psi(\theta, \phi)$ = tide-producing potential

$2\pi/\sigma$ = period of oscillation

The problem of forced gravitational oscillations in a rotating atmosphere is one of solving eight basic equations for eight unknowns. The basic equations are for (1) hydrostatic equilibrium, (2) adiabatic equilibrium, (3) perfect gas law both for the static and the perturbed case, (4) equation of continuity, and (5) the three equations of motion containing terms involving the gravitational potential of the body. The unknowns are $u, v, w, p_0 , \rho_0 , T_0 , p, \rho, T$; T_0 or H depends on the choice of models and is assumed known. We are then left with eight equations and as many unknowns. Ordinarily, it is most convenient to get the final differential equation in terms of χ(since it represents three variables in one), and it turns out that the other unknowns can be expressed in terms of χ and $d\chi/dz$. In considering a thermal forcing function as well as a gravitational one, the adiabatic gas law must be replaced by

$$\frac{D\bar{p}}{Dt} - c^2 \frac{D\bar{\rho}}{Dt} = g\bar{\rho}Q \qquad (1)$$

where c is the speed of sound, and where the source function $Q(z, \theta, \phi) = q(z)\, \psi(\theta, \phi)$ is defined in the manner of Wilkes [9] to have the dimensions of velocity.

Omitting unnecessary details, it can be shown that

$$\frac{p(z)}{\rho_0} = -\Omega(z) + \frac{h}{i\sigma}\left[-\gamma g\chi + \gamma g H\frac{d\chi}{dz} - g\left\{-\frac{1}{H}\left(1+\frac{dH}{dz}\right)q + \frac{dq}{dz}\right\}\right] \quad \ldots\ldots(2)$$

$$w(z) = -\frac{i\sigma\Omega}{g} + \left(Hh\frac{d}{dz} + H - h\right)\left(\gamma\chi - \frac{q}{H}\right) \quad \ldots\ldots(3)$$

$$\gamma H\frac{d^2\chi}{dz^2} + \gamma\left(\frac{dH}{dz} - 1\right)\frac{d\chi}{dz} + \left[\gamma\frac{dH}{dz} + (\gamma - 1)\right]\frac{\chi}{h}$$
$$= \frac{1}{Hh}\left(\frac{dH}{dz} + 1\right)q - \frac{d}{dz}\left[\frac{1}{H}\left(\frac{dH}{dz} + 1\right)q\right] + \frac{d^2q}{dz^2} \quad \ldots\ldots(4)$$

when the usual approximations are made of variables separable, neglect of the earth's ellipticity, neglect of the variation with height of the radius vector, g, and $d\Omega/dz$, and neglect of vertical acceleration. Only the first of these approximations is really serious. The present theory is also subject to the usual restriction that the departures from static values of pressure, density, and temperature are so small that their squares and products may be neglected. We are thus working within the framework of a linearized theory, so that χ is given by

$$\chi = \chi_{\text{gravitational}} + \chi_{\text{thermal}} \quad \ldots\ldots(5)$$

Using equation (5), equations (2), (3), and (4) may more readily be obtained by drawing upon the corresponding equations for the purely thermal and gravitational cases. Note that the last term in Wilkes' equation (18) should be omitted [11]. This error does not affect his treatment.

The amplification factor at the ground is found by employing equation (2), subject to the condition that the vertical velocity at the ground vanishes, that is, $w(0) = 0$,

$$\text{Ampl.} = \frac{p}{p_{\text{equi.}}} = -\frac{ig}{\sigma\Omega}\left[\gamma H_0\chi(0) - q(0)\right] \quad \ldots\ldots(6)$$

where it may be recalled that $p_{\text{equi.}} = -\Omega\rho_0$ for the equilibrium tide.

In the manner of Pekeris [1], we define [12] a new coordinate y' by $T = T_0 - \beta' z \equiv \beta' y'$ and a new coordinate x' by $x'^2 = 4my'$, where $m = [(\gamma - 1)n - 1]/\gamma h$ and $n + 1 = g/R\beta'$. Expressing T as a linear function of z is justifiable as follows. This substitution, as we shall use it, enters only in the particular solution, that is, in the thermal effect; and the thermal input producing the oscillations in question is confined to tropospheric regions where the lapse rate, β', is observed to be constant throughout. With a further transformation, $f(x') = x'^{(n+1)}\chi$, equation (4) reduces to the form

$$\left.\begin{aligned}\frac{d^2f}{dx'^2} + \frac{1}{x'}\frac{df}{dx'} + \left[1 - \frac{(n+1)^2}{x'^2}\right]f(x') \\ = \frac{x'^{(n+3)}}{4m^2}\frac{n+1}{\gamma y'}\left[\frac{d^2q}{dy'^2} + n\frac{d}{dy'}\left(\frac{q}{y'}\right) + \frac{nq}{hy'}\right] \\ = R(x'), \qquad \text{say.}\end{aligned}\right\} \quad \ldots\ldots(7)$$

The complementary solution of this differential equation is analogous to the purely gravitational solution obtained by Pekeris in terms of the independent solutions of Bessel's equation of order $(n + 1)$, namely,

$$\chi = x'^{-(n+1)}[AJ_{n+1}(x') + BY_{n+1}(x')] \quad (8)$$

where, however, A and B now depend on the source function. The particular solution, P.I., is found by the method of variation of parameters to be

$$\text{P.I.} = J_{n+1}(x') \int \frac{Y_{n+1}(x')R(x')}{J'_{n+1}(x')Y_{n+1}(x') - J_{n+1}(x')Y'_{n+1}(x')}\,dx' - Y_{n+1}(x') \int \frac{J_{n+1}(x')R(x')}{J'_{n+1}(x')Y_{n+1}(x') - J_{n+1}(x')Y'_{n+1}(x')}\,dx' \quad (9)$$

The denominators in the above integrands are recognized as the negative of the Wronskian of $J_n(x')$ and $Y_n(x')$ [13],

$$W = \begin{vmatrix} J_n(x') & Y_n(x') \\ J'_n(x') & Y'_n(x') \end{vmatrix} = \frac{2}{\pi x'} \quad (10)$$

so that the following expression for $F(= x'^{-(n+1)}$ P.I.) is found,

$$F = -\frac{\pi}{2} x'^{-(n+1)} \left[J_{n+1}(x') \int_{x_1'}^{x'} x' Y_{n+1}(x')R(x')\,dx' - Y_{n+1}(x') \int_{x_1'}^{x'} x' J_{n+1}(x')R(x')\,dx' \right] \quad (11)$$

The above integrals will be evaluated in the appendix (see Section 5).

3. *The Source Function Q*

The source function can be obtained semi-empirically. One first examines equation (19) of Wilkes [9] reproduced below,

$$\frac{i\sigma RT}{g} = Q - w\frac{dH}{dz} - (\gamma - 1)H\chi \quad (12)$$

valid for our present case.

The second term on the right vanishes at the ground $[w(0) = 0]$, while the last term is due to adiabatic compression arising from the mechanical term $\bar{p}\delta(1/\bar{\rho})$ in equation (1) for the first law of thermodynamics. At the ground, therefore, we may rewrite equation (12) as

$$\frac{i\sigma R\tau'(0)}{g} \simeq q(0) \quad (13)$$

where τ' is the value of τ corrected for adiabatic heating and cooling in the manner of Chapman [3], and $q(z)$ and $\tau(z)$ refer to the z-variations only of Q and T, respectively. Still from the work of Chapman, [14],

$$\tau(0) = 0°.4 \sin(2t + 75°) = 0°.4e^{-15°i}$$

Hence,

$$\tau'(0) \simeq 0°.4e^{-38°i} \quad \ldots\ldots(14)$$

Also,

$$\tau(z) = \tau(0)e^{-\beta z/H_0} \quad \ldots\ldots(15)$$

where

$$(\beta/H_0)^2 = i\sigma/K \quad \ldots\ldots(16)$$

and where K is the coefficient of thermometric conductivity, so $q(0)$ at the ground is known. If $w(z)$ remains very small in the neighborhood of the ground, then

$$q(z) \simeq q(0)e^{-\beta z/H_0} \quad \ldots\ldots(17)$$

The values of K and β found from the diurnal temperature variations at various points on the Eiffel Tower [3] give

$$K \simeq 10^5 \text{ cgs units} \qquad \text{and} \qquad \therefore\ |\beta| \simeq 21.5 \quad \ldots\ldots(18)$$

Balloon observations by H. Riehl in the Eastern Caribbean, analyzed by B. Haurwitz [4], show large semi-diurnal temperature variations above 1.5 km, pointing up the possible importance of heating aloft. Were this effect due to eddy transport from the ground, it would imply much smaller β-values.

4. *Isothermal and Adiabatic Atmospheric Models*

For an *isothermal* atmosphere, $dH/dz = 0$, and equation (4) reduces to

$$\gamma H \frac{d^2\chi}{dz^2} - \gamma \frac{d\chi}{dz} + \frac{\gamma - 1}{h}\chi = \frac{q(0)}{H^2 h}[H + \beta(\beta + 1)h]e^{-\beta z/H} \quad \ldots\ldots(19)$$

where according to the preceding section

$$q(z) = q(0)e^{-\beta z/H_0}$$

The complementary solution of equation (19) is

$$\chi(z) = Ae^{\lambda z} \quad \ldots\ldots(20)$$

where λ is given by (taking $\gamma = 1.4$)

$$\lambda = \frac{1}{2H}\left[1 \pm \sqrt{1 - \frac{8}{7}\frac{H}{h}}\right] \quad \ldots\ldots(21)$$

the sign in (21) depending on the boundary condition at infinitely high layers [6], and the complete solution becomes

$$\chi(z) = Ae^{\lambda z} + \frac{q(0)}{H}\frac{H + \beta(\beta + 1)h}{(\gamma - 1)H + \beta(\beta + 1)\gamma h}e^{-\beta z/H} \quad \ldots\ldots(22)$$

The particular solution is just that given by Wilkes [9]. Imposing the condition that the vertical velocity at the ground must vanish, equation (3) can be solved for the constant of integration A, yielding

$$A \simeq \frac{i\sigma}{g\gamma}\frac{\Omega(0) + R\tau'(0)/\beta\gamma}{Hh\lambda + H - h} \quad \ldots\ldots(23)$$

e $q(0)$ as given by equation (13) is employed and where terms of order $1/\beta^2$ gher are neglected (we assume $\beta > 1$). Substitution of equations (22) and (23) the expression (6) for the amplification yields

$$\text{Ampl.} \simeq \frac{H}{H(h\lambda + 1) - h}\left[1 + \frac{R}{\beta\gamma}\frac{\tau'(0)}{\Omega(0)}\right] \quad \ldots\ldots(24)$$

may identify β for the isothermal case with Wilkes [7], Section 4, expression n_3, so that

$$\beta = e^{i\pi/4}H\sqrt{\frac{\sigma\gamma}{K}} \quad \ldots\ldots(25)$$

n equation (24),

$$\frac{\text{Thermal effect}}{\text{Gravitational}} = \frac{R\tau'(0)}{\beta\gamma\Omega(0)} \quad \ldots\ldots(26)$$

rt from the factor $1/\gamma$, this is the same as the expression obtained by Chapman or a plane parallel atmosphere. If we take the Eiffel Tower value for K (10^5 cgs) hapman and Wilkes have done, the ratio of thermal to gravitational effect is it two, and if further $h \simeq H$, then λ, from (21), $\simeq 1/2H$, and the amplification bout 4.7 $e^{72°i}$, as compared with the observed value of 100 $e^{64°i}$ based on bson's observations. In considering an atmosphere in *adiabatic* equilibrium, ave

$$\frac{dH}{dz} = -\frac{\gamma - 1}{\gamma}, \qquad \frac{dH}{dx} = -\frac{\gamma - 1}{\gamma}H, \qquad H = H_0 e^{-(\gamma - 1/\gamma)x}$$

re x is defined by $x = \int(dz/H)$. Defining $y = e^{-\frac{1}{2}x}\chi$, equation (4) reduces to

$$\frac{d^2y}{dx^2} - \frac{1}{4}y = R(x) \quad \ldots\ldots(27)$$

setting $q = q(0)\, e^{-\beta x}$, the solution of equation (27) becomes

$$y = Ae^{-1/2x} + \frac{q(0)}{h\gamma^2(\beta^2 + \beta)}e^{-(1/2+\beta)x} + \frac{q(0)}{H_0\gamma}e^{-[1/2+\beta-(\gamma-1/\gamma)]x} \quad \ldots\ldots(28)$$

ing $w(z)$ in (3) equal to zero and, as in the isothermal case, solving for A, we in

$$A = \frac{i\sigma\Omega(0)/g + q(0)/\beta\gamma}{\gamma(H_0 - h)} \quad \ldots\ldots(29)$$

stitution of equation (28) for $y(= e^{-\frac{1}{2}x}\chi)$ and of (29) into expression (6) for amplification yields

$$\text{Ampl.} = \frac{H_0}{H_0 - h}\left[1 + \frac{R\tau'(0)}{\beta\gamma\Omega(0)}\right], \quad \text{when} \quad \beta > 1 \quad \ldots\ldots(30)$$

h leads to the same expression for the ratio of thermal to gravitational effect the isothermal case, namely, equation (26).

Equation (30) was obtained by Chapman in 1924 for both isothermal and

adiabatic cases, from which he concluded that the resonance amplification was independent of the atmospheric model (p. 190, first paragraph).

Wilkes in his 1951 paper on thermal oscillations also attempted to treat gravitational and thermal oscillations together for an isothermal atmosphere. He introduced an equivalent gravitational potential and obtained finally an expression for the pressure variation in terms of an unknown "equivalent" pressure variation (see his eq. 41). However, Wilkes obtained no relations such as our equations (24) or (26) and came to the conclusion that "near resonance the complementary function far outweighs the particular integral even near the ground."

5. *The Particular Integral and Its Application to an Arbitrary Atmospheric Profile*

It may be recalled that the fundamental differential equation for the radial component of the pure gravitationally excited oscillations had been reduced to the following simplified wave equation by Weekes and Wilkes [8],

$$\frac{d^2y}{dx^2} + \mu^2(x)y = 0 \qquad (31)$$

where

$$\mu^2(x) = \frac{1}{h}\left(\frac{dH}{dx} + \frac{\gamma - 1}{\gamma} H\right) - \frac{1}{4}$$

Jacchia and Kopal [2] assume the complete primitive of equation (31) to be of the form

$$y = (P + iQ)(y_1 \pm iy_2) \qquad (32)$$

where $(P + iQ)$ is a complex constant of integration. However, when both thermal and gravitational excitation are considered, the complete solution for $\chi(z)$ is then of the form

$$\chi(z) = e^{1/2z}(P + iQ)(y_1 \pm iy_2) + F(z) \qquad (33)$$

where $F(z)$ is given by equation (11). The value of $(P + iQ)$ is found from the condition $w(0) = 0$, and the analysis proceeds as in the previous section. It is found that

$$P + iQ = [i\sigma\Omega(0)/g - H_0 h\gamma F'(0) - \beta h q(0)/H_0 - \gamma(H_0 - h)F(0) + q(0)\left(1 - \frac{h}{H_0}\frac{n}{n+1}\right)] \Big/ \gamma h(a_1 + ia_2) \qquad (34)$$

where we use the abbreviations of Jacchia and Kopal [2] for a_1 and a_2 that

$$a_1 = \left[\frac{dy_1}{dx} + \left(\frac{H}{h} - \frac{1}{2}\right)y_1\right]_{x=0} \qquad (35)$$

and

$$a_2 = \left[\frac{dy_2}{dx} + \left(\frac{H}{h} - \frac{1}{2}\right)y_2\right]_{x=0} \qquad (36)$$

ly,

$$F'(0) = \left(\frac{dF}{dz}\right)_0$$

equations (33) and (34) and expression (6), it is clear that the amplification depend upon $F(0)$ and $F'(0)$, so that it is necessary to evaluate $F(0)$ and explicitly.

n Appendix I, it is shown that

$$F(0) \simeq q(0)/\gamma H_0 \quad \ldots\ldots (37)$$

e terms involving squares and higher powers of $(1/\beta)$ are neglected, since essive terms decrease sufficiently fast, even for values of β as small as 3.

Ve may compute $F'(0)$ by taking the derivative of equation (11) with respect

$$= m\pi x_0'^{-(n+2)}\left[Y_{n+2}(x_0') \int_{x_1'}^{x_0'} x' J_{n+1}(x') R(x')\, dx' - J_{n+2}(x_0') \int_{x_1'}^{x_0'} x' Y_{n+1}(x') R(x')\, dx' \right]$$

integrals in the above expression have already been calculated in the process nding $F(0)$. Expressing $F'(0)$ in decreasing powers of β, we have

$$\left(\frac{dF}{dz}\right)_0 \simeq -\frac{(n+1)}{\gamma} q(0)\left[\frac{\beta}{H_0 y_0'} - \frac{1}{y_0'^2} + \frac{H_0(n - mh)}{\beta h y_0'^2}\right] \quad \ldots\ldots (38)$$

ne same degree of approximation as equation (37).

The expressions for $F(0)$ and $F'(0)$, together with equations (33), (34), and give the amplification for any general atmospheric profile,

$$\text{Ampl.} = \mathbf{M}\left(1 + \frac{R\tau'(0)}{\gamma\beta\Omega(0)}\right) \quad \ldots\ldots (39)$$

e, according to Jacchia and Kopal, we have, in effect,

$$\mathbf{M} = \frac{H_0}{h}\left(\frac{y_1 + iy_2}{a_1 + ia_2}\right)_0 \quad \ldots\ldots (40)$$

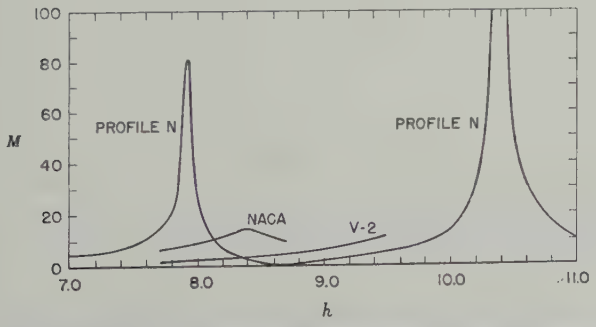

—Resonance spectra for NACA profile, V-2 profile, and profile N; amplification factor M plotted against equivalent depths h (after Jacchia and Kopal)

Jacchia and Kopal [2] have made extensive numerical and mechanical integrations of the wave equation (31) for various atmospheric profiles and were thus able to obtain the magnitude M of the amplification factor for the purely gravitational case. They did not concern themselves with the phase of **M**, however. Values of M will be taken from their computations. From equation (39), one sees that the ratio of thermal to gravitational action is given by the same expression as for the isothermal and adiabatic models, again in close agreement with Chapman [that is eq. (26)]. From equation (39) and the M-values of Jacchia and Kopal, plotted in Figure 1, we are able to construct Table 1, using $h = 7.9$.

TABLE 1—*The amplification factor for various atmospheric models and values of β at $h = 7.9$ km*

Atmosphere	M	Amplification		
		$\beta = 5e^{45°i}$	$\beta = 20e^{45°i}$	$\beta = 50e^{45°i}$
Martyn-Pulley*	26.	425.	107.	47.2
NACA	$7.43e^{-12°i}$	$121.e^{82°i}$	$30.5e^{71°i}$	$13.5e^{52°i}$
V-2	$1.76e^{-20°i}$	$28.8e^{73°i}$	$7.25e^{62°i}$	$3.21e^{44°i}$
Jacchia-Kopal atmosphere N†	$80.6e^{-88°i}$	$1320.e^{5.°5i}$	$331.e^{-5°i}$	$146.e^{-24°i}$

*Only absolute values of the quantities given.
†The resonant h-value (= 7.93) for atmosphere N is used here.

6. *General Discussion and Conclusions*

Table 1 allows us to compare two parameters, namely, the atmospheric model and β-value, with the observed amplification factor over equilibrium tide $\simeq 10$ $e^{64°i}$, based on Simpson's observations for the solar semi-diurnal pressure variation at the ground. It is at once seen that the theoretical amplification factor depends as critically, if not more so, upon the atmospheric model as on the value of β, a fact not fully appreciated before [3]. In constructing Table 1, β is allowed to vary only over the pertinent range $1 \leq \beta \leq 100$ (see Section 3). Over most of this range in β, the atmosphere N gives too great an amplification factor; this is to be expected since in the design of the atmosphere N only a gravitational forcing function was considered. Inclusion of a thermal forcing function as well eliminates the need for a highly resonant atmosphere. Considering next the phase for the atmosphere N, it is apparent that within the purely gravitational framework of the Jacchia-Kopal [2] treatment, atmosphere N gives an amplification factor $M \simeq 80.6\ e^{-88°i}$ that differs from that observed $\simeq 100\ e^{64°i}$ by 152°. Even when thermal effects are introduced (see Table 1), the phases cannot be reconciled.

Refering again to Table 1, it is seen that both the NACA and V-2 atmospheres will give the observed amplification in regards both magnitude and phase for

10, from which it is concluded that thermal $\gg$ gravitational effect. Of course, conclusion is subject to the very great uncertainties associated with the NACA V-2 models current for 1949. One unlikely alternative to the above conclusion d be to discard the resonant theory of atmospheric pressure oscillations ely. However, there are other reasons which support the resonant theory and ACA-type atmosphere. These reasons follow from the resonance curve for the A-profile (Fig. 4 of Jacchia and Kopal [2]) and reproduced here in Figure 1 he reader's convenience: (1) From the trend of this curve, it appears that the olar hour period would be far enough removed from resonance so as to make solar diurnal oscillation much smaller than the solar semi-diurnal oscillation; he need for an amplification factor of 3 to explain the observed lunar semi- al oscillation (corresponding to $h \simeq 7.1$ km) seems satisfied [15]; (3) a sharply ant atmosphere is no longer required. Thus, if we do accept an NACA type le as being the correct one, then from Table 1, $\beta \simeq 5$, and the ratio of thermal ravitational action $\simeq 16$; physically this means that the smaller β is, the er will be the layer over which the heating source is spread and the more rtant the thermal to the gravitational effect. Now eddy conductivity upward portant only very close to the ground. A value of $\beta \simeq 5$ corresponds to a paratively thick layer and implies impossibly large values of the coefficient of conductivity k. The work of Riehl and Haurwitz and the present results however, be reconciled with $K \simeq 10^5$, if radiative absorption is more important eddy conductivity over the layer corresponding to $\beta \simeq 5$ [16] or if eddy con- ion from above were important. Another explanation could be that the large -diurnal heating effects are due to a coupling between the diurnal temperature tion and a diurnal component K_1. In considering the observational material he coefficient of eddy conductivity, Chapman himself pointed out that the for $\tau(z)$ and $\tau'(z)$ are all rather uncertain; the values over the great oceans probably those of chief importance, and yet the least known. Thus, it would that $\beta \simeq 5$ is not impossible.

ne of the authors is at present engaged in studying the above-mentioned ional heating effects, including ozonospheric heating, with particular appli- n to the semi-diurnal winds aloft.

Appendix I—*Derivation of* $F(0)$

is seen from equation (11) that it is necessary to evaluate integrals of the

$$\int_{x_1'}^{x_0'} x' J_{n+1}(x') R(x')\, dx'$$

tituting for $R(x')$ from equation (7) and changing from the independent ble x' to y', we obtain

$$x' J_{n+1}(x') R(x')\, dx' = \int_{y_1'}^{y_0'} \left[G(y') \frac{d^2 q}{dy'^2} + G_1(y') \left(\frac{dq}{dy'} + \frac{q}{h} \right) - G_2(y') q \right] dy'. \quad (1)$$

where we define

$$G(y') = J_{n+1}(\sqrt{4my'}) \cdot \frac{2(n+1)}{\gamma} \cdot (4my')^{(n+1)/2}$$

and

$$G_1(y') = \frac{nG(y')}{y'}, \qquad G_2(y') = \frac{nG(y')}{y'^2} \qquad \text{.....(2)}$$

Integrating equation (1) by parts and arranging in powers of $1/\beta$, we obtain

$$\int_{x_1'}^{x_0'} x' J_{n+1}(x') R(x')\, dx' \simeq \left[\frac{\beta}{H_0} G(y_0') - \{G'(y_0') - G_1(y_0')\} + \frac{H_0}{\beta}\left\{G''(y_0') + \frac{G_1(y_0')}{h} - G_1'(y_0') - G_2(y_0')\right\} - \frac{H_0^2}{\beta^2}\left\{G''(y_0') + \frac{G_1'(y_0')}{h} - G_1''(y_0') - G_2'(y_0')\right\}\right] q(0) \qquad \text{....(3}$$

where terms involving the cube and higher powers of $(1/\beta)$ are neglected. No that considerable simplification occurs because the integrated terms vanish at th lower limit due to the factor $e^{-\beta y_0'/H_0}$ in the expression for $q(y')$:

$$q = q(0) e^{-\beta y_0'/H_0} e^{-\beta y'/H_0} \qquad \text{.....(}$$

Expressing the G's explicitly and carrying out their differentiations, equatio (3) becomes

$$\int_{x_1'}^{x_0'} x' J_{n+1}(x') R(x')\, dx' \simeq \frac{2(n+1)}{\gamma} \cdot (4m)^{(n+1/)2} q(0) \left\{\left[\frac{\beta}{H_0} y_0'^{(n+1)/2} - y_0'^{(n-1)/2} + \frac{H_0}{\beta}\left(\frac{n}{h} - m\right) y_0'^{(n-1)/2}\right] J_{n+1}(\sqrt{4my_0'}) + \sqrt{m}\, y_0'^{n/2} J_{n+2}(\sqrt{4my_0'})\right\} \qquad \text{..(}$$

and a similar expression is obtained for

$$\int_{x_1'}^{x_0'} x' Y_{n+1}(x') R(x')\, dx'$$

Upon substitution of the above integrated expressions into equation (11) of t text for $F(0)$, we obtain

$$F(0) \simeq q(0)/\gamma H_0 \qquad \text{.....(}$$

where we have used the expression $y_0' = H_0 (n+1)$ and the formula relati J's and Y's [13]

$$J_{n+2}(\sqrt{4my_0'})\, Y_{n+1}(\sqrt{4my_0'}) - J_{n+1}(\sqrt{4my_0'})\, Y_{n+2}(\sqrt{4my_0'}) = \frac{2}{\pi\sqrt{4my_0'}}$$

References

[1] C. L. Pekeris, Proc. R. Soc., A, **158**, 650 (1937).
[2] L. G. Jacchia and Z. Kopal, J. Met., **9**, 13 (1952).
[3] S. Chapman, Q. J. R. Met. Soc., **50**, 165 (1924).

[4] H. Riehl, Bull. Amer. Met. Soc., **28**, 311 (1947); B. Haurwitz, Bull. Amer. Met. Soc., **28**, 319 (1947).
[5] M. V. Wilkes, Oscillations of the Earth's Atmosphere, Cambridge, University Press (1949); Chap. I.
[6] S. Chapman, Compendium of Meteorology (T. F. Malone, Editor), Amer. Met. Soc. (1951); p. 510.
[7] G. I. Taylor, Proc. R. Soc., A, **156**, 318 (1936).
[8] K. Weekes and M. V. Wilkes, Proc. R. Soc., A, **192**, 80 (1947).
[9] M. V. Wilkes, Proc. R. Soc., A, **207**, 358 (1951).
[10] H. K. Sen and M. L. White, Mixed Commission on the Ionosphere, Proceedings of the Fourth Meeting, Brussels, August 16–18, 1954 (pp. 174–181).
[11] We are indebted to Mr. Manfred Siebert, Geophysikalisches Institut, Göttingen, for bringing this error in Wilkes' paper to our attention.
[12] We have used β' in place of the Pekeris β in order to avoid confusion with the β used later in the heat source function in equation (17). Similarly, we use y' and x' in place of the Pekeris y and x to be consistent with the notation of Wilkes and Jacchia and Kopal. Finally, the small h used here corresponds to the Pekeris H.
[13] Watson's Bessel Functions, Cambridge, University Press, 2nd ed. (1944); pp. 76–77.
[14] The expression for $\tau(0)$ is a slightly modified Hann's law, the modifications being based on data taken by the U. S. Weather Bureau at various Pacific stations and kindly furnished to us by Mr. Isadore Enger, statistician.
[15] This amplification is found by comparing the lunar semi-diurnal barometric pressure variation p ($= 0.062$ mm) observed for Batavia (Chapman, 1939) with the value computed from equilibrium tidal theory, namely, $p = -\Omega\rho_9 = +2 \times 10^4 \times 1.3 \times 10^{-3}$ cgs units $= 0.020$ mm Hg.
[16] M. Siebert, Naturwiss., **19**, 446 (1954).

REGULARLY-OBSERVABLE ASPECT-SENSITIVE RADIO REFLECTIONS FROM IONIZATION ALIGNED WITH THE EARTH'S MAGNETIC FIELD AND LOCATED WITHIN THE IONOSPHERIC LAYERS AT MIDDLE LATITUDES

BY A. M. PETERSON, O. G. VILLARD, JR., R. L. LEADABRAND, AND P. B. GALLAGHER

Radio Propagation Laboratory, Stanford University, Stanford, California

(Received August 12, 1955)

ABSTRACT

Aspect-sensitive radio reflections in the frequency range from 6 to 30 Mc have been regularly obtained from scattering sources located within the ionosphere at locations quite far south of the auroral zone. Observations have been made at two locations on the west coast of the United States (Stanford, California, geomagnetic latitude 43.75°, and Spokane, Washington, geomagnetic latitude 55°). With few exceptions, the echoes occur when the line of sight from the transmitter intersects a magnetic field line at perpendicular incidence at heights corresponding to those of the *E* and *F* layers. Thus, the *E*-layer echoes are obtained from areas in the immediate vicinity of the observing stations. The echoes may be detected with relatively low-power radars during the majority of the hours of darkness on almost every night. The reflection geometry and the characteristics of the echoes themselves—occurrence frequency, fading rate, etc.—all suggest that the observed low-latitude phenomenon is caused by the same general type of particle bombardment which is believed to cause the aurora.

INTRODUCTION

Studies of the ionosphere by the scatter-sounding technique [see 1 and 2 of "References" at end of paper] have been conducted at Stanford University since 951. The primary purpose of this work has been to learn more of the character-tics of sporadic-*E* clouds of ionization. The sounding equipment [3,4] has con-isted of several fixed-frequency rotating-beam radars working in the high-requency range. This type of sounding takes advantage of energy scattered back o a high-frequency transmitter from irregularities on the ground at or beyond ne edge of the skip zone. The usefulness of the technique is greatly enhanced y the circumstance that ground-scatter echoes are normally very strong in omparison with the energy that is scattered directly back from an undisturbed ayer. Thus, the normal ionosphere can be pictured as a reasonably smooth surface; hen its reflecting power at a given radio frequency becomes sufficiently great, ne ground at some distant point is mirrored in the layer, and echoes from scatter-ng at that point can be displayed on a plan position indicator.

When geomagnetic disturbances occur, however, this simple picture becom more complex. In particular, echoes of considerable strength can be obtain from scattering sources within the ionosphere itself. Such echoes have be detected relatively frequently by observers close to the auroral zone [5] a relatively infrequently by observers farther away. It is presently believed th echoes of this type are reflections from ionization caused by charged partic —or groups of charged particles—colliding with the earth's atmosphere. As consequence of their charge, such particles will follow the lines of force of t earth's magnetic field. Many workers believed that the strongest radar echo fr the ionization is obtained when the line of sight to the transmitter is perpendicul to the track of the particles.

It was shown not long ago [6] that very long-distance echoes from ionizati in the vicinity of the northern auroral zone can be detected as far south as Stanfo University (geomagnetic latitude 43.75 degrees). The slant ranges of such echo may be as great as 4700 km. The echoes are relatively intermittent in nature particular one may last anywhere from one to thirty minutes, and the total ti they are seen during a typical day on which they are detected is of the order one or two hours.

DISCUSSION

It is the purpose of this paper to describe the characteristics of a new class echo, regularly obtained from scattering sources located within the E and layers of the ionosphere at points relatively close to Stanford University. Refl tions from these sources are highly aspect-sensitive, behaving in a manner wh would be consistent with expectations based on the assumption that the sour took the form of ion columns lying parallel to the earth's magnetic field. Th are seen most frequently at night and in the geomagnetic north direction.

Radio echoes of this type have been observed ever since the inception of scatt sounding measurements at Stanford. It was originally believed that the reflecti were ground-scatter propagated by small sporadic-E clouds lying to the north, the ranges at which the echoes were observed are comparable to those of grou scatter propagated by sporadic-E clouds lying in other directions. The ra fading, which is a striking characteristic of these echoes, was considered to b consequence of the small cloud size and of possible turbulent motion.

The rate at which echoes of the new class fade is very great in compari with the fading rate of sporadic-E or F-layer propagated ground-scatter ech The fading rate is, in fact, roughly comparable to that of long-distance reflecti from the auroral zone [6,7]. Echoes of either type have a "fuzzy" or filled-in pearance, which is quite distinctive when they are viewed on a radar Class A displ Figure 1 illustrated the difference in appearance between a short-range echo of rapidly-fading type, and a typical sporadic-E-propagated ground-scatter ec With practice, rapidly-fading echoes can usually be identified on a PPI sc although positive identification is more difficult. When the echoes are strong, fading fluctuations tend to be obliterated by the effects of clipping or ampli saturation.

As a check on the hypothesis that the rapidly-fading echoes were due to grou

catter, an experiment was undertaken in the early spring of 1955 whereby the gnal of the continuously-operating 17-Mc scatter-sounder at Stanford was ecorded at Spokane, Washington. Spokane is located approximately in the eomagnetic north direction from Stanford, California, and at a distance (roughly

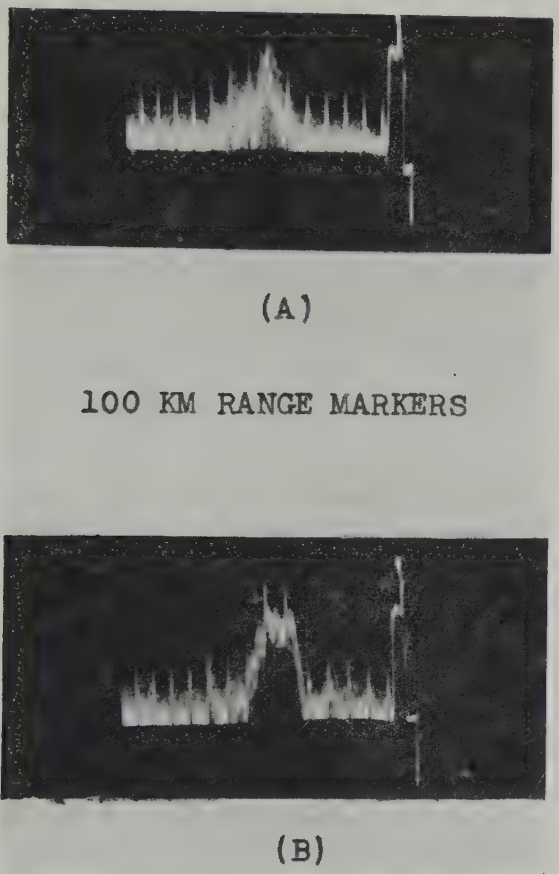

g. 1—Examples of 17-Mc radar echoes with Class A display: (*a*) Rapidly-fading echo seen when am pointed toward geomagnetic north direction; (*b*) slowly-fading sporadic-*E*-propagated ound-scatter echo seen when beam pointed south. Time is approximately 2100 PDT, 25 June 55; sweep moves from right to left; transmitted pulse length 0.4 milliseconds; range marks every 100 km; PRF 90 cps.

00 km) which corresponds to the slant range of an echo of the rapidly-fading pe which has been seen very consistently on the above sounder at Stanford iversity. If the echo were due to ground-scatter, its appearance at Stanford ould be accompanied by strong one-way transmission to Spokane. On the other nd, if no such transmission developed, the most reasonable expectation would that the echo was being returned from the ionosphere above Spokane.

The field-strength recordings were made over a period of 76 days. During s period, there were some 10 clear-cut instances of slowly-fading sporadic-*E*-

propagated echoes in the direction and range corresponding to Spokane. Duri
all but two of these instances, strong one-way propagation was recorded at Spokan
The remaining two instances were, for one reason or another, doubtful. On t
other hand, rapidly-fading echoes in the right direction and range were observ
during 14 of the nights. On none of the latter occasions was the strength of t
one-way signal stronger than the normal background level of meteor bursts.

As a consequence, the possibility that the fuzzy echo originates within t
ionosphere came under active study. As a second test of the ground-scatter expl
nation, a portable scatter-sounder substantially identical to the Stanford equi
ment—and operating on the same radio frequency of 17.31 Mc—was set up
Spokane [8]. If the echo to the north of Stanford were due to ground-scatt
propagated by a sporadic-*E* cloud, then it should be possible to "see" substantial
the same cloud when looking back towards Stanford from that city. This equipme
was operated for a period of about two months, and on no occasion when a rapidl
fading echo was seen in the right range and direction from Stanford could
equivalent echo be seen looking south from Spokane. Furthermore, there was
evidence on these occasions of strong one-way propagation between the t
sounders, as would be unmistakable in view of the common radio frequency us
On the other hand, there were several occasions when a typical slowly-fadi
sporadic-*E* ground-scatter echo did appear in the Spokane direction and range
viewed from Stanford. On each occasion of this type not only did strong one-w
transmission take place between the sounders, but also a back-scatter echo su
stantially equivalent to that at Stanford was seen at the right range and in t
correct bearing as viewed from Spokane.

TESTS FOR ALIGNMENT WITH MAGNETIC FIELD

It is reasonable to suspect that an echo appearing most frequently in t
geomagnetic north direction may be obtained by perpendicular reflection fr
ionization aligned with the earth's magnetic field. Chapman [10] has worked o
the points at which such perpendicular reflection would take place, for vario
observing locations on the earth's surface. It is also plausible to suspect th
whatever the nature and cause of the ionization, the greatest amount might

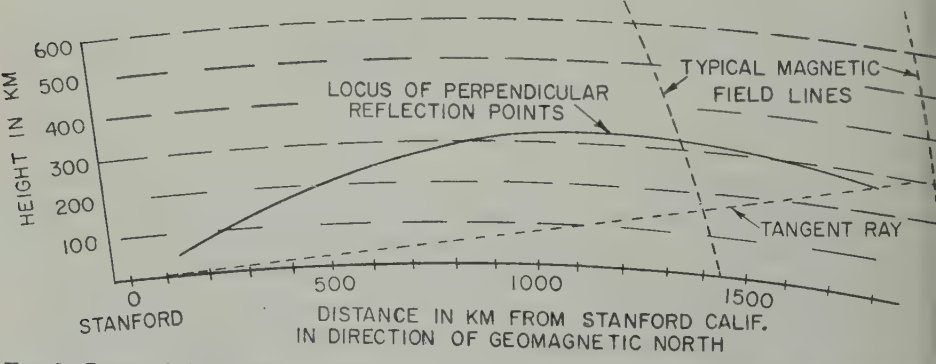

FIG. 2—Locus of those points at which the line of sight in the geomagnetic north direction fr
Stanford, California, meets the earth's magnetic field lines at perpendicular incidence

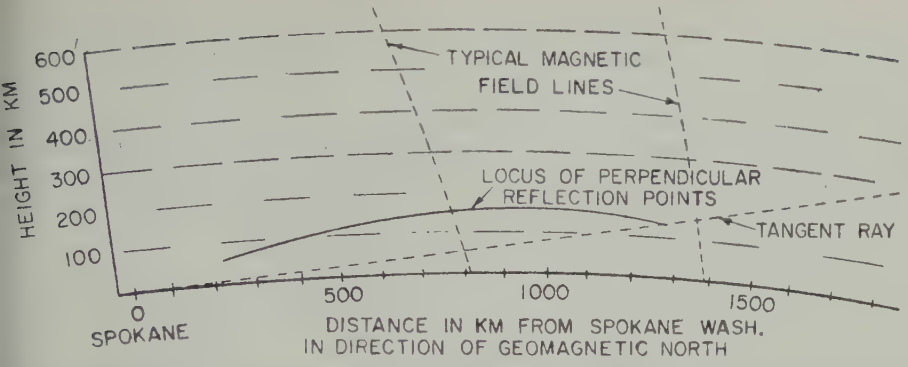

g. 3—Locus of those points at which the line of sight in the geomagnetic north direction from pkane, Washington, intersects the earth's magnetic field lines at perpendicular incidence

ınd at heights corresponding to the *E* and the *F* layers of the ionosphere. vidence obtained at Stanford indicates that the long-distance radio reflections ɔm ionization at the auroral zone do in fact originate at *F*-layer heights, or eater [5].)

With these circumstances in mind, calculations similar to those of Chapman 0] were carried out to determine the locus of those points at which the line of ht in the geomagnetic north directions from Stanford and Spokane would meet e earth's magnetic field lines at perpendicular incidence. The resulting loci are own in Figures 2 and 3, respectively. It will be observed that the locus from anford passes through the *E* region at a slant range of 220 km, and through the region at slant ranges varying between 600 and 1700 km. The locus from Spokane sses through the *E* region at a range of 500 km, but does not pass through the region at all.

It has been found that one group of rapidly-fading echoes observed in the ɔmagnetic north direction from Stanford occurs at ranges varying between 600 d 1700 km. The relative frequency of occurrence of these echoes has been plotted a function of range in the histogram of Figure 4. The curve has a peak corresnding to a range of 800 km. Thus, an *F*-layer origin for these echoes is strongly ggested.

Further substantiation has been obtained through vertical angle-of-arrival asurements made by comparing echo strength when the radar is switched ween identical antennas at varying heights above ground. The angle of arrival echoes of this type is found to be that which would be expected if the echoes ginate within the *F* layer. (The measurements were made at times of day when likelihood of strong bending in the lower ionosphere was very remote.)

Echoes of the rapidly-fading type were also observed at Spokane, Washington, the geomagnetic north direction, and they were found for the most part to be anges of the order of 500 km. Longer-range echoes were not seen. This evidence nterpreted as being in support of the *E*-region origin of the echoes seen from kane.

During February, 1955, a 23-Mc short-pulse radar was placed in service at nford University primarily for conducting certain studies of small meteors.

This equipment has a peak power output of 50 kw, and an average power roughly one kilowatt. Quite unexpectedly, weak but steady echoes at a sla range of approximately 220 km were found to be detectable with this equipme on the majority of nights. The strength of these echoes reached its diurnal pe during the hours around midnight. With the aid of a rotatable antenna, the dir tion in which the echoes were strongest was found to be geomagnetic north. It now quite certain that these echoes are the central California equivalent of t

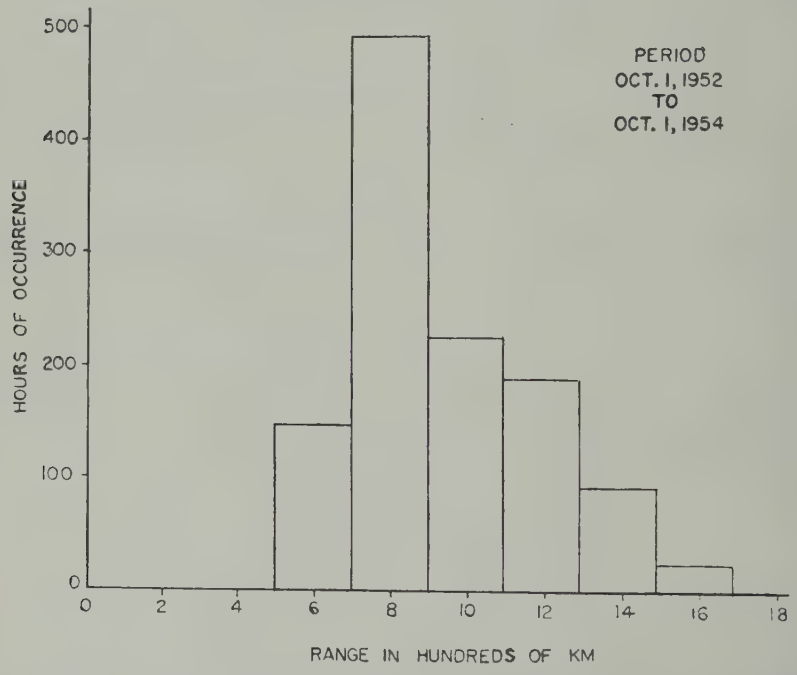

FIG. 4—Histogram showing distribution in range of the longer-range group of rapidly-fa echoes seen in geomagnetic north direction from Stanford, California, during the period Octob 1952, to October 1, 1954

E-region echoes seen from Spokane. This second, shorter-range group of ech in the geomagnetic north direction had not originally been observed on the 17- sounder at Stanford because of the long pulse length (order of 2 millisecon employed in that equipment, which had been designed primarily for lon distance back-scatter studies. As soon as the pulse length of the 17-Mc sour was reduced, however, the short-range echoes were found. The peak power out of the 17-Mc sounder is about two kilowatts, with an average power of roug 50 watts. Judging by the relative strength of the *E*-layer echoes observed a and at 23 Mc, it seems clear that their amplitude falls off very rapidly with creasing radio frequency. Quantitative measurements remain to be made, howe On a very few occasions, such echoes have been seen on a low-power 30-Mc sou at Stanford University.

The *E*-region echo has been found to occur at both 17 and 30 mc on nearly e

ght during the late spring and early summer of 1955, with much the same con-stency as the *F*-region echo. However, there seems to be little relation between the vo as far as exact times of occurrence are concerned.

The *F*-layer echoes are found to be spread out over a four-to-six millisecond nge interval. Their *E*-region equivalents, however, are much more concentrated range, being individually seldom wider than a 100-microsecond transmitted ılse. These differences are consistent with expectations based on the geometry Figure 2. It can be seen that perpendicular reflections can occur only within relatively limited slant-range interval in the *E*-region, whereas in the case of the layer they can occur anywhere within a much larger slant-range interval. The arrow range spread of the *E*-region echoes of this type is a distinctive feature which lps still further in their recognition, since sporadic-*E* ground-scattered echoes e almost invariably spread out over a relatively large slant-range interval, even hen a short transmitted pulse is used.

It is interesting to note that if the electron density in the ionosphere does not ecrease appreciably in the height interval between *E* and *F* layers, as suggested rocket data [11,12], then one would expect to find echoes occurring at ranges rresponding to intermediate heights of reflection. However, echoes are seldom en at such ranges.

Direct reflection from the layers are also found to occur in directions to the st and to the west of geomagnetic north. For reflection at right-angles to the agnetic field, the locus of points at which the perpendicular reflection can occur a particular altitude moves out in range when the radar beam is directed to

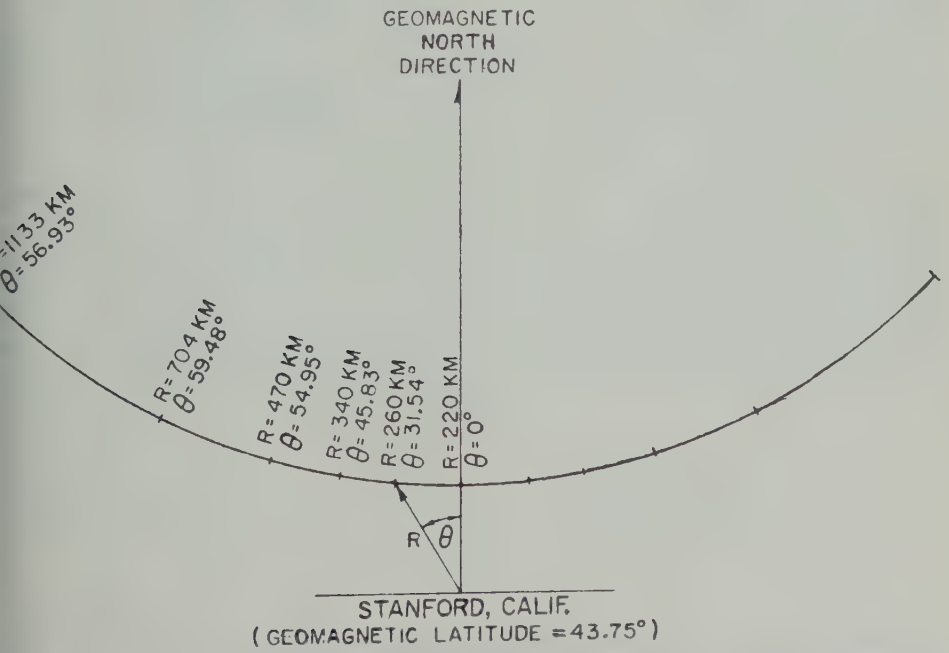

. 5—Plan view showing locus of those points at which the line of sight from Stanford, California, meets a magnetic field line at perpendicular incidence at an altitude of 100 km

either side of geomagnetic north [10]. A plan view of the locus of perpendicu reflection points as a function of azimuth is shown in Figure 5 for a height reflection of 100 km and a radar located at the geomagnetic latitude of Stanfo University. It is seen that the direct-reflected echo would be returned from point approximately 220 km away when the radar beam is pointed directly geomagnetic north, whereas it would be returned from a point 600 km away the radar beam were pointed to either side of geomagnetic north by approximat 60 degrees of azimuth.

This behavior has been regularly observed with the short-range group echoes on both the 17- and 23-Mc sounders. The analogous effect has also be observed in the case of the longer-range echoes. A short-range example at 17 Mc illustrated by the series of A-scope photographs shown in Figure 6. A furth example is given in Figure 7, which shows a number of range-azimuth photograp

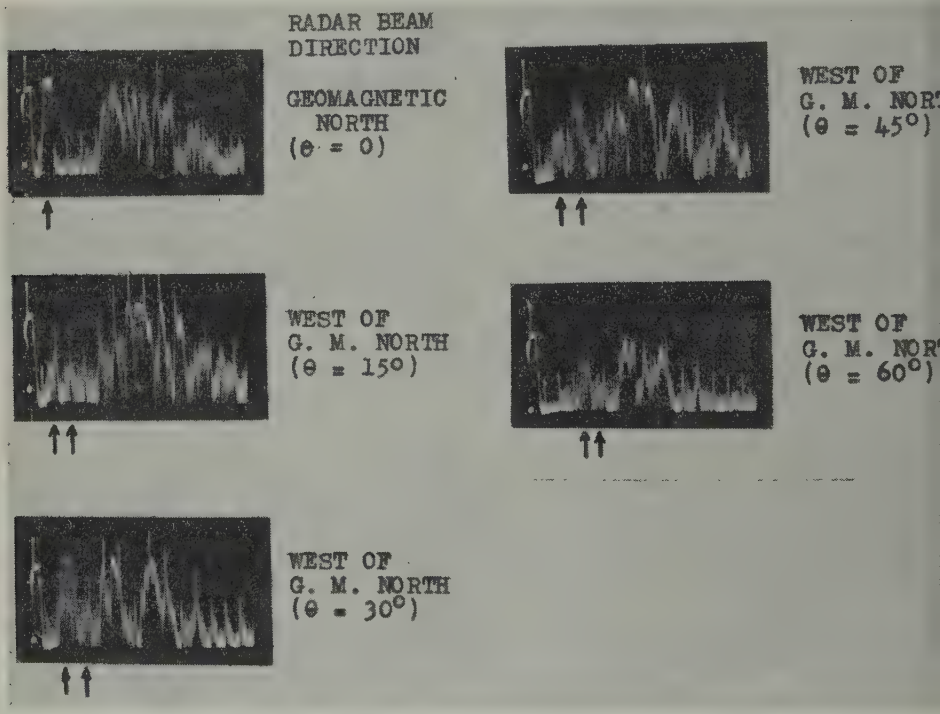

FIG. 6—Variation in range of short-range rapidly-fading echoes, as radar beam is directed to side of geomagnetic north direction; 17-Mc radar, 28 June 1955, 2200 PST, Class A display, sw travel left to right, 100-km range marks, transmitted pulse length 0.3 millisecond; θ is ang deviation in azimuth from geomagnetic north direction; arrows indicate short-range rapidly-fa echoes; slowly-fading echoes at longer range are sporadic-*E*-propagated ground-scatter

(in rectangular, rather than polar form) made with the 23-Mc equipment different times on a particular night. Figure 8 is a superposition of the indivi displays of Figure 7. The agreement between the superimposed echoes and perpendicular-reflection locus for a 100-km reflection height is quite evident.

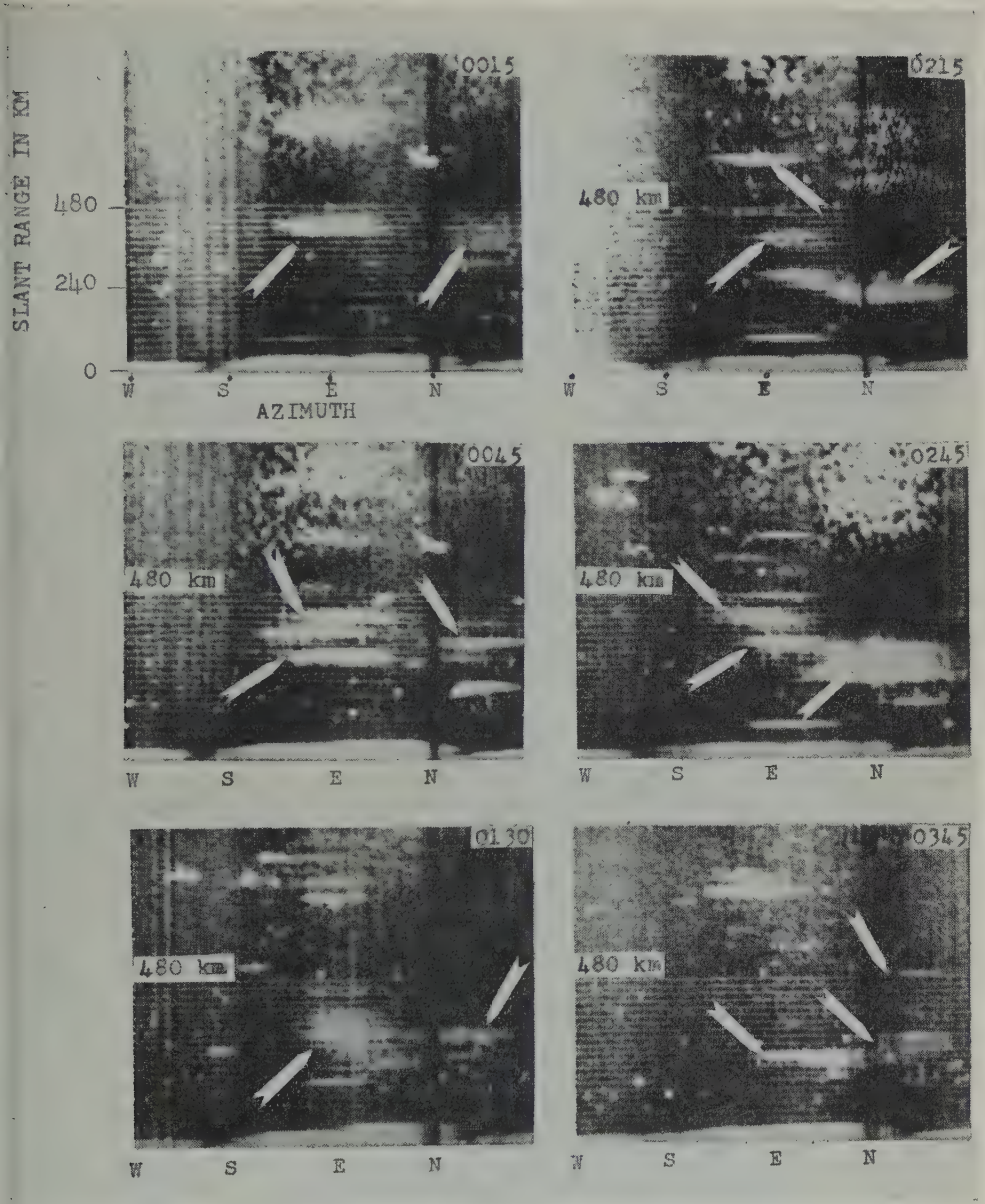

FIG. 7—Range-azimuth photographs made with high-power 23-Mc rotating-beam radar; pulse length 150 microseconds; transmitted pulse at bottom of each photograph; range marks every 20 km up to maximum of 480; arrows indicate rapidly-fading echoes; others are meteors or sporadic-*E*-propagated ground-scatter; date June 28, 1955; local standard time shows in upper right-hand corners of photos; time required for complete azimuth sweep 2 minutes

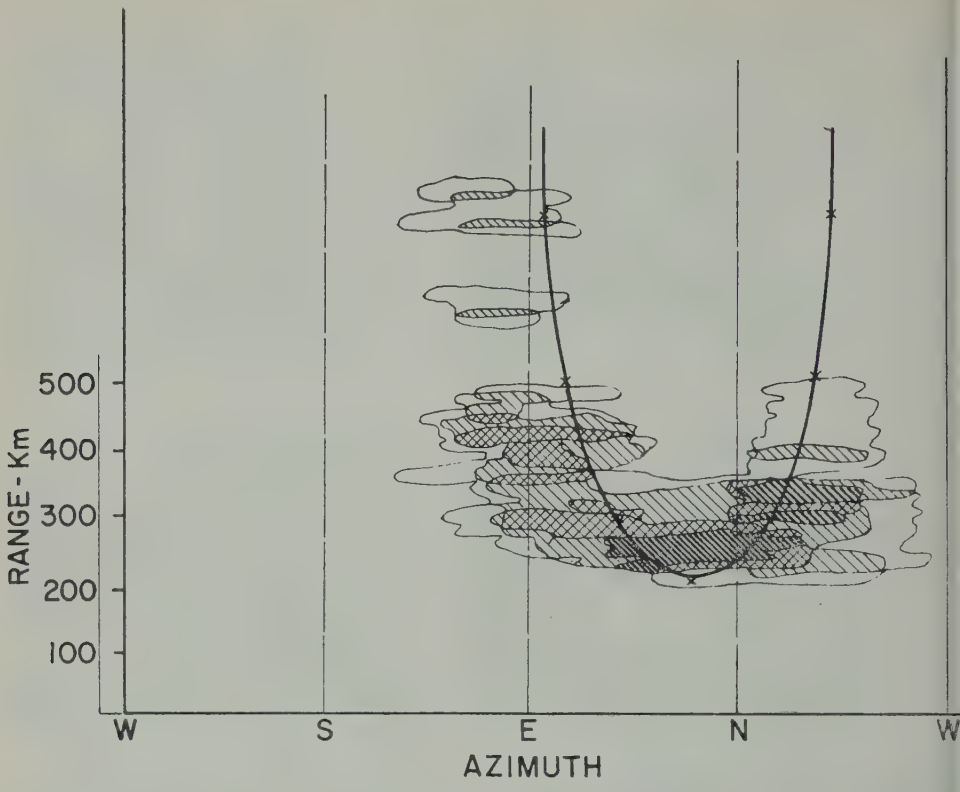

FIG. 8—Superposition of rapidly-fading echoes of Figure 7; solid line is perpendicular-reflection locus of Figure 5

Tests have been conducted at a location 250 km to the east of Stanford, bu with the same geomagnetic latitude. Their purpose was to determine if the rapidly fading reflections could be used for east-west communication in the same manne that auroral ionization can be utilized for this purpose [13,14]. When the antenna at Stanford and at the field-site at Dinuba, California, were pointed approximatel north, a 17-Mc pulse signal was found to propagate from Stanford to the nort and back to the more easterly location. During these tests, rapidly-fading signal were obtained which corresponded to oblique reflections from *both E* and *F* regions Examples of the signals observed over this path are shown in Figure 9. The delay time difference between the *E*-region and the *F*-region reflection is readily seen.

POSSIBILITIES FOR FURTHER STUDY

The results obtained thus far suggest a number of possibilities for futur study. Since echoes of the new type can be obtained from the *F* region, and ar obtained most frequently at night, it is reasonable to look for a connection betwee the echoes and the "spread *F*" condition seen on vertical-incidence sounder Preliminary attempts have been made to correlate the echoes with "spread *F*" a observed on a C-3 recorder at Stanford University. Little correlation on an hour-to

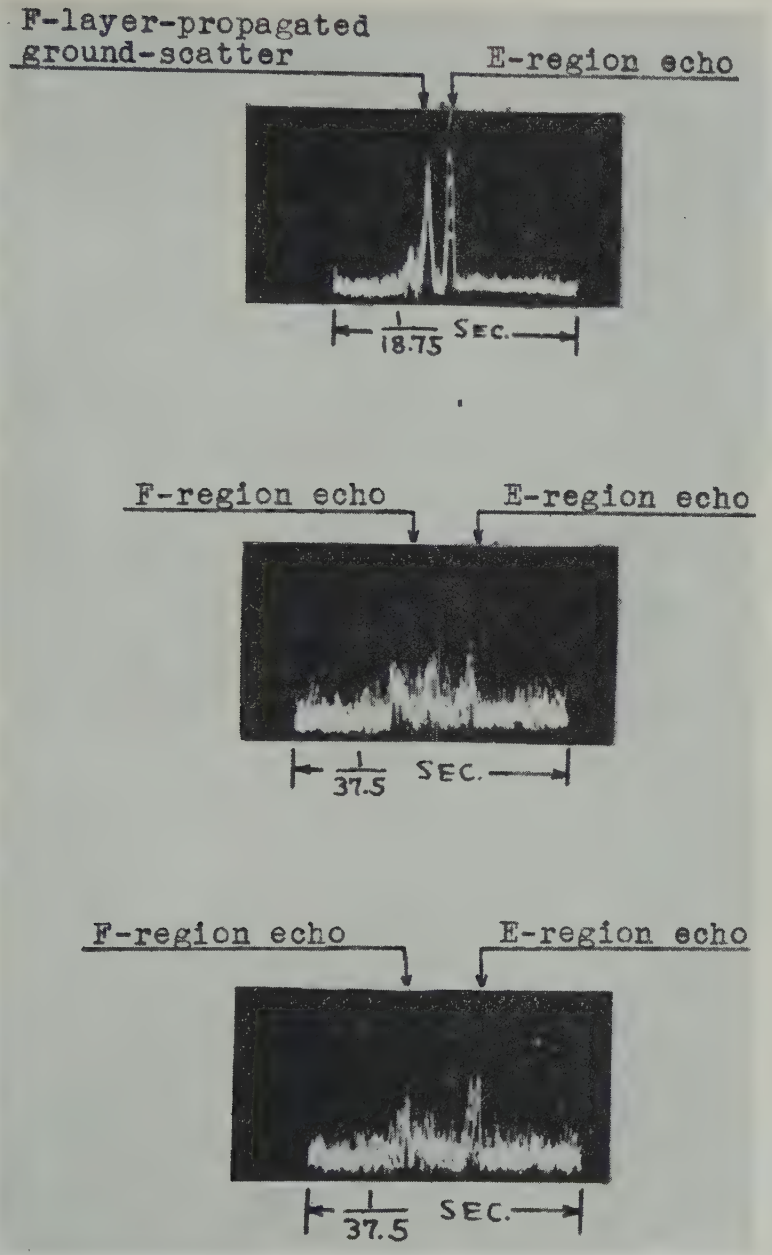

FIG. 9—Rapidly-fading reflections received at Dinuba, California (same geomagnetic latitude but 250 km east of Stanford, California), on 30 May 1955 from the 17-Mc transmitter at Stanford. Note the slowly-fading *F*-layer ground-scatter echo at 2100, which later disappeared; note also both *E*- and *F*-layer echoes of the rapidly-fading type at 2300 and 2400; sweep moves from right to left.

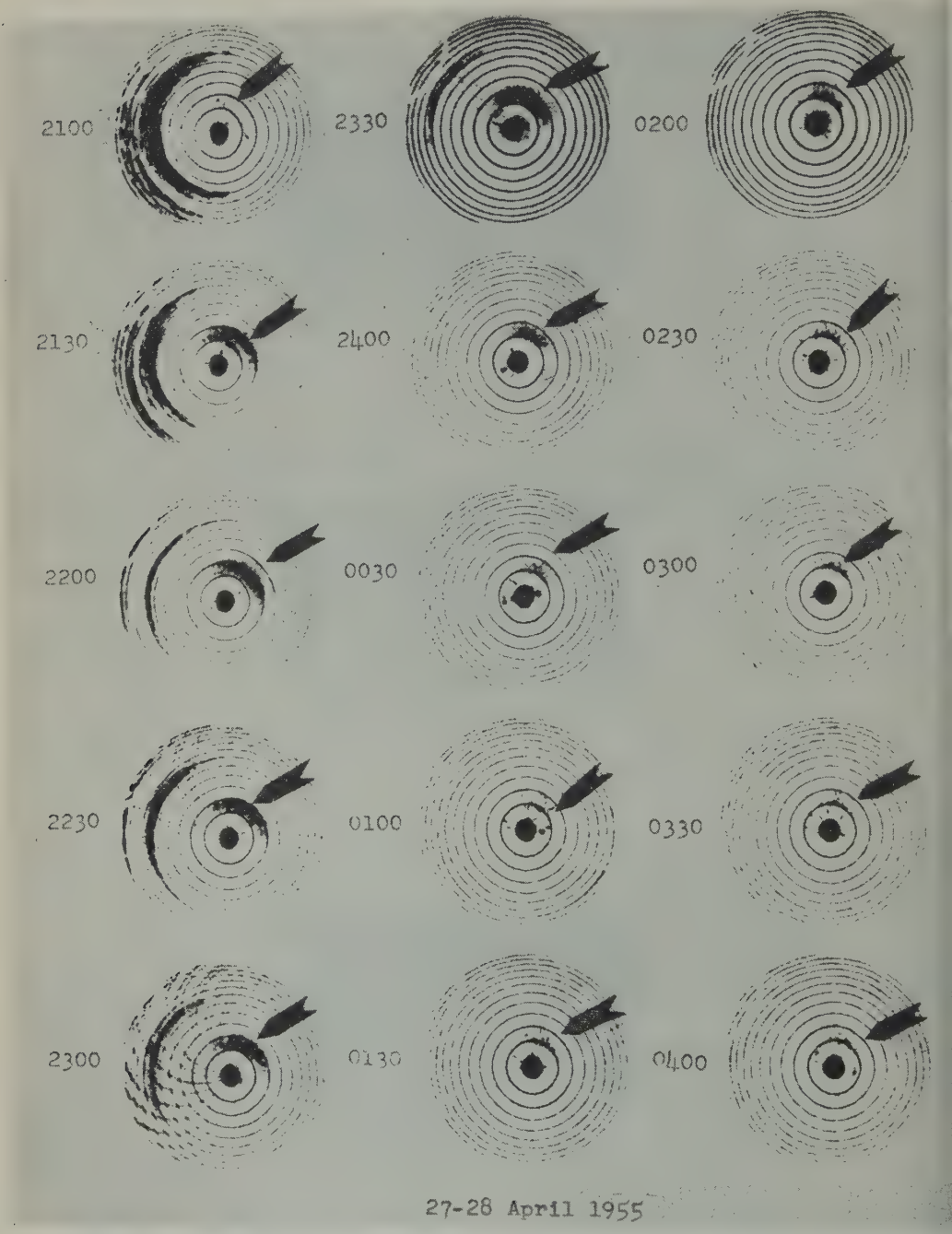

FIG. 10—Plan-position photographs taken at half-hourly intervals, illustrating the steady nature of the long-range (or *F*-layer) rapidly-fading echo. In these plots, north is at 12 o'clock, east at 3 o'clock, etc.; the geomagnetic north direction is 15°; 17-Mc rotating-beam radar; night of April 19–20, 1955; 500-km range marker circles.

hour basis was found. However, when "spread F" was seen at Stanford, the long-range echoes were usually found to occur sometime during the night. Since "spread F" varies with latitude, as pointed out by Reber [15,16], a high correlation would not be expected under these conditions, since the long-range echo has its point of origin in the ionosphere some 1200 km away from the point at which the vertical-incidence measurements were taken.

Another condition which may in some way be related to the rapidly-fading echoes is that which causes "twinkling" of radio stars.

Certain features of the variable portion of the light of the night sky resemble the general behavior of the newly-identified radio echoes. It will clearly be important to look for a possible connection between these two effects.

The F-region echoes described here represent the first direct evidence of a type of scattering occurring within the F-layer itself. It is clear that these reflections can be used for long-distance point-to-point communication under conditions

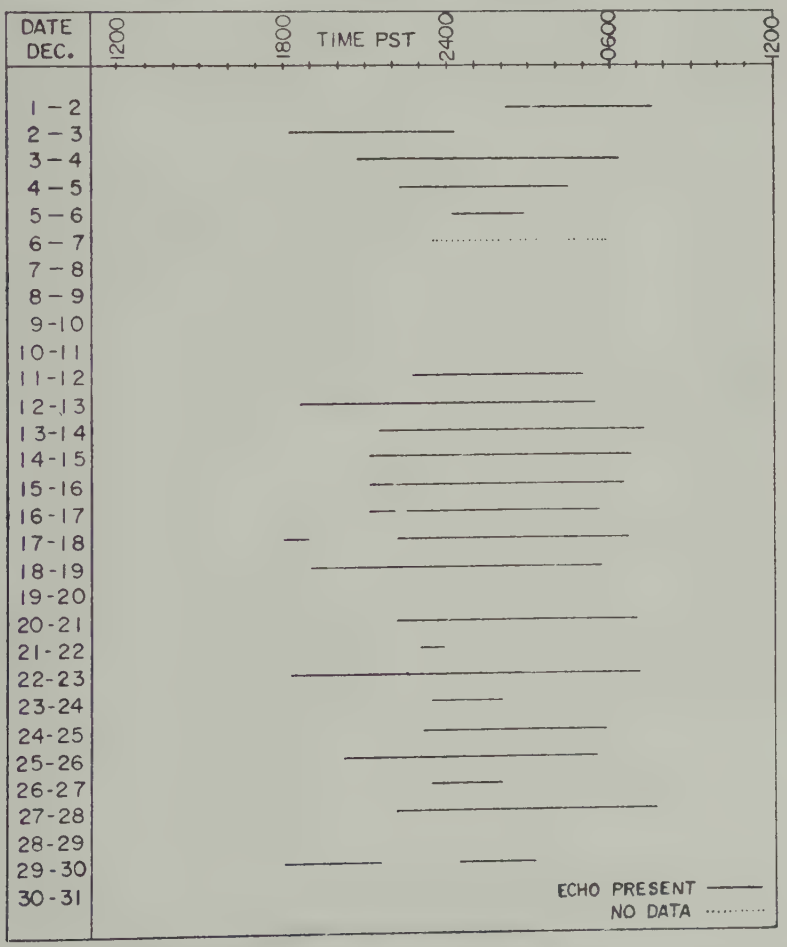

FIG. 11—Occurrences of the long-range (or F-layer) rapidly-fading echo for the month of December, 1952; 17.3-Mc scatter-sounder

where the perpendicular-reflection requirement is satisfied. Over suitably-located paths, this in itself should make possible communication at frequencies above the F-layer maximum usable frequency over distances somewhat longer than the longest which can be spanned with the aid of scattering in the E-region.

The regularity with which echoes of the new type are seen should be sufficient to make them of some practical importance. Figure 10 will serve to illustrate the remarkably consistent nature of the F-layer echo as observed at 17.31 Mc on a particular night. Figures 11 and 12 show the number of hours in each 24-hour

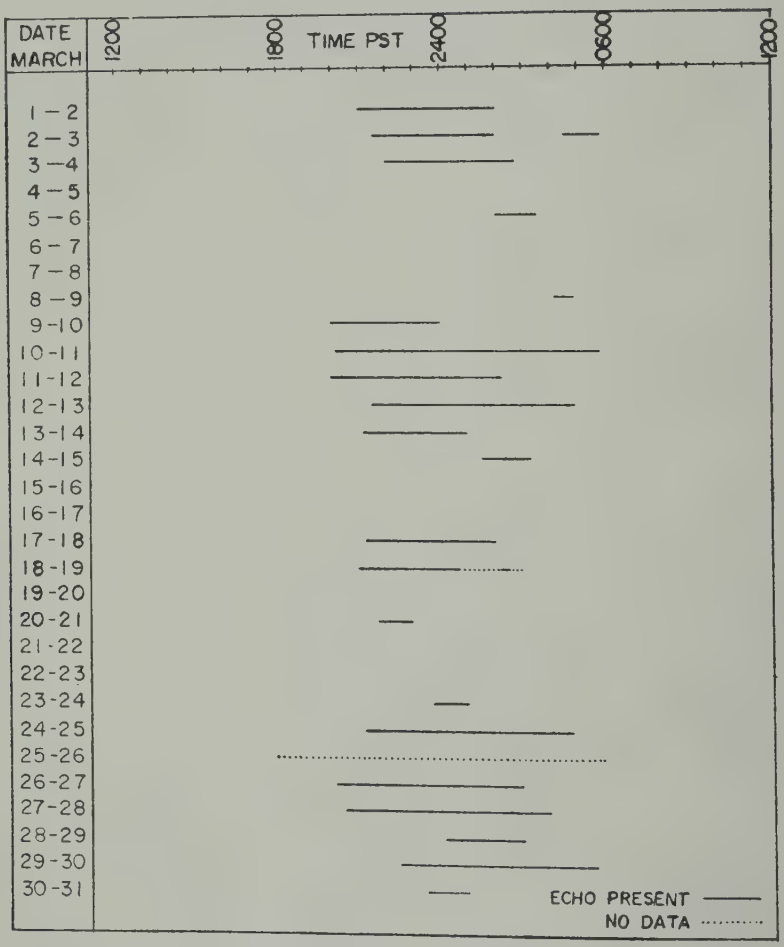

FIG. 12—Occurrences of the long-range (or F-layer) rapidly-fading echo for the month of March, 1955; 17.3-Mc scatter-sounder

period during which the echo was detectable on the 17.31-Mc radar at Stanford. Figure 11 is for the month of December, 1952; Figure 12 is for March, 1955. There is no very great difference in this behavior from month to month or year to year.

Still another interesting possibility is that the new echoes are in some way

related to one of the major types of sporadic-E ionization. On a number of occasions, appearance of the close-range or E-region echo on the scatter-sounders has been found to coincide with a general increase in the penetration frequency of sporadic-E reflections as measured on the C-3 vertical-incidence ionosphere recorder at Stanford University. Furthermore, on the scatter-sounders themselves, onset of a strong short-range fluctuating echo is usually followed by appearance of a slowly-fading ground-scatter echo at twice the slant range. For example, ground-scatter echoes can be seen at roughly twice the range of the rapidly-fading echoes in the photographs of Figure 7. No such effect is apparent in the case of the rapidly-fading long-distance or F-layer echoes.

CONCLUSIONS

Aspect-sensitive radio echoes in the 6- to 30-Mc frequency range have been regularly obtained from scattering sources located within the ionosphere at locations on the west coast of the United States, well south of the auroral zone. These echoes are consistent with the hypothesis that the energy is scattered from ionization in the form of columns (or some equivalent shape) lying along the earth's magnetic field lines. The scattering is found to arise within the E and F layers at points at which the line of sight from the transmitter meets the earth's magnetic field lines at perpendicular incidence. Echoes are seldom seen which would correspond to scattering at heights between the E and F layers. Results to date indicate that the strength of the echoes falls off very rapidly with increasing frequency, although quantitative evaluation remains to be done. High fading rates are ordinarily observed, suggesting rapid motion of the scatterers or an irregular pattern of ion production. Present indications are that the echoes arise within relatively localized, although fairly sizeable, areas. The regions from which echoes are obtained can shift within a matter of minutes from one location to another.

The echoes are observed during some portion of almost every night, magnetically quiet as well as active. Preliminary indications are that the onset of these echoes is often followed by appearance of one type of night-time sporadic-E ionization. It is suggested that whatever mechanism produces the rapidly-fading echoes may, if intense enough, also produce a sporadic-E patch.

Observations to date are very suggestive of a particle bombardment of the ionosphere at lower latitudes, perhaps similar to the more violent rain of particles responsible for the aurora further north. The possibility that a southward extension of auroral activity might exist has been proposed in the literature by a number of authors [9,10,17]. This is perhaps the most obvious interpretation of the present observations. However, the apparent lack of correlation with magnetic disturbance is a significant departure from the expected behavior if an aurora-like particle bombardment is assumed to be the cause. A comparison of the aspect-sensitive radio reflections with photometric measurements of the night-sky light should prove instructive. Photometric observations have been made of auroral spectral lines, and certain variations in the light of the night sky have been attributed to a southward extension of auroral activity [18].

ACKNOWLEDGEMENT

The work reported in this paper was supported jointly by the Army, the Navy, and the Air Force under contract ONR-N6-251-T7 and OOR-DA-04-200-ORD 181 with Stanford University. It could not have been performed without the generous assistance of Messrs. R. O. Beaudette and J. P. Swann of Spokane, Washington. The help of R. D. Egan, L. Juste, T. Harroun, A. Ruiz-Sanchez, and S. Stein, all students at Stanford University, is gratefully acknowledged.

References

[1] A. M. Peterson, The mechanism of *F*-layer propagated back-scatter echoes, J. Geophys. Res., **56**, 221–237 (1955).

[2] O. G. Villard, Jr., and A. M. Peterson, A method for studying sporadic-*E* clouds at a distance, Proc. Inst. Radio Eng., **40**, 992–994 (1952).

[3] A. M. Peterson, A scatter-sounder for the study of sporadic ionization in the upper atmosphere, Radio Prop. Lab., Stanford University, Contract DA-04-200-ORD 181, Tech. Rep. No. 1 (Sept. 1953).

[4] O. G. Villard, Jr., and A. M. Peterson, Instantaneous prediction of radio transmission paths, QST, **34**, 11–15 (1952).

[5] G. Hellgren and J. Meos, Localization of aurorae with 10 m high power radar technique, using a rotating antenna, Research Laboratory of Electronics, Rep. No. 26 [reprint from Tellus, **4**, 249–261 (1952)].

[6] A. M. Peterson and R. L. Leadabrand, Long-range radio echoes from auroral ionization, J. Geophys. Res., **59**, 306–309 (1954).

[7] K. L. Bowles, Doppler shifted radio echoes from aurora, J. Geophys. Res., **59**, 553–555 (1954).

[8] O. G. Villard, Jr., A. M. Peterson, and R. L. Leadabrand, Simultaneous scatter-sounding observations of sporadic *E* clouds at two separated locations, paper presented at the International Scientific Radio Union meeting, May 1955, Washington, D. C.

[9] R. K. Moore, Theory of radio scattering from the aurora, Trans. Inst. Radio Eng., Prof. Group on Antennas and Propagation, No. 3, 217 (1952).

[10] S. Chapman, The geometry of radio reflections from the aurora, J. Atmos. Terr. Phys., **3**, 1–29 (1952).

[11] J. C. Seddon, A. D. Pickar, and J. E. Jackson, Continuous electron density measurements up to 200 km, J. Geophys. Res., **59**, 513–524 (1954).

[12] J. C. Seddon, Electron densities in the ionosphere, J. Geophys. Res., **59**, 463–466 (1954).

[13] R. K. Moore, A V.H.F. propagation phenomena associated with aurora, J. Geophys. Res., **56**, 97–106 (1951).

[14] R. Dyce, More about V.H.F. auroral propagation, QST, **34**, 11–15 (1955).

[15] G. Reber, Spread *F* over Hawaii, J. Geophys. Res., **59**, 257–265 (1954).

[16] G. Reber, Spread *F* over Washington, J. Geophys. Res., **59**, 445–448 (1954).

[17] H. G. Booker, C. W. Gartlein, and B. Nichols, An interpretation of radio reflections from the aurora, J. Geophys. Res., **60**, 1–22 (1955).

[18] F. E. Roach, D. R. Williams, and H. B. Pettit, The diurnal variation of [OI] 5577 in the nightglow: Geographical studies, J. Geophys. Res., **58**, 73–82 (1953).

FORMATION OF THE LOWER IONOSPHERE

BY K. WATANABE,* F. F. MARMO, AND JEROME PRESSMAN
Geophysics Research Directorate,
Air Force Cambridge Research Center,
Air Research and Development Command,
Cambridge, Massachusetts

(Received July 29, 1955)

ABSTRACT

According to new absorption data on O_2 and N_2 in the spectral region 850-1100A, photoionization of atmospheric O_2 at its first ionization potential should occur in the *E* layer rather than the *D* layer. In particular, Lyman beta in the solar spectrum is expected to be an important line, as it can ionize O_2 while it is quite transparent to N_2 . A flux of about 10^9 photons cm^{-2} sec^{-1} for this line can account for the lower *E* layer, while the higher region may be in part ascribed to an observed preionization of the Hopfield bands. Thus, it is not possible yet to reject the oxygen theory in favor of the x-ray theory of the *E* layer.

INTRODUCTION

Of the several processes suggested for the formation of the *E* layer, the following have the strongest support: (*A*) Photoionization of molecular oxygen at its first ionization potential, and (*B*) ionization of air by soft x-rays of about 40A. Recent theoretical studies [see 1, 2, 3, 4, 5 of "References" at end of paper] of the problem indicate that additional data are necessary in order to establish the relative importance of these processes.

The case for the x-rays has been greatly strengthened by rocket measurements of solar radiation, particularly by means of photon counters [6]. Byram, *et al.* [7], have claimed that the sun supplies an adequate amount of soft x-rays to account for the production of the entire *E* layer. Their most recent report [8] states that the flux over the entire x-ray region is about 0.1 erg cm^{-2} sec^{-1}, which is about 2×10^8 photons cm^{-2} sec^{-1}. This result appears to be consistent with theoretical estimates of emission from the solar corona [2,9].

On the other hand, there have been several objections to the theory that the *E* layer is due to the process

$$O_2(X^3\Sigma_g^-) + h\nu(\sim 900\text{–}1000\text{A}) \rightarrow O_2^+(X^2\Pi_g) + e \quad \ldots\ldots\ldots\ldots (1)$$

These are:

(*a*) The transition layer for dissociation of O_2 calculated on the basis of photochemical equilibrium, such as that by Penndorf [10], is too narrow ($\sim$ 10 km).

*Present address: Department of Physics, University of Hawaii, Honolulu, Hawaii.

(*b*) The cross-section of the ionization continuum associated with process (1) has been assumed to be very small ($\sim 10^{-20} - 10^{-21}$ cm^2), which would place (1) in the *D* layer.

(*c*) Use of the strong absorption bands of O_2 in the same spectral region in place of the continuum as proposed by Nicolet [11] requires experimental confirmation of the process,

$$O_2 + h\nu \text{ (at Hopfield bands)} \rightarrow O_2^* \rightarrow O_2^+(X^2\Pi_g) + e \quad . \quad . \quad . \quad . \quad (2)$$

where the second step represents preionization.

(*d*) Rawer and Argence [4] have doubted whether the radiation in the region 900-1000A penetrates into the *E* layer.

(*e*) Byram, *et al.* [7], have rejected process (1) on the basis that the estimated energy available in the relevant spectral region is very small ($\sim$ 0.0004 erg cm^{-2} sec^{-1} per 100A).

It appears that all of these objections rely on assumptions or incomplete data. In this respect, the present paper is an attempt to remove most of these objections and to show that process (1) probably makes a major contribution to the *E* layer on the basis of some new absorption data. The *D* layer is also discussed in terms of these data.

EXPERIMENTAL DATA

In this section, experimental results relevant only to the discussion of the lower ionosphere are presented. Description of the experimental method, which is similar to those described previously [12,13], and more detailed discussion of the data will be reported elsewhere.

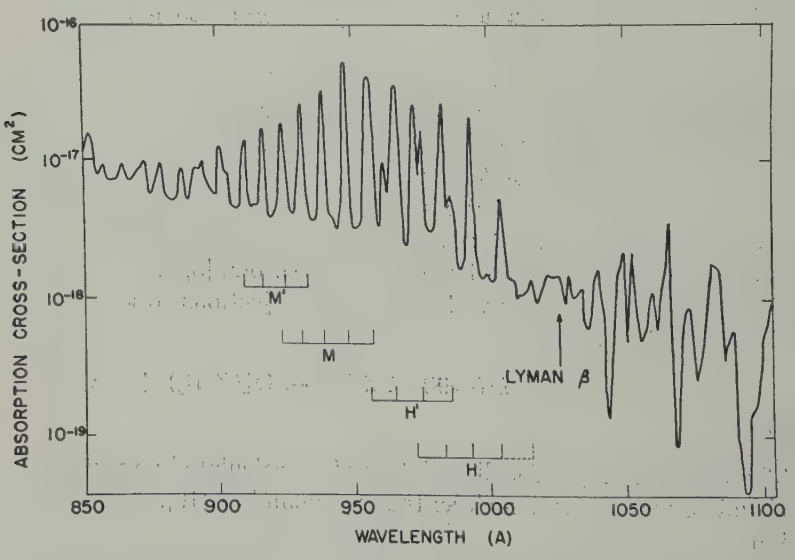

FIG. 1—Absorption cross-section of O_2 in the spectral region 850-1100A

1. *Absorption Cross-Section of* O_2

The total absorption cross-section, σ, of O_2 for the spectral region 850-1100A, shown in Figure 1, is an extension of our previous work [12]. The curve is based on measurements at nearly 200 wavelengths, one to three angstroms apart. This absorption spectrum agrees well with photographs by Price and Collins [14] and by Tanaka and Takamine [15]. The intense Hopfield bands, which Price and Collins [14] have identified as Rydberg bands (designated H, H′, M, M′) leading to the second ionization potential, were not completely resolved although they are diffuse bands, and the σ-values at the band maxima may be somewhat low. Otherwise the σ-values below about 1035A were independent of pressure, indicating a true continuum underlying these bands. The result, shown in Figure 1, gives a more detailed picture than previously reported results [16,17] for this region and appears to be sufficiently quantitative for application to the ionosphere.

2. *First Ionization Potential of* O_2

By the photoionization method [13,18], the first ionization potential was found to be 12.07 $\pm$ 0.01 ev (1027A). This is preferred to the preliminary result 12.04 $\pm$ 0.01 ev obtained by Inn [19], as the latter measured only the appearance wavelength and not the shape [18] of the ionization continuum. These values are consistent and are somewhat lower than the accepted value [20], 12.2 ev. The difference is very important in connection with the E layer, as only the lower values would allow Lyman beta (1025.7A) to ionize O_2 .

3. *Ionization Yield of* O_2

By the method described previously [13,18], ionization yields of O_2 were found to vary from about 40 to 100 per cent for about a hundred wavelengths in the region 855-1027A. The H bands at 993.1, 983.1, and 972.5A gave the lowest yields, 40-50 per cent; the other bands showed higher yields up to 80 per cent. The yields for the region outside of the bands varied from about 60 to 100 per cent. In particular, the σ-value at Lyman beta was 1.54×10^{-18} cm^2 and the ionization cross-section was 58 per cent of this value. Thus, the curve for ionization cross-section of O_2 in the region 855-1028A is very similar to Figure 1, so the latter will be used in our discussion. Wainfan, *et al.* [21], obtained ionization yields (30-70 per cent) at three wavelengths in the above spectral region.

4. *Absorption Spectrum of* N_2

Since a strong absorption by atmospheric N_2 may remove solar radiation required for process (1), it is necessary to know the absorption cross-section of N_2 in the same spectral region. Our measurements showed that in the region 995-1050A N_2 is very transparent (σ values $\sim 10^{-20}$ or less). For example, at Lyman beta, the cross-section is about 4×10^{-21} cm^2, which is much lower than the values obtained by Weissler, *et al.* [22] ($\sim 2 \times 10^{-18}$ cm^2), and Clark [17] ($\sim 3 \times 10^{-19}$ cm^2). The latter values are probably too high, as their measurements were not designed for small cross-sections.

In the region below 995A, there are many strong sharp bands, as well as deep

windows, in the N_2 absorption spectrum. It was not possible to resolve these bands with rotational structure [23], and the absorption cross-section obtained for the region 850-995A is only semiquantitative. The values ranged from 3×10^{-17} cm^2 at the band head of the strongest bands to about 2×10^{-20} cm^2 at the deepest windows, but the values for the maxima are no doubt too low and minima too high. The result above is consistent with photographs by Worley [23], which do show a number of windows in the N_2 absorption spectrum.

DISCUSSION

1. *D Layer*

The formation of the *D* layer by process (1) may be eliminated by showing that the required radiation does not penetrate into this layer. Previously, Bates and Seaton [24] had suggested that this is the case on the basis of spectrograms by Hopfield [25]. We have estimated [26] likewise that the minimum absorption cross-section of *air* is higher (about 10^{-19} cm^2) than other estimates ($\sim 10^{-21}$ cm^2) used by Mitra [27]. Figure 1 shows that the minimum absorption cross-section of O_2 in the spectral region 1027-850A is about 10^{-18} cm^2. For this cross-section, the maximum absorption rate probably occurs at about 95 km, as discussed in the following section on the *E* layer, and process (1) cannot be used for the formation of the *D* layer.

If we accept the preceding conclusion, minor constituents such as ozone with ionization potentials higher than about 12 ev cannot be used for the formation of the *D* layer by the action of solar ultraviolet. On the other hand, Bates and Seaton [24] have examined the processes

$$\mathrm{Na} + h\nu(> 5.1 \text{ ev}) \rightarrow \mathrm{Na}^+ + e \quad \ldots\ldots\ldots\ldots\ldots\ldots (2)$$

proposed by Jouaust and Vassy [28], and

$$\mathrm{O}(^1\mathrm{S}) + \text{Ly } \alpha \rightarrow \mathrm{O}(^1\mathrm{P})$$

$$\mathrm{O}(^1\mathrm{P}) + \mathrm{X} \rightarrow \mathrm{O}^+(^4\mathrm{S}) + \mathrm{X} + e + 0.75 \text{ ev} \quad \ldots\ldots\ldots\ldots\ldots\ldots (3)$$

proposed by Chapman and Price [29], which require photon energy less than 12 ev, and concluded that these processes do not appear to have ionization rates high enough to account for the normal *D* layer.

Although high energy photons of wavelength less than about 10A can penetrate into the *D* layer, rocket measurements [6] show that the amount of soft x-rays in this energy range is insufficient to produce the normal *D* layer.

In view of these considerations, the most probable process appears to be the photoionization of nitric oxide by ultraviolet in the region 1100-1340A. Recent rocket spectrograms [30,31] show that most of the energy in this spectral region is concentrated in the Lyman alpha line (1215.6A), and hence the *D* layer may be due mainly to

$$\mathrm{NO} + \text{Ly } \alpha \rightarrow \mathrm{NO}^+(v = 0, 1, 2, 3) + e \quad \ldots\ldots\ldots\ldots\ldots\ldots (4)$$

where the vibrational levels of NO^+ are inferred from laboratory data [18].

2. *E Layer*

In this section, we consider the several objections to the oxygen theory of the *E* layer which were listed in the introduction.

Objection (*a*) on the width of the transition layer of O_2, dissociation appears to be removed by recent rocket data [6,32], which indicate a broad transition region of nearly 50 km. Furthermore, Nicolet and Mange [33] have shown that mixing and diffusion must be included in a photochemical theory, because the observed solar flux [6] in the spectral region around 1500A effective for the dissociation of O_2 is much less than that from a black body of 6000°K and, consequently, the time for photochemical equilibrium is in the order of days. Nicolet [34] has obtained a distribution curve of O_2 very close to that observed by Byram, *et al.* [32], in the region 100-130 km. To calculate optical densities, we have used these results with extrapolation down to 90 km.

To discuss objections (*b*) and (*c*), we refer to Figure 1. The minimum absorption cross-section of O_2 varies from about 10^{-18} to 5×10^{-18} cm^2 in the spectral region from 1027 to 900A. For these cross-sections, maximum rate of absorption occurs at about 95 to 105 km for vertical incidence, using the above data for oxygen distribution and neglecting absorption by N_2. On the other hand, the strong bands in this spectral region are all preionized, and the strongest of them has a cross-section of about 5×10^{-17} cm^2, the height for maximum rate of absorption being about 120 km. Thus, the entire absorption spectrum of O_2 in the region 1027-900A meets the altitude requirement for the *E* layer. As the ionization yield ranges from 40 to 100 per cent of total absorption, any absorption by O_2 in this spectral region, including the bands, contributes to the *E* layer. Thus, objections (*b*) and (*c*) are removed.

Rawer and Argence [4] have suggested that process (1) is not as important as x-ray ionization, on the basis that the absorption coefficient of N_2 in the spectral region 900-1000A appears to be uniformly high. From published data [22], they adopted a coefficient of 500 cm^{-1} over the region below 980A and allowed for only one shallow minimum near Lyman beta with a coefficient of 60 cm^{-1}. This interpretation is not consistent with the absorption spectrum of N_2, for no strong absorption continua have been observed in this spectral region and, in fact, photographs by Worley [23] show that there are windows as well as many sharp bands. The absorption cross-sections of these windows, according to our data, are about 10^{-19} cm^2, and even this value is considered to be too high, because the spectrum was not well resolved in our measurements. At Lyman beta, the cross-section is about 4×10^{-21} cm^2, much less than that reported by Weissler, *et al.* [22]. Thus, objection (*d*) does not appear to be serious, although a considerable portion of solar radiation in the region 900-995A may be removed by N_2 rather than by O_2.

In objection (*e*), Byram, *et al.* [7], have assumed that the solar energy available in the spectral region around 1000A corresponds to that from a black body of about 4500°K. However, as yet, there are no quantitative energy measurements in this region of the solar spectrum, and it seems they have neglected the possible contribution from emission lines such as Lyman beta which may greatly exceed that from the continuum. In the spectral region 1100-1300A, there are several estimated experimental values of incident flux expressed in ergs cm^{-2} sec^{-1}: 0.4

by thermoluminescent phosphor [35], 1-10 by photon counters [6], 0.5 for Lyman alpha by a spectrograph [30], and 0.1 by photon counters [36]. Moreover, as mentioned earlier, most of the energy is apparently concentrated in the Lyman alpha line. The large spread in these values may be ascribed mostly to experimental uncertainties and partly to real variation in the emission intensity; for the present, about 0.2 erg cm^{-2} sec^{-1} or 1.2×10^{10} photons cm^{-2} sec^{-1} may be a realistic value for Lyman alpha. Nicolet [37] has estimated that the Lyman alpha line is about 2×10^{10} photons cm^{-2} sec^{-1}, Lyman beta about 3×10^{9}, and Lyman gamma 4×10^{8}. In this connection, it may be noted that the intensity of Lyman beta from our laboratory hydrogen lamp is about one order of magnitude lower than that of Lyman alpha. From these considerations, it would appear that the intensity of solar Lyman beta greatly exceeds that from the continuum around 1000A and is by no means negligible.

In order to show that processes (1) and (1*a*) may make a major contribution to the *E* layer, we consider a few members of the Lyman series.

(1) *Lyman beta* (1025.7A)—This line should be absorbed almost entirely by O_2, as N_2 is quite transparent. The σ-value for O_2 being 1.54×10^{-18} cm^2, most of the absorption should occur in the altitude range 95 to 110 km. Since more than half of the absorption leads to ionization, about 10^9 photons cm^{-2} sec^{-1} should account for the lower *E* layer. This intensity is not inconsistent with that observed for Lyman alpha.

(2) *Lyman gamma* (972.5A)—A strong N_2 band should absorb most of this line; however, if N_2 is dissociated above the *E* layer, some absorption by O_2 in one of the Hopfield bands with a cross-section of 2.6×10^{-17} cm^2 may contribute electrons near the top of the *E* layer by process (1*a*).

(3) *Lyman delta* (949.7A)—This line lies in a relatively transparent portion of the N_2 absorption spectrum and also between two bands in the O_2 spectrum where the σ-value is 3.3×10^{-18} cm^2 and ionization yield is about 90 per cent. Most of the absorption should occur in the altitude range 100 to 115 km, but the amount may be small, as the intensity of this line is expected to be much weaker than that of Lyman beta.

The above estimate is hardly satisfactory, but does indicate that at least Lyman beta is important to the formation of the *E* layer. In this connection, it is interesting to note that the observed changes of the distribution of electron density in the *E* layer may be due to changes in the O_2 distribution. Process (1) will be sensitive to this change, while photoionization by x-rays will be much less affected.

References

[1] D. R. Bates, Proc. R. Soc. (London), A, **196**, 562 (1949).
[2] M. Nicolet, Ann. Géophys., **8**, 141 (1952).
[3] D. C. Choudhury, Phys. Rev., **88**, 405 (1952).
[4] K. Rawer and E. Argence, Phys. Rev., **94**, 253 (1954).
[5] T. Sato, Rep. Ionosphere Res. Japan, 8, 49 (1954).
[6] H. Friedman, S. W. Lichtman, and E. T. Byram, Phys. Rev., **83**, 1025 (1951).
[7] E. T. Byram, T. Chubb, and H. Friedman, Phys. Rev., **92**, 1066 (1953).
[8] E. T. Byram, T. Chubb, and H. Friedman, Phys. Rev., **96**, 860 (1954); also private communication.

[9] H. Bondi, F. Hoyle, and R. A. Lyttleton, Mon. Not. R. Astr. Soc., **107**, 184 (1947); R. v. d. R. Woolley and C. W. Allen, *ibid.*, **108**, 292 (1948); **110**, 358 (1950); G. Elwert, Zs. Naturf., **7a**, 202 (1952).
[10] R. Penndorf, J. Geophys. Res., **54**, 7 (1949).
[11] M. Nicolet, Mém. Inst. R. Mét. Belgique, **19**, 124 (1945).
[12] K. Watanabe, E. C. Y. Inn, and M. Zelikoff, J. Chem. Phys., **21**, 1026 (1953).
[13] K. Watanabe, F. F. Marmo, and E. C. Y. Inn, Phys. Rev., **91**, 1155 (1953).
[14] W. C. Price and G. Collins, Phys. Rev., **48**, 714 (1935).
[15] Y. Tanaka and Y. Takamine, Sci. Pap., Inst. Phys. Chem. Res. (Japan), **39**, 437 (1942).
[16] G. L. Weissler and P. Lee, J. Optical Soc. Amer., **42**, 200 (1952).
[17] K. C. Clark, Phys. Rev., **87**, 271 (1952).
[18] K. Watanabe, J. Chem. Phys., **22**, 1564 (1954).
[19] E. C. Y. Inn, Phys. Rev., **91**, 1194 (1953).
[20] G. Herzberg, Spectra of Diatomic Molecules, D. Van Nostrand Co., Inc., New York (1950); p. 459.
[21] N. Wainfan, W. C. Walker, and G. L. Weissler, J. Appl. Phys., **24**, 1318 (1953).
[22] G. L. Weissler, P. Lee, and E. I. Mohr, J. Optical Soc. Amer., **42**, 84 (1952).
[23] R. E. Worley, Phys. Rev., **64**, 207 (1943).
[24] D. R. Bates and M. J. Seaton, Proc. Phys. Soc. (London), B, **63**, 129 (1950).
[25] J. J. Hopfield, Astroph. J., **104**, 208 (1946).
[26] K. Watanabe, F. F. Marmo, and E. C. Y. Inn, Phys. Rev., **90**, 155 (1953).
[27] A. P. Mitra, J. Geophys. Res., **56**, 373 (1951).
[28] R. Jouaust and E. Vassy, Paris, C.-R. Acad. sci., **213**, 139 (1941).
[29] S. Chapman and W. C. Price, Rep. Prog. Phys. (The Physical Society, London), **3**, 55 (1936).
[30] W. A. Rense, Phys. Rev., **91**, 299 (1953).
[31] F. S. Johnson, J. D. Purcell, and R. Tousey, Phys. Rev., **95**, 621 (1954).
[32] E. T. Byram, T. Chubb, and H. Friedman, J. Optical Soc. Amer., **44**, 353 (1954); also private communication.
[33] M. Nicolet and P. Mange, J. Geophys. Res., **59**, 15 (1954).
[34] M. Nicolet, Pennsylvania State University, Ionosphere Res. Lab., Sci. Rep. No. 61 (1954).
[35] R. Tousey, K. Watanabe, and J. D. Purcell, Phys. Rev., **83**, 165 (1951).
[36] E. T. Byram, T. Chubb, H. Friedman, and N. Gailar, Phys. Rev., **91**, 1278 (1953).
[37] M. Nicolet, in Physics and Medicine of the Upper Atmosphere, University of New Mexico Press, Albuquerque (1952); p. 195.

JOURNAL OF GEOPHYSICAL RESEARCH VOLUME 60, No. 4 DECEMBER, 1955

VISCOSITY IN THE *F* REGION

BY J. W. DUNGEY AND A. J. WILLSON

Cavendish Laboratory, Cambridge, England

(Received July 26, 1955)

ABSTRACT

The problem of viscosity for disturbances whose scale is smaller than the mean free path is attacked by means of Boltzmann's equation. It is shown that the phenomenon cannot be described by an "effective coefficient of viscosity" and that viscosity is of primary importance under these conditions. The implications for the aerodynamics of the *F* region are discussed.

In his recent discussion of viscosity in the high atmosphere, Yerg [see 1 of "References" at end of paper] has considered the effect of viscosity for disturbances whose scale is smaller than the mean free path λ. The usual mean-free-path method gives a formula for the coefficient of viscosity of a gas which is independent of the density, so that the corresponding kinematic viscosity is inversely proportional to the density. When λ is large compared with the scale of variation of the velocity, it is well known that this method of calculation is invalid. If the effect of viscosity could be described by an "effective coefficient of (kinematic) viscosity," it seems probable that such an effective coefficient would be smaller than that given by the usual formula which leads to infinite kinematic viscosity when λ tends to infinity. Yerg (1) attacks the problem by means of an expansion in powers of λ, thus involving higher spatial derivatives of the velocity than the first, and concludes that, at least for a particular example of shear flow, an effective coefficient of viscosity can be used, which varies like λ^{-1} when λ is large.

However, Yerg's method is a mean-free-path method, and is therefore hardly appropriate when λ is large. In this note, a different approach is adopted, which shows that an effective coefficient of viscosity cannot be used, and that the phenomenon of viscosity is so important that any initial motion on a scale small compared with λ disappears very rapidly. This has important consequences for the *F* region.

In the extreme case, in which collisions can be neglected altogether and there are no external forces, each gas molecule travels in a straight line with constant velocity. Given a simple initial velocity distribution, Boltzmann's equation can then be integrated. Consider a gas of uniform density and initial mean velocity $[U(z), 0, 0]$; let the velocity distribution function f have the form $F(u - U)G(v)H(w)$, where u, v, w are the velocity components and F, G and H are even functions of their arguments. Boltzmann's equation reduces to

$$\frac{\partial f}{\partial t} = -w \frac{\partial f}{\partial z}$$

and the solution is

$$f = F\{u - U(z - wt)\}G(v)H(w)$$

The mean value $\bar{u}(z, t)$ of u at time t is then given by

$$\bar{u}\int_{-\infty}^{\infty} H(w)\,dw = \int_{-\infty}^{\infty} U(z - wt)H(w)\,dw$$

which shows that $\bar{u}$ is linearly related to U. It is, therefore, sufficient to consider a Fourier component of U; let $U(z) = U_0 \cos(\beta z)$. Then

$$\bar{u}\int_{-\infty}^{\infty} H(w)\,dw = U_0 \cos(\beta z)\int_{-\infty}^{\infty} \cos(\beta wt)H(w)\,dw$$

and the time variation of $\bar{u}$ is given by the Fourier transform of $H(w)$. When the initial distribution is Maxwellian, $H(w) \propto \exp[-mw^2/2kT]$, and it is well known that the Fourier transform is proportional to $\exp[-kT\beta^2t^2/2m]$. Hence

$$\bar{u} = U_0 \cos(\beta z) \exp[-kT\beta^2t^2/2m]$$

For a situation in which the motion may be described by a coefficient of viscosity, there would be an exponential decay with time of a Fourier component of velocity; hence, we must conclude that the problem considered above cannot be described in terms of an effective coefficient of viscosity. Nevertheless, the solution does show that the velocity decreases very rapidly after a time of order $(2m/kT\beta^2)^{\frac{1}{2}}$. This is the time taken by a particle of velocity $(kT/2m)^{\frac{1}{2}}$ to travel the distance β^{-1}, and is small compared with the time-scale of the flow, provided the velocity of flow is much smaller than the velocity of sound.

It may be noted that, if the velocity distribution is to remain unchanged in time, the velocity profile must be linear. This is also true when a coefficient of viscosity can be used. Such a profile might be relevant to the flow between solid plates, but in this note the scale of the flow must be regarded as limiting the distance over which the profile can approximate to linearity.

Because there is nothing in the F region capable of maintaining velocity differences over distances small compared with λ, it may be concluded that the scale of variation of the mean velocity of neutral molecules is at least as large as λ. Then, if turbulence should occur, eddies smaller than λ must be negligible. The numerical values suggested by Bates [2] give $\lambda \sim 200$ km at 400-km altitude, and the majority of workers accept this order of magnitude. It then follows that the patches of ionisation, which cause the scintillation of radio stars, cannot be due to turbulence in the neutral gas, as suggested by Maxwell [3].

Viscosity need not prevent a general circulation in the F region, whose existence was previously suggested by Yerg [4]. If such a circulation were driven by heating lower in the atmosphere, however, it could be treated as a thermal tide, and Wilkes [5] has shown that tidal motions are heavily attenuated even below the F region. Any general circulation must therefore be driven locally.

Acknowledgments—We are indebted to Dr. K. Weekes for a valuable discussion. One of us (J.W.D.) is indebted to Imperical Chemical Industries for a fellowship

and one (A.J.W.) to the Department of Scientific and Industrial Research for a grant.

References

[1] D. G. Yerg, J. Geophys. Res., **60**, 87 (1955).
[2] D. R. Bates, Rocket Exploration of the Upper Atmosphere (edited by R. L. F. Boyd and M. J. Seaton), Pergamon Press, Ltd., London (1954); p. 347.
[3] A. Maxwell, Phil. Mag., **45**, 1247 (1954).
[4] D. G. Yerg, J. Met., **8**, 244 (1951).
[5] M. V. Wilkes, Oscillations of the Earth's Atmosphere, University Press, Cambridge (1949); p. 39.

GEOMAGNETIC AND SOLAR DATA

INTERNATIONAL DATA ON MAGNETIC DISTURBANCES, SECOND QUARTER, 1955

Preliminary Report on Sudden Commencements

S.c.'s given by five or more stations are in italics. Times given are mean values, with special weight on data from quick-run records.

Sudden commencements followed by a magnetic storm or a period of storminess (s.s.c.)

1955 April *24d 12h 13m:* fourteen (s.i.?).—*27d 16h 24m:* thirty-nine.
1955 May 05d 14h 54m: Ci Ap.—*25d 14h 33m:* thirty-seven.
1955 June *06d 17h 28m:* twenty-six.—*22d 10h 39m:* twenty-nine.

Sudden commencements of polar or pulsational disturbances (p.s.c.)

1955 April 01d 19h 25m: So Tn.—*01d 21h 05:* seventeen.—01d 21h 32: MB Ba Hr.—*02d 13h 12:* five.—*02d 21h 13:* twelve.—*02d 21h 23:* six.—03d 21h 13: Ma Gi.—*04d 22h 01:* thirteen.—04d 22h 40: SM Ta Ba.—05d 13h 28: Ta Ap To Am.—05d 19h 31: Do Le Es El.—*06d 21h 04:* fifteen.—06d 23h 01: Wn SM.—07d 00h 16: CF Va.—07d 02h 01: CF Va.—*08d 20h 57:* eleven.—09d 03h 39: CF Bi.—*09d 22h 07:* twenty-five.—11d 03h 16: CF SM Bi.—12d 01h 52: CF Eb Bi.—12d 02h 07: CF MB Va.—13d 22h 44: SM Ta.—14d 22h 06: Eb Ta El.—*15d 00h 40:* eleven.—15d 01h 55: CF MB.—15d 03h 13: CF Ta.—16d 12h 40: Eb Tl Ka To.—19d 03h 42: CF Bi.—19d 13h 13: Ka Ta.—20d 01h 00: CF SM.—21d 04h 36: El Va.—22d 01h 50: CF Eb Ta El.—*22d 19h 36:* eleven.—22d 20h 53: Eb Gi.—24d 04h 27: Qu Bi.—*25d 19h 10:* seven.—25d 23h 56: Ma Ta Bi.—*26d 20h 04:* fourteen.—*26d 22h 43:* fourteen.—28d 00h 33: SM MB El Hr.—*28d 20h 36:* nine.—*29d 20h 39:* nine.—*30d 22h 40:* twelve.

1955 May 01d 21h 00m: CF Ta Bi Hr.—*01d 21h 09:* sixteen.—*02d 21h 58:* twelve.—*03d 01h 17:* nine.—03d 01h 32: IK MB El Va.—06d 12h 10: Ka Ap.—*06d 22h 25:* thirteen.—08d 11h 56: Ka To.—08d 18h 29: Ta El Hr.—08d 22h 36: Ci MB.—*08d 23h 21:* seventeen.—*09d 23h 54:* nine.—10d 11h 02: Ap Am.—10d 20h 31: Bi Tn.—*10d 21h 01:* ten.—11d 20h 43: CF Bi El.—11d 22h 48: CF Bi.—*12d 21h 23:* eight.—12d 21h 41: Do Ci SM MB.—*13d 17h 45:* six.—13d 18h 08: So Do.—17d 23h 22: CF El.—18d 14h 38: Do Hr.—19d 19h 40: Bi El Tn.—27d 19h 19: Bi El Tn.—27d 21h 52: El Hr.—*31d 22h 27:* five.

1955 June 01d 13h 20m: MB Ba.—*01d 17h 05:* seven.—02d 19h 40: Tr So El. —*02d 23h 03:* five.—03d 02h 21: CF MB Va.—03d 19h 11: Ma Tn.—*04d 19h 54:* seven.—*04d 20h 29:* ten.—*07d 12h 18:* five.—*07d 22h 55:* twenty-three.—*08d 22h 05:* fifteen.—09d 20h 58: Ma Fu Eb Qu.—10d 23h 00: Bi Hr.—*15d 22h 39:* five.—17d 21h 29: CF Ta.—17d 22h 25: SM Ta.—*19d 02h 33:* six.—*22d 00h 04:* twelve.—*23d 18h 54:* five.—23d 20h 34: Do Wn Tn.—25d 01h 14: SM Ta Va.—*26d 22h 07:* ten.—27d 23h 38: Tl Bi.—*28d 22h 53:* nineteen.

TABLE 1—*Geomagnetic planetary three-hour-range indices Kp, preliminary magnetic character-figures C, average amplitudes Ap (unit 2_γ), and final selected days, April to June, 1955*

April 1955									
E	1	2	3	4	5	6	7	8	Sum
1	3+	3+	3−	3o	2o	1o	1+	5o	22−
2	3o	3+	3−	3−	4−	3o	3o	4o	25+
3	2+	3−	3−	3+	3o	3−	2+	2−	21−
4	2o	2o	2−	4−	3−	3+	4−	4o	23o
5	4+	3o	4−	3o	5−	2−	3o	2−	25o
6	4−	4−	2o	4−	3o	3−	1o	4−	23+
7	4+	4o	3+	4o	2+	2o	3−	3−	25+
8	2o	3−	3o	1o	1+	2o	1+	2+	16−
9	2−	2+	1+	1+	0+	0+	1−	3o	11o
10	1o	0+	0+	4−	4o	3o	1+	2+	16o
11	2o	3+	3−	2−	2o	2o	1+	2−	17−
12	3o	3+	2+	2+	3o	1+	2+	3−	20+
13	4o	4o	3−	2o	2o	2+	2+	4o	23+
14	3−	3o	2+	2+	2−	1−	0+	1−	14−
15	1+	1+	1+	1o	2+	2o	1o	1o	11+
16	1−	1o	1o	1−	1+	1−	2o	2−	9o
17	1−	1−	2o	2o	2+	1o	2−	1−	11o
18	0+	0o	0o	1−	1o	2−	1−	0+	5−
19	1+	2o	1−	0+	1−	1−	1o	1o	8−
20	2o	3−	4−	1−	2−	2o	2−	1+	16−
21	1+	2−	2+	2−	3−	2o	1+	2o	15o
22	2+	3+	2−	2o	1o	1o	2+	1+	15o
23	0o	0+	0+	1+	1+	1o	0+	0+	5o
24	2−	2o	2−	2−	5o	4o	4−	4+	24o
25	3−	3+	2−	1+	3−	3−	3+	3−	20+
26	4−	3+	3+	4−	2o	2−	3o	4o	25−
27	4−	3+	3−	1−	1+	5−	8−	7+	31+
28	7o	4−	5−	4o	3−	3+	4+	6−	35+
29	5ó	4−	3+	4−	4−	4−	4+	4+	32−
30	4+	4o	2+	3+	2o	2o	3−	3+	24o
31									

May 1955									
1	2	3	4	5	6	7	8	Sum	
2+	3−	1o	1o	0+	1−	1+	2o	11+	
0+	0+	1+	1+	2o	2−	1+	2−	10o	
2o	1+	2−	1o	1o	2o	2o	1+	12+	
1+	0+	0+	1+	2o	2−	2o	2+	11+	
2−	2+	2o	2−	3−	3+	2−	2+	18−	
3+	3o	3o	4+	6o	3+	3+	5+	32−	
5−	4+	4+	4+	2+	3−	3o	4o	30−	
4o	5+	4−	4o	5−	4−	4+	4+	34o	
2+	2+	2+	2−	2−	2o	2+	2+	17o	
3−	3o	2o	3+	1o	2−	2o	3−	18+	
1o	1+	2o	1o	1−	1+	1+	1o	10−	
1o	2−	2−	1+	1o	1+	2o	3+	13+	
3−	1−	2o	2+	2+	2+	3−	2+	17+	
2+	3+	3o	4−	2o	2+	2o	2o	21−	
2o	2+	2o	0+	1−	1o	1+	2o	12−	
4−	5+	2+	3−	1+	1−	1−	1o	18−	
1+	1+	1+	1−	1−	1−	0o	1+	7+	
2−	1+	1−	0o	1o	2o	1o	1−	8+	
1−	1−	1+	1−	1−	1−	1−	1−	6o	
1−	2o	1o	2o	1o	1+	1+	2−	11o	
0+	1−	1−	1−	2−	1o	0+	1+	7−	
2−	2−	1−	1−	0+	1o	2o	1o	9o	
0+	0+	0+	1−	1+	1+	0o	0+	5−	
0+	1−	1o	1−	1o	1+	1+	1−	7o	
1o	1−	0+	0+	4o	4o	6+	7−	23+	
6+	6o	5−	5+	3−	3+	2o	1+	32−	
2−	1+	2−	1o	4o	5−	5o	4+	24−	
4o	4+	5−	4+	4−	2+	2+	3o	29−	
2+	2o	3−	2o	1+	2+	1−	2−	15o	
1−	0+	2−	1−	1o	2o	1+	1+	9o	
2−	2−	2o	1o	1o	1o	1o	2−	11o	

June 1955									
E	1	2	3	4	5	6	7	8	Sum
1	2−	2+	2−	1o	3−	3−	1+	1o	14+
2	2o	1+	2+	2−	2+	1+	1+	2−	14o
3	1o	2−	1+	1o	1o	2o	2+	2−	12o
4	1+	2−	3o	2o	2+	2−	2−	1+	15o
5	1o	0+	1o	2−	1+	2−	2−	1−	9+
6	0+	1−	1+	1o	2−	2+	4o	4o	15+
7	3+	3o	2o	3−	3−	2o	1o	3+	20o
8	3o	5o	3o	3−	4o	5−	2+	4−	28+
9	0+	2−	2+	2+	3−	1+	2o	3−	15+
10	2−	1o	2−	2−	1o	1+	1o	1−	10o
11	0+	1−	1+	2o	2o	2−	2−	3o	13−
12	2+	3o	2+	3−	3+	1−	1+	2+	18o
13	1+	1−	2+	1+	3+	3−	2o	2+	16o
14	2−	2o	3o	4+	4−	3+	2+	1o	21+
15	4−	4−	4+	4−	3o	2+	3o	3+	27o
16	4o	3o	3o	4−	4−	3−	1+	2o	23+
17	2+	2+	3−	4−	3−	3−	2−	3o	21o
18	1+	3−	3−	3−	1o	1+	1+	2−	15−
19	3+	3+	2+	2o	2o	2−	1o	1−	16+
20	1o	1o	1+	1o	1+	3o	2−	1o	11+
21	2o	1−	1−	1−	1o	1o	1o	1o	8o
22	1+	1−	0+	3+	3−	3o	2+	3−	16+
23	3+	3+	3o	2−	2o	2o	5−	4o	24o
24	4o	3+	4o	4−	4−	2+	2+	3−	26o
25	3o	2−	4−	3+	3−	1+	3−	1o	19+
26	1o	2−	0+	1−	1−	1o	1−	2−	8−
27	1+	1+	2o	2−	1+	2o	2o	1−	12+
28	2−	3−	1o	2−	2−	1o	1o	3−	13+
29	2−	1−	1+	2o	2o	1+	2+	1o	12+
30	2o	1o	1−	1−	0+	1−	1−	1−	7−
31									

	Preliminary *C*. 1955			Average amplitude *Ap*		
	Apr.	May	June	Apr.	May	June
	1.1	0.2	0.5	16	6	7
	1.1	0.2	0.3	17	5	6
	0.8	0.2	0.3	12	6	6
	1.0	0.3	0.5	15	5	7
	1.0	0.7	0.1	19	9	4
	0.9	1.4	0.8	16	32	10
	1.0	1.3	0.8	18	25	12
	0.4	1.3	1.2	8	32	23
	0.3	0.6	0.5	6	8	8
	0.6	0.7	0.1	11	10	5
	0.4	0.2	0.4	8	5	6
	0.7	0.4	0.6	12	7	10
	1.0	0.6	0.6	16	9	8
	0.2	0.7	0.8	7	12	14
	0.4	0.2	0.9	5	6	19
	0.1	0.9	0.9	4	14	16
	0.2	0.1	0.7	5	4	12
	0.1	0.2	0.3	2	4	8
	0.0	0.0	0.5	4	3	9
	0.5	0.4	0.4	8	5	6
	0.4	0.2	0.1	7	4	4
	0.6	0.2	0.8	8	4	10
	0.0	0.2	1.1	3	3	17
	1.3	0.1	1.1	19	4	18
	0.9	1.5	0.7	12	34	12
	1.0	1.5	0.2	17	39	4
	1.7	1.1	0.2	54	21	6
	1.6	1.1	0.4	44	23	7
	1.3	0.4	0.3	27	7	6
	0.9	0.2	0.0	16	4	4
		0.1			5	

TABLE 1—(Concluded)—*Final selected days, April to June, 1955*

Month	Five quiet days	Ten quiet days	Five disturbed days
1955			
April	16 17 18 19 23	9 14 15 16 17 18 19 21 22 23	5 7 27 28 29
May	17 19 21 23 24	2 11 17 18 19 21 22 23 24 30	6 7 8 25 26
June	5 10 21 26 30	3 5 10 11 20 21 26 27 29 30	8 15 16 23 24

Sudden impulses found in the magnetograms (s.i.)

1955 April 05d 14h 54m: Ba Tu.—05d 17h 50: Qu MB Ba.—07d 09h 18: Ba Bi Hr.—17d 20h 55: IK MB Bi.—*27d 18h 53:* seven.—27d 22h 32: Wn IK Eb Hr.

1955 May 06d 13h 10m: Ma Db MB.—*06d 13h 54:* twelve.—06d 19h 11: Ta MB.—13d 12h 42: Ka Qu Hr.—13d 21h 36: Tr So Bi.—16d 10h 50: IK Bi.—*20d 05h 29:* sixteen.—20d 09h 51: Ka Ta MB Hr.—*23d 15h 12:* eight.—25d 17h 30: Ci Ta.—*25d 18h 36:* six.

1955 June *02d 02h 41m:* six.—08d 16h 00: Ci Ta.—08d 16h 58: Ci Ta.—*14d 05h 11:* seven.—15d 22h 47: Ci SF Ta.—20d 16h 46: SM MB.—22d 16h 06: SM Ta Ba.—*23d 15h 57:* five.—*23d 19h 14:* seven.—29d 19h 31: Tr Eb.

Preliminary Report on Solar-Flare Effects

Effects confirmed by ionospheric or solar observations are in italics.

1955 April 02d 13h 11m–13h 38m: El.—06d 14h 25–15h 00: El.—06d 15h 13–15h 43: El.—06d 18h 55–.....: Hu.—07d 13h 56–14h 06: Bi.—09d 14h 14–14h 20: SM.—15d 16h 13–16h 29: Bi.—29d 14h 18–14h 40: Ch.—30d 21h 51–.....: Hu.

1955 May 18d 14h 42m–15h 13m: El.

1955 June 02d 23h 02m–23h 20: Tu Ap(?).—09d 14h 27–14h 33: Bi.—*18d 12h 30–13h 05:* Wn CF.—18d 19h 05–19h 40: Ch Tu.—20d 11h 55–12h 05: El.—23d 00h 09–.....: Ap(?).

Ionospheric or solar disturbances without clear geomagnetic effect

1955 June 23d 10h 37m–.....: CF(?).

Minor disturbances reported by one station only are listed in the De Bilt quarterly circular, but omitted here.

TABLE 2—*Monthly mean values of Ci, Cp, and Ap*

Index	Apr. 1955	May 1955	June 1955
Mean *Ci*	0.72	0.55	0.54
Mean *Cp*	0.66	0.50	0.50
Mean *Ap*	14	11	9

COMMITTEE ON RAPID VARIATIONS AND EARTH CURRENTS
A. ROMAÑÁ, *Chairman*, Observatorio del Ebro, Tortosa, Spain

COMMITTEE ON CHARACTERIZATION OF MAGNETIC DISTURBANCES
J. BARTELS, *Chairman*
University
Göttingen, Germany

J. VELDKAMP
Kon. Nederlandsch Meteorologisch Instituut
De Bilt, Holland

PROVISIONAL SUNSPOT-NUMBERS FOR JULY TO SEPTEMBER, 1955

(Dependent on observations at Zurich Observatory and its stations at Locarno and Arosa)

Day	July	Aug.	Sep.
1	35	25	89
2	38	20	88
3	38	16	80
4	43	0	85
5	48	26	78
6	60	46	70
7	47	61	74
8	47	77	68
9	39	83	64
10	41	87	52
11	35	85	40
12	25	77	40
13	25	77	40
14	37	60	33
15	29	44	46
16	22	28	25
17	20	16	38
18	7	10	41
19	26	13	29
20	32	17	23
21	11	22	7
22	9	23	0
23	0	23	7
24	0	14	25
25	8	11	30
26	0	26	11
27	11	40	21
28	12	54	12
29	16	55	9
30	20	49	32
31	26	62	
Means.....	26.0	40.2	41.9
No. days.....	31	31	30

Means for quarter: 36.0 (92 days)

M. Waldmeier

Swiss Federal Observatory
Zurich, Switzerland

CHELTENHAM THREE-HOUR-RANGE INDICES K FOR JULY TO SEPTEMBER, 1955

[$K9 = 500\gamma$; scale-values of variometers in γ/mm: $D = 5.4$; $H = 2.4$; $Z = 4.3$]

Gr. day	July 1955		August 1955		Sep. 1955	
	Values K	Sum	Values K	Sum	Values K	Sum
1	2231 1111	12	1101 2111	8	2132 2222	16
2	2221 2354	21	3110 0023	10	5434 3211	23
3	3423 2122	19	4331 2222	19	3334 2132	21
4	2220 0011	8	3435 4333	28	4415 2323	24
5	2111 0122	10	2353 2344	26	5454 2222	26
6	1111 1224	13	4455 3334	31	2443 1213	20
7	4321 2223	19	3443 3243	26	3133 1120	14
8	2333 2333	22	3123 3222	18	1232 1212	14
9	2222 3113	16	3221 2132	16	3221 2122	15
10	2223 3233	20	1323 1112	14	2232 2111	14
11	3233 3343	24	2200 1122	10	2221 1012	11
12	5134 3134	24	2211 1111	10	3452 3223	24
13	3311 2312	16	2223 1113	15	4544 2221	24
14	1233 2121	15	3233 1243	21	0233 1112	13
15	1112 4433	19	3332 2111	16	3311 1121	13
16	4322 2222	19	1330 1122	13	3333 1112	17
17	2332 0033	16	2101 1222	11	2354 1122	20
18	2442 1111	16	2332 2122	17	2334 1202	17
19	1111 1001	6	1332 1112	14	3322 1112	15
20	2111 1111	9	2111 1211	10	3233 0122	16
21	2101 0122	9	2321 1122	14	2212 1022	12
22	1211 1112	10	1000 1111	5	4321 1122	16
23	3221 1234	18	0120 0011	5	1133 2233	18
24	4432 1122	19	1222 2122	14	4221 1112	14
25	2231 2122	15	2121 2121	12	2111 0112	9
26	1333 3224	21	2302 2122	14	1110 1011	6
27	3222 1111	13	0111 0123	9	3323 2333	22
28	2110 1111	8	1464 2132	23	2433 2132	20
29	3221 1142	16	3222 1144	19	3223 2443	23
30	1122 1123	13	2111 1122	11	4675 4324	35
31	3230 2212	15	1212 1122	12		

J. B. Campbell
Observer-in-Charge

Cheltenham Magnetic Observatory
Cheltenham, Maryland, U.S.A.

PRINCIPAL MAGNETIC STORMS

(Advance knowledge of the character of the records at some observatories as regards disturbances)

servatory Observer- -Charge)	Green-wich date	Storm-time GMT of begin.	Storm-time GMT of ending[1]	Sudden commencement Type[2]	Amplitudes[3] D	H	Z	C-figure, degree of activity[4]	Maximal activity on K-scale 0 to 9 Gr. day	Gr. 3-hr. period	K-index	Ranges D	H	Z
(1)	(2)	(3)	(4)	(5)	(6)	(7)	(8)	(9)	(10)	(11)	(12)	(13)	(14)	(15)
	1955	*h m*	*d h*		′	γ	γ					′	γ	γ
ege	July	None												
J. Beers)	Aug.	None												
	Sep. 13	02 ..	13 22	.....	....	....	....	ms	13	3,4	6	150	1040	860
	Sep. 30	04 ..	30 24	.....	....	....	....	ms	30	3,4	7	260	1620	980
a	July	None												
L. Skillman)	Aug. 6	05 ..	6 14	.....	....	....	....	ms	6	3	7	81	470	677
	Sep. 5	05 ..	5 21	.....	....	....	....	ms	6	4,5	6	74	334	412
	Sep. 13	20 ..	13 21	.....	....	....	....	ms	13	3	7	85	394	322
	Sep. 29	15 ..	30 24	.....	....	....	....	ms	30	3,4	7	104	752	586
eveen	July 2	10 00	3 07	.....	....	....	....	m	2	6,7,8	5	30	135	50
an Sabben)	Aug. 3	11 00	7 24	.....	....	....	....	ms	6	8	6	30	200	75
	Sep. 27	02 00	27 22	.....	....	....	....	ms	27	7	6	30	150	40
	Sep. 29	15 00	30 24	.....	....	....	....	ms	30	2,3	6	40	165	70
ltenham	July	None												
.Campbell)	Aug. 6	04 ..	8 03	.....	....	....	....	m	6	3,4	5	26	104	103
	Aug. 28	03 ..	28 11	.....	....	....	....	ms	28	3	6	25	74	55
	Sep. 12	04 ..	13 13	.....	....	....	....	m	12	3	5	25	69	48
									13	2	5			
	Sep. 29	14 ..	30 20	.....	....	....	....	ms	30	3	7	40	107	91
son	July	None												
F. White)	Aug. 2	21 00	8 15	.....	....	....	....	ms	6	3	6	15	106	45
	Sep. 2	02 ..	5 17	.....	....	....	....	m	3	4	5	13	87	27
									5	2,3,4	5			
	Sep. 29	08 ..	1 01	.....	....	....	....	ms	30	2,3,4	6	19	115	32
Juan	July	None												
G. Ledig)	Aug.	None												
	Sep.	None												
olulu	July	None												
L. Cleven)	Aug. 28	03 00	28 14	.....	....	....	....	ms	28	2	6	4	120	20
	Sep. 30	04 00	31 01	.....	....	....	....	ms	30	2,3	6	7	100	30
ag	Apr. 10	03 ..	11 00	.....	....	....	....	m	10	4	5	4	119	21
S. Chaubal)	Apr. 24	01 ..	25 01	.....	....	....	....	m	24	5	5	4	139	32
	Apr. 27	16 25	1 00	s.c.	−1	+31	−5	m	27	7	5	7	113	62
	May 5	08 ..	7 09	.....	....	....	....	m	6	4,5	5	7	170	50
	May 25	14 33	26 20	s.c.	0	+33	−6	s	25	7	6	8	165	56
	June 6	17 28	8 23	s.c.	0	+14	−3	m	8	5,6	5	10	101	79
	June 22	10 39	24 00	s.c.	0	+29	−9	m	22	4	5	6	74	49
									23	7	5			
ituto	July 26	04 05	27 03	.....	....	....	....	m	26	5,6	5	5	124	17
ísico de	Aug. 5	03 58	7 22	s.c.	0	+23	0	m	6	6	5	9	217	54
ncayo	Sep. 29	13 21	30 22	.....	....	....	....	ms	29	7	6	6	269	38
..Giesecke, .)														

[1] Approximate time of ending of storm construed as the time of cessation of reasonably marked disturbance movements in the s; more specifically, when the *K*-index measure diminished to 2 or less for a reasonable period.
s.c. = sudden commencement; s.c.* = small initial impulse followed by main impulse (the amplitude in this case is that of the *impulse only*, neglecting the initial brief pulse; ... = gradual commencement.
Signs of amplitudes of *D* and *Z* taken algebraically; *D* reckoned positive if towards the east and *Z* reckoned positive if verti- downwards.
Storm described by three degrees of activity: *m* for moderate (when *K*-index as great as 5); *ms* for moderately severe (when 6 or 7); *s* for severe (when *K* = 8 or 9).

PRINCIPAL MAGNETIC STORMS—*Concluded*

Observatory (Observer-in-Charge)	Greenwich date	Storm-time GMT of begin.	Storm-time GMT of ending[1]	Sudden commencement Type[2]	Amplitudes[3] *D*	*H*	*Z*	*C*-figure, degree of activity[4]	Maximal activity on *K*-scale 0 to 9 Gr. day	Gr. 3-hr. period	*K*-index	Ranges *D*	*H*
(1)	(2)	(3)	(4)	(5)	(6)	(7)	(8)	(9)	(10)	(11)	(12)	(13)	(14)
	1955	*h m*	*d h*		′	γ	γ					′	γ
Elisabethville	Jan. 17	03 22	19 24	s.c.	−1	+33	0	s	17	4 à 8	...	13	177
(A. Alexandre)	Feb.	Néant											
	Mar. 22	03 20	22 24	s.c.	0	−8	+1	ms	22	4,5	...	10	264
	Apr. 27	16 24	28 24	s.c.	−1	+25	−2	s	27	7,8	...	6	196
	May 25	14 34	26 14	s.c.	−1	+35	−2	s	25	7,8	...	8	198
									26	1	...		
	June	Néant											
	July	Néant											
	Aug.	Néant											
	Sep.	Néant											
Apia	July	None											
(A. L. Burrows)	Aug. 6	06 18	7 15	.....	.....	.....	.....	m	6	3	5	6	57
	Aug. 27	21 42	29 04	.....	.....	.....	.....	m	28	2,3	5	3	156
	Sep.	None											
Hermanus	July 2	15 ..	3 07	.....	.....	.....	.....	m	2	7	5	14	99
(A. M.	July 12	00 25	12 02	s.c.		(bay)		m	12	1	5	5	45
van Wijk)	Aug. 3	23 01	7 23	s.c.	.....	.....	.....	m	4	4	5	22	93
									6	8	5		
									7	4	5		
	Sep. 3	09 ..	3 13	.....	.....	.....	.....	m	3	4	5	9	80
	Sep. 12	01 ..	12 14	.....	.....	.....	.....	m	12	3	5	10	71
	Sep. 27	01 ..	27 22	.....	.....	.....	.....	m	27	7	5	14	92
	Sep. 29	08 ..	1 01	.....	.....	.....	.....	m	29	6,7	5	19	99
									30	4,8	5		
Binza	Apr. 27	16 23	28 20	s.c.	−1	+30	−3	ms	27	6,7,8	...	6	193
(Ch. Staes)	May 25	14 34	26 16	s.c.	−1	+41	−3	ms	25	5,6,7	...	.....	210
	(*Note:* Trace invisible during one hour due to meteorological storm)												
	June 22	10 40	23 21	s.c.	−1	+37	−3	ms	22	4,5,6	...	4	138
	July	None											
	Aug.	None											
	Sep.	None											
Watheroo	July	None											
(A. F. Tillott)	Aug.	None											
	Sep.	None											
Toolangi	July	None											
(I. B.	Aug. 2	19 03	8 15	.....	.....	.....	.....	m	4	4	5	17	122
Everingham)									6	3,5	5		
	Aug. 28	03 00	28 17	.....	.....	.....	.....	m	28	3,4	5	21	95
	Sep.	None											
Amberley	July	None											
(A. L.	Aug. 2	21 ..	8 15	.....	.....	.....	.....	m	4	4	5	22	127
Cullington)									6	3	5		
	Aug. 27	21 ..	29 23	.....	.....	.....	.....	m	28	3	5	14	120
	Sep. 1	6 ..	7 14	.....	.....	.....	.....	m	3	4	5	19	133
									5	4	5	11	115
	Sep. 11	23 ..	14 15	.....	.....	.....	.....	m	13	4	5	15	107
	Sep. 29	15 ..	(Storm continuing)				....	m	30	2,3,4,5	5	20	124

LETTERS TO EDITOR

EXTENSION OF THE SEN-WHITE PAPER ON ATMOSPHERIC OSCILLATIONS

A general solution of the radial wave equation obtained by Sen and White[1] for the excitation of large-scale oscillations in an atmosphere on a rotating globe by gravitational and thermal forcing functions is

$$\chi = \frac{q(z)}{\gamma H(z)} + e^{\frac{1}{2}x}[(P + iQ)(y_1 + iy_2) + (R + iS)(y_1 - iy_2) + I(x)] \quad \ldots(1)$$

consisting of the complementary function, and a particular integral, $q(z)/\gamma H(z) + e^{\frac{1}{2}x}I(x)$, where

$$I(x) = y_1 \int_{\infty}^{x \geq 0} \frac{y_2 T(x)}{y_1' y_2 - y_1 y_2'}\,dx - y_2 \int_{\infty}^{x \geq 0} \frac{y_1 T(x)}{y_1' y_2 - y_1 y_2'}\,dx \quad \ldots(2)$$

and where $T(x) = qe^{\frac{1}{2}x}/\gamma^2 h$ and $y_k' = dy_k/dx$. The symbols are those used by Sen and White. With this value of χ, the expressions for the oscillatory winds (u, v, w) and the oscillatory pressure variation $(=p)$ reduce to the corresponding equations for the purely gravitational case,[2] except now the wave function y must be replaced by $[y + I]$. With this interpretation, the equations of Wilkes and Pekeris[2] become generally valid. The inclusion of a heat-source function in an atmosphere of any arbitrary temperature profile can be carried out exactly by numerical integration for $I(x)$.

With a change of variables $(r = r_1 e^{b(x - x_1)/2})$, $I(r)$, and χ can be found for any portion of the atmosphere with a straight-line temperature profile of slope $b = dH/dz$ from

$$\left.\begin{aligned} \chi &= \frac{q}{\gamma H} + e^{\frac{1}{2}x}[(P + iQ)H_{1/b}^{(1)}(r) + (R + iS)H_{1/b}^{(2)}(r) + I(r)] \\ \text{where} \\ I(r) &= -\frac{\pi}{2}\left(\frac{2}{b\gamma}\right)^2 \frac{q_0}{h}(r_1 e^{-bx_1/2})^{1/b}\left[J_{1/b}(r)\int_{\infty}^{r} e^{-\beta'(r^2 - r_1^2)^2} r^{-\left(\frac{1}{b}+1\right)} Y_{1/b}(r)\,dr \right. \\ &\qquad \left. - Y_{1/b}(r)\int_{\infty}^{r} e^{-\beta'(r^2 - r_1^2)^2} r^{-\left(\frac{1}{b}+1\right)} J_{1/b}(r)\,dr\right] \end{aligned}\right\} \quad \ldots(3)$$

where $q = q_0 \exp[-\beta(z - z_1)^2]$, say, and where $H_{1/b}^{(1)}$ is a Hankel function. For a top with constant temperature gradient, $H_{1/b}^{(1)}$ represents an outgoing and $H_{1/b}^{(2)}$ an incoming wave. From boundary conditions, only $H_{1/b}^{(1)}$ need be retained at the top.

[1]H. K. Sen and M. L. White, J. Geophys. Res., **60**, 483 (1955).

[2]M. V. Wilkes, Oscillations of the Earth's Atmosphere, Cambridge, University Press (1949); p. 31.

The amplification over equilibrium tide for thermal input anywhere in an atmosphere having an isothermal top but with an otherwise arbitrary temperature profile is given by

$$\text{Ampl. } (z) = 1 + \mathbf{N} - \frac{i\gamma gh}{\sigma\Omega} e^{\frac{1}{2}x}\left[\left\{\frac{\left(\frac{H_0}{h} - \frac{1}{2} + \frac{\mathrm{d}}{\mathrm{d}x}\right)I(x)}{\left(\frac{H_0}{h} - \frac{1}{2} + \frac{\mathrm{d}}{\mathrm{d}x}\right)(y_1 + iy_2)}\right\}_0 \left(\frac{\mathrm{d}}{\mathrm{d}x} - \frac{1}{2}\right)(y_1 + iy_2) - \left(\frac{\mathrm{d}}{\mathrm{d}x} - \frac{1}{2}\right)I(x)\right] \quad \ldots\ldots(4)$$

where

$$\mathbf{N} = -e^{\frac{1}{2}x}\left[\frac{\left(\frac{\mathrm{d}}{\mathrm{d}x} - \frac{1}{2}\right)(y_1 + iy_2)}{\left\{\left(\frac{H_0}{h} - \frac{1}{2} + \frac{\mathrm{d}}{\mathrm{d}x}\right)(y_1 + iy_2)\right\}_0}\right] \quad \ldots\ldots\ldots\ldots\ldots(5)$$

represents the ratio for the dynamical over the equilibrium tide, while the last term represents the contribution to the amplification by thermal sources only. One can also obtain that contribution to the amplification in a given layer due to solar heating in any other layer or layers by appropriately adjusting the limits of integration of $I(x)$ over which the heating function q is integrated.

As a brief application, the solar semi-diurnal wind observations in the E-region, compiled by Briggs and Spencer[3] (Table 3), are found to be internally consistent (from the expression for u/v), the same azimuthal dependence being found in the E region as on the ground (Schmidt's law), thus serving to vindicate the assumption of variables separable.

A full account of this work has been prepared and will be published shortly.

MARVIN L. WHITE

NATIONAL BUREAU OF STANDARDS,
Boulder, Colorado, September 16, 1955
(Received September 19, 1955)

[3]B. H. Briggs and M. Spencer, Rep. Prog. Phys., 17, 245 (1954); see p. 256.

NIGHT-TIME MEASUREMENT OF POSITIVE AND NEGATIVE ION COMPOSITION TO 120 KM BY ROCKET-BORNE SPECTROMETER

The ambient positive and negative ion composition in the mass range 5 to 58 atomic mass units was measured between 98 and 120 km[1] by two Bennett radio-frequency mass spectrometers. The spectrometers were flown in Aerobee rocket NRL No. 23 at White Sands Proving Ground, New Mexico, at 01:39 MST, July 8, 1955. The spectrometers and associated instrumentation performed well throughout flight. The rocket did not acquire measurable potential, nor was a large quantity of rocket gas observed, as was the case in the positive-ion spectrometer experiment flown in Viking 10.[2] It can therefore be reasonably assumed that these complicating factors had negligible influence on this Aerobee experiment. Interpretation of the telemetered data was simple and unambiguous. Positive ions appeared only at atomic mass number 28. The position of the mass 28 peak on the flight record checked laboratory calibrations within an error of less than plus or minus one-half a mass unit. Positive ions of mass number other than 28 would have been detected if their concentration had been as much as one per cent of the concentration of mass 28 ions. Mass 28 is attributed here to N_2^+ ; the possibility that it could be CO^+ seems remote, considering their non-ionized relative abundances. There was no indication of negative ions at the operating altitudes of the spectrometer. Assuming the collection properties of the negative and positive ion spectrometers to be identical, negative ions of a given mass would have been detected if their concentration had been as much as one per cent of the concentration of N_2^+ ions.

Ionosphere records taken at 15-second intervals from the White Sands station during the time the rocket was in the *E*-region showed sporadic-*E* reflections at maximum frequencies varying between 2.8 and 5.0 Mc/sec at a virtual height of 100 km. Records taken at 5-minute intervals between 01:00 and 02:00 MST showed relatively stable sporadic-*E* reflections. These sporadic-*E* conditions are a common occurrence at White Sands at that time of the year. Magnetograms from the Tucson Observatory, located 425 km west of White Sands, did not show any appreciable magnetic disturbance during the two-day period centered on the firing time.

The various theories and ideas which have been set forth to explain nocturnal *E*-region ionization, both regular and sporadic, have quite generally attributed this ionization to oxygen atoms and molecules, and (or) oxides such as NO. It is thus particularly significant that in this measurement the ion composition was found to be N_2^+ . A daytime flight with identical instrumentation is scheduled for November 1955. A complete description of the experiment and results for both the July 8 night flight and the scheduled daytime flight, if successful, will be presented at a later date.

CHARLES Y. JOHNSON AND JAMES P. HEPPNER

NAVAL RESEARCH LABORATORY,
Washington 25, D. C., September 16, 1955
(Received September 17, 1955)

[1]Altitudes have been computed from the best trajectory data available at this writing.
[2]C. Y. Johnson and E. B. Meadows, J. Geophys. Res., **60**, 193 (1955).

SOME REMARKS CONCERNING IONOSPHERIC ABSORPTION-WORK

In a study of the frequency dependence of observed (monthly median) absorption decrements, we found in most cases a variation which did not agree with the simple formula $(f + f_L)^{-2}$. There was mostly evidence for an increased absorption near the critical frequency f^oE. This may be understood quite well on the basis of an estimation of the absorbing effect which this region should have (using the thickness and electron density known from sounding and the collision frequency obtained by rocket measurements). We were thus able to determine the effective collision-frequency times layer thickness, using the absorption values of Slough and Freiburg for a number of years.

Now, if we consider these monthly presentations in detail, we may often note important irregularities. This is even more the case with most daily observations. We feel that these irregularities are not due to the magnetic field (its influence has been calculated in detail for one model case absorption in a parabolic layer, and it was found to be small).

If one observes the amplitudes of the successive echoes, one must state that they often do not fit at all with the simple theory which is generally used. This theory introduces a horizontally-stratified plane ionosphere, the total absorption being characterized by an effective reflection-coefficient. Rather often one has observations giving an apparent reflection-coefficient greater than "1" (that is, a negative absorption-decrement). We think that this is due to focusing effects. A rather small curvature of the reflecting layer, in fact, is sufficient to account for such effects.

We first thought that there should be focusing and defocusing of nearly equal importance. But in calculating the correction term due to the curvature of the reflecting layer, one finds that the effect is nearly negligible for defocusing and that it is only important in the neighborhood of the focusing value. This latter is at $H/r = 1$ for the first echo, $H/r = 1/2$ and 1 for the second, $H/r = 1/4$, $3/4$, and 1 for the third (H = virtual height of the reflection level and r = radius of curvature of this level).

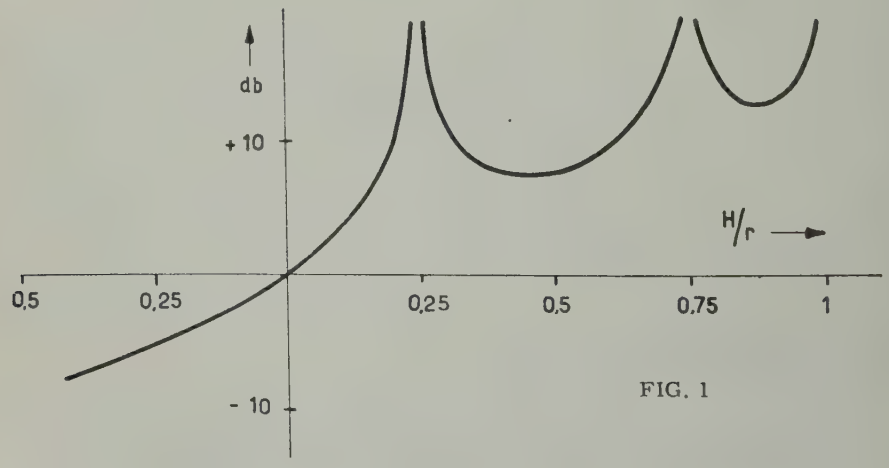

FIG. 1

A number of night observations on the $F2$-layer has been evaluated in terms of these considerations. When applying the usual simple evaluation method, we found a negative absorption-decrement in about 30 per cent of all cases. If now the correction term were introduced into the evaluation, these cases could be considered as focalization cases and the effective curvature could accordingly be deduced. (With three successive echoes, one may determine three parameters, that is, the vertical radiated power, the decrement of absorption, and the effective curvature.) Very often we found a curvature of $H/r \approx 1/4$ (focalization for the third echo), very rarely for $H/r \approx 1/2$, and never for $H/r \approx 1$. This result fits well with observations of Pierce and Mimno (1940), who found ripples of the order of nearly a kilometer of depth at two points separated approximately by 100 km.

A practical conclusion from this is that we should prefer first- and second-order echoes for absorption work, the third being often troubled by focusing.

An important difficulty for a correct analysis of absorption observations is the following: In order to eliminate rapid fading, we must have a certain time for every measurement, at least some minutes (generally, several readings are made of the varying echo-amplitude, the observation being repeated about ten minutes later). If now the focusing on a given frequency were constant during that time, the evaluation is no problem in terms of our theory. (Different curvature on different reflection-levels could be admitted.) But if we have rapid variations and movements of the "ripples," we must discuss the statistical effect of these variations on our data. Unfortunately, there are reasons for a rapid variation, in the daytime, at least. On the other hand, daytime observations are less influenced by focusing, because the absorption is higher in daytime. Nevertheless, every month we find some two or three daily observations where an important focusing should be admitted (cases of negative decrement with the simple theory). We think, therefore, that one should discuss the influence of the ripples also for the usual noon observations of absorption.

K. Rawer

Ionospheric Station of S.P.I.M. (France),
Neuershausen b. Freiburg, Germany, August 3, 1955
(Received August 6, 1955)

RELATIONS BETWEEN SOLAR ACTIVITY AND THE CENTER OF GRAVITY OF THE PLANETARY SYSTEM

Though there are astronomers who consider the planetary influence on the solar activity as non-existent, there are others who have investigated certain relations between the two phenomena, which, although partial, seem to be real. Before rejecting this hypothesis definitely, I thought it advisable to make a study in which the influence of the whole planetary system would be considered. So I set out to search for some influence of the center of gravity of the planetary system on the solar activity.

I have tried to plot the trajectory of the center of gravity of the planetary

system during the years 1870 to 1960, taking into consideration the four major planets Jupiter, Saturn, Uranus, and Neptune, neglecting the remaining ones whose masses are so small in comparison with the former four that they would alter the trajectory only 1/146, an error much smaller than that inherent to the drawing.

To this effect, I have plotted the elliptical orbits at the corresponding proportional distances, taking the direction of the perihelion at its mean value for the period covered by my work, that is, for the year 1900. The orbits have been projected on the plane of the ecliptic. The longitudes of the planets have been computed for January 1 of each year. The centers of gravity have been computed separately for the pairs Jupiter-Saturn and Uranus-Neptune.

Results—After having plotted the various trajectories, the following results have been found:

(1) All the maxima of solar activity of the 90 years covered by this work coincide approximately with the times when the three centers of gravity (Jupiter-Saturn, Uranus-Neptune, resulting center) are collinear with the sun; in other words, when the centers of gravity are in relative conjunction with the center of the sun.

(2) Out of the eight minima belonging to the same period, six correspond to the times when the centers of gravity Jupiter-Saturn and Uranus-Neptune stand in quadrature with respect to the sun; the remaining two minima coincide with conjunctions like the maxima.

(3) Whenever besides these cases occurs a conjunction, in the middle of the period there is a notable increase of the solar activity.

(4) The trajectory of the center of gravity Jupiter-Saturn, after a period of 59 years, repeats itself almost exactly; the trajectory of the center of gravity Uranus-Neptune repeats itself every 171–172 years approximately. Thus, we should get a total cycle of about 1,534 years for the trajectory of the center of gravity of the four planets. This cycle could be divided into nine periods of about 170 years, which period is nearly the same as that found by C. N. Anderson (J. Geophys. Res., **59**, 455, 1954) concerning the repetition of the solar activity.

(5) It seems to me that the small differences observed throughout these comparisons could easily be explained.

A future hypothesis of the solar activity would rest, therefore, on the following assumptions. (1) The planetary system produces a tidal effect on the surface of the sun. (2) During the minima, there is a resonance between the tidal wave and the rotation of the sun. (3) The time necessary for the occurrence of a resonance is a period of 11.5 years. (4) The rupture of this resonance is the cause of the solar activity. (In the drawing, it can be seen that the center of gravity has a considerable variation in its angular velocity.)

The comparisons of dates and other details will be published in the next number of *Acta Scientifica* of the Observatorio de San Miguel, Argentina.

Nilo Arriaga, S.J.

Head, Heliophysics Department,
Observatorio de Física Cósmica,
San Miguel, F.C.N.G.S.M., Argentina, August 26, 1955
(Received September 7, 1955)

INTERPRETATION OF IONOSPHERIC RESULTS DURING ECLIPSES

Even though it is clearly established from solar eclipse results that the radiation responsible for the ionization of the E layer is due to photons, it is not yet possible to have a consistent picture of the whole mechanism. All the published results show that the solar emission may come from a "uniform" disk having various additional sources, and that the recombination coefficient is relatively small, namely, between 1×10^{-8} and 2×10^{-8} cm^3 sec^{-1}. However, other considerations must be taken into account in order to obtain a consistent picture of the solar emission for interpretation of ionospheric data, such as those taken during the eclipse of February 25, 1952.[1,2,3,4] First, it is not possible to represent the solar emission as coming from a *uniform* disk with the addition of *identical* sources. Some sources do seem to coincide with areas of rather high solar activity, but their positions deduced from the experimental data of several stations do not agree closely. Second, the numbers of photons, q_0 , emitted by the sun at the top of the earth's atmosphere are not identical for all stations when obtained by extrapolation from ionospheric data. Third, the recombination coefficient α is not well determined and may be considered variable.

Instead of the conventional law, we have considered the following approximation,

$$\frac{\mathrm{d}(n_e)_{\max}}{\mathrm{d}t} = q_0 \cos^n \chi - \alpha(n_e^2)_{\max}$$

in which we have introduced the exponent n arising from the effect of scale-height variation with height.[5] Such a parameter has a physical meaning, in that it corresponds to the possible variation of the temperature gradient, depending on latitude. This method of analysis was used for our ionospheric data obtained on February 25, 1952, at Lwiro (Belgian Congo), at the station of the "Institut pour la Recherche Scientifique en Afrique Centrale" (IRSAC), and afterwards was applied to the published results for the same eclipse, namely, those for Bangui,[1] Khartoum,[2] Ibadan,[3] and Gao.[4] It is significant that the solar emission can be represented by a model in which the quiet disk emission is not uniform, but which is partly coronal in nature, following the 21-cm model[6] (elliptic distribution with equatorial brightening and polar darkening, and 15 per cent of the ionizing radiation outside the visible disk). Neglecting small anomalies in the ionospheric results, only one additional source is needed, namely, a hot spot emitting only 7 per cent of the total radiation, situated about 260° on the limb of the disk and corresponding to an active bright Ca^+ area with strong emission of the 5393A coronal line.

[1]S. Estrabaud, Mesures ionosphériques effectuées à Bangui . . . , Proc. Meet. Mixed Comm. Ionosphere, **3**, 34 (1953); Paris, C.-R. Acad. sci., **236**, 833 (1953); Notes preliminaires L.B.N., No. 174 (1954).

[2]C. M. Minnis, Ionospheric measurements at Khartoum . . . , Proc. Meet. Mixed Comm. Ionosphere, **3**, 38 (1953); J. Atmos. Terr. Phys., **6**, 91 (1955).

[3]R. W. Piggott, Ionospheric measurements at Ibadan . . . , Proc. Meet. Mixed Comm. Ionosphere, **3**, 42 (1953).

[4]F. Delobeau, L'éclipse du soleil à Gao, Ann. Géophys., **9**, 317 (1953).

[5]M. Nicolet, J. Atmos. Terr. Phys., **1**, 141 (1951).

[6]W. N. Christiansen and J. A. Warburton, Observatory, **75**, 9 (1955).

The published results concerning the February 25 eclipse are different from our general conclusion. However, the more recent work of Minnis[7] for the eclipse of June 30, 1954, which occurred when the sun was almost quiet, could be considered as leading to a result identical with ours if a coronal effect is introduced. The various values of n show that the vertical distributions of atmospheric temperature cannot be the same at the stations at the equator and northward.

Finally, the data presently considered indicate a high value for the recombination coefficient. It was found that the analysis of data is very sensitive to the value adopted for it between 1×10^{-8} and 3×10^{-8} cm^3 sec^{-1}. It is almost certain that the recombination coefficient in the E layer cannot be less than 4×10^{-8} cm^3 sec^{-1} and is certainly greater than all published values. Such a high value is consistent with the existence of a gradient of the scale height and emission beyond the visible disk of the sun.

This work was carried out as a part of the program of IRSAC, and a detailed communication will be published elsewhere.

J. Hunaerts
M. Nicolet

Royal Observatory,
Royal Meteorological Institute,
Uccle, Belgium, October 18, 1955
(Received October 21, 1955)

[7]C. M. Minnis, Nature, **176**, 652 (1955).

NOTES

(36) *New officers, Society of Exploration Geophysicists*—The Society of Exploration Geophysicists has elected the following 1955–1956 officers to serve beginning October 6, 1955: president, R. C. Dunlap, Jr., Dallas, vice-president of Geophysical Service, Inc.; vice-president, Dave P. Carlton, Houston, chief geophysicist, Humble Oil and Refining Company; secretary-treasurer, George A. Grimm, Midland, district geophysicist, Tide Water Associated Oil Company. Dr. Norman Ricker, Tulsa, senior research physicist, Carter Oil Company, was elected editor for a two-year term. At the meeting in Denver, October 3–6, 1955, marking the 25th Anniversary Meeting of the Society, some 40 technical papers were presented.

(37) *Announcement of staff by U.S. National Committee for the International Geophysical Year*—Joseph Kaplan, chairman of the U.S. National Committee for the International Geophysical Year (USNC-IGY) and former chairman of the department of physics at the University of California at Los Angeles, has announced that the secretariat of the committee now includes the following: executive secretary, Hugh Odishaw, former assistant to the director of the National Bureau of Standards; administrative officer, R. C. Peavey, formerly administrative head of the NBS Central Radio Propagation Laboratory; and program officer, G. F. Schilling, since 1949 a member of the Institute of Geophysics at the University of California, Los Angeles. The planning for the United States' program by the U.S. National Committee (Joseph Kaplan, chairman, A. H. Shapley, vice-chairman, and N. C. Gerson, recording secretary) has been achieved through the assistance of 14 technical subcommittees and panels. These groups have worked closely with the USNC Secretariat and with many public and private institutions that are cooperating in the US-IGY effort. The International Geophysical Year program is an unprecedented study of man's physical environment which will take place in 1957–58. More than 40 nations are participating in the coordinated, simultaneous geophysical investigations.

(38) *United States' proposed satellite program*—On July 29, 1955, Dr. Detlev W. Bronk, president of the National Academy of Sciences, and Dr. Alan T. Waterman, director of the National Science Foundation, announced plans for the construction of a small, unmanned, earth-circling satellite vehicle, to be used for basic, non-secret scientific observations during the coming International Geophysical Year 1957–58. This first satellite has been described as a basketball-sized globe filled with recording and transmitting devices. Once established in its orbit, the satellite could telemeter information to earth about conditions in the outer edge of the atmosphere. It is hoped that the vehicle will flash around the earth for a period of days at a height of 200 to 300 miles and at a velocity of 18,000 miles per hour, gradually circling back down into the upper atmosphere where air friction will burn or disintegrate it harmlessly.

(39) *Airborne radioactivity surveys*—A photomosaic map showing radioactivity anomalies detected during an airborne survey of an area of 1,700 square miles in Apache County, Arizona, was released on August 30, 1955, by the United States Geological Survey, as part of a program of airborne reconnaissance for radioactive materials being carried on for the Atomic Energy Commission. The survey was made with scintillation detection equipment in a plane flying regularly spaced traverses about 500 feet above the ground. The map released is Geophysical Investigations Map 124, and is available for purchase at 50 cents.

The location of a number of radioactivity anomalies in the interior of Alaska by the United States Geological Survey was announced on August 19, 1955. Graphically recording the radioactivity responses, a four-inch scintillation crystal was used in a light "bush" plane flying at an average elevation above the ground of about 100 feet and at a speed of about 80 miles per hour. The data give only those localities of greater than average radioactivity, and only suggest areas favorable for prospecting for uranium and thorium deposits. The radioactivity anomalies were located earlier this summer and have not been checked on the ground. The coordinates of these areas may be obtained from Geological Survey offices in Washington, D.C., or in Alaska at Fairbanks, Anchorage, and Juneau.

(40) *Release of geologic map for public inspection*—The United States Geological Survey is releasing in open files for consultation, at the Geological Survey office, Science Hall, University of Wisconsin, Madison, Wisconsin, electrical-resistivity measurements made by H. C. Spicer and G. J. Edwards in the Neillsville area of Wisconsin.

(41) *Fall meeting of URSI*—A fall meeting, sponsored by the USA National Committee of the International Scientific Radio Union (URSI), was held at the University of Florida, Gainesville, Florida, on December 15, 16, and 17, 1955. Besides a combined technical meeting, sessions were also held in the fields of radio and troposphere, ionospheric radio, radio noise of terrestrial origin, and radio astronomy.

(42) *A new British rocket program*—A rocket program for research in upper atmosphere physics is being organized and coordinated by a newly formed subcommittee of the Gassiot Committee of the Royal Society, with Prof. H. S. W. Massey of Imperial College as Chairman. A solid-propellant rocket is being designed at the Royal Aircraft Establishment that will reach altitudes of 80 to 90 km. About 100 pounds of equipment will be carried, exclusive of telemetering, and the rockets will be tracked by radar. A number of preliminary tests will be made during the year 1956, and the major program should be well under way by the time of the International Geophysical Year, 1957–58.

(43) *English translations of Russian papers on high energy physics*—Arrangements have been made between the Soviet Academy of Sciences and the editors of *Nuovo Cimento* for the publication in the latter journal of English translations of papers on high energy and cosmic ray physics appearing in Russian in Soviet journals. The time for publication of articles in *Nuovo Cimento* is only six weeks, so that prompt publication in English of important Russian papers in this field is promised.

(44) *Geomagnetic activities of the United States Coast and Geodetic Survey*—

Capt. Vera Suvannus of Thailand and Sr. Sergio Ferraes G. of Mexico have been studying the methods and procedures of the U.S. Coast and Geodetic Survey in office and field work in geomagnetism.

Mr. Joel B. Campbell has been assigned to International Geophysical Year (IGY) operations in geomagnetism and will be responsible for much of the detailed work of the Survey's IGY field activity. He has been relieved as Observer in Charge of Cheltenham Magnetic Observatory by Mr. Ralph R. Bodle.

The new Fredericksburg (Virginia) Magnetic Observatory has a resident staff of four geophysicists and one instrument maker, with Mr. Robert E. Gebhardt as Observer in Charge. Routine operation of some of the magnetic instruments is expected to be under way before the end of the year 1955. Coordinates of the station are as follows: *Geographic*—38° 12′.2 north and 282° 37′.6 east; *geomagnetic*—49°.6 north and 349°.8 east.

(45) *Special scatter-propagation issue of the Proceedings of the IRE*—In line with its practice of occasionally publishing a special number of its *Proceedings* devoted entirely to one topic of unusual importance and timeliness, the Institute of Radio Engineers in its issue of October 1955 (Vol. 43, No. 10) selected "Scatter Propagation." In some 36 articles, the nature of scatter propagation and its practical significance are described. The printed material presents the results of four years of intensive work on the subject.

(46) *Personalia*—Sir *Harold Spencer Jones*, Astronomer Royal at the Royal Greenwich Observatory, will retire on December 31, 1955, after a long and distinguished career as an astronomer. The tenth Astronomer Royal, he will always be associated with the move of the Royal Observatory from Greenwich to Herstmonceux. Sir Harold was made a Knight of the British Empire in the Queen's Birthday Honors List.

Prof. *R. v. d. R. Woolley*, present Commonwealth Astronomer of Australia, has been chosen the eleventh Astronomer Royal, to succeed Sir Harold Spencer Jones beginning in 1956. Under his able direction, the Commonwealth Observatory at Canberra has become one of the leading observatories in the world.

Dr. *Edison Pettit*, an astronomer noted for his studies of ultraviolet radiation of the sun and solar prominences, retired on July 1, 1955, from the staff of Mount Wilson and Palomar Observatories. Shortly before his retirement, he completed a long series of photoelectric measurements, begun in 1947, of brightnesses and colors of galaxies, data important in the problem of the expanding universe.

Dr. *W. Heiskanen*, formerly director of the Isostatic Institute, Helsinki, Finland, and more recently Research Professor at Ohio State University, has been granted a seven-months leave of absence by the University to devote to writing his share of a text-book with Dr. Felix A. Vening-Meinesz on the earth and its gravity field, which is expected to be published by the McGraw-Hill Book Company, Inc.

Oliver H. Gish has been appointed visiting professor of physics at Southern Illinois University, Carbondale, Illinois, for the academic year 1955–56. From 1922 until his retirement in 1948, Mr. Gish was on the staff of the Department of Terrestrial Magnetism of the Carnegie Institution of Washington, first as physicist and later as chief of the section of terrestrial electricity and as assistant director of

the Department. Since his retirement, he has been part-time consulting physicist to the U.S. Air Force and the U.S. Navy Mine Defense Laboratory.

It is with regret that we have learned of the death, on October 19, 1955, of Dr. *E. Sucksdorff*, of Finland, who for so many years was associated with the Geophysical Observatory at Sodankylä. He served on numerous committees of the International Union of Geodesy and Geophysics, among them being magnetic activity, characterization of magnetic disturbances, registration of giant- and micro-pulsations, and aurora.

Lloyd V. Berkner was promoted on June 1, 1955, from Captain to the rank of Rear Admiral in the United States Naval Reserves. Admiral Berkner was on the staff of the Department of Terrestrial Magnetism, Carnegie Institution of Washington for many years. Since 1951, he has been president of Associated Universities, Inc., New York City, and played a large part in the first moves in 1951 for initiating the International Geophysical Year, 1957-58. He has participated in all of the international conferences relating to the I.G.Y., and is vice-president of the special committee for the I.G.Y. established by the International Council of Scientific Unions.

LIST OF RECENT PUBLICATIONS

BY W. E. SCOTT

Department of Terrestrial Magnetism,
Carnegie Institution of Washington,
Washington 15, D.C.

(Received September 30, 1955)

A—*Terrestrial Magnetism*

ALFVÉN, H. On the electric field theory of magnetic storms and aurorae. Tellus, **7**, No. 1, 50–64 (1955).

BARTELS, J., A. ROMAÑÁ, AND J. VELDKAMP. International data on magnetic disturbances, first quarter, 1955. J. Geophys. Res., **60**, No. 3, 351–354 (1955).

BATES, L. F., AND D. H. MARTIN. A study of domain structures in Alnico. Proc. Phys. Soc., B, **68**, No. 428, 537–540 (1955).

BIREBENT, R. Appareil pour la mesure de l'intensité du champ magnétique terrestre. Paris, C.-R. Acad. sci., **241**, No. 4, 368–369 (1955).

BLOCK, L. Model experiments on aurorae and magnetic storms. Tellus, **7**, No. 1, 65–86 (1955).

CAMPBELL, J. B. Cheltenham three-hour-range indices *K* for April to June, 1955. J. Geophys. Res., **60**, No. 3, 355 (1955).

CATTALA, L. Quelques mesures de déclinaison magnétique à Madagascar. Paris, C.-R. Acad. sci., **241**, No. 4, 435–436 (1955).

CHERNOSKY, E. J. Long-period variations in geomagnetic activity. Trans. Amer. Geophys. Union, **36**, No. 4, 591–595 (1955).

COPENHAGEN, DET DANSKE METEOROLOGISKE INSTITUT. Magnetisk Årbok. 2den del: Grönland—Annuaire magnétique, 2ème partie: Le Groenland, 1949, A: Godhavn. Köbenhavn, 27 pp. (1955). 32 cm.

DAY, A. A., AND S. K. RUNCORN. Polar wandering—some geological dynamical and palaeomagnetic aspects. Nature, **176**, 422–426 (Sept. 3, 1955). [A colloquium held recently by the Department of Geodesy and Geophysics, University of Cambridge, Mr. B. C. Browne in the chair.]

DU BOIS, P. M. Paleomagnetic measurements of the Keweenawan. Nature, **176**, 506–507 (Sept. 10, 1955). [Letter to Editor.]

EGEDAL, J., AND N. AMBOLT. The effect on geomagnetism of the solar eclipse of 30 June 1954. J. Atmos. Terr. Phys., **7**, Nos. 1/2, 40–48 (1955).

ELSASSER, W. M., AND H. TAKEUCHI. Nonuniform rotation of the earth and geomagnetic drift. Trans. Amer. Geophys. Union, **36**, No. 4, 584–590 (1955).

FORBUSH, S. E., AND E. H. VESTINE. Daytime enhancement of size of sudden commencements and initial phase of magnetic storms at Huancayo. J. Geophys. Res., **60**, No. 3, 299–316 (1955).

GRAHAM, J. W. Evidence of polar-shift since Triassic time. J. Geophys. Res., **60**, No. 3, 329–347 (1955).

IVANOV, A. G., AND V. A. TROYIÇKAYA. The Ivanov-Troyiçkaya earth current oscillations. Ottawa, Defense Research Board, No. T174R, xiii + 10 pp. + 7 figs. (March, 1955). 28 cm. [Translations by E. R. Hope, with comments, of three papers from Dok. Akad. Nauch, **81**, No. 5, 807–810 (1951), **91**, No. 2, 241–244 (1953), and **93**, No. 2, 261–264 (1953).]

KATO, Y., AND T. WATANABE. A possible explanation of the cause of giant pulsations. Sci. Rep. Tôhoku Univ., Ser. 5, Geophysics, **6**, No. 2, 95–104 (1955).

KATO, Y., J. OSSAKA, AND M. OKUDA. Investigation on magnetic disturbance by the induction magnetograph, Part IV. Sci. Rep. Tôhoku Univ., Ser. 5, Geophysics, **6**, No. 3, 137–149 (1955).

Lovö. Ergebnisse der Beobachtungen des magnetischen Observatoriums zu Lovö (Stockholm) im Jahre 1953. Von Folke Eleman und Kjell Borg. Stockholm, Kungl. Sjökarteverket, 30 pp. (1955). 31 cm.

Rikitake, T. Magneto-hydrodynamic oscillations in the earth's core. Bull. Earthquake Res. Inst., Tokyo Univ., **33**, pt. 1, 1–25 (1955).

Roberts, W. O., and D. E. Trotter. Solar prominences and geomagnetic disturbance. J. Atmos. Terr. Phys., **6**, No. 5, 282–283 (1955). [Research note.]

Runcorn, S. K., Palaeomagnetism of sediments from the Colorado Plateau. Nature, **176**, 505–506 (Sept. 10, 1955). [Letter to Editor.]

Runcorn, S. K. The permanent magnetization of rocks. Endeavour, **14**, No. 55, 152–159 (1955).

Runcorn, S. K. The earth's magnetism. Sci. Amer., **193**, No. 3, 152–162 (1955).

Smart, J. S. The Néel theory of ferrimagnetism. Amer. J. Physics, **23**, No. 6, 356–370 (1955).

Spinicci, G. L. Sul campo geomagnetico regionale per la Sicilia. Riv. Geof. appl., Milano, **15**, No. 2, 105–123 (1954).

Sucksdorff, E. Ergebnisse der magnetischen Beobachtungen des Observatoriums zu Sodankylä in den Jahren 1943–1944. Helsinki, Suomalainen Tiedeakatemia, 46 pp. (1954). [Veröff. Geophys. Obs. Finn. Akad. Wiss. Nr. 34.]

Toledo, Observatorio Central Geofisíco. Geomagnetismo, año 1950. [Prepared by J. Sancho de San Roman.] Madrid, Instituto Geografico y Catastral, 143 pp. (1954). 24 cm.

Van Wijk, A. M. Magnetic effects during solar eclipses. J. Geophys. Res., **60**, No. 3, 297–298 (1955).

Wingst Observatorium. Magnetogramme Wingst, 1953. D. Hydrogr. Inst., Hamburg, pub. No. 2503, 99 pp. (1955). 25 cm.

B—*Terrestrial Electricity*

Best, A. C. Atomic explosions and condensation nuclei. Met. Mag., **84**, No. 997, 201–204 (1955).

Clark, J. F., and J. H. Kraakevik. The charge on the earth. J. Atmos. Terr. Phys., **6**, No. 6, 344–345 (1955). [Research note.]

Israël, H. An experimental problem in the atmospheric-electrical synopsis—The separation of conduction current and Maxwell's displacement current in measurements of the air-earth current. J. Atmos. Terr. Phys., **6**, No. 6, 322–327 (1955).

Ortner, G., and Abdel Fattah el Nadi. Intermediate and large atmospheric ions at Cairo-Giza. J. Atmos. Terr. Phys., **7**, Nos. 1/2, 31–39 (1955).

Phillips, B. B., P. A. Allee, J. C. Pales, and R. H. Woessner. An experimental analysis of the effect of air pollution on the conductivity and ion balance of the atmosphere. J. Geophys. Res., **60**, No. 3, 289–296 (1955).

Stergis, C. G., S. C. Coroniti, A. Nazarek, D. E. Kotas, D. W. Seymour, and J. V. Werme. Conductivity measurements in the stratosphere. J. Atmos. Terr. Phys., **6**, No. 5, 233–242 (1955).

Whitlock, W. S. Apparatus for the accurate and continuous measurement of the earth's electric field. J. Atmos. Terr. Phys., **7**, Nos. 1/2, 61–72 (1955).

C—*Cosmic Rays*

Meredith, L. H., M. B. Gottlieb, and J. A. Van Allen. Direct detection of soft radiation above 50 kilometers in the auroral zone. Phys. Rev., **97**, No. 1, 201–205 (1955).

Meredith, L. H., J. A. Van Allen, and M. B. Gottlieb. Cosmic-ray intensity above the atmosphere at high latitudes. Phys. Rev., **99**, No. 1, 198–209 (1955).

Ray, E. C. Effects of a ring current on cosmic radiation. Iowa City, State University of Iowa, Dept. of Phys., Pub. No. SUI-55-10, 24 pp. + 9 figs., mim. (Aug. 1955).

Sandström, A. E. On the correlation between geomagnetic activity and the diurnal variation of cosmic rays. Tellus, **7**, No. 2, 204–214 (1955).

Sarabhai, V., N. W. Nerurkar, and P. D. Bhavsar. Study of the anisotropy of cosmic rays with narrow angle telescopes. Proc. Indian Acad. Sci., **41**, No. 6, Sec. A, 245–252 (1955).

Sittkus, A. Untersuchung des Tagesganges der kosmischen Ultrastrahlung mit einer grossen Ionisationskammer. J. Atmos. Terr. Phys., **7**, Nos. 1/2, 80–89 (1955).

Soberman, R. K. High altitude cosmic ray neutron intensity variations. New York University, Cosmic Ray Project, tech. rep., 52 pp., mim. (1955). 28 cm.

Webber, W. R. A new determination of the intensities of primary cosmic ray alpha particles and Li, Be, B, nuclei at $\lambda = 41°.5$ using a Cerenkov detector. Iowa City, State University of Iowa, Dept. of Phys., Pub. No. SUI-55-9, 24 pp., mim. (1955).

D—*Upper Air Research*

Akasofu, S. Thermal upward flow in the ionosphere. Sci. Rep. Tôhoku Univ., Ser. 5, Geophysics, **6**, No. 3, 150–161 (1955).

Ashburn, E. V., and L. G. LaMarca. The measurement of the atmospheric density distribution by the searchlight technique. J. Geophys. Res., **60**, No. 3, 361–362 (1955). [Letter to Editor.]

Banerji, R. B. Distribution-in-speed of fading of 150 kc/s. waves. Nature, **176**, 131 (July 16, 1955). [Letter to Editor.]

Barbier, D. Analyse du spectre du ciel nocturne. Ann. Géophys., **11**, No. 2, 181–208 (1955).

Becker, W. Dir Bestimmung der wahren Verteilung der Elektronendichte, in der Ionosphäre I. Archiv Elektr. Uebertrag., **9**, Heft 6, 277–284 (1955).

Berg, O. E. Day sky brightness to 220 km. J. Geophys. Res., **60**, No. 3, 271–277 (1955).

Blamont, J.-E., et G. Courtès. Nouveau procédé d'étude photométrique des émissions monochromatiques du ciel nocturne. Ann. Géophys., **11**, No. 2, 252–254 (1955). [Note.]

Bramley, E. N. Some aspects of the rapid directional fluctuations of short radio waves reflected at the ionosphere. Proc. Inst. Elec. Eng., **102**, Pt. B, 533–540 (1955).

Budden, K. G. The numerical solution of the differential equations governing the reflexion of long radio waves from the ionosphere, II. Phil. Trans. R. Soc., A, **248**, No. 939, 45–72 (1955).

Byram, E. T., T. A. Chubb, and H. Friedman. Dissociation of oxygen in the upper atmosphere. Phys. Rev., **98**, No. 6, 1594–1597 (1955).

Chatterjee, B. A discussion on the variation of *F*-region height. J. Geophys. Res., **60**, No. 3, 325–327 (1955).

Crombie, D. D. Measurement of the arrival angle of "whistlers." J. Geophys. Res., **60**, No. 3, 364–365 (1955). [Letter to Editor.]

Davids, N. The diffusion thermo effect in the atmosphere above 120 km. Pennsylvania State University, Ionosphere Res. Lab., Sci. Rep. No. 76, 25 pp. (July 1, 1955). 28 cm.

Delobeau, F. Nouvelle représentation de l'effet de longitude dans la couche ionosphérique F_2. Paris, C.-R. Acad. sci., **241**, No. 4, 439–441 (1955).

Dominici, P., e F. Mariani. Considerazioni critiche sulla regione *F* della ionosfera. Ann. Geofis., Roma, **8**, No. 1, 103–120 (1955).

Dufay, M., et J. Dufay. Contribution à l'étude du spectre du ciel nocturne dans le violet et le proche ultraviolet. Ann. Géophys., **11**, No. 2, 209-213 (1955).

Dyce, R. B. Auroral echoes observed north of the auroral zone. J. Geophys. Res., **60**, No. 3, 317–323 (1955).

Elterman, L. Reply to comments by Ashburn and LaMarca. J. Geophys. Res., **60**, No. 3, 363 (1955). [Letter to Editor.]

Elvey, C. T., and F. E. Roach. Aurora and airglow. Sci. Amer., **193**, No. 3, 140–151 (1955).

Elvey, C. T., H. Leinbach, J. Hessler, and J. Noxon. Preliminary studies of the distribution of auroras in Alaska. Trans. Amer. Geophys. Union, **36**, No. 3, 390–394 (1955).

Friedman, H. The solar spectrum below 2,000 angstroms. Ann. Géophys., **11**, No. 2, 174–180 (1955).

Gautier, T. N. The ionosphere. Sci. Amer., **193**, No. 3, 126–139 (1955).

Gerson, N. C. Diurnal variation in auroral activity. Proc. Phys. Soc., B, **68**, No. 427, 408–414 (1955).

Gerson, N. C. Radio observations of the aurora. J. Atmos. Terr. Phys., **6**, No. 5, 263–267 (1955).

Gibbons, J. J., and J. D. Wolf. Methods of determining long wave reflection coefficients for a specific ionospheric model. Pennsylvania State University, Ionosphere Res. Lab., Sci. Rep. No. 75, 50 pp. (June 1, 1955). 28 cm.

Heading, J. The reflexion of vertically-incident long radio waves from the ionosphere when the earth's magnetic field is oblique. Proc. R. Soc., A, **231**, No. 1186, 414–435 (1955).

Hines, C. O. Hydromagnetic resonance in ionospheric waves. J. Atmos. Terr. Phys., **7**, Nos. 1/2, 14–30 (1955).

Hirono, M. Researches on the geomagnetic distortion in the ionosphere. Part 4—Effect of gravity and ionization pressure gradient on the vertical drift in the $F2$ region. Rep. Ionosphere Res. Japan, **9**, No. 2, 95–104 (1955).

Hirono, M., and H. Maeda. Researches on the geomagnetic distortion in the ionosphere. Part 3—Characteristics of $F2$ layer on the magnetic equator. Rep. Ionosphere Res. Japan, **9**, No. 2, 86–94 (1955).

Hirono, M., and H. Maeda. Geomagnetic distortion of the $F2$ region on the magnetic equator. J. Geophys. Res., **60**, No. 3, 241–255 (1955).

Horner, F., and C. Clarke. Some waveforms of atmospherics and their use in the location of thunderstorms. J. Atmos. Terr. Phys., **7**, Nos. 1/2, 1–13 (1955).

Humby, A. M., C. M. Minnis, and R. J. Hitchcock. Performance characteristics of high-frequency radiotelegraph circuits. Proc. Inst. Elec. Eng., **102**, Pt. B, 513–522 (1955). [Discussion follows.]

International Council of Scientific Unions, Mixed Commission on the Ionosphere. Proceedings of the fourth meeting held in Brussels, from August 16th to 18th, 1954. Secrétariat Général de l'U.R.S.I., Bruxelles, 238 pp. (1955). 24 cm. [This publication may be obtained from the General Secretariat of the U.R.S.I., 42 rue des Minimes, Brussels, Belgium, at the following price: 300 Belgian francs, or £2.3.0, or $6.00 U.S., postpaid.]

International Scientific Radio Union, Commission IV on Radio Noise of Terrestrial Origin. Proceedings of the Eleventh General Assembly held in The Hague from August 23rd to September 2nd, 1954. Secretary General of U.R.S.I., Brussels, Vol. X, Pt. 4, 60 pp. (1954). 25 cm. [This publication is available from the General Secretariat of the U.R.S.I., 42 Rue des Minimes, Brussels, Belgium, at the following price: 60 Belgian francs, or 8/8 sh., or $1.20 U.S. (postage included).]

International Scientific Radio Union. Proceedings of the Eleventh General Assembly held in The Hague from August 23rd to September 2nd, 1954 (Administrative Proceedings). Secrétariat-Général de l'U.R.S.I., Bruxelles, **10**, Pt. 8, 125 pp. (1954). 24 cm. [This publication may be obtained from the Secretary General of the U.R.S.I., 42 rue des Minimes, Brussels, Belgium, at the following price: 100 Belgian francs, or 14/6 shillings, or $2.00 U.S., postpaid.]

Jelley, J. V., and W. Galbraith. Light pulses from the night sky and Čerenkov radiation. Part II. J. Atmos. Terr. Phys., **6**, No. 6, 304–312 (1955).

Jowett, J. K. S., and G. O. Evans. A study of commercial time lost on transatlantic radio circuits due to disturbed ionospheric conditions. Proc. Inst. Elec. Eng., **102**, Pt. B, 505–512 (1955). [Discussion follows.]

Kaiser, T. R., and S. Evans. Upper atmospheric data from meteors. Ann. Géophys., **11**, No. 2, 148–152 (1955).

Lange-Hess, G. Erdmagnetische Unruhe und Durchschnittsabweichungen der F_2-Schicht-Tagesgrenzfrequenzen in verschiedenen geomagnetischen Breiten. J. Atmos. Terr. Phys., **7**, Nos. 1/2, 49–60 (1955).

Maeda, H. Researches on the geomagnetic distortion in the ionosphere. Part 1—Observed facts of the geomagnetic distortion in the ionosphere. Rep. Ionosphere Res. Japan, **9**, No. 2, 59–70 (1955).

Maeda, K. Researches on the geomagnetic distortion in the ionosphere. Part 2—Theoretical study on the geomagnetic distortion in the $F2$ layer. Rep. Ionosphere Res. Japan, **9**, No. 2, 71–85 (1955).

McNamara, A. G. Double-Doppler radar investigations of aurora. J. Geophys. Res., **60**, No. 3, 257–269 (1955).

Meek, J. H. The location and shape of the auroral zone. J. Atmos. Terr. Phys., **6**, No. 6, 313–321 (1955).

Mitra, S. N., and S. C. Mazumdar. Effect of solar activity on ionosphere and earth's magnetic field. Indian J. Phys., **28**, No. 12, 563–580 (1955).

Nagata, T., Y. Nakata, T. Rikitake, and I. Yokoyama. Effect of the solar eclipse on the lower parts of the ionosphere and the geomagnetic field. Rep. Ionosphere Res. Japan, **9**, 121–135 (1955).

Naismith, R. An improved chart for ionospheric forecasting in the British zone. Proc. Inst. Elec. Eng., **102**, Pt. B, 503–504 (1955).

Newell, H. E., Jr. Rocket data on atmospheric pressure, temperature, density, and winds. Ann. Géophys., **11**, No. 2, 115–144 (1955).

Obayashi, T. Movements of irregularities in the *E* region. J. Radio Res. Lab. Japan, **2**, No. 7, 59–67 (1955).

Omholt, A. The auroral *E*-layer ionization and the auroral luminosity. J. Atmos. Terr. Phys., **7**, Nos. 1/2, 73–79 (1955).

Peiffer, H. R., and A. P. Mitra. The effect of vertical ion transport on the night-time *E*-region. J. Atmos. Terr. Phys., **6**, No. 6, 291–303 (1955).

Phillips, G. J., and M. Spencer. The effects of anisometric amplitude patterns in the measurement of ionospheric drifts. Proc. Phys. Soc., B, **68**, No. 428, 481–492 (1955).

Rastogi, R. G. The occurrence of high multiple reflections from the *F*2 region of the ionosphere based on a study of the Ahmedabad records. Proc. Indian Acad. Sci., **41**, No. 6, Sec. A, 253–260 (1955).

Roach, F. E. A review of observational results in airglow photometry. Ann. Géophys., **11**, No. 2, 214–231 (1955).

Seaton, M. J. Theory of the airglow spectrum. Ann. Géophys., **11**, No. 2, 232–248 (1955).

Seddon, J. C., and J. E. Jackson. L'application des fusées a l'étude de l'ionosphère. Ann. Géophys., **11**, No. 2, 169–172 (1955).

Sedra, R. N., and I. B. Hazzaa. Effect of radiation from solar flares on the ionosphere and the earth's magnetic field. Phys. Rev., **99**, No. 4, 1070–1072 (1955).

Shepherd, G. G., and D. M. Hunten. On the measurement of rotational temperature from unresolved auroral nitrogen bands. J. Atmos. Terr. Phys., **6**, No. 6, 328–335 (1955).

Shimazaki, T. World-wide daily variations in the height of the maximum electron density of the ionospheric *F*2 layer. J. Radio Res. Lab. Japan, **2**, No. 7, 85–97 (1955).

Shmoys, J. Long-range propagation of low-frequency radio waves between the earth and the ionosphere. New York University, Res. Rep. No. EM-79, 28 pp. mim. (1955). 28 cm.

Sinno, K. Studies on the disturbances in *F*2 layer associated with geomagnetic disturbances. J. Radio Res. Lab. Japan, **2**, No. 7, 69–76 (1955).

Spencer, M. The shape of irregularities in the upper ionosphere. Proc. Phys. Soc., B, **68**, No. 428, 493–503 (1955).

Sprenger, K., und E. A. Lauter. Beobachtungen der tiefen Ionosphäre während der Sonnenfinsternis am 30.6.1954. Beitr. Geophysik, **64**, Heft 4, 284–327 (1955).

Theissen, E. L'influence du cycle solaire sur le facteur de transmission $(M\ 3000)F_2$. J. Atmos. Terr. Phys., **6**, No. 5, 243–249 (1955).

Trolese, L. G. Characteristics of tropospheric scattered fields. Trans. Inst. Radio Eng. Prof. Group on Antennas and Propagation, **AP-3**, No. 3, 117–122 (July, 1955).

Vallance Jones, A., and A. W. Harrison. Rotational temperatures of the auroral N_2^+ bands. J. Atmos. Terr. Phys., **6**, No. 6, 336–343 (1955).

Yonezawa, T. On the influence of electron-ion diffusion on the electron density and height of the nocturnal *F*2 layer. J. Radio Res. Lab. Japan, **2**, No. 8, 125–136 (1955).

E—*Radio Astronomy*

Akabane, K. Lunar radiation at 3,000 Mc/s. Proc. Japan Acad., **31**, No. 3, 161–165 (1955). [Tokyo Astr. Obsy. reprint No. 115.]

Bracewell, R. N. Correcting for Gaussian aerial smoothing. Aust. J. Phys., 8, No. 1, 54–60 (1955).

Davies, R. D., and D. R. W. Williams. An alternative identification of the radio source in the direction of the galactic centre. Nature, **175**, 1079–1081 (June 18, 1955). [Letter to Editor.]

Elsmore, B., and G. R. Whitfield. Lunar occultation of a radio star and the derivation of an upper limit for the density of the lunar atmosphere. Nature, **176**, 457–458 (Sept. 3, 1955). [Letter to Editor.]

Hatanaka, T., S. Suzuki, and A. Tsuchiya. Observations of polarization of solar radio bursts. Proc. Japan Acad., **31**, No. 2, 81–87 (1955). [Tokyo Astr. Obsy. reprint No. 113.]

Heeschen, D. S. Some features of interstellar hydrogen in the section of the galactic center. Astroph. J., **121**, No. 3, 569–584 (1955).

Helfer, H. L., and H. E. Tatel. Preliminary 21-cm meridian plane surveys. Astroph. J., **121**, No. 3, 585–603 (1955).

Ko, H. C., and J. D. Kraus. Radio frequency radiation from the Rosette nebula. Nature, **176**, 221–222 (July 30, 1955).

Kraus, J. D., and H. C. Ko. The radio position of the galactic nucleus. Astroph. J., **122**, No. 1, 139–145 (1955).

Kraus, J. D., H. C. Ko, and D. V. Stoutenburg. A fluctuating celestial radio source at 242 megacycles per second. Nature, **176**, 304–305 (Aug. 13, 1955). [Letter to Editor.]

Lilley, A. E. Association of gas and dust from 21-cm hydrogen radio observations. Astroph. J., **121**, No. 3, 559–568 (1955).

Ryle, M., and P. A. Scheuer. The spatial distribution and the nature of radio stars. Proc. R. Soc., A, **230**, No. 1183, 448–462 (1955).

F—*Earth's Crust and Interior*

Bhattacharyya, B. K. Electromagnetic induction in a two-layer earth. J. Geophys. Res., **60**, No. 3, 279–288 (1955).

Forester, R. D. Calculated travel times of seismic core waves. Bull. Seis. Soc. Amer., **45**, No. 3, 187–195 (1955).

Gutenberg, B. Wave velocities in the earth's crust. Geol. Soc. Amer. Memoir, special paper 62, 19–34 (1955).

Kay, M. The origin of continents. Sci. Amer., **193**, No. 3, 62–66 (1955).

Menard, H. W. Deformation of the northeastern Pacific basin and the west coast of North America. Bull. Geol. Soc. Amer., **66**, No. 9, 1149–1198 (1955).

Oliver, J., M. Ewing, and F. Press. Crustal structure of the Arctic regions from the L_g phase. Bull. Geol. Soc. Amer., **66**, No. 9, 1063–1074 (1955).

Rey Pastor, A. Contribución de la ciencia del magnetismo a la geológia. Rev. Geofísica, Madrid, **14**, No. 53, 13–30 (1955).

Shimazu, Y. Equation of state of materials composing the earth's interior, Part I. J. Earth Sci. Nagoya Univ., **2**, No. 1, 15–93 (1954).

Shimazu, Y. Equation of state for the earth's mantle based upon a theory of pressure- and temperature-dependences of elasticity of solid. J. Phys. Earth, **2**, No. 2, 55–61 (1954).

Suzuki, Z., and H. Sima. On forms of seismic waves generated by explosion, II. Sci. Rep. Tôhoku Univ., Ser. 5, Geophysics, **6**, No. 3, 162–170 (1955).

Takeuchi, H., and W. M. Elsasser. Fluid motions near the core boundary and the irregular variations in the earth's rotation. J. Phys. Earth, **2**, No. 2, 39–44 (1954).

Toledo, Observatorio Central Geofísico. Corrientes telúricas, año 1952. [Prepared by Luis de Miguel y González-Miranda.] Madrid, Instituto Geografico y Catastral, 51 pp. + 11 figs. (1955). 24 cm.

Tomaschek, R. Earth tilts in the British Isles connected with far distant earthquakes. Nature, **176**, 24–25 (July 2, 1955).

G—*Miscellaneous*

Counseil International des Unions Scientifiques. Huitième rapport de la Commission pour l'étude des Relations entre les Phénomènes Solaires et Terrestres. Paris, 184 pp. (1954). 21 cm.

Ferraro, V. C. A. Magneto-hydrodynamics. Nature, **176**, 234–237 (Aug. 6, 1955). [Discussion on magneto-hydrodynamics, organized by Sir Edward Bullard, held in rooms of the Royal Society, May 5, 1955.]

Waldmeier, M. Final relative sunspot-numbers for 1954. J. Geophys. Res., **60**, No. 3, 349–351 (1955).

Waldmeier, M. Provisional sunspot-numbers for April to June, 1955. J. Geophys. Res., **60**, No. 3, 355 (1955).

INDEX OF AUTHORS

Volume 60, 1955

NOTICE

When available, single unbound volumes can be supplied at $6 each and single numbers at $2 each, postpaid.

Charges for reprints and covers

Reprints can be supplied, but prices have increased considerably and costs depend on the number of articles per issue for which reprints are requested. It is no longer possible to publish a schedule of reprint charges, but if reprints are requested approximate estimates will be given when galley proofs are sent to authors. Reprints without covers are least expensive; standard covers (with title and author) can be supplied at an additional charge. Special printing on covers can also be supplied at further additional charge.

Fifty reprints, without covers, will be given to institutions paying the publication charge of $8 per page.

Alterations

Major alterations made by authors in proof will be charged at cost. Authors are requested, therefore, to make final revisions on their typewritten manuscripts.

Orders for back issues and reprints should be sent to Editorial Office, 5241 Broad Branch Road, N.W., Washington 15, D.C., U.S.A.

Subscriptions are handled by The Editorial Office, 5241 Broad Branch Road, N.W., Washington 15, D.C., U.S.A.

CONTENTS—Concluded